

The amidase AmiC2 and its peptidoglycan substrate in filamentous cyanobacteria

Dissertation

der Mathematisch-Naturwissenschaftlichen Fakultät
der Eberhard Karls Universität Tübingen
zur Erlangung des Grades eines
Doktors der Naturwissenschaften
(Dr. rer. nat.)

vorgelegt von
Eva Bok
aus Horb a. N.

Tübingen
2020

Gedruckt mit Genehmigung der Mathematisch-Naturwissenschaftlichen Fakultät der
Eberhard Karls Universität Tübingen.

Tag der mündlichen Qualifikation:

27.10.2020

Stellvertretender Dekan:

Prof. Dr. József Fortágh

1. Berichterstatter:

Prof. Dr. Karl Forchhammer

2. Berichterstatter:

Prof. Dr. Friedrich Götz

Declaration

„Ich erkläre hiermit, dass ich die zur Promotion eingereichte Arbeit mit dem Titel: „The amidase AmiC2 and its peptidoglycan substrate in filamentous cyanobacteria“ selbständig verfasst, nur die angegebenen Quellen und Hilfsmittel benutzt und wörtlich oder inhaltlich übernommene Stellen (alternativ: Zitate) als solche gekennzeichnet habe. Ich erkläre, dass die Richtlinien zur Sicherung guter wissenschaftlicher Praxis der Universität Tübingen (Beschluss des Senats vom 25.5.2000) beachtet wurden. Ich versichere an Eides statt, dass diese Angaben wahr sind und dass ich nichts verschwiegen habe. Mir ist bekannt, dass die falsche Abgabe einer Versicherung an Eides statt mit Freiheitsstrafe bis zu drei Jahren oder mit Geldstrafe bestraft wird.“

Tübingen,

Eva Bok

Acknowledgements

First of all, I want to acknowledge and thank Prof. Dr. Karl Forchhammer for giving me the opportunity to study a very interesting and fascinating issue; the cell wall of filamentous cyanobacteria. He supported me throughout the 4 years of my PhD, and gave me a lot of professional advices to answer the question how AmiC2 drills little nanopores into the cell wall or let's say to track down the secret.

Secondly, I sincerely and cordially thank Dr. Iris Maldener for her supervision and the opportunity to make and earn my PhD in her working group. I really liked to be a part of the "cell wall people" and appreciated her ideas, support and advices.

I really want to highlight the roles of Dr. Mark Stahl and Dr. Ute Bertsche. Dr. Ute Bertsche guided me through the highly complex world of peptidoglycan, and explained me how to prepare samples as well as to analyse LC-MS data of peptidoglycan. Thank you very much for your support, Ute! Dr. Mark Stahl exceptionally helped me to analyse peptidoglycan by LC-MS and became an integral part of my PhD. He measured hundreds of my samples to help me elucidating the cell wall of multicellular cyanobacteria. I really appreciated working with him and would not have been able to lift the secret without him. Really, really thank you a lot, Mark!

The identification of AmiC2 substrates was a challenging task and I am so gratefully thankful for the support and help of Dr. Philipp Spät. He optimized methods to detect highly crosslinked peptides by tandem mass spectrometry. Furthermore, he analysed tryptic digests of *N. punctiforme* cell walls. But the most important thing was his loving support during my "roller-coaster ride" especially at the final stage of my PhD. Thank you for always being there for me; no matter how fast and deleterious my "roller-coaster ride"-style was!

I want to acknowledge José Manuel Beltrán Belena from the Institute of Organic Chemistry. He helped me to fractionate peptidoglycan samples by HPLC and to analyse all these fractions by LC-MS.

Moreover, I want to thank Dr. Mulugeta Nega to give me the opportunity to use the HPLC and for all the fruitful discussions about amidases and peptidoglycan. Thank you, Mulu!

I want to thank Andreas Kulik for performing the amino acid analysis by HPLC.

Furthermore, I want to acknowledge Dr. Felix Büttner for making the AmiC2cat/peptidoglycan docking model and his suggestions for site-specific mutants.

I want to thank my family and friends. I know that it was really hard to understand my project, but I appreciated it that you tried to understand each detail of it and gave me so much advice. Thank you for giving me support, when I needed it the most and cheered me up. I love you all!

Last but not least, I want to thank all the members of my working group. When I started my PhD, I felt so welcomed by all of you and I really enjoyed spending time with you, even or especially outside the work. I got to know so many lovely people and became friends with nice, but also a bit crazy, let's say interesting, people (just kidding☺). I will miss the time!

Abstract

Multicellularity is an advantageous ability of cyanobacteria to successfully inhabit diverse ecological niches. The development of specialized cell types like N₂-fixing heterocysts, spore-like akinetes or short motile hormogonia expanded their repertoire to survive and proliferate in a rapid changing, partially harsh environment. A recently detected structure in the septal peptidoglycan between adjacent cells in the filaments of heterozygous cyanobacteria became evident to be indispensable for differentiation or adaptation. This structure is relevant for intercellular communication and consists of numerous perforations, with a diameter of 15 - 20 nm, in the central part of septal disks. This nanopore-array is the framework for septal junction proteins, which connect neighbouring cells in the filaments and enable intercellular communication. N-acetylmuramyl-L-alanine amidases, homologous to AmiC from *E. coli*, are involved in nanopore formation, but differ functionally and structurally from those in unicellular bacteria. While AmiC enables the release of daughter cells during cell division in unicellular bacteria, it drills the regularly formed nanopores into septal disks of multicellular cyanobacteria. An inhibitory α -helix, which is crucial for catalytic activation of AmiC in *E. coli*, is missing in AmiC from heterocyst-forming cyanobacteria. This points to a novel regulation mechanism of AmiC in filamentous cyanobacteria.

This work characterizes the interaction between the amidase AmiC2 from the multicellular cyanobacterium *Nostoc punctiforme* with its natural substrate, the peptidoglycan (PGN). The first part describes the chemical composition of *Nostoc* PGN, which revealed some differences to other Gram-negative bacteria. Extensive analysis of the amino acid composition, the muropeptide fragment pattern and the type of modification uncover the complex PGN network of *Nostoc punctiforme*. The glycan chains consist of alternating disaccharide units of N-acetylglucosamine (GlcNAc) and N-acetylmuramic acid (MurNAc) which are crosslinked by short peptides containing alanine (Ala), glutamic acid (Glu) and meso-diaminopimelic acid (mDAP). LC-(ESI-TOF)-MS analysis of PGN fragments revealed highly amidated side chains of the peptide stem. Furthermore, dimeric, trimeric and higher PGN oligomers were detected. These oligomers are formed by peptide bond formation between mDAP, the third amino acid from one peptide stem and the fourth alanine residue from another peptide stem.

The amino acid analysis revealed several PGN typical amino acids indicating the presence of either covalently linked or associated proteins. Tandem mass spectrometry detected numerous peptides in tryptic digests of *Nostoc* PGN, which were assigned to putative PGN interacting proteins, like lipoproteins, parts of transporters and of two-component systems. Moreover, a polysaccharide might be covalently linked to MurNAc by a phosphodiester bond. HPAEC-analysis determined glucose, arabinose, galactose and mannose/xylose at almost equal stoichiometry in acid PGN-hydrolysates. Interestingly, disruption of *amiC2*, encoding the amidase AmiC2 in *N. punctiforme*, altered the composition of this PGN-polysaccharide. Glucose was enriched in acid PGN-hydrolysates while arabinose, mannose/xylose and galactose were consistently reduced. The inactivation of *amiC2* in *N. punctiforme* affected polysaccharide modification, since amino acid analysis of HCl-hydrolysed PGN components revealed exclusively PGN derived amino acids, whereas further amino acids, as has been shown for the wild-type, were missing. The basic PGN composition of the *amiC2* mutant was identical to the wild-type.

The second part of this work focused on the enzymatic activity and PGN binding capability of the amidase AmiC2 from *N. punctiforme*. The AmiC2 was unable to hydrolyse purified wild-type cell walls but degraded the peptidoglycan derived from the *amiC2* mutant. Released peptides were collected and subjected to tandem mass spectrometry. Highly cross-linked species were identified as substrates of the amidase AmiC2. The substrate-binding characteristic of AmiC2 was investigated by amino acid exchanges in the catalytic site. Substitution of residues F564, E529 and L576 decreased the hydrolytic activity of the catalytic domain of AmiC2 (AmiC2cat) on Remazol Brilliant Blue labelled *E. coli* PGN. Different genetic, and experimental procedures were performed to detect the interaction between PGN and the amidase AmiC2 as well as to analyse the influence of site-specific mutations. Biolayer interferometry (BLI) measurements efficiently determined the binding of *E. coli* PGN to the catalytic domain of AmiC2. The replacement of F564, E529 and L576 did not significantly change the binding behaviour of AmiC2cat, indicating the reduced activity of these variants is not due to impaired substrate binding but likely due to a defect in the catalytic mechanism.

In this work the chemical composition of PGN from *N. punctiforme* and its *amiC2* mutant, was elucidated. In addition a direct interaction between PGN and the catalytic domain of AmiC2 was demonstrated. Furthermore, highly cross-linked peptides were identified as substrates for the amidase, which points to a novel regulatory mechanism of the amidase on substrate level.

Zusammenfassung

Die Mehrzelligkeit ist eine nützliche Fähigkeit von Cyanobakterien diverse ökologische Nischen erfolgreich zu besiedeln. Die Entwicklung von spezialisierten Zelltypen wie N_2 -fixierenden Heterozysten, Sporen-ähnlichen Akineten oder kleinen beweglichen Hormogonien erweiterten ihr Repertoire um in einer sich schnell ändernden, teils harschen Umwelt zu überleben und zu vermehren. Es hat sich herausgestellt, dass eine kürzlich entdeckte Struktur im septalen Peptidoglykan, zwischen benachbarten Zellen eines Filaments von Heterozysten-bildenden Cyanobakterien, unverzichtbar für die Differenzierung oder Anpassung ist. Diese Struktur ist für die zelluläre Kommunikation wichtig und besteht aus zahlreichen Perforationen im zentralen Bereich der Septen, mit einem Durchmesser von 15 – 20 nm. Dieser „Nanopore-Array“ bildet das Grundgerüst für septale Junction-Proteine, die benachbarte Zellen eines Filaments miteinander verbindet und somit die interzelluläre Kommunikation ermöglicht. N-Acetylmuramyl-L-Alanine-Amidasen, homolog zu AmiC aus *E. coli*, sind an der Bildung der Nanoporen beteiligt, unterscheiden sich aber in Funktion und Struktur von denen aus einzelligen Bakterien. Während AmiC in einzelligen Bakterien beide Tochterzellen während der Zellteilung trennt, bohrt es in vielzelligen Cyanobakterien regelmäßig geformte Nanoporen in deren Septen. Eine hemmende α -Helix, wie sie für die katalytische Aktivierung von AmiC aus *E. coli* benötigt wird, fehlt in AmiC aus Heterozysten-bildenden Cyanobakterien. Dies deutet auf einen neuen Regulationsmechanismus für AmiC aus filamentösen Cyanobakterien hin.

Diese Arbeit beschreibt die Interaktion zwischen der Amidase AmiC2 aus dem vielzelligen Cyanobakterium *Nostoc punctiforme* und seines natürlichen Substrates, dem Peptidoglykan (PGN). Der erste Part erläutert die chemische Zusammensetzung des *Nostoc* PGNs, welches einige Unterschiede zum PGN von Gram-negativen Bakterien aufweist. Umfangreiche Analysen zur Zusammensetzung der Aminosäuren, zum Muropeptid-Profil und zur Art der Modifikation deckten das komplexe PGN-Netzwerk von *Nostoc punctiforme* auf. Die Glykanstränge bestehen aus sich wiederholenden Disaccharid-Einheiten von N-Acetylglucosamin (GlcNAc) und N-Acetylmuraminsäure (MurNAc), die über kurze Peptide aus Alanin (Ala), Glutaminsäure (Glu) und meso-Diaminopimelinsäure (mDAP) miteinander verbunden sind. LC-(ESI-TOF)-MS- Analysen von PGN-Fragmenten wiesen amidierete Carboxylseitenketten des Peptidstammes auf. Des Weiteren wurden dimere, trimere und höhere oligomere PGN-Fragmente entdeckt. Diese Oligomere weisen Peptidbindungen zwischen der dritten Aminosäure des einen Peptidstammes, mDAP, und der vierten Aminosäure des anderen Peptidstammes, Ala, auf.

Die Aminosäure-Analyse wies mehrere kanonische Aminosäuren auf, die sich auf kovalent gebundene oder lose assoziierte Proteine zurückführen lässt. Tandem-Massenspektrometrie detektierte zahlreiche Peptide in tryptischen Verdauen des *Nostoc* PGNs, die zu möglichen PGN interagierenden Proteinen wie Lipoproteine, Teile von Transportern oder Zweikomponentensystemen zugeordnet werden konnten. Außerdem, könnte ein Polysaccharid kovalent an MurNAc, über eine Phosphodiesterbindung, verknüpft sein. HPAEC detektierte Glukose, Arabinose, Galaktose und Mannose/Xylose zu beinahe gleichen Teilen in sauren PGN-Hydrolysaten. Interessanterweise wies *N. punctiforme* eine veränderte Zusammensetzung des Polysaccharids auf wenn das Gen für die Amidase AmiC2 mutiert wurde. Glukose war in sauren PGN-Hydrolysaten stark angereichert während Arabinose, Mannose/Xylose und Galaktose konstant reduziert waren. Die Inaktivierung von *amiC2* in *N. punctiforme* beeinträchtigte außerdem die Polysaccharid-Modifikation

des PGNs, da die Aminosäure-Analyse von HCl-hydrolysierten PGN-Komponenten ausschließlich PGN-Aminosäuren und keine weiteren Aminosäuren, wie man sie im wildtypischen PGN vorfand, aufwies. Die Grundzusammensetzung des PGNs war dennoch identisch zu dem des Wildtyps.

Der zweite Teil der Arbeit konzentrierte sich auf die enzymatische Aktivität und PGN-Bindungsfähigkeit der Amidase AmiC2 aus *N. punctiforme*. AmiC2 war unfähig gereinigtes Wildtyp-PGN zu hydrolysieren, baute das Peptidoglykan der *amiC2*-Mutante aber fast vollständig ab. Die durch AmiC2 abgetrennten Peptide wurden durch Tandem-Massenspektrometrie analysiert. Stark vernetzte Spezies wurden als Substrate der Amidase AmiC2 identifiziert. Die Substratbindeeeigenschaft von AmiC2 wurde durch Aminosäureaustausche im katalytischen Zentrum untersucht. Der Austausch von F564, E529 und L576 beeinträchtigte die Hydrolyse von Remazol Brilliant Blue gefärbten *E. coli* PGN durch die katalytische Domäne von AmiC2 (AmiC2cat). Unterschiedliche genetische und experimentelle Vorgehen wurden angewandt, um eine Interaktion zwischen dem PGN und der Amidase AmiC2cat sowie den Einfluss von Aminosäureaustauschen nachzuweisen. Biolayer Interferometrie (BLI)-Messungen ermöglichten die Detektion der Bindung zwischen *E. coli* PGN und der katalytischen Domäne von AmiC2. Der Austausch von F564, E529 und L576 sorgte für keine signifikante Änderung im Bindungsverhalten der Amidase, was darauf hindeutet, dass die geringere katalytische Aktivität dieser Varianten nicht aufgrund einer verminderten Substratbindung herrührt, viel wahrscheinlicher aufgrund eines Defekts im katalytische Mechanismus.

In dieser Arbeit wurde die chemische Zusammensetzung des PGNs von *N. punctiforme* und seiner *amiC2* Mutante aufgeklärt. Außerdem wurde die direkte Interaktion zwischen dem PGN und der katalytischen Domäne der Amidase nachgewiesen. Des Weiteren wurden stark vernetzte Peptide als Substrate der Amidase identifiziert, was auf einen neuen Regulationsmechanismus der Amidase auf dem Substratlevel hindeutet.

Abbreviations

Abbreviation	
μE	Micro Einstein
A	Amidation
AA	Amino acid
ABC	ATP binding cassette
Ac	Acetylation
AFM	Atomic Force Microscopy
ACN	Acetonitrile
ALP	Actin-like protein
AmiC2cat	Catalytic domain of AmiC2
APS	Ammonium persulfate
ATCC	American Type Culture Collection
ATP	Adenosine triphosphate
BCA	Bicinchoninic acid
BG	Blue Green
BLI	Biolayer interferometry
BPI	Base peak ion
BSA	Bovine Serum Albumin
CAP	Capsular polysaccharide
CM	Cytoplasmic membrane
CV	Column volume
DMSO	Dimethyl sulfoxide
DNA	Deoxyribonucleic acid
dNTP	deoxyribonucleoside triphosphates
DRA	Dye-release Assay
DTT	Dithiothreitol
EDTA	Ethylenediaminetetraacetic acid
ES+	Electrospray ionization, positive mode
ESI	Electrospray ionization
FRAP	fluorescence recovery after photobleaching
G	gravitational force equivalent
GAF	cGMP-specific and -regulated cyclic nucleotide phosphodiesterases, adenylyl cyclase, and transcription factor FhIA
GFP	Green fluorescent protein
GlcNAc	N-acetylglucosamine
GST	Gluthation-S-transferase
GTP	Guanosine triphosphate
HAMP	Histidine kinases, Adenylate cyclases, Methyl accepting proteins and Phosphatases
HCD	Higher-energy collisional dissociation
HCl	Hydrochloride acid
HEP	heterocyst envelope polysaccharides
HGL	heterocyst-specific glycolipid
HMW	High molecular weight
HPAEC	High Performance Anion Exchange Chromatography
HPLC	High Performance Liquid Chromatography
HR	High-resolution

Abbreviation	
IMP	Inner membrane protein
IPTG	Isopropyl- β -D-thiogalactopyranosid
IR	Infrared
kDa	Kilo Dalton
L	Litre
LB	Lysogeny broth
LC	Liquid chromatography
LED	light-emitting diode
LMW	Low molecular weight
LP	Lipoprotein
LPS	Lipopolysaccharide
LTA	Lipoteichoic acid
m	Meter
m/z	Mass-to-charge
mDAP	Meso-diaminopimelic acid
Min	Minute
MS	Mass spectrometry
MST	Microscale Thermophoresis
MurNAc	N-acetylmuramic acid
NTA	Nitrilotriacetic acid
OD	Optical density
OMP	Outer membrane protein
OPA	o-Phthaldialdehyde
PAGE	Polyacrylamide Gel Electrophoresis
PBP	Penicillin Binding Protein
PBS	Phosphate buffered Saline
PCR	Polymerase chain reaction
PES	Polyethylensulfone
PG	Peptidoglycan
PGN	Peptidoglycan
Pos.	Position
Ppm	Parts per million
PTFE	Polytetrafluorethylen
PVDF	polyvinylidene difluoride
RBB	Remazol Brilliant Blue
Rpm	Rounds per minute
SDM	Site-directed mutagenesis
SDS	Sodium Dodecyl sulfate
SP	Signal peptide
SPR	Surface Plasmon Resonance
Sub.	Substituion
TB	Terrific broth
TEM	Transmission electron microscopy
TFA	Trifluoric acid
TIC	Total Ion Current
TOF	Time of Flight
TRIC	temperature related intensity change
Tris	tris(hydroxymethyl)aminomethane
UDP	Uridine diphosphate

Abbreviation	
UPLC	Ultra Performance Liquid Chromatography
UV	Ultraviolet
Wt	Wild-type
WTA	Wall teichoic acid
YFP	Yellow fluorescent protein

Table of contents

Declaration	V
Acknowledgements	VI
Abstract	VII
Zusammenfassung.....	IX
Abbreviations	XI
Table of contents.....	XIV
1. Introduction.....	1
1.1. Cyanobacteria – an overview	1
1.1.1. Evolution and classification of cyanobacteria	1
1.1.2. Filamentous cyanobacteria and the ability of cell differentiation	2
1.1.3. Successful survival strategies of filamentous cyanobacteria	4
1.2. Peptidoglycan – a giant macromolecule	5
1.2.1. Cell envelope of Gram-negative and Gram-positive bacteria	5
1.2.2. Composition and biosynthesis of peptidoglycan.....	6
1.2.3. Peptidoglycan during the cell cycle: cell division and elongation	9
1.3. The peptidoglycan in cyanobacteria	12
1.3.1. The cell envelope of cyanobacteria.....	12
1.3.2. Remodelling of cyanobacterial peptidoglycan	14
1.3.3. Cell-cell communication in multicellular cyanobacteria	16
1.3.4. Septal junctions enable direct cell-cell communication.....	17
1.3.5. Formation of the nanopore array.....	18
1.3.6. Regulation mechanism of AmiC and its homologues.....	20
1.4. Research objectives.....	22
2. Material and methods.....	23
2.1. Chemicals and enzymes	23
2.2. Kits	23
2.3. Software and programmes.....	23
2.4. Strains and maintenance.....	24
2.5. Media and buffers	25
2.6. Cultivation of cyanobacteria	28
2.7. Cultivation of <i>E.coli</i>	29
2.8. Molecular genetic methods	29
2.8.1. Oligonucleotides.....	29

2.8.2.	Plasmids.....	30
2.8.3.	Polymerase chain reaction	31
2.8.4.	Gibson Cloning.....	32
2.8.5.	Site-directed mutagenesis.....	33
2.8.6.	Transformation of electro or chemical competent cells	33
2.9.	Biochemical methods	33
2.9.1.	Protein determination.....	33
2.9.2.	SDS-PAGE (Laemmli, 1970 (251))	33
2.9.3.	Western blot.....	34
2.9.4.	Determination of SDS (Hayashi, 1975 (252)).....	35
2.9.5.	Protein-interaction assays.....	35
2.9.6.	Monitoring AmiC2cat hydrolytic activity.....	37
2.10.	Analytical methods.....	39
2.10.1.	High Performance liquid chromatography (HPLC)	39
2.10.2.	Mass spectrometry.....	39
2.11.	Compositional analysis of peptidoglycan	40
2.11.1.	Amino acid analysis	40
2.11.2.	Release of muropeptides for HPLC and LC-MS	41
2.12.	Purification of AmiC2cat and its mutant variants	41
2.12.1.	Protein expression and cell lysis.....	41
2.12.2.	Affinity chromatography	42
2.12.3.	Size exclusion chromatography.....	42
2.13.	Isolation and purification of peptidoglycan	43
2.13.1.	Modified dePedro et al protocol	43
2.13.2.	Optimized dePedro et al protocol.....	43
2.13.3.	Kühner et al. method.....	44
3.	Results	45
3.1.	The peptidoglycan composition of the filamentous cyanobacterium <i>Nostoc punctiforme</i> ..	45
3.1.1.	Isolation and purification of cyanobacterial peptidoglycan.....	45
3.1.2.	Determination of peptidoglycan derived amino acids.....	48
3.1.3.	Muropeptide profile of <i>N. punctiforme</i> and its <i>amiC2</i> mutant.....	52
3.1.4.	Differences between lateral and septal peptidoglycan of wild-type <i>N. punctiforme</i> ...	61
3.1.5.	Polysaccharides are covalently bound to cyanobacterial peptidoglycan.....	63
3.1.6.	Putative proteins associated or covalently bound to the peptidoglycan.....	66
3.2.	The amidase AmiC2 and its substrate peptidoglycan	70

3.2.1.	Ami2cat hydrolyses <i>amiC2</i> mutant PGN but not wild-type PGN	70
3.2.2.	Ami2cat prefers complex peptidoglycan fragments	74
3.2.3.	Putative catalytic residues: F564, E529 and L576	83
4.	Discussion	91
4.1.	<i>Nostoc punctiforme</i> and its Gram-negative type peptidoglycan	92
4.1.1.	The general composition of <i>Nostoc</i> peptidoglycan.....	93
4.1.2.	Modifications of <i>Nostoc</i> peptidoglycan.....	95
4.1.3.	<i>Nostoc</i> PGN and its putative associated proteins	97
4.1.4.	Minor differences in the septal and lateral cell wall of <i>N. punctiforme</i>	100
4.1.5.	The peptidoglycan model of <i>N. punctiforme</i>	101
4.2.	The amidase AmiC2 and its substrate, the peptidoglycan	101
4.2.1.	Disruption of <i>amiC2</i> altered peptidoglycan modification	102
4.2.2.	Highly crosslinked peptidoglycan is the substrate of AmiC2.....	103
4.2.3.	Site-specific mutations alter hydrolytic activity but not peptidoglycan binding	106
5.	Supplementary information	109
5.1.	LC-MS analysis of <i>Nostoc</i> muropeptides	109
5.2.	Muropeptides in septal and lateral cell wall fractions	111
5.3.	Domain organization and <i>in-silico</i> interactions of putative PGN-interacting proteins	114
5.4.	Factors affecting MST measurements.....	117
5.5.	BLI-measurements.....	119
5.6.	Peptidoglycan-polysaccharide of <i>Nostoc</i> sp.PCC 7120.....	121
5.7.	Ami2cat digestion of wild-type peptidoglycan.....	121
5.8.	Efficiency of mutanolysin cleavage	122
5.9.	Site-specific AmiC2 mutants.....	122
5.10.	MS/MS fragmentation of muropeptides derived from wild-type <i>N. punctiforme</i> PGN..	123
5.11.	MS/MS profiles of muropeptides from <i>N. punctiforme amiC2::ck3</i> PGN	128
5.12.	Proteins identified in tryptic digests from <i>Nostoc</i> PGN.....	133
5.13.	MS/MS fragmentation of Ami2cat released peptides	144
5.13.1.	MS2-spectra and fragmentation pattern of PGN-peptides.....	144
5.13.2.	MS1-spectra of wild-type and <i>amiC2</i> mutant PGN derived peptides in the range between 200 and 500 m/z	151
5.13.3.	Further m/z detected in wild-type and <i>amiC2</i> mutant PGN samples digested by Ami2cat152	
6.	Literature.....	153

1. Introduction

1.1. Cyanobacteria – an overview

1.1.1. Evolution and classification of cyanobacteria

Cyanobacteria are among the oldest organisms on earth that inhabit the planet already since several thousand million years (6, 7). First records date back to the early Proterozoic era, also known as the “Great Oxidation Event”, 2.5 to 2.3 billion years before today (8-10). The fast oxygenation of the atmosphere in this period is ascribed to the nascent ability of early cyanobacteria to perform oxygenic photosynthesis (11, 12). Interestingly, already older fossil records from the Archaen eon, around 3.5 billion years before now, were identified as cyanobacteria, although evidences were not conclusive (13-15). Unambiguous identifications occurred only after the “Great Oxidation Event” around 2 billion years in the Proterozoic era (14). *Eoentophysalis belcherensis*, for example, was detected in silicified stromatolites from the Belcher Supergroup in Canada with an age of around 1.9 to 1.8 billion years (16). This ancient coccoid cyanobacterium was identified by its unique cell envelope consisting of multiple concentric extracellular layers harbouring a dark coloured UV-absorbing pigment (16, 17). Morphological characteristics also clearly identified *Polybessurus bipartitus* found in 1.3–1.0 billion years old microfossils. It produced cylindrical mucopolysaccharide stalks to elevate from the water sediment (18).

First filamentous structures of cyanobacteria were found in the Gunflint formation (*Gunflintia grandis* or *Huroniospora*) (19, 20) and the Belcher Supergroup (*Halythrix* sp) (16), both of which are approximately 2 billion years old. The first primeval forms of specialized cell types, in this case spore-like cells, were detected in 1.5 billion years old microfossils in Siberian cherts (21, 22). Pang et al. also reported a filamentous microfossil from the Tonian Liulaobei Formation (~1.00 – 0.72 billion years), *Anhuithrix magna*. This organism might have formed additionally a special cell type advantageous for the survival under nitrogen depleting conditions (23).

These primeval representatives of cyanobacteria already display the morphological diversity of modern cyanobacteria as well as their ability to colonize different habitats all over the planet. For a long time, cyanobacteria were designated as “blue-green algae” and assigned to the plant kingdom as “Cyanophyta”, despite the fact that cyanobacteria are true prokaryotes (24, 25). In 1979, Rippka et al. classified cyanobacteria under bacteriological aspects and grouped them into five morphologically distinct sections (26). Section I and II comprise unicellular cyanobacteria whereby species assigned to section I divide via binary fission (e.g. *Synechocystis* or *Synechococcus*) or budding (e.g. *Chamaesiphon*) and section II cyanobacteria divide in multiple planes, which result in the formation of smaller daughter cells, the “baeocytes”. The following three sections represent filamentous cyanobacteria, which are distinguished by the branching morphology and the ability to differentiate. Cyanobacteria of section III, such as *Spirulina*, *Oscillatoria* or *Lyngbya*, grow in long helical or straight chains of vegetative cells and are unable to differentiate (26). Cyanobacteria from section IV and V evolved as a monophyletic group to a later time point as demonstrated by 16S-RNA analysis (21, 27, 28). Section IV cyanobacteria are unbranched, whereas section V species have a branched morphology. Both sections comprise cyanobacteria that are able to specialise vegetative cells into spore-like akinetes, nitrogen-fixing heterocysts or short motile hormogonia.

1.1.2. Filamentous cyanobacteria and the ability of cell differentiation

Multicellularity is a tremendous advantage for cyanobacteria, enabling them to adapt to rapid changing environmental conditions and to colonize a broad range of different habitats. The differentiation of vegetative cells into highly specialized cell types like heterocysts, akinetes or hormogonia (Fig. 1) significantly contributed to the successful distribution of multicellular cyanobacteria and represents unique survival strategies.

Heterocysts are produced in a semi regular pattern along the filament when combined nitrogen sources are limited. The main function of these terminally differentiated cells is to fix atmospheric nitrogen and provide neighbouring cells with nitrogen-containing organic compounds like amino acids (29, 30). The oxygen-sensitive nitrogenase incorporates atmospheric nitrogen gas into ammonia and needs to be protected from atmospheric oxygen (31, 32). The heterocyst exhibits a unique cell envelope structure to restrict the oxygen diffusion. The envelope consists of characteristic glycolipid and polysaccharide layers surrounding the entire heterocyst but omitting the septum (Fig. 2A and B) (1, 33). The laminated HGL-layer (heterocyst-specific glycolipid) is composed of long-chain polyhydroxy or ketohydroxy alkanes glycosidically bound to hexoses (34, 35). The outermost layer comprises heterocyst envelope polysaccharides (HEP) of repeating mannose and glucose residues containing side chains of glucose, xylose, galactose or mannose (36).



Fig. 1. Different cell types of multicellular cyanobacteria. Heterocysts develop under nitrogen depleting conditions and generate a microoxic compartment for the oxygen-sensitive nitrogenase that fixes atmospheric nitrogen. Hormogonia are short motile fragments of vegetative cells. The spore-like akinetes represent dormant cells for the survival under harsh environmental conditions. Images were kindly provided by Rebeca Perez.

Additionally, the heterocyst increases the oxygen-consuming respiratory activity from the so-called 'honeycomb' membranes, near the polar neck and lacks the oxygen-producing photosystem II (37, 38) to generate a microoxic environment for the nitrogenase. Vegetative cells counterbalance the absence of carbon fixation and photosystem II and transport carbon sources and reductants to the heterocysts. In return, the heterocyst provides vegetative cells with nitrogenous compounds. In electron micrographs, polar granules containing cyanophycin, a reserve polymer consisting of aspartate and arginine, appear as a plug stacked at the cell poles of heterocysts (Fig. 2A). These granules possibly contribute to nitrogen homeostasis as nitrogen storage (39).

Akinetes are thick-walled, nonmotile cells formed by some heterozygous cyanobacteria to withstand unfavourable conditions in a dormant state (40, 41). These cells resemble endospores from other bacteria, are resistant to cold and desiccation but are heat sensitive (41). The terrestrial, filamentous cyanobacterium *Nostoc punctiforme* induces akinete formation upon phosphate starvation (42). More than 70% of vegetative cells turned into akinetes after 18 days in phosphate-poor cultivation medium. More than 95% akinetes were even detected in cultures of *Anabaena variabilis* under low

light conditions. The morphological and metabolic changes that accompany akinete development are quite diverse and differ from species to species (42). Generally, the cell size increases enormously, storage compounds accumulate, thylakoid membranes are rearranged and the cell envelope is remodelled (43). Interestingly, the akinete cell envelope is multi-layered and resembles the envelope structure of heterocysts. A polysaccharide layer surrounds the entire akinete but omits the septum when the akinete is still attached to the filament. *Anabaena variabilis* and *Cylindrospermum licheniforme* produce a 1,3-linked sugar backbone consisting of glucose and mannose residues branched by glycan side chains (44). One or two glycolipid layers are subjacent, followed by a mucilaginous layer in some cyanobacterial species (42, 45). Perez et al. identified heterocyst specific glycolipids in extracts of *N. punctiforme* and *A. variabilis* akinetes and indicate thereby an evolutionary closer relationship between heterocysts and akinetes (46).

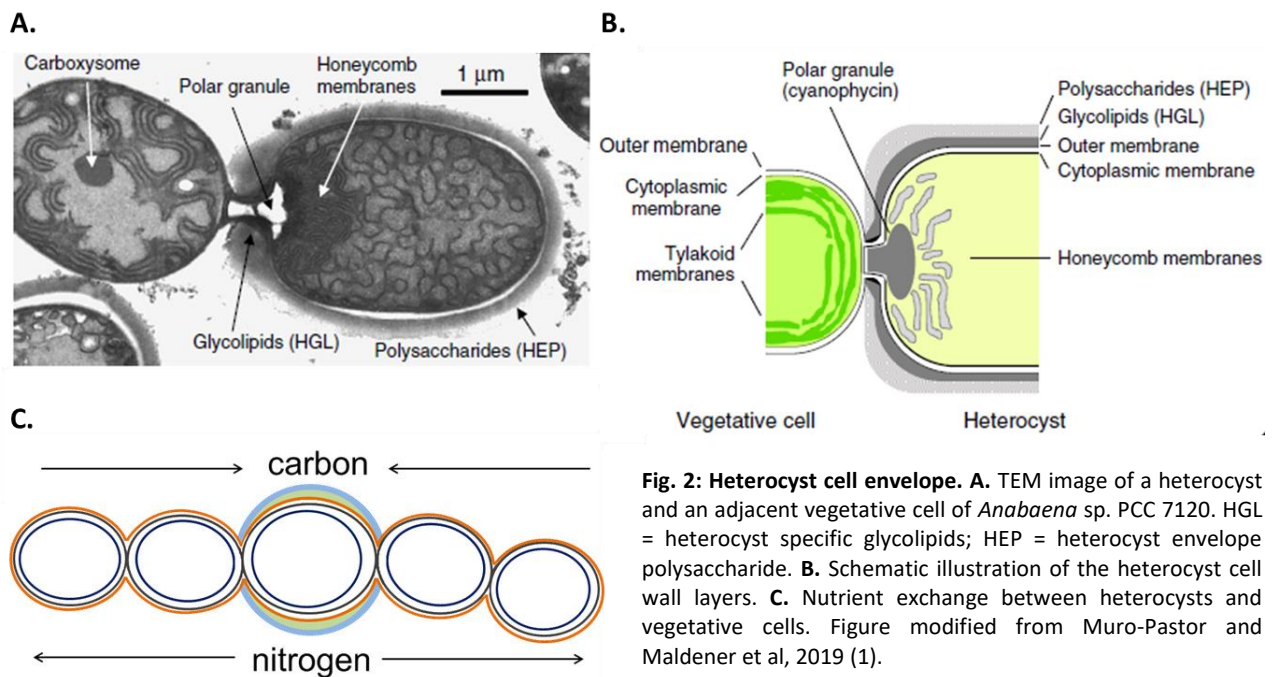


Fig. 2: Heterocyst cell envelope. A. TEM image of a heterocyst and an adjacent vegetative cell of *Anabaena* sp. PCC 7120. HGL = heterocyst specific glycolipids; HEP = heterocyst envelope polysaccharide. B. Schematic illustration of the heterocyst cell wall layers. C. Nutrient exchange between heterocysts and vegetative cells. Figure modified from Muro-Pastor and Maldener et al, 2019 (1).

As soon as the environmental factors improve, akinetes start to germinate. The release of newly formed vegetative cells is also very different. *Nostoc* sp. PCC 6720, *C. ripphae*, *C. raciborskii* and *N. punctiforme*, for example, degrade the cell wall at polar regions for the release of the new filament (46-49) whereas akinetes from *Anabaena variabilis* rupture, maybe due to high pressure (46).

The third developmental stage of many filamentous cyanobacteria is the transient formation of short, motile hormogonia. These short filaments of vegetative cells are characterized by a smaller cell size accompanied by a different cell shape, lack of heterocysts and their ability to be motile either by gliding or gaseous vacuoles (50). Several factors induce the formation of hormogonia like nutrient limitations (51), light quality (52) or symbiotic interactions with, for example, plants (53).

1.1.3. Successful survival strategies of filamentous cyanobacteria

Specialized cell types like heterocysts, akinetes or hormogonia enable filamentous cyanobacteria the survival under harsh, nutrient-depleting conditions. The planktonic bloom-forming cyanobacterium *Aphanizomenon ovalisporum* involves all these cell types in its life cycle to cope with seasonal fluctuations (54). *A. ovalisporum* grows pelagic during the summer and reacts to nitrogen starvation by the formation of N₂-fixing heterocysts. When the temperature drops below 25°C during autumn, it starts to produce akinetes that sink to the water sediment and remain in a dormant state. As soon as the environmental conditions improve during spring, new filaments germinate and subsequently fragment at higher temperatures into short motile hormogonia (55). Gaseous vacuoles help to reach the water surface so that *A. ovalisporum* continues pelagic growth.

The production of akinetes, heterocysts or hormogonia represents successful strategies of filamentous cyanobacteria to overcome or escape challenging environmental conditions. But how do cyanobacteria survive in regions with constant extreme conditions as in Polar Regions or hot deserts? *Phormidium* species are common representatives in mats or films in hydro-terrestrial habitats of Arctic and Antarctic regions and have to face several stresses, most notably desiccation and freezing. A first protective barrier against freezing in winter is the production of a thick exopolysaccharide sheath that enables the community to overwinter in frozen mats while the cells stay in a viable condition (56). In parallel, trehalose and sucrose are accumulated (57), photosynthesis is decreased to a minimum and growth is arrested, until melting ice rehydrates the community during spring (58). Cyanobacteria living in hot and dry regions are likewise exposed to extreme environmental conditions. *Nostoc flagelliforme*, an important part of desert soil crusts, increases the synthesis of proteins involved in DNA repair mechanisms and oxidative stress responses upon UV-stress. It additionally produces UV-absorbing compounds, such as mycosporine-like amino acids and scytonemin. Furthermore, it enhances the secretion of proteins like the water stress protein WspA to support the structure and function of the exopolysaccharide sheath (59).

These examples provide broad insights into the numerous adaptation mechanisms of multicellular cyanobacteria and their capability to colonize diverse ecological niches. But unicellular cyanobacteria are certainly no less innovative. The non-diazotrophic cyanobacterium *Synechocystis* sp. PCC 6803, for example, is able to survive long periods of nitrogen depletion in a dormant-like state. Therefore, cells drive a genetically determined program when combined nitrogen becomes limited. The fast degradation of abundant phycobiliproteins feeds the intracellular nitrogen pool for the *de novo* synthesis of survival-associated proteins (60, 61), and glycogen is accumulated as an energy resource to drive resuscitation (62). These changes are accompanied by a colour change of liquid cultures from green to yellow, a process called chlorosis, due to the almost complete degradation of the photosynthesis apparatus. Metabolism and growth are arrested; photosynthesis is decreased to a minimum, but restarts as soon as nitrogen gets available again. This resuscitation follows a highly organized program that bases on respiration of glycogen in a first, and reactivates photosynthesis in a second phase, before cellular growth continues (63-65).

1.2. Peptidoglycan – a giant macromolecule

1.2.1. Cell envelope of Gram-negative and Gram-positive bacteria

Cyanobacteria exhibit a great ecological diversity and have to withstand various environmental stresses, as outlined above. A natural protection against these stresses and a hostile environment is the multi-layered cell envelope. Generally, bacteria are classified into two distinct groups according to differences in the cell envelope structure: Gram-negative and Gram-positive bacteria. In the late 19th century, the bacteriologist Christian Gram used a complex of crystal violet and iodine to stain infected lung tissue and observed that some bacteria retained the purple dye after decolouration while others did not (66).

The fundamental principle underlying this staining procedure is the different thickness of the peptidoglycan layer and the presence of an outer membrane. Gram-negative bacteria are surrounded by a cytoplasmic membrane and a thin peptidoglycan layer (Fig. 3, top). The outermost layer is an asymmetrical lipid bilayer, consisting of lipopolysaccharides. These lipopolysaccharides are protruding into the extracellular space and are anchored in the membrane bilayer by a glycolipid, lipid A. The crystal violet/iodine complex penetrates into any gap of the peptidoglycan layer and can be easily washed out upon alcohol treatment that dissolves the lipid bilayer. Gram-positive bacteria do not have an outer leaflet that is composed of lipid components but a thick peptidoglycan layer (Fig. 3). This cell-spanning macromolecule shrinks when it is exposed to alcohol and traps the purple dye. This technique is commonly known as Gram-staining.

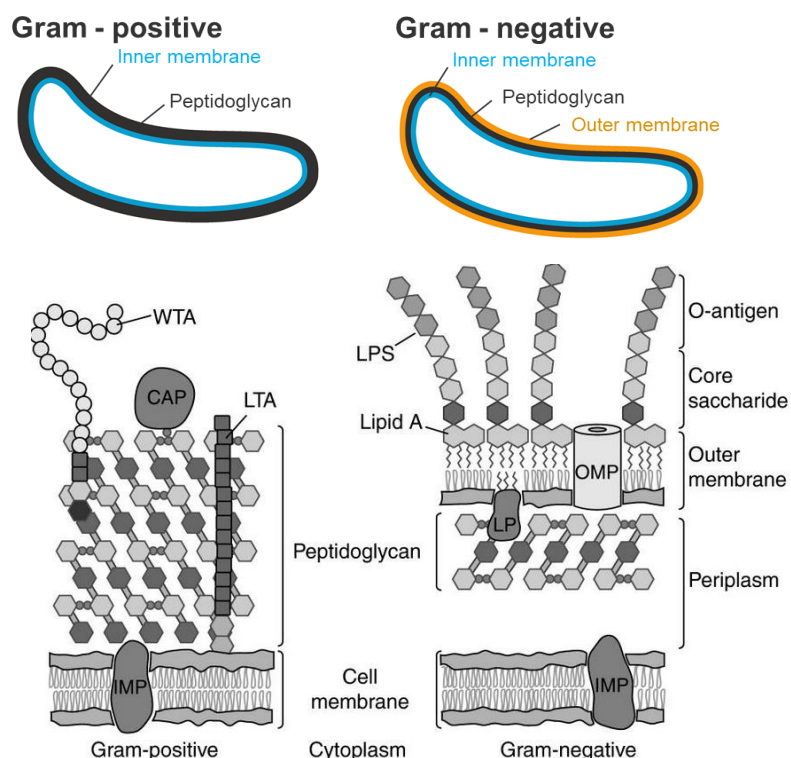


Fig. 3: The cell envelope of Gram-negative and Gram-positive bacteria. IMP = inner membrane protein; LTA = Lipoteichoic acid; WTA = Wall teichoic acid; CAP = Capsular polysaccharide; LPS = Lipopolysaccharide; LP = Lipoprotein; OMP = Outer membrane protein (detailed illustration of envelope structure obtained from Silhavy et al. 2010 (5))

Cyanobacteria possess an outer membrane (67, 68) and are therefore ascribed to Gram-negative bacteria. Notably, they also share the feature of a thick peptidoglycan layer with Gram-positive bacteria (69). Thus, cyanobacteria are positioned between Gram-positive and Gram-negative bacteria.

The following sections describe first the general composition, structure and function of the peptidoglycan found in Gram-negative and Gram-positive bacteria (1.2.2 and 1.2.3). The second part focuses on cyanobacterial peptidoglycan (1.3.1 and 1.3.2) and especially how it is involved in intercellular communication of filamentous cyanobacteria (1.3.3-0).

1.2.2. Composition and biosynthesis of peptidoglycan

The peptidoglycan is a giant macromolecule in the periplasm that surrounds the entire bacterial cell. Since decades, researchers are trying to elucidate the composition, structure and function of this mesh-like polymer (70-75). In 1972, Schleifer and Kandler summarized all the hitherto gained knowledge and described the basic peptidoglycan structure found in both, Gram-negative and Gram-positive, bacteria (76). The peptidoglycan, or murein (lat. murus = wall), consists of linear glycan chains that are crosslinked by short peptides. The glycan strands are composed of alternating units of two β -1,4-linked acetylated amino sugars, N-acetylglucosamine (GlcNAc) and N-acetylmuramic acid (MurNAc). A peptide with varying length is covalently linked to the disaccharide unit. In most bacteria, the first amino acid in the stem peptide is L-alanine that forms an amide bond with the lactoyl group of MurNAc. Variation of the first position occurs for example in *Mycobacterium leprae*, in which L-alanine is substituted by glycine (77) or in *Butyrubacterium rettgeri*, where L-serine represents the first amino acid in the peptide (78). The second amino acid is D-iso-glutamic acid that is connected to a diamino acid by its γ -carboxyl group. Interestingly, the α -carboxyl group of D-iso-glutamate is often highly amidated (72). The conversion of D-iso-glutamate into D-iso-glutamine is involved in the β -lactam antibiotic resistance in *Staphylococcus aureus* (79) and plays a crucial role in crosslinking reactions, as has been shown for *Streptococcus pneumoniae* (80). In Gram-negative bacteria, *Mycobacteria* and *Bacilli*, a diamino acid is on the third position in the peptide stem, usually meso-diaminopimelic acid (mDAP), whereas L-lysine is present in most Gram-positive bacteria (72). Two D-alanine residues are covalently attached to the diamino acid and complete the peptidoglycan building block that is represented in Fig. 4.

This building block is synthesized in the cytoplasm (see Fig. 5) (81). The amino acids are step wise attached to the precursor UDP-MurNAc by the ATP-dependant Mur-ligases C, D, E and F. MraY, an integral membrane protein, couples the activated UDP-MurNAc-pentapeptide to the lipid carrier undecaprenylpyrophosphate yielding lipid I. Subsequently lipid I is glycosaminylated by MurG with UDP-GlcNAc, resulting in the formation of lipid II. At this step, many Gram-positive bacteria modify the monomeric peptidoglycan subunit either by the amidation of the α -carboxyl group of D-iso-glutamate or by the incorporation of additional amino acids (72, 82). *Staphylococcus aureus*, for example, sequentially connects five glycine residues to L-lysine by the nonribosomal peptidyltransferases FemABX (83, 84) whereas *Enterococcus faecium* introduces D-aspartate to the ϵ -amino group of L-lysine (85). The newly formed lipid II is then translocated across the membrane by the flippase MurJ (86) and is integrated into the existing peptidoglycan sacculus by glycosyltransferases and transpeptidases (74, 87).

Early studies revealed that the β -lactam antibiotic Penicillin inhibited enzymes with glycosyltransferase and transpeptidase activity that are involved in the peptidoglycan metabolism (88, 89). These enzymes were designated as Penicillin Binding Proteins (PBP) and are categorized into high molecular weight (HMW) and low molecular weight (LMW) proteins (89-92). The HMW proteins are subclassified into A and B groups. Class A PBPs are bifunctional membrane-embedded enzymes that polymerize and crosslink glycan chains, whereas class B PBPs are monofunctional transpeptidases. LMW PBPs are D,D-carboxypeptidases, that trim the peptide stem, and D,D-endopeptidases, that cleave peptide crosslinks between the glycan strands. Meanwhile, it is well known that Penicillin mimics the D-alanyl-D-alanyl peptide, which is the binding site for transpeptidases and prevents crosslinking reactions (88, 93).

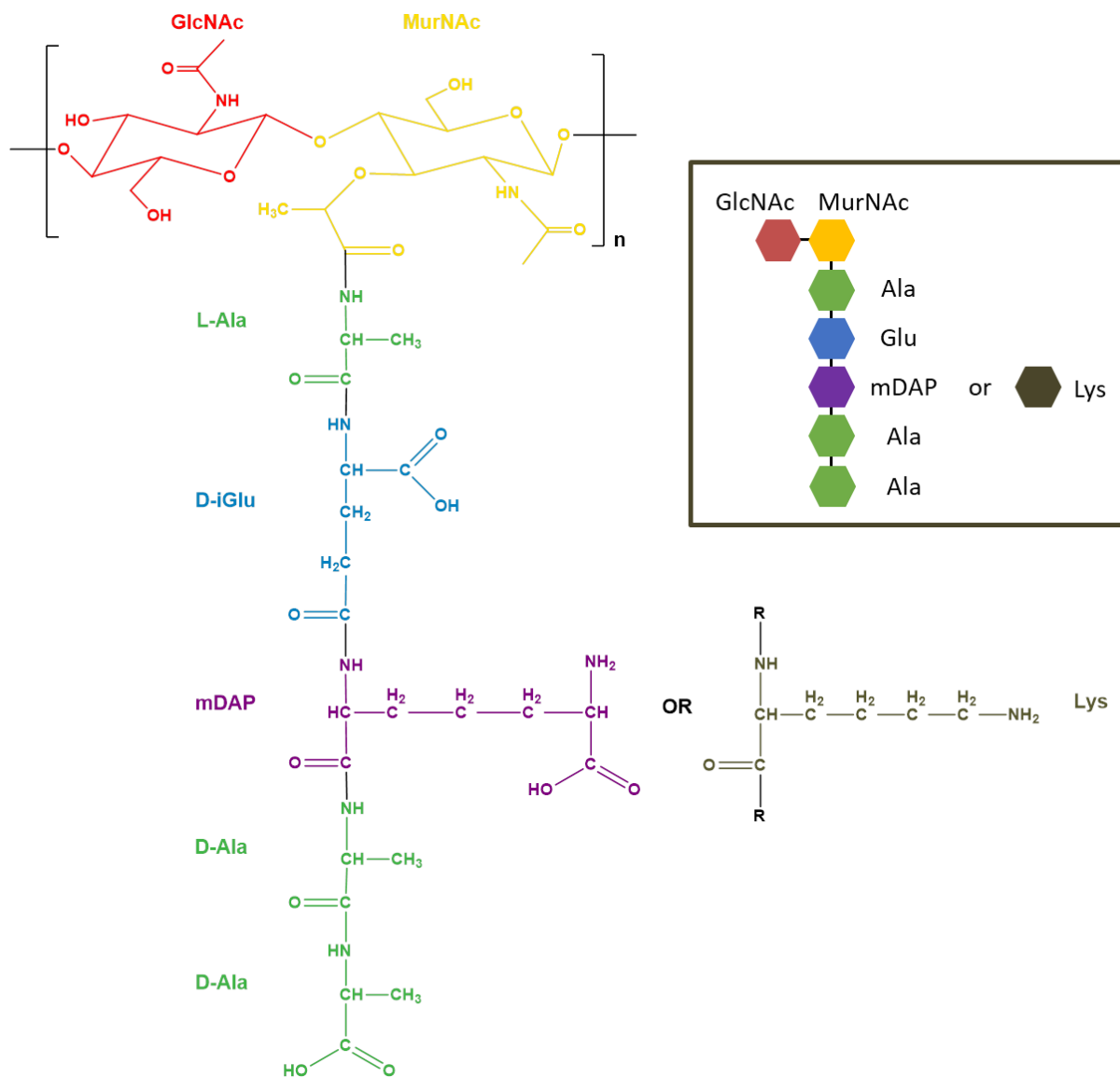


Fig. 4: The peptidoglycan building block. Alternating N-acetylglucosamin (GlcNAc) and N-acetylmuramic acid (MurNAc) units form the carbohydrate backbone of the peptidoglycan that are connected by a peptide stem consisting of D/L-alanine, D-glutamic acid and a dibasic amino acid like meso-diaminopimelic acid or L-lysine.

The most common crosslinks in the peptidoglycan are 3-4 linkages between the carboxyl group of D-Ala at position 4 with the ϵ -amino group of the diamino acid from the 3. position of another glycan strand (72). These 3-4 linkages are generated by D,D-transpeptidases that use the energy from the

cleavage of the D-Ala-D-Ala peptide bond. The 3-4 crosslink can be either direct or indirect via an interpeptide bridge as the glycine bridge found in *Staphylococcus aureus* (83, 84). In some bacteria, L,D-transpeptidases connect the glycan strands via the diamino acids resulting in 3-3-crosslinks. *Mycobacterium tuberculosis*, for example, remodels its peptidoglycan when it enters stationary growth phase. In this phase, the transpeptidase Ldt_{Mt1} substitutes 3-4 crosslinks by 3-3 crosslinks. This enables *M. tuberculosis* to subsequently connect glycan strands during stationary growth without the need for D,D-transpeptidases that act only during peptidoglycan synthesis (94). Furthermore, *Enterococcus faecium* M512 increases 3-3 crosslinks mediated by the L,D-transpeptidase Ldt(fm) in the presence of ampicillin to evade the suicidal effect of β -lactam antibiotics (95).

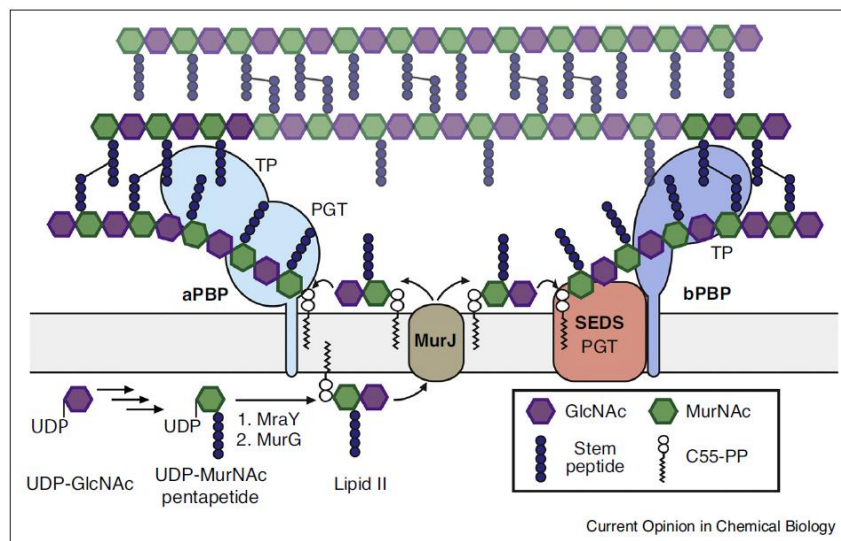


Fig. 5: Insertion of nascent peptidoglycan into the sacculus. UDP-GlcNAc is converted to UDP-MurNAc whose lactoyl group carries a peptide stem. MraY links UDP-MurNAc-pentapeptide to undecaprenylpyrophosphate (C55-PP) and MurG attaches GlcNAc. The peptidoglycan precursor is translocated by MurJ into the periplasm where it is incorporated into the peptidoglycan sacculus either by class A Penicillin Binding Proteins (aPBP) or class B Penicillin Binding Proteins (bPBP) that work in concert with SEDS proteins (sporulation, elongation, division, and septation). Figure from Taguchi et al, 2019 (3)

L,D-Transpeptidases also catalyse the covalent linkage of the Braun lipoprotein to the peptidoglycan in Gram-negative bacteria (96). This triacylated protein is anchored to the outer membrane by its N-terminal lipid moiety and forms a covalent bond with mDAP by its C-terminal lysine (97, 98). In that way, it provides structural integrity for the cell envelope. Moreover, it is a crucial determinant for the size of the periplasm. Experiments in *Salmonella enterica* showed that the distance between the peptidoglycan and the outer membrane changed proportionally to the length of the lipoprotein (Lpp) (99). The Braun lipoprotein has a major impact on various cellular processes involved in virulence, nutrient uptake, signal transduction and others (100). Remarkably, it is the only known lipoprotein that is covalently linked to the peptidoglycan (101).

Gram-positive bacteria have a thick peptidoglycan layer, which is modified by glycopolymers (102). These polymers consist of alternating ribitol-phosphate or glycerol-phosphate units, linked to a disaccharide of N-acetylmannosamine and N-acetylglucosamine-1-phosphate (103). This phosphate group forms an ester bond with the C6-hydroxyl group of N-acetylmuramic acid and connects the wall teichoic acid with the peptidoglycan (104). Wall teichoic acids (WTA) play important roles in cell

morphology and growth, as indicated by the fact that rod-shaped bacteria like *Bacillus subtilis* or *Listeria monocytogenes* become spherical in the absence of WTAs (105, 106). Previous studies also demonstrated higher levels of WTA in pathogenic community-acquired methicillin-resistant *S. aureus* (MRSA) strains and show that WTAs are involved in *S. aureus* virulence (107).

Wall teichoic acids or lipoproteins, like the Braun lipoprotein, are only two examples of the whole spectrum of peptidoglycan modifications. Numerous alterations are reported to date that fulfil various functions. *Streptococcus pneumoniae* or *Bacillus anthracis* remove the N-acetyl group from GlcNAc to confer lysozyme resistance (108-110), whereas *Neisseria gonorrhoeae* acetylates the C6-hydroxyl group of MurNAc (111). *Mycobacteria* species hydroxylate the N-acetyl group of MurNAc to trigger a stronger immune response for an advantageous effect during host infection (112). Also, capsular polysaccharides can be attached to the peptidoglycan to contribute to bacterial virulence. The type of linkage can thereby vary. *S. pneumoniae*, for example, attaches the polysaccharides directly to GlcNAc via 1,6-glycosidic bonds (113), while *S. aureus* forms phosphodiester bonds between MurNAc and the capsular polysaccharides (114). Many bacteria form an intramolecular ring between the C1 and C6 of MurNAc, but the function of this cyclisation is still unknown (72).

1.2.3. Peptidoglycan during the cell cycle: cell division and elongation

The coupling of peptidoglycan synthesis and hydrolysis, during cell division or elongation, is one of the most complex tasks in the bacterial cell cycle. Hereby, the synthesis of peptidoglycan is a highly organized process that underlies the coordinated activities of several enzymes. This involves major protein complexes, which accomplish the peptidoglycan remodelling while maintaining cell shape and integrity. The divisome is an assemblage of diverse proteins that drives cytokinesis (see Fig. 6) (2, 115). One of the first proteins that localizes to the division site is FtsZ, a tubulin homologue and a core component of the divisome (116, 117). Several FtsZ proteins polymerize during this process in a GTP-dependant manner into single-stranded filaments (118-120) that are tethered to the membrane by FtsA and ZipA (121-123). These filaments can be crosslinked by ZapA that stabilizes Z-ring formation (124, 125). In *E. coli*, ZapA further interacts with the linker protein between the Z-ring and the replication terminus, ZapB (126). This interaction is important for the position of the Z-ring. Two additional systems also influence the spatial orientation of the Z-ring. The first one is the Min-system that prevents septation at the cell poles (127-129). The second one is the nucleoid occlusion system that blocks FtsZ – polymerization over the chromosomes, except at the replication terminus (130-132). After the assembly of the Z-ring, several proteins are recruited to the division site in a strictly hierarchical order. In *E. coli*, two major subcomplexes are subsequently formed: FtsL-FtsQ-FtsB and FtsW-FtsI (133). FtsW is an integral membrane protein belonging to the SEDS family and an essential part of the divisome (134). It connects the cytoplasmic peptidoglycan synthesis with the division machinery by translocating lipid II (135), but acts also as a peptidoglycan polymerase in complex with a class B PBP (136). FtsI is a class B PBP transpeptidase, that is involved in septal peptidoglycan synthesis in *E. coli* (137, 138) and interacts directly with FtsW (139) and the peptidoglycan synthase PBP1b (140). This ternary complex of FtsW-FtsI and PBP1b is regulated by FtsQLB. The latter complex was shown to inhibit the glycosyltransferase activity of PBP1b and the transpeptidase activity of FtsI and prevents septal peptidoglycan synthesis *in-vitro* (141). FtsN is the last protein joining the divisome and triggers septal peptidoglycan synthesis, thus acting antagonistically to FtsQLB (142). Fluorescent imaging of FtsAZ - filaments and PBP2b in *B. subtilis* demonstrated that the peptidoglycan synthesis follows the treadmilling of FtsAZ-filaments, resulting in septum formation

(143). The cleavage of the septum and the subsequent release of the daughter cells are mediated by peptidoglycan hydrolases. In most Gram-negative bacteria, the cleavage of the septum follows parallel to its synthesis, while Gram-positive bacteria synthesize the whole septum and split it afterwards (144).

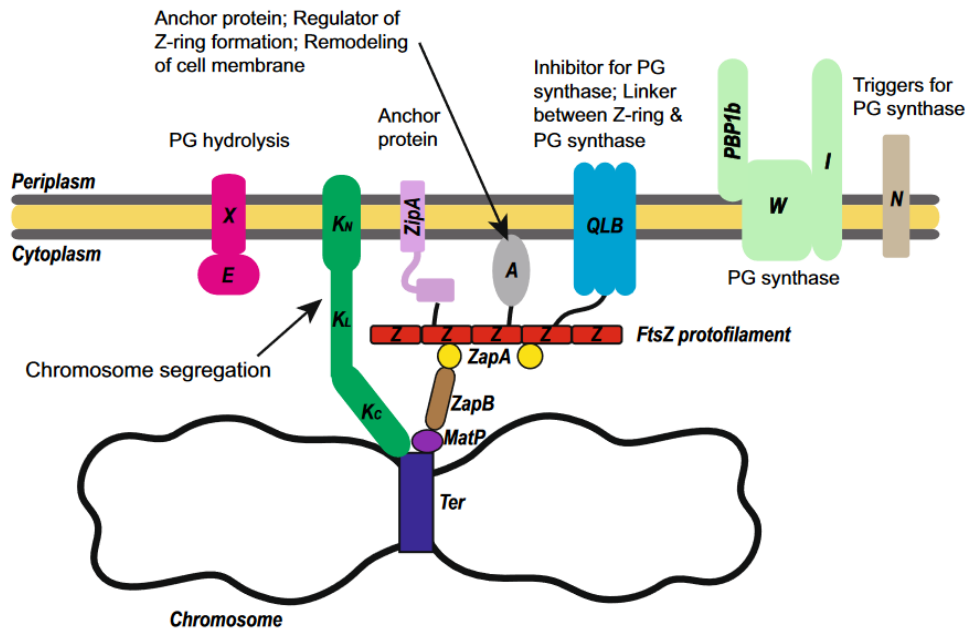


Fig. 6: The divisome of *E. coli*. FtsZ forms treadmilling filaments that are anchored to the membrane by FtsA and ZipA. ZapB connects FtsZ and the replication terminus via ZapA and MatP. The PGN synthesis machinery PBP1, FtsW and FtsI is regulated by FtsQ, L and B as well as by FtsN. The ATP-binding cassette transporter complex FtsX and FtsE are critical components for septal PGN cleavage. FtsK is involved in the segregation of chromosomes. Figure from Wang et al. 2019 (2).

E. coli possesses three LytC-type peptidoglycan hydrolases, namely AmiA, B and C, which are important key players in the cleavage of septal peptidoglycan by their ability to cleave the covalent bond between L-alanine and MurNac. Mutants lacking all three hydrolases are impaired in cell division and grow filamentous with each cell encased by peptidoglycan (145). The amidases are usually autoinhibited and can be activated by the LytM containing proteins EnvC or NlpD (146-148). NlpD is a lipoprotein that is anchored in the outer membrane and is recruited to the division site for the activation of AmiC (146). Deletion of *nlpD* affects cell morphology as has been shown for *N. gonorrhoeae*, that formed large aggregates unable to separate (149). Similarly, *Haemophilus influenzae* lacking *nlpD* grows in long cell chains with aberrant septa and exhibits a decreased outer membrane stability by the increased release of outer membrane vesicles (150). Recently, Tsang et al. reported a possible mechanism how NlpD mediates the activation of AmiC in *E. coli*. The Tol/Pal system, that coordinates outer membrane constriction and YraP, a protein of yet unknown function, reduce the distance between NlpD and AmiC by the invagination of the outer membrane and enable direct interaction (148). Furthermore, the enzymatic active site of AmiC from *E. coli* is blocked by a α -helix, which prevents peptidoglycan hydrolysis. Deletion of this helix leads to peptidoglycan hydrolysis without prior activation by NlpD (151). The amidases AmiA and AmiB are both regulated by EnvC (152). This regulation is presumably mediated through the M23 peptidase domain of EnvC since point mutations in this region abolish amidase activation (147). During cell division, EnvC is recruited to the divisome by the transporter FtsEX (153). AmiB, like AmiC, contains

an N-terminal targeting domain and localizes at the division site, whereas AmiA lacks the peptidoglycan-targeting domain and is distributed throughout the periplasm in a cell-cycle independent mode (154, 155). Interestingly, *V. cholerae* encodes a single putative amidase for the cleavage of septal peptidoglycan that is activated by both, EnvC and NlpD whereby NlpD has a greater impact on infection of infant mice and resistance towards bile salts or detergents (156)

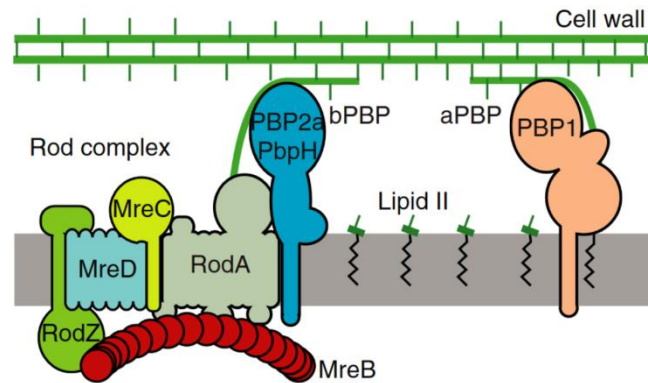


Fig. 7: The elongosome of *B. subtilis*. Two enzyme machineries mediate the insertion of peptidoglycan during growth of *B. subtilis*. Class A PBPs exhibit glycosyltransferase and transpeptidase activity and work independently from MreB filaments that direct PGN synthesis by the Rod complex. RodA and PBP2 are regulated by MreCD and incorporate nascent PGN into the sacculus. Figure from Dion et. al 2019 (4)

Overall, cell division is a complex network of temporally tight organized interactions and relocations of proteins that coordinate septum formation, constriction and separation. After the cell accomplished a successful fission, it enters the next critically important stage of growth and elongation. This process is dependent on the insertion of new peptidoglycan material into the existing sacculus, without affecting its functionality and stability. The expansion of the peptidoglycan polymer is well examined in rod-shaped bacteria like *E. coli* or *B. subtilis* (157). *In-vivo* studies of the polymerase activity in *E. coli* revealed that even two interdependent major enzyme machineries mediate the insertion of peptidoglycan, the Rod system and bifunctional class A PBPs (see Fig. 7) (158). PBP1, a major peptidoglycan synthase in *B. subtilis*, shifts dynamically from the division site to the cylindrical part of the cell and is able to synthesize both, septal and lateral peptidoglycan (159). The regulatory protein GpsB binds to the cytoplasmic part of PBP1 and accomplishes the relocalization from the septum to the lateral wall. Besides this, it also interacts with the critical shape determinant protein MreC and connects it thereby with PBP1 (160). MreC and PBP1 directly interact as confirmed by bacterial-two-hybrid assays (161). Severe effects on the cell morphology were seen upon depletion of *mreC*, which prevented the incorporation of lateral peptidoglycan. Instead, the insertion of peptidoglycan at the division site was increased (162). Localization studies of MreC demonstrated a helical or banded pattern (162) as has been seen for MreB (163). MreB is a structural homologue of eukaryotic actin and polymerizes into tightly membrane associated helical filaments in *E. coli* (164). These filaments appear in discrete patches and move circumferentially around the cell to coordinate the PGN synthesis machinery (163). MreB binds to RodZ (165), a bitopic membrane protein, and is thereby connected to the Rod complex, the second major enzyme machinery for elongation.

The Rod complex consists of the aforementioned Mre proteins and RodZ as well as RodA, an integral membrane protein, and PBP2, a transpeptidase. RodA and PBP2 form a stable complex which is regulated by MreC and D as demonstrated in *E. coli*. Hereby, MreC interacts directly with PBP2 and stimulates the RodA – PBP2 interaction whereas MreD is the counteracting part (166). As recently demonstrated, RodA exhibits glycosyltransferase activity in *B. subtilis* (167) which explains the previous observations of viable and lateral cell wall producing *B. subtilis* lacking all four class A PBP peptidoglycan synthases (168). The Rod complex follows the axial movements of MreB filaments in both directions at the periphery (163), while class A PBPs are independent from MreB motion (158). Cho et al. showed in *B. subtilis* that aPBPs and the Rod system cooperate semi-autonomously and might have specialized functions. They hypothesized that the Rod complex builds the frame of the peptidoglycan matrix and the aPBPs fill in the gaps (158). Examinations on the diameter of *B. subtilis* cells revealed that an increased Rod complex activity reduced the cell diameter whereas enhanced aPBPs activity increased the cell diameter (4).

1.3. The peptidoglycan in cyanobacteria

1.3.1. The cell envelope of cyanobacteria

For decades, cyanobacteria were classified as “blue-green algae” despite their prokaryotic nature (24-26). Particularly, the similarity of the photosynthetic apparatus with that of higher plants and algae contributed the most to this classification (169). However, cyanobacteria lack common eukaryotic features, like a nucleus or membrane-bound organelles (170). Furthermore, evidences for a multi-layered cell envelope, containing peptidoglycan, accumulated. Reports from the early 1950s describe the inability of several cyanobacteria to withstand the osmotic pressure, when they were treated with lysozyme (171, 172) or stopped to grow in the presence of penicillin (173). In parallel, Work and Dewey identified the non-proteinogenic amino acid meso-diaminopimelic, a key component of cell walls in Gram-negative bacteria, *Mycobacteria* and *Bacilli*, in hydrolysates of *Anabaena cylindrica*, *Oscillatoria* sp. and *Mastigocladus laminosus* (174).

An extensive examination of unicellular and filamentous cyanobacteria of all orders by electron microscopy from Ris and Singh in 1961 demonstrated an electron dense layer encaptured between the outer membrane and the cytoplasmic membrane, as was observed for Gram-positive and Gram-negative bacteria (175). Moreover, the thickness of this intermediate layer varied widely from 10-20 nm (in *Anacystis*, *Calothrix*, *Nostoc*, *Gloeotrichia*, *Anabaena*, *Gloeocapsa*, *Fischerella*) up to 200 nm in *Oscillatoria* species. The structure of this multilayered cell envelope consisting of an outer membrane, an electron-dense layer and the cytoplasmic membrane, seemed to be common amongst cyanobacteria (176, 177). Interestingly, this electron dense layer disappeared from isolated cell wall fractions obtained from *Phormidium uncinatum* in the presence of lysozyme and showed drastic defects when *P. uncinatum* was grown in medium supplemented with penicillin (178). Furthermore, the same study performed, for the first time, chemical analyses of cell wall fractions to determine the single components of the assumed peptidoglycan layer. Indeed, muramic acid, glucosamine and the amino acids alanine, glutamate and meso-diaminopimelic acid were detected. Drews and Meyer successfully identified these peptidoglycan components also in two further cyanobacteria, *Anacystis nidulans* and *Chlorogloea fritschii* (179). In the following years, studies accumulated confirming the presence of peptidoglycan components in the cell envelope of many cyanobacteria and determined the exact localization of the peptidoglycan layer (180-182).

Jürgens and colleagues pioneered in the elucidation of the primary peptidoglycan structure of *Synechocystis* sp. strain PCC 6714 (183). The researchers partially hydrolysed the peptidoglycan and isolated different peptidoglycan fragments. They identified tripeptides and tetrapeptides covalently linked to MurNAc residues. The amino acid composition of these peptides corresponded to those found in Gram-negative bacteria. Furthermore, they suggested that the peptidoglycan of this unicellular cyanobacterium contains direct crosslinks due to the presence of mDAP-Ala dipeptides in the partial acid hydrolysates. Another important finding, in that study, was the identification of polysaccharides possibly linked to MurNAc. A follow-up study revealed the composition of this covalently linked polysaccharide, containing glucosamine, mannosamine, galactosamine, mannose, and glucose, and confirmed the binding on MurNAc via a phosphate group (184). Polypeptides with the respective masses of 67 kDa and 61 kDa were found to be associated with the peptidoglycan, but were not identified until now (185).

Cell envelope of *N. punctiforme*

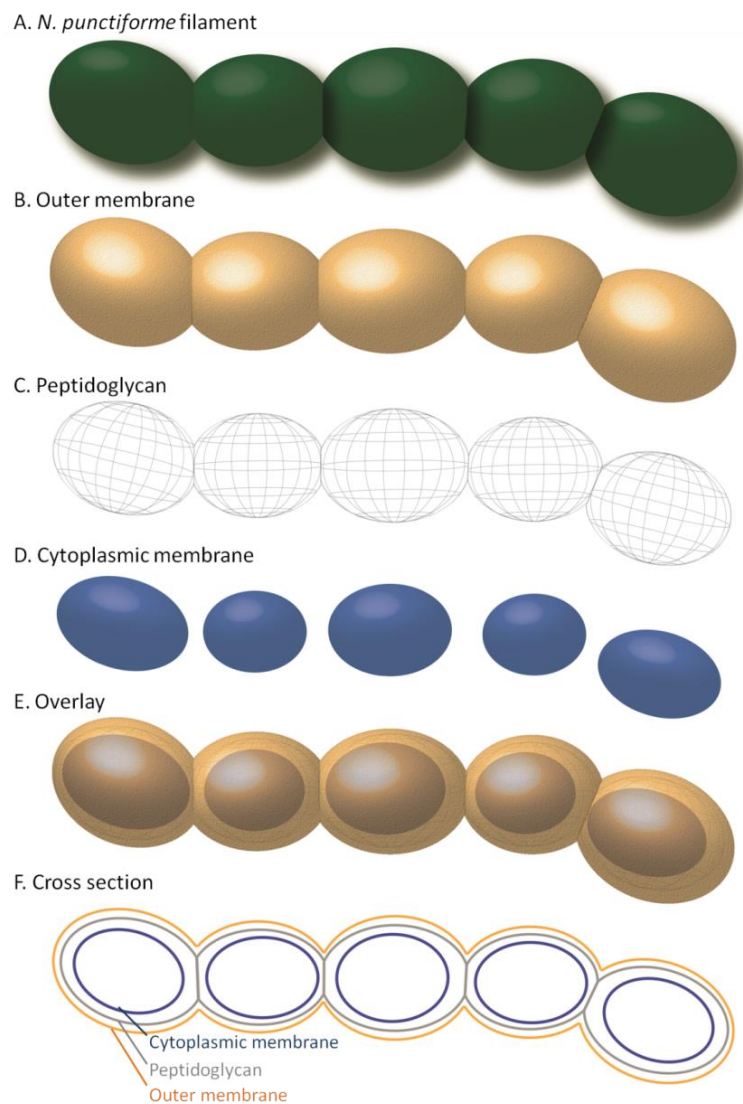


Fig. 8: *Nostoc* cell envelope. *N. punctiforme* grows in long green filaments (A) that are covered by the outer membrane (B). This outermost layer does not enter the septum and allows the periplasm to be continuous (F). Neighbouring cells share a common peptidoglycan layer (C) but are separately surrounded by a cytoplasmic membrane (D).

The outermost external layer, nowadays known as outer membrane, appeared in the first electron micrographs of cyanobacteria as a double lined structure (175, 186). In filamentous cyanobacteria, it was observed that the outer membrane covers the whole filament, only slightly invaginating between neighbouring cells without separating them (175, 186). As a result, the periplasm appears continuous throughout the filament (187, 188). Later, it was shown that this external layer contained lipopolysaccharides, the major constituent in outer membranes of Gram-negative bacteria (67, 68).

These early studies showed that the formerly known blue-green algae are prokaryotes with a multi-layered envelope that encompasses peptidoglycan (Fig. 8). The presence of peptidoglycan requires enzymes for its synthesis, but to date, information about the peptidoglycan synthesis in cyanobacteria is rare. In 1999, Kodani et al. were able to extract the peptidoglycan precursor UDP-N-acetylmuramyl-pentapeptide from *Anabaena cylindrica* (189), that occurs in almost all bacteria. The presence of this precursor suggests that cyanobacteria have a similar peptidoglycan synthesis as other Gram-negative or Gram-positive bacteria. Recently, homologues of the enzymes UDP-N-acetylmuramyl-L-alanine ligase MurC (*alr5065*) and UDP-N-acetylenolpyruvoylglucosamine reductase MurB (*alr5066*) were identified in *Anabaena* sp. PCC 7120. Complementation of temperature-sensitive *E. coli* strains, deficient of either *murC* or *murB*, with the corresponding *Anabaena* genes *alr5065* or *alr5066* were able again to grow again at nonpermissive temperatures (190).

1.3.2. Remodelling of cyanobacterial peptidoglycan

Interestingly, depletion of the aforementioned *mur* gene homologues *murC* and *murB* in *Anabaena* sp. PCC 7120 (hereafter named *Anabaena*) affected heterocyst differentiation and resulted in short and distorted filaments (190). These extensive consequences due to the absence of two peptidoglycan synthesis enzymes on heterocyst development indicate a crucial role of peptidoglycan remodelling during differentiation. Transposon mutagenesis of *Anabaena* revealed a putative Penicillin Binding Protein (PBP), homologous to *E. coli* bifunctional PBPs, that has a pivotal role in heterocyst formation (191). The disruption of this putative PBP gene (*alr5101*) resulted in heterocysts with very thin envelope layers lacking cyanophycin granules and a reduced nitrogen activity under nitrogen depleting conditions.

Besides this, two additional putative PBPs encoding genes were identified in *Anabaena* that are involved in the formation of a functional polysaccharide layer in heterocysts (192). The gene products of *all2981* and *alr4579* are homologous to the D,D-carboxypeptidase PBP6 and the transpeptidase PBP3, which is also known as FtsI in *E. coli* (137, 138). Mutations of these putative PBPs resulted in an impaired closure or the complete absence of the polysaccharide layer (192). An extensive comparative genomic analysis revealed that the number of PBPs in 12 cyanobacterial genomes increases by the genome size. Unicellular marine cyanobacteria with a genome of roughly 2 Mb encode a minimal set of four putative PBPs. These are a bifunctional class A PBP, two class B PBPs probably involved in elongation and septum formation and one LMW-PBP that is similar to *E. coli* PBP4, a carboxy- and endopeptidase (192). It is astonishing that these organisms realize cell division, elongation and remodelling events by possessing only four Penicillin Binding Proteins.

The complex regulatory network during cell division and elongation is also partially conserved in cyanobacteria. The unicellular freshwater cyanobacterium *Synechocystis* PCC 6803 (hereafter *Synechocystis*) uses the major cell division protein FtsZ to assemble a ring-like structure at the division plane as a scaffold for other proteins (193, 194), similar to *E. coli* (2, 115). The position of the

Z-ring is amongst others determined by the Min-system. Depletion of *minCDE* abolished the spherical phenotype of *Synechocystis* and led to spiral cell growth with aberrant FtsZ-polymers (194). Bacterial-two-hybrid assays elucidated the interplay between the major division proteins FtsZ and ZipN (194), a new division protein that occurs only in cyanobacteria and plastids (195), with other division proteins like FtsQ, FtsI and FtsW (193). FtsI belongs to class B PBPs and functions as a transpeptidase involved in the inward synthesis of peptidoglycan during cell division of *Synechocystis*. It interacts directly with two class A HMW-PBPs analogous to *E. coli*, where FtsI interacts with the bifunctional peptidoglycan synthase PBP1b (140). Transposon mutagenesis in *Synechococcus elongatus* PCC 7942 identified two more genes, *ftn6* and *cikA*, that are important for Z-ring assembly and unique to cyanobacteria (196). Whereas the former gene is still under investigation, the latter one encodes a Histidine kinase that modulates the phase-setting of the circadian clock (197). Cells lacking *cikA* revealed elongated cell lengths and abrogated Z-rings (196). Remarkably, this is the first hint for a direct connection between the circadian clock and the cell division.

Unfortunately, not much is known about the septum cleavage in unicellular cyanobacteria. Marbouty et al. investigated two putative endopeptidases in *Synechocystis*, Slr0646 and Slr0804, that might be involved in septation (193). Mutants carrying deletions in either *slr0646* or *slr0804* had pleiotropic morphological defects and were impaired in cell separation.

Noteworthy, integral parts of the *E. coli* divisome are not encoded in any of the annotated cyanobacterial genomes. FtsL and FtsB, that form a complex with FtsQ (133), as well as the positive regulator FtsN (142) and the FtsZ-interacting FtsA (122, 123) are missing (198). Several studies appeared describing analogues for the corresponding *E. coli* division proteins in cyanobacteria. For example, cyanobacterial ZipN was found to act similarly as FtsA (195), and CyDiv was recently identified in *Anabaena* substituting for FtsB (199). A homologous *ftsZ* gene was also identified in the genome of the filamentous cyanobacterium *Anabaena* (200, 201), indicating that FtsZ also plays a major role in the cell division of multicellular cyanobacteria. GFP-fusion located FtsZ at midcell position in *Anabaena*, where it formed a Z-ring (202). Interestingly, when *Anabaena* FtsZ was overexpressed in *E. coli*, it became filamentous without having septa between neighbouring cells in the filament. Purified recombinant FtsZ exhibited GTPase-activity (203) which fuels FtsZ polymerization in *E. coli* (118). Moreover, only vegetative cells expressed FtsZ, whereas mature heterocysts did not (203). A *hetC* mutant showed elevated levels of FtsZ in proheterocysts and was unable to stop cell division (204). HetC is an ABC protein or peptide exporter (205) with regulatory function in early heterocyst differentiation. The filaments of the *hetC* mutant displayed actively dividing proheterocysts that could not transform into mature heterocysts (204). The expression of *ftsZ* has to be suppressed to allow heterocyst maturation. Lately, the interaction between ZipN and several putative divisome components of *Anabaena* sp. PCC 7120 was elucidated (206) and clearly showed that the underlying molecular mechanism of cell division using FtsZ as scaffold for regulatory proteins and peptidoglycan synthesis enzymes is shared not only between unicellular and multicellular cyanobacteria, but also between cyanobacteria and other Gram-negative and Gram-positive bacteria.

In comparison to cell division, little is known about elongation and growth of cyanobacteria. The cytoskeletal protein MreB, the critical determinant for cell shape and an important part of the elongosome of most rod-shaped bacteria (157) was identified in *Anabaena*. Cells lacking MreB appeared larger and were almost coccoid compared to the wild-type (207). Disruption of a putative PBP2 transpeptidase encoded by *alr5045* in *Anabaena*, which is homologous to the RodA interacting

transpeptidase in *E. coli* (166), altered cell shape and filament length (208). These studies show that main constituents of the elangosome of rod-shaped bacteria exist as well in cyanobacteria. Furthermore, investigations on the adaptation behaviour of the filamentous cyanobacterium *Fremyella diplosiphon* to red or green light revealed the presence of the MreB counteracting partner BolA (209). The morphogene *bolA* was first described in *E. coli* where it induces spherical morphology during stress-bearing conditions (210) or stationary growth (211). *F. diplosiphon* increases *bolA* expression in response to red light that suppresses *mreB*. This comes along with the morphological remodelling from rod-shaped into spherical cells. Upon green light, *bolA* expression is inhibited while *mreB* expression is enhanced that leads to a rod-shaped morphology (209).

1.3.3. Cell-cell communication in multicellular cyanobacteria

Communication between cells within a filament is a prerequisite for the survival and maintenance of the entire filament especially during rapid environmental changes. The observation that the outer membrane does not enter the septum, so that the periplasm seems to be continuous (Fig. 8) led to the hypothesis that communication might also occur via the periplasm (187, 188). Several tracking studies addressed the periplasmic movements based on GFP fluorescence, but reported contradictory results (188, 212, 213). Initially, Mariscal et al expressed GFP under the promoter of *patS*, a gene specific for proheterocysts and heterocysts. Such expressed GFP diffused to neighbouring vegetative cells, when it was exported into the periplasm by the Tat-system (188). Later, Zhang et al. fused GFP to different Tat signal sequences specific for heterocysts or vegetative cells and observed a GFP export into the periplasm but no diffusion to neighbouring cells (212). Hereafter, they expanded their research by attaching a Tat-signal sequence to the smaller fluorescent protein iLOV, in order to examine the diffusion of this marker within the periplasm. An interesting observation of this study was that the 13 kDa protein did not diffuse from the producing cell to adjacent cells in the periplasm. This suggests that only smaller molecules can pass freely through the periplasm (214). The question whether communication through the periplasm is possible or not remains still open. But, it is clear that molecules are exchanged between the cells. FRAP-experiments based on calcein labeled *Anabaena* cells demonstrated an exchange of this small fluorescent molecule between the cells cytoplasm through the filament (215). Calcein is a fluorescein-derivative and available as an acetoxymethyl-ester enabling a diffusion through membranes. This hydrophobic ester-group is cleaved by cytoplasmic esterases and thus turns calcein into a hydrophilic fluorescent dye. Mullineaux et al. used this technique to measure the exchange of molecules between cells in a filament. They labelled the cells with calcein and showed in the first case, that it accumulates in the cytoplasm. In the second, one single cell within the filament was photobleached, so that the calcein fluorescence was irreversibly destroyed. Surprisingly, fluorescence recovered within several seconds. This increase of fluorescence signals occurred through the influx of calcein from neighbouring cells (215).

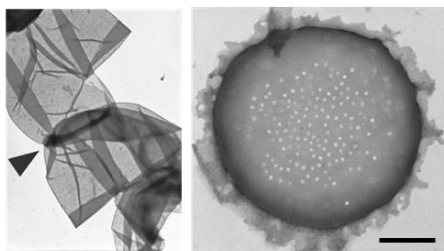
Calcein is a hydrophilic molecule that cannot pass the cytoplasmic membrane. The uptake of calcein from neighbouring cells indicates cell joining structures between adjacent cells. Electron micrographs obtained from early studies demonstrated intercellular connections perpendicular to the cytoplasmic membrane between different cells in the filaments of heterocyst-forming cyanobacteria (216-218). The continuous improvement of electron microscopy techniques enabled higher resolution images of these cell joining structures, which were designated as “septal junctions” and assumed that these channels are proteinaceous (219, 220). The number of septal junctions observed between

neighbouring cells varies amongst different species from around 100 in *Anabaena* (221, 222), over 155 in *N. punctiforme* (223), up to 250 in *Anabaena cylindrica* (224).

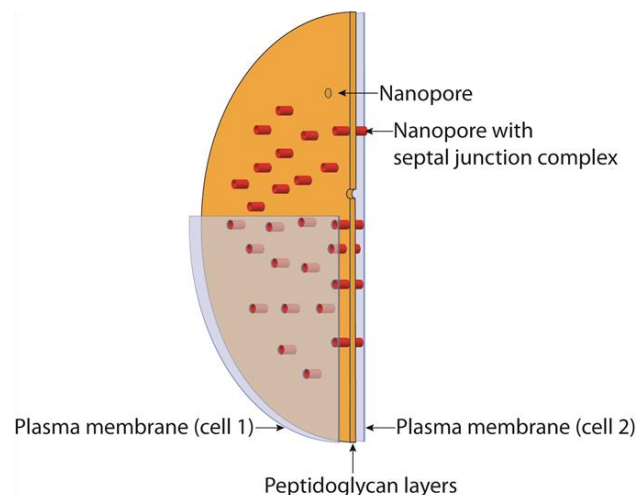
1.3.4. Septal junctions enable direct cell-cell communication

Random transposon mutagenesis in *Anabaena* identified a gene (*alr2338*) encoding for the septal protein SepJ (also known as FraG = fragmentation, glycolipid), when screening for non-diazotrophic mutants. *Anabaena* strains lacking *alr2338* were impaired in heterocyst maturation and fragmented drastically, when nitrogen was depleted. Subcellular localization studies based on GFP-fusion detected SepJ at the cell poles in septa between adjacent cells (225, 226). Moreover, FRAP-experiments demonstrated an affected intercellular communication in *alr2338* mutant strains (215). Mullineaux et al. suggested SepJ as a major structural component of the septal junction. However, ultrastructural images revealed that the septal junctions were still present in mutant cells (219, 220). One possible explanation to explain these contradicting observations could be a role in septum maturation rather than in septal junction formation. Bacterial-two-hybrid assays revealed a strong interaction between SepJ and the cell division protein FtsQ (227), that regulates peptidoglycan synthesis during cell division (141). Besides, SepJ possesses a coiled-coil peptidoglycan binding domain at its N-terminus (228).

A. TEM-image of peptidoglycan from *N. punctiforme*



B. Nanopore-array accommodates septal junction complexes



C. Septal junction architecture of *Nostoc* sp. PCC 7120

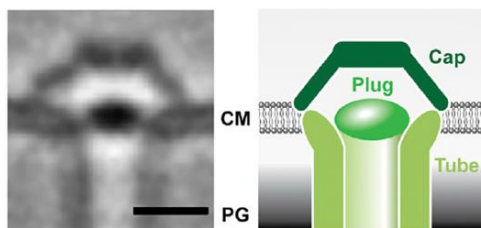


Fig. 9: Fundamentals of cell-cell-communication in filamentous cyanobacteria. **A.** Electron micrographs of purified peptidoglycan sacculi and a perforated septum obtained from *N. punctiforme*. Scale bar = 300 nm; arrow points to a septal disk. Images from Lehner et. al, 2013 **B.** Schematic illustration of a perforated septal disk harbouring septal junction complexes. Image provided by Jan Bornikoel. **C.** Averaged cryotomogram of a septal junction from *Nostoc* sp. PCC 7120 with a schematic illustration displaying cap, plug and tube structures. Scale bar = 10 nm. Image from Weiss et al., 2019.

Further studies that involved the role of N-acetylmuramyl-L-alanine amidases gave more details about the function of SepJ. It was observed that septal disks of heterocyst-forming cyanobacteria harbour numerous pores in the central part with a diameter of 15 – 20 nm (222, 223). The inactivation of Npun_F1846, encoding for a N-acetylmuramyl-L-alanine amidase, had severe morphological defects in *N. punctiforme* (229) and abolished the nanopore array in the septum (223).

Mutation of the homologous amidase gene *alr0092* (*amiC1*) in *Anabaena* reduced the number of nanopores in the septal disks (221). Interestingly, disruption of *amiC1* in the *sepJ* mutant abolished the fragmentation phenotype (221). Overexpression of *SepJ* in *Anabaena* increased the number of nanopores in the septa (230), that are mainly drilled by the amidase *AmiC1*. These findings indicate that *SepJ* might be involved in the regulation of the amidase *AmiC1* in *Anabaena* (231).

Recently, Weiss et al. revealed the architecture of the septal junctions by high resolution 3D cryo-microscopy (232). Accordingly, septal junctions consist of a tube, traversing the septal peptidoglycan, as well as cap and plug structures at both sides of the tube. The authors further showed that the channel can actively be opened and closed. The gating in the *sepJ* mutant of *Anabaena* was unaffected, but the transfer of fluorescent tracers between the cells was nevertheless strongly decreased (232). A possible explanation for the impaired cell-cell communication could be due to the reduced number of nanopores in the *sepJ* mutant (222). Furthermore, *FraD* was identified as a structural component of the septal junctions. It is anchored in the cytoplasmic membrane and protrudes into the tube with its N-terminus (232). *FraD* is encoded in an operon-like structure together with *fraC* and *fraE*. Immunogold-labelling and GFP fusions experiments confirmed the localization of the integral membrane proteins *FraD* and *FraC* in intercellular septa (233, 234). Mutants lacking single or multiple *fra* genes displayed only short filaments, were impaired in cell-cell communication, and showed less nanopores in the septal disks (222, 233-235). Alcian blue staining demonstrated the presence of heterocysts in these *fra* mutants, that were active and contained heterocyst-specific polysaccharides, as well as glycolipids. However, the nitrogenase activity was diminished compared to the wild-type (233). Moreover, *fraC* and *fraD* mutants displayed an impaired localization of *SepJ* (233), indicating a closer relationship between those three proteins, although clear evidences for a direct interaction are still missing (231).

1.3.5. Formation of the nanopore array

Septal junctions are crucial for cell-cell communication and are conserved amongst multicellular cyanobacteria (232). Great progress has been made in the elucidation of the architectural structure and the mode of intercellular communication, whereas the molecular mechanism of nanopore formation remains still unclear. Several proteins, affecting the nanopore drilling in the septal disk upon mutation were identified. These are the septal proteins *SepJ*, *FraC* and *FraD* (222), as well as the aforementioned N-acetylmuramyl-L-alanine amidase *AmiC* (221, 223).

Multicellular, heterocyst-forming cyanobacteria encode two copies of the *amiC* gene with an high similarity to *amiC* from *E. coli* (236). *Anabaena* and *Nostoc* species have a conserved gene cluster with both *amiC* genes located between *kefB*, encoding a subunit of a K^+/H^+ -antiporter, and *murl*, encoding a glutamate racemase. Both *AmiC* proteins, *AmiC1* and *AmiC2*, contain two septal targeting AMIN domains at the N-terminus and a catalytic domain at the C-terminus. The function of both *AmiC* proteins was extensively studied in the model organisms *N. punctiforme* and *Anabaena* (223, 229, 236). Whereas *AmiC* in *E. coli* is involved in septation and the release of daughter cells during cell division (145), a novel function was ascribed to the homologous *AmiC* proteins in multicellular heterocystous cyanobacteria. The disruption of *Npun_F1846*, corresponding to *amiC2*, had pleiotropic defects (223, 229). Filaments were distorted and appeared as cell aggregates with aberrant septa of varying sizes. Differentiation was impaired, neither heterocysts, nor akinetes or hormogonia could differentiate, and intercellular communication was abolished (229). Electron micrographs of purified peptidoglycan sacculi from the *amiC2* mutant displayed septa without

nanopores (223). Taken together, all these findings suggest AmiC2 as a key player in the formation of the nanopore array in *N. punctiforme*, that is likely the scaffold for septal junctions. Moreover, localization studies demonstrated that AmiC2 is dependent on the cell cycle and the differentiation pattern (223). When *N. punctiforme* was grown in medium with combined nitrogen sources, GFP-AmiC2 was detected in the septa of dividing vegetative cells, but when nitrogen components were removed, GFP-AmiC2 accumulated mainly at septa of developing heterocysts. Depletion of nitrate induces hormogonia formation in *N. punctiforme* (237) and led to an even distribution of GFP-AmiC2 in the septa of dividing cells (223), due to a simultaneous cell division during hormogonia differentiation (29). AmiC2 has a pivotal role in peptidoglycan remodelling during differentiation of hormogonia and heterocysts. But unfortunately it was not possible to inactivate *amiC1* in *N. punctiforme* (229).

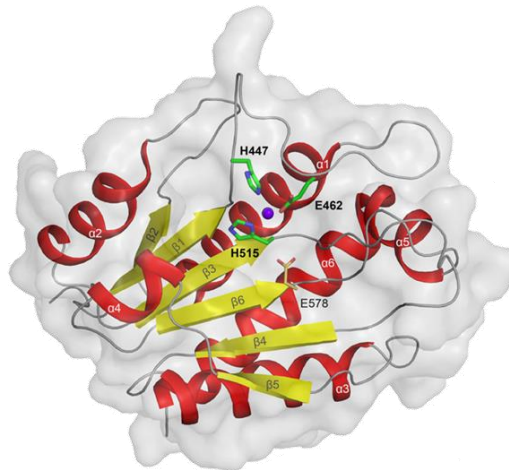
Depletion of *amiC1* in *Anabaena* impaired heterocyst differentiation and prevented intercellular transfer of calcein (236). Ultrastructural images showed less nanopores in the central part of the septal disk, compared to the wild-type (221). Like AmiC2 from *N. punctiforme*, AmiC1 localized to the intercellular septa of dividing vegetative cells, but shifted to the septal peptidoglycan of maturing heterocysts under nitrogen starvation. Furthermore, overexpression of AmiC1 led to an uncontrolled cleavage activity, resulting in cell lysis (236). Taken together, AmiC1 in *Anabaena* seems to act similarly to AmiC2 from *N. punctiforme*. AmiC2 (*alr0093*) from *Anabaena* was first described by Zhu et al. as a peptidoglycan hydrolase, that is required for heterocyst differentiation, and was termed HcwA (for heterocyst cell wall) (238). The inactivation of *alr0093* impaired growth under nitrogen depleting conditions. Zhu et al. hypothesized that the amidase removes peptide crosslinks in the peptidoglycan layer of heterocysts to facilitate the transport of polysaccharides or glycolipids. Berendt et al. inactivated *alr0093* by a single recombination insertion of an antibiotic resistance cassette and observed no phenotypic alterations. These contradictory results from both reports were somehow clarified from Bornikoe et al. (221). The researchers noticed, that the mutants behave differentially in BG11 or AA/8 medium deficient of nitrogen sources. But both *amiC2* mutant variants could not grow diazotrophically in AA/8 medium lacking combined nitrogen sources (221, 238). Recently, Brenes-Álvarez et al. found out, that the strictly, conserved small RNA Yfr1 positively regulates expression of AmiC2 in *Anabaena* (239).

Mutational analysis of *fra* or *amiC* genes in diverse filamentous cyanobacteria displayed various malfunctions in morphology, growth and differentiation. Nanopore formation was affected regarding quantity and size of nanopores. Recently, another protein, SjcF1, was identified, coupling nanopore and septal junction formation (240). SjcF1 is a transmembrane protein with a SH3 domain, capable of protein-protein interaction, and two peptidoglycan binding domains, that directly interact with *Anabaena* sp. PCC 7120 peptidoglycan. An insertional mutant did not show any growth defects in the presence or absence of combined nitrogen, but the diameter of nanopores in purified *Anabaena* sacculi was bigger whereas intercellular communication was reduced. Based on this observation, it was hypothesized, that SjcF1 organizes the positioning of the septal junction by the interaction with SepJ and FraC. Cryotomographs of a *scjF1* mutant revealed fully assembled septal junction complexes (232). SjcF1 might be rather involved in nanopore formation.

1.3.6. Regulation mechanism of AmiC and its homologues

The activity of the cell wall hydrolase AmiC in *E. coli* is tightly regulated (146, 148). It is assumed that a conformational change induced by NlpD leads to the activation of AmiC (148). The structural elucidation of AmiC reveals that an α -helix obstructs the active site and prevents peptidoglycan cleavage (Fig. 10C, blue helix) (151). The exact molecular mechanism on the removal of the helix by NlpD remains unclear.

A. Crystal structure of the catalytic domain of AmiC2 from *N. punctiforme*



B. Domain architecture of AmiC2 from *N. punctiforme*



C. Surface conservation of AmiC homologs of *E. coli* and *N. punctiforme*

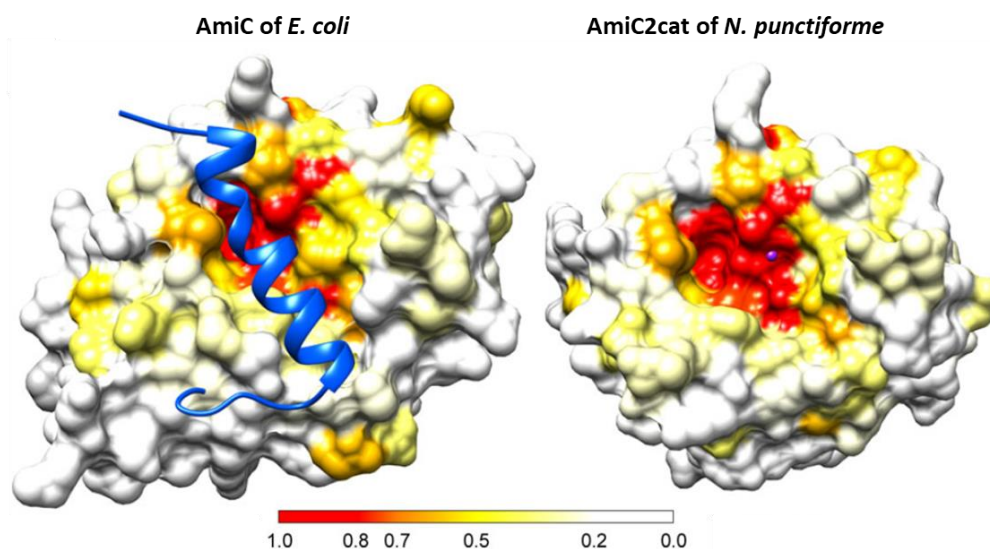


Fig. 10: Catalytic domain of AmiC2 from *N. punctiforme*. A. Crystal structure of the catalytic domain of AmiC2 from Büttner et al., 2016. B. Domain architecture of the full-length AmiC2 from *N. punctiforme*. SP = signal peptide. C. Representation of conserved regions in the binding site of AmiC from *E. coli* and AmiC2cat from *N. punctiforme*. Colour bar indicates conservation level. Image from Büttner et al., 2016.

The mechanism of autoinhibition seems to be conserved for cell division dependant hydrolases, since the active site of AmiB orthologues in *Bartonella henselae* and other Gram-negative bacteria is also blocked for substrate binding by an inhibitory α -helix (241). Structural examinations on the catalytic domain of *N. punctiforme* demonstrated the absence of an inhibitory α -helix (Fig. 10A and C) (242). This indicates a novel, to date unknown, regulation mechanism.

The domain architecture from AmiC2 differs from that of *E. coli* AmiC insofar, that AmiC2 contains two AMIN domains (Fig. 10B). Both domains are separated by a proline rich, 160 amino acid residue long linker region, modulating the enzymatic activity (hereafter modulator). Purification of the full-length AmiC2 protein revealed two bands of approximately 69 and 55 kDa molecular weight by western blot analysis, using polyclonal antibodies against the modulator. The authors hypothesized that AmiC2 undergoes proteolysis, which might be a regulation mechanism, as demonstrated for some cell wall modifying cysteine peptidases (243). Furthermore, recombinant expressed fusion proteins containing the modulator and the catalytic domain attached to a GST-tag showed a reduced activity *in-vitro*, compared to the catalytic domain alone (244).

Büttner et al. suggested a possible involvement of the AMIN domains or the modulator in the regulation mechanism. The zinc-dependant peptidoglycan hydrolase Rv3717 from *Mycobacterium tuberculosis*, lacking any AMIN domains, harbours a short flexible hairpin turn, obstructing the active site, analogous to the α -helix in homologous amidases (245). AmiC2 does not have any structural component in the catalytic domain, that could prevent substrate binding and cleavage (242). Unfortunately, it was not possible to obtain crystal structures from the full length AmiC2 protein with its AMIN domains together with the modulator (F. Büttner, personal communication). Another difference between AmiC2 from *N. punctiforme* and AmiC from *E. coli* is the mode of translocation. Whereas AmiC is translocated in its folded state by the Twin-arginine-translocation system into the periplasm, AmiC2 from *N. punctiforme* carries a Sec signal peptide and is translocated in an unfolded state.

Apart from structural components, that modulate the enzymatic activity, interacting proteins play an important role in the recruitment and activation of amidases. NlpD and EnvC are known activators of peptidoglycan amidases (146-148). A genomic screening of *Anabaena* sp. PCC 7120 for homologues of *envC* or *nlpD* revealed open reading frames similar to those of *envC* and *nlpD* from *E. coli* (246). The NlpD homologue (*alr3353*) lacks any transmembrane regions and is predicted to be a soluble periplasmic protein. YFP-fusion experiments located NlpD in the cell wall with higher intensities at the septa between neighbouring cells, but not at the polar neck of heterocysts. This strongly indicates its role in septum constriction during heterocyst maturation. Disruption of the putative *nlpD* gene affected filament morphology and exhibited fewer nanopores in the septal disks of purified *Anabaena* sacculi. Heterocysts were formed in this mutant, but had a reduced nitrogenase activity and the communication between vegetative cells and the heterocysts was disturbed. A direct interaction between the putative NlpD homologue and AmiC1 could be determined by MST-analysis. Together with a potentiated activity in Dye-release assays, these findings suggest that the periplasmic NlpD homologue likely activates AmiC.

1.4. Research objectives

Intercellular communication of heterozygous cyanobacteria requires two essential processes, namely nanopore drilling and septal junction formation. Mutational analysis of *fraDC* (222), *sepJ* (225, 226), *sjcF1* (240) or *amiC* (223, 236) affected the perforation of the septal disk as well as the intercellular transfer of fluorescent tracers, indicating that both processes are likely interdependent. The tight regulation of proteins and enzymes involved in one of these processes is therefore highly relevant. Uncontrolled hydrolytic activity of amidases like AmiC1 from *Anabaena* sp. PCC 7120 or AmiC2 from *N. punctiforme*, for example, would lead to cell lysis instead of nanopore formation.

Previous studies showed that peptidoglycan cleavage is reduced, when the modulator is fused to the catalytic domain of AmiC2 from *N. punctiforme* (244), indicating a structural inhibition analogous to the inhibitory α -helix of AmiC from *E. coli* (151). Furthermore, AmiC2 localization is altered, when just one AMIN domain or the modulator is deleted, (244) displaying the high importance of these domains for the spatial distribution of AmiC2. Purification of recombinantly expressed AmiC2 indicates an autoproteolytic activity, thus AmiC2 localisation could be controlled by protein cleavage (242). Moreover, NlpD homologues (*Npun_F5024* and *alr3353*) were found in *N. punctiforme* (244) and *Anabaena* (246), affecting hydrolytic activity upon mutation.

However, there is another possibility, how nanopore formation by AmiC2 might be regulated. Although little is known about the specificity of the amidase AmiC2, the enzyme might prefer a specific type of peptidoglycan fragment that is accumulating at future sites of nanopores in the septal disks. Following this hypothesis, *N. punctiforme* could incorporate cleavage sites for AmiC2 into the septal peptidoglycan. The verification of this assumption requires a full elucidation of the peptidoglycan composition and the determination of the substrate specificity of AmiC2.

The first part of this work focuses on the substrate of the amidase AmiC2 from *N. punctiforme*, the peptidoglycan:

1. Establishing a protocol for the isolation of cyanobacterial peptidoglycan
2. Identification of PGN amino acids in HCl hydrolysates of crude peptidoglycan.
3. Analysis of muropeptide profiles of wild-type and the *amiC2* mutant from *N. punctiforme*.
4. Differences between the lateral and septal cell wall wild-type *N. punctiforme*
5. Determination of covalently linked polysaccharides
6. Identification of putative peptidoglycan linked proteins

The second part will deepen the functional characterization of AmiC2 regarding enzymatic activity and peptidoglycan binding capacity:

1. Development of new analytical methods to determine the so far elusive hydrolytic activity of AmiC2.
2. Detection and identification of AmiC2 released peptides to get information on the molecular structure of presumed cleavage sites in the septum. The main focus of this section will be on the establishment of a sensitive method to determine the interaction between AmiC2 and the peptidoglycan.
3. Mutational analysis of site-specific amino acids in the binding cleft of AmiC2

2. Material and methods

2.1. Chemicals and enzymes

All chemicals were purchased either from Carl Roth, Sigma-Aldrich, Fluka or Merck, except those listed below:

Table 1: List of chemicals and enzymes.

Chemicals or enzymes	Company
ReproSil® OPA	Dr. Maisch GmbH
Fluoraldehyde™ o-Phthaldialdehyde Crystals	ThermoFisher Scientific
Glycerol	Honeywell Riedel-de-Haën
Bicinchoninic acid	ThermoFisher Scientific
Instant blue	Expedeon
Imidazole	Acros Organics
Agarose	Genaxxon

2.2. Kits

Table 2: List of kits and corresponding manufacturers.

Kit	Company
Monarch Plasmid Miniprep Kit	New England BioLabs, Ipswich, USA
Monarch DNA Gel Extraction Kit	New England BioLabs, Ipswich, USA
Q5 Site-directed Mutagenesis Kit	New England BioLabs, Inc., Ipswich, USA
Monolith His-Tag Labeling Kit RED-tris-NTA	NanoTemper, Munich, Germany

2.3. Software and programmes

Plasmid constructs were made with the help of CloneManager9 (Sci Ed Software LLC, Westminster, USA). Cloning experiments were planned with PlasmidMaster. Luminescence was monitored by GEL LOGIC 1500 Imaging system and processed by the software Kodak MI. Biolayer interferometry interaction assays were defined by the Octet System Data Acquisition 7.1 (FortéBio, Fermont, USA) and subsequently processed by Data Analysis HT software (FortéBio, Fermont, USA). Microscale thermophoresis was carried out by a Monolith®NT.115 device equipped with the NT control software which was needed to define all necessary parameters. MST data were further processed by the software NT Analysis v.1.5.41. Amino acid analysis by HPLC (see chapter 2.10.1 and 2.11.1) was performed by ChemStation for LC 3D, Rev. A.08.03 (Agilent Technologies, Santa Clara, USA). Muropeptide structures, sum formulas and fragmentation simulations were obtained from ChemBioDraw Ultra 12.0 (PerkinElmer, Waltham, USA).

Summary of all web-based programs, which were used in this work, are listed below:

Table 3: Summary of all web-based programs and the corresponding web address

Designation	Web address
BLASTp	https://blast.ncbi.nlm.nih.gov/Blast.cgi?PROGRAM=blastp&PAGE_TYPE=BlastSearch&LINK_LOC=blasthome
CELLO	http://cello.life.nctu.edu.tw/
Clustal Omega	https://www.ebi.ac.uk/Tools/msa/clustalo/
Cyanobase	http://bacteria.kazusa.or.jp/cyanobase/
InterPro	https://www.ebi.ac.uk/interpro/
NEB TM calculator	https://tmcalculator.neb.com/#!/main
Nick Anthis	http://nickanthis.com/tools/a205.html
ProtParam	https://web.expasy.org/protparam/
SignalP-5.0	http://www.cbs.dtu.dk/services/SignalP/
STRING	https://string-db.org/
TMHMM	http://www.cbs.dtu.dk/services/TMHMM/
UniProt	https://www.uniprot.org/

2.4. Strains and maintenance

Table 4: *Nostoc* and *E.coli* strains

Strain	Genotype	reference
<i>Nostoc punctiforme</i> ATCC 29133	Wild-type	ATCC
<i>Nostoc punctiforme</i> ATCC 29133 <i>Npun_F1846::C.K3</i> (rev.)	<i>Npun_F1846::C.K3</i> (rev.); Nm ^r	Lehner et al. 2011 (229)
<i>E. coli</i> K-12 MG1655	F- <i>lambda- ilvG- rfb-50 rph-1</i>	Jensen et al., 1993 (247)
<i>E. coli</i> DH5 α	F- 80 <i>dlacZ</i> M15 (<i>lacZYA-argF</i>) U169 <i>recA1 endA1, hsdR17</i> (rk-, mk+) <i>phoA supE44 -thi-1 gyrA96</i> <i>relA1</i>	Hanahan et al. 1983 (248)
<i>E. coli</i> DH10 β	F-, <i>mcrA</i> , Δ (<i>mrr-hsdRMS-mcrBC</i>), ϕ 80 <i>lacZ</i> Δ M15, Δ <i>lacX74</i> , <i>recA1</i> , <i>endA1, araD139, \Delta(ara, leu)7697</i> <i>,galU, galK, \lambda-rpsL, nupG</i>	Hanahan et al. 1991 (249)
<i>E. coli</i> Lemo21 (DE3)	<i>fhuA2</i> [lon] <i>ompT gal</i> (λ DE3) [dcm] Δ <i>hsdS</i> / pLemo(CamR) λ DE3 = λ sBamHlo Δ EcoRI-B int::(<i>lacI::PlacUV5::T7 gene1</i>) i21 Δ nin5 pLemo = pACYC184- <i>PrhaBAD-lysY</i>	NEB Biolabs

E. coli strains were stored on LB agar plates supplemented with appropriate antibiotics (see Table 24) for several days at 4°C. Long-term storage was performed in 30% glycerol at -80°C. Cyanobacterial strains were stored on BG11 agar plates, with or without nitrogen sources with the appropriate antibiotics, on room temperature or at 28°C under constant light conditions. Addition of 8% (v/v) DMSO to liquid cultures enabled preservation at -80°C.

2.5. Media and buffers

BG11 modified according to Rippka et. al (26)

Cyanobacteria were cultivated in liquid or solid BG11 medium supplemented with 5 mM NaHCO₃. Nitrogenous compounds were omitted for the maintenance of heterozygous cyanobacteria on BG11₀ agar plates. Neomycin (50 µg/ml final concentration) was added to liquid or solid BG11 medium for the cultivation of the *amiC2* mutant strain of *N. punctiforme*.

Components, listed in Table 5, were dissolved in ddH₂O water and sterilized as 200x stock solutions. The 200x stock solution containing citric acid and ferric (III)-citrate has to be protected from light. All 200x stock solutions were store at room temperature. Table 6 summarizes all components for the BG11 trace element solution. The aqueous solution, containing all listed trace elements, was filtered through a sterile PTFE membrane filter with a cut-off of 0.22 µm and stored at room temperature.

For 1 l of 1x BG11 medium, 5 ml of each 200x stock solution, listed in Table 5, and 1 ml of the 1000x trace element stock solution were added to 500 ml ddH₂O and filled to 1 l with ddH₂O. NaHCO₃ was added after sterilization to a final concentration of 5 mM.

Table 5: 200x stock solutions for BG11 medium

Substance	200x stock [mM]
NaNO ₃	3530
K ₂ HPO ₄ ×3H ₂ O	35
MgSO ₄ ×7H ₂ O	60
CaCl ₂ ×2H ₂ O	49
Citric acid & Ferric(III)-citrate	6.25 4.9
EDTA	0.68
Na ₂ CO ₃	7550

Table 6: 1000x stock solution of trace elements

Substance	1000x stock [mM]
H ₃ BO ₃	46.3
MnCl ₂ ×4H ₂ O	9.2
ZnSO ₄ ×7H ₂ O	0.77
Na ₂ MoO ₄ ×2H ₂ O	1.6
CuSO ₄ ×5H ₂ O	0.32
Co(NO ₃) ₂ ×6H ₂ O	0.267

BG11 or BG11₀ medium was supplemented with 1.5% Bacto agar, sterilized and supplemented with the appropriate antibiotics. Petri dishes were filled with solid medium and stored at 4°C.

Lysogeny broth (LB)-medium

Table 7: Ingredients for LB-medium

Substance	g/l
Tryptone	10
Yeast extract	5
NaCl	10

Tryptone, yeast extract and NaCl were dissolved in 1l ddH₂O water and sterilized. For the preparation of LB agar plates, 1.5% Bacto agar were added to LB medium, sterilized and subsequently distributed on Petri dishes, supplemented with Ampicillin (100 µg/ml) or Kanamycin (50 µg/ml) (see chapter 2.8.2), if necessary.

Terrific broth (TB)-medium

Tryptone, yeast extract and glycerol were dissolved in 900 ml ddH₂O water and autoclaved. The 10x salt stock solution was prepared separately and also sterilized. Afterwards, 100 ml of the 10x TB salt stock solution were added to the 900 ml TB medium under the sterile hood.

Table 8: TB medium

Substance	g/l
Tryptone	12
Yeast extract	24
Glycerol	5

Table 9: 10x TB salts

Substance	g/l
KH ₂ PO ₄	23.1
K ₂ HPO ₄	125.4

Autoinduction medium according to Studier et al. (250)

The autoinduction medium was used for the cultivation of *E. coli* Lemo21 (DE3) strains, expressing GST-tagged AmiC2cat proteins or AmiC2cat mutant variants and consists of tryptone (1%), yeast extract (0.5%), salts (Table 10), sugars (Table 11) and trace elements (Table 13). The salts and the sugars were separately prepared as 25x stock solutions and autoclaved. A 0.1 M solution of FeCl₃ was prepared in 0.12 M HCl and diluted 1:1 with the 2000x trace metal stock solution (Table 12), which was prepared in advance and autoclaved, to obtain a 1000x trace element stock solution.

Table 10: 25x M stock solution

Substance	mM
Na ₂ HPO ₄	25
K ₂ HPO ₄	25
NH ₄ Cl	50
Na ₂ SO ₄	5

Table 11: 25x 5052 stock solution

Substance	%
Glycerol	12.5
Glucose	1.25
Lactose	5

Table 12: 2000x trace metal stock solution

Substance	mM
CaCl ₂	40
MnCl ₂	20
ZnSO ₄	20
CoCl ₂	4
CuCl ₂	4
NiCl ₂	4
Na ₂ MoO ₄	4
Na ₂ SeO ₃	4
H ₃ BO ₃	4

Table 13: 1000x trace element stock solution

Substance	mM
FeCl ₃	50
CaCl ₂	20
MnCl ₂	10
ZnSO ₄	10
CoCl ₂	2
CuCl ₂	2
NiCl ₂	2
Na ₂ MoO ₄	2
Na ₂ SeO ₃	2
H ₃ BO ₃	2

For 500 ml of autoinduction medium, tryptone and yeast extract were dissolved in 460 ml ddH₂O water and autoclaved. After cooling, 20 ml of each 25x stock solution was added under the sterile hood. The medium was subsequently supplemented with 2 mM MgSO₄ and 500 µl of the 1000x trace element stock solution. The medium was always freshly prepared just before use.

Sodium phosphate buffer

Buffer systems, containing sodium phosphate, were prepared according to the Promega guidelines “Buffers for Biochemical Reactions”. Sodium phosphate buffer, with a pH of 8, was used in almost all experiments and was prepared using 0.2 M stock solutions of Na₂HPO₄ and NaH₂PO₄. For a 0.1 M sodium phosphate buffer, with a pH of 8, 47.35 ml of solution A and 2.65 ml of solution B were mixed. Subsequently, the pH was measured and, if necessary, adjusted to 8 using NaOH or HCl. For sodium phosphate buffers with different pH values, the ratio between Na₂HPO₄ and NaH₂PO₄ taken from the Promega guidelines “Buffers for Biochemical Reactions” or calculated using the Henderson-Hasselbalch equation.

Table 14: Solution A

Substance	M
Na ₂ HPO ₄ ·x2H ₂ O	0.2

Table 15: Solution B

Substance	M
NaH ₂ PO ₄ ·xH ₂ O	0.2

Borate buffer

Boric acid and sodium tetraborate were dissolved in ddH₂O water according to Table 16. The pH was adjusted to 9 or 10.7 using boric acid or NaOH.

Table 16: Preparation of 1M borate buffer with pH 9 or 10.7

Substance	pH	
	9	10.7
Boric acid	39.3 g/l	2.1 g/l
Sodium tetraborate	73.4 g/l	194.4 g/l

Buffers for GSTrap affinity chromatography

Table 17: GST-binding buffer

Component	mM
Tris-HCl, pH 8	50
NaCl	300
(v/v) Glycerol	10%
DTT	1

Table 18: GST-elution buffer

Component	M
Tris-HCl, pH 8	50
NaCl	300
(v/v) Glycerol	10%
DTT	1
reduced glutathione	15

All components were dissolved in ddH₂O water, filtered through a 0.22 µm PVDF membrane and degassed for several hours. Buffers were stored at 4°C.

Buffers for HiTrap affinity chromatography

The components, listed above, were dissolved in ddH₂O and filtered through a 0.22 µm PVDF membrane. The buffers were degassed, before use, for several hours and stored at 4°C.

Table 19: HiTrap-binding buffer

Component	mM
Sodium phosphate, pH 8	50
NaCl	300
(v/v) Glycerol	10%
DTT	1

Table 20: HiTrap-elution buffer

Component	M
Sodium phosphate, pH 8	50
NaCl	300
(v/v) Glycerol	10%
DTT	1
Imidazol	300

Friendly-Towbin buffer

For 1 l buffer, 25 ml of a 1M stock solution of Tris-HCl, pH 8.5 and 14.4 g glycine were filled into 500 ml ddH₂O water. Afterwards, 50 ml iso-propanol were added and the buffer filled up to 1l with ddH₂O water.

Table 21: Composition of Friendly-Towbin buffer.

Component	mM
Tris-HCl, pH 8.5	25
Glycine	192
2-propanol	5%

Phosphate buffered saline (PBS)

All components were dissolved in 1l ddH₂O water and stored at room temperature.

Table 22: 1x PBS buffer

Component	mM
NaCl	137
KCl	2.7
Na ₂ HPO ₄	10
KH ₂ PO ₄	1.8

2.6. Cultivation of cyanobacteria

N. punctiforme and its *amiC2* mutant variant were cultivated in liquid and solid BG11 or BG11₀ medium whereas Neomycin was added to cultures and agar plates of the *amiC2* mutant. Freshly inoculated liquid cultures were grown under microaerophilic and low light conditions. When the cultures were in exponential growth phase, or the optical density reached 0.4, cultures were exposed to constant illumination with 30 μ E at 28°C, slightly shaken at 300 rpm. Biomass upscaling to 700 ml culture volume was carried out in bottles with a working volume of 800 ml. Generally, a 50 ml densely grown culture was used as inoculum, reaching approximately an OD_{750nm} of 0.2. The cultures were continuously bubbled with 2% CO₂ enriched air. Light intensity was increased from 30 to 50 μ E depending on the optical density of the culture. Wild-type strains were cultivated on BG11₀ agar plates whereas the *amiC2* mutant of *N. punctiforme* was grown on BG11 agar plates at 28°C under constant illumination with 10 - 20 μ E.

2.7. Cultivation of *E.coli*

Precultures of *E. coli* strains, harbouring different plasmids, contained 10 ml LB-medium in glass tubes and were inoculated by a single colony. The cultures were incubated overnight at 37°C and 180 rpm. Antibiotics were added according to Table 24. The cultures were subsequently used to inoculate main cultures for protein expression or harvested to isolate plasmids.

Protein expression was carried out in different growth media: *E. coli* Lemo21 (DE3) pGEX-4-T *amiC2cat* (expressing GST-tagged proteins) was grown in autoinduction medium whereas *E. coli* Lemo21 (DE3) pET28a-His8x-*amiC2cat* (expressing His-tagged proteins) was cultivated in TB medium. Main cultures, consisting of 500 ml autoinduction or TB medium in 2l baffled flasks, were inoculated to an OD_{600nm} of 0.01. Cultures in autoinduction medium were grown for three days at 20°C and 110 rpm. Whereas *E. coli* cultures, in TB medium, were grown at 37°C and 110 rpm, until the OD_{600nm} was reached 0.6 to 0.8. Thereafter, 0.5 mM IPTG was added to induce protein expression, and cultivation was continued at 30°C and 110 rpm overnight.

In general, *E. coli* strains were cultivated on LB-agar plates and were grown overnight at 37°C.

2.8. Molecular genetic methods

2.8.1. Oligonucleotides

Table 23: Oligonucleotides. Nucleotide exchanges in the sequence of site-directed mutagenesis (SDM) primers are underlined. DNA sequence of the *amiC2* gene was amplified from genomic DNA from *N. punctiforme* ATCC 29133 and used as template in PCR. All plasmids contained exclusively sequence of the catalytic domain from *amiC2* (*amiC2cat*).

Number	Name	Purpose	Sequence (3'-5')
1641 fw	F564A	SDM-PCR	CCGCAAAGCCAGAG <u>CGT</u> TACGTTCTCAGG
1642 fw	F564S	SDM-PCR	CCGCAAAGCCAGAAGCTACGTT <u>CT</u> CAGG
1643 rv	F564	SDM-PCR	GTTCTCGGTTTTTATTGATGATCGATGTTTTGCAGAATA
1646 rv	R568	SDM-PCR	GCGGGCTTTGCGGGTTCCTC
1647 fw	R563D R568D	SDM-PCR	CCGCAAAGCCGATTTCTACGTTCTCGATAAAAGCTC
1648 fw	S518A	SDM-PCR	CAGCATTACGCTAATG <u>CGG</u> TTGACAATCG
1649 rv	S518	SDM-PCR	ACAAATGCAGTTGCATTAACCTCGCTCGGCAATTC
1650 fw	E529A	SDM-PCR	CGCCCTGATGTGAATGGGTTAG <u>CGG</u> TATATTATTACG
1651 rv	E529	SDM-PCR	ATTGTCAACAGAATTAGCGTGAATGCTGACAAATGC
1681 fw	R563A R568A	SDM-PCR	GAACCCGCAAAGCCGCGTTCTACGTTCTCGCGAAAAGC TC
1745 fw	L576A	SDM-PCR	CCCTCGATTG <u>CGG</u> TAGAAACAG
1746 rv	L576	SDM-PCR	CATAGAGCTTTTCTGAGAACGTAGAATC
1752 fw	L576S	SDM-PCR	CCCTCGATTAG <u>CGG</u> TAGAAACAG
1753 fw	V519T	SDM-PCR	ACGCTAATTCTA <u>CCG</u> ACAATCG
1754 rv	V519	SDM-PCR	GAATGCTGACAAATGCAGTTGCATTAACCTC
1755 fw	D520A	SDM-PCR	ACGCTAATTCTGTTG <u>CGA</u> ATCG
1756 fw	E529Q	SDM-PCR	CGCCCTGATGTGAATGGGTTA <u>CAGG</u> TATATTATTACG
1757 fw	F564V	SDM-PCR	CCGCAAAGCCAGAGTGTACGTTCTCAGG
1758 fw	F564T	SDM-PCR	CCGCAAAGCCAGA <u>ACCT</u> ACGTTCTCAGG
1888 fw	E578A	SDM-PCR	CGATTTTAGTAG <u>CC</u> ACAGGTTATATG
1889 rv	E578	SDM-PCR	AGGGCATAGAGCTTTTCCTG
995 fw	pGEX-4T-3	Sequencing	AGAGCGTGCAGAGATTC

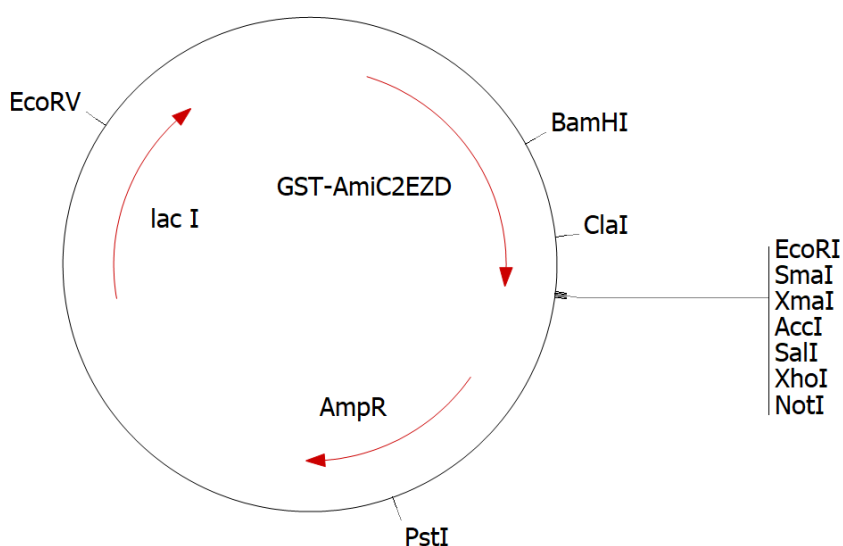
Number	Name	Purpose	Sequence (3'-5')
1000 rv	pGEX-4T-3	Sequencing	GGAGCTGCATGTGTCAGAG
1079 fw	pGEX-4T-3- <i>amiC2cat</i>	PCR	GCGGCACTCGACAGAATTGG
1080 rv	pGEX-4T-3- <i>amiC2cat</i>	PCR	CCTATGCCTACAGCATCCAG
1884 fw	pET28a <i>amiC2cat</i>	Gibson cloning	CATCATCATCATCATCACCATCATAGCAGCGGCCTGGTGC CCGCGCGGCAGCGGGAAATTACTAGTTGTG
1885 rv	pET28a <i>amiC2cat</i>	Gibson cloning	GCGACCCATTTGCTGTCCACCAGTCATGCTAGCCATATG TTAACGCTGTAAGTATTTTAGG
1939 fw	pET28a	Sequencing	CACGATGCGTCCGGCGTAGAGG
1940 rv	pET28a	Sequencing	GATCCGCGACCCATTTGCTG
2219 fw	GGGS	PCR	CGGCGGCGGCAGCAGCGGCCTGGTGCCG
2220 rv	GGGS	PCR	CTGCCGCCCATGATGGTGATGATGATGATGATGGCT GCTGC

2.8.2. Plasmids

Table 24: Plasmids. The plasmids, pGEX-4T-3 and pET28a (+), contain a thrombin cleavage site between the affinity tag and the *amiC2* sequence. A GGS amino acid linker was introduced into pET28a, between the His8x tag and the *amiC2* sequence. Amp = Ampicillin; Kan = Kanamycin

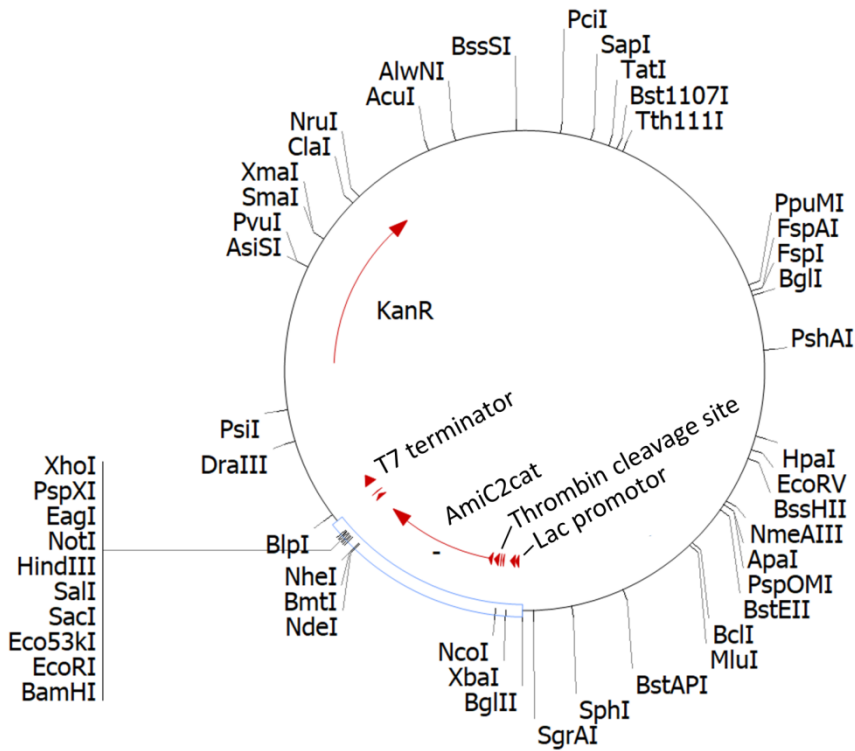
Plasmids	Resistance	Tag	Reference
pGEX-4T-3- <i>amiC2cat</i> (pIM 629)	Amp	N-term GST	Büttner et al. (242)
pET28a (+)	Kan	C and N-term His6x	Addgene
pET28a His8x- <i>amiC2cat</i>	Kan	N-term His8x	This work
pET28a His8x-GGS- <i>amiC2cat</i>	Kan	N-term His8x	This work

Plasmid pGEX-4T-3-*amiC2cat* (pIM 629)



EcoRV, BamHI, ClaI and PstI contain restriction sites for restriction enzymes. A repressor protein is encoded by *lacI*, which suppresses expression of *amiC2cat* (EZD on plasmid card) until IPTG is added. AmpR encodes the ampicillin resistance. A multiple cloning site with seven restriction sites is also represented on the map.

Plasmid pET28a His8x-amiC2cat



Multiple restriction sites on the plasmid as well as a multiple cloning site. KanR encodes for kanamycin resistance. The catalytic domain is cloned into NdeI restriction site with an N-terminal His-tag and a thrombin cleavage site for the enzymatic removal of the His-Tag after purification.

2.8.3. Polymerase chain reaction

Amplification of DNA sequences was performed by the polymerase chain reaction using either the Q5 High-Fidelity DNA Polymerase (New England BioLabs Inc.) or the Taq DNA Polymerase (Sigma-Aldrich). Protocols and PCR conditions are summarized in the tables listed below:

Table 25: Q5-PCR.

Component	50 µl total volume
5x Q5 Reaction Buffer	10 µl
Q5-polymerase	0.5 µl
10 mM dNTPs	1 µl
10 µM fw primer	2.5 µl
10 µM rv primer	2.5 µl
<1 ng template DNA	variable
Nuclease-free water	variable

Table 26: Q5-PCR conditions.

Step	Temp	Time
Denaturation	98	2 min
Denaturation	98	30 s
Annealing	variable	30 s
Extension	72	variable
Extension	72	2 min

} 30x

Table 27: Colony-RedTag-PCR.

Component	50 µl total volume
2x RedTag Master mix	25 µl
10 µM fw primer	2.5 µl
10 µM rv primer	2.5 µl
Template DNA	colony
Nuclease-free water	20µl

Table 28: RedTag-PCR conditions.

Step	Temp	Time
Denaturation	94	10 min
Denaturation	94	30 s
Annealing	variable	30 s
Extension	72	variable
Extension	72	2 min

} 30x

2.8.4. Gibson Cloning

The interaction between AmiC2cat and peptidoglycan was analysed using different experimental procedures, which required the presence of a His-tag. Therefore, the sequence of the catalytic domain was incorporated into the plasmid pET28a (+) by Gibson cloning. This method allows the fast assembly of multiple overlapping DNA fragments, without the need for extensive restriction enzyme digestions.

First, pET28a (+) was overproduced in *E. coli* Lemo21 (DE3) and isolated using the Monarch Plasmid Miniprep Kit according to the manufacturer's instructions. Afterwards, pET28a (+) was digested by NdeI overnight (Table 29), and purified by chloroform extraction and dialysis against water, according to standard procedures. In parallel, the sequence of the catalytic domain was amplified by Q5-PCR using pGEX-4T-3 *amiC2cat* as template and the primer pair 1884 and 1885 (see Table 25 and Table 26 for PCR conditions) to yield overlapping parts with the NdeI linearized plasmid pET28a (+). The PCR product was gel-purified and extracted using the Monarch DNA Gel Extraction Kit.

Specific amounts of the linearized plasmid and the PCR amplified *amiC2cat* sequence, calculated by the program PlasmidMaster (see chapter 2.3), were added to 15 µl of Gibson Mix (Table 30). The reaction mixture was incubated for 1h at 50°C. Afterwards, the mixture was extracted by chloroform and dropped onto a Type-VS Millipore membrane (MF type, VS filter, 0.025 µm, Millipore, Inc), which was placed into a Petri dish filled with ddH₂O. Dialysis was performed for 30 min at room temperature. A total of 10 µl was used for transformation into electro-competent *E. coli* DH10β cells.

Table 29: NdeI-restriction enzyme digestion.

components	20 µl total volume
10 x CutSmart buffer	2 µl
NdeI	1 µl
>20 ng template DNA	variable
Nuclease-free-water	variable

Table 30: Preparation of the Gibson-Mastermix.

components	1.2 ml total volume
5x Isothermal Master Mix	320 µl
T5 exonuclease (10 U/µl)	0.64 µl
Phusion DNA-Polymerase (2 U/µl)	20 µl
Taq DNA Ligase (40 U/µl)	160 µl
Nuclease-free-water	860 µl

2.8.5. Site-directed mutagenesis

Substitution of specific amino acids in the active site of AmiC2 from *N. punctiforme* occurred through site-directed mutagenesis. Forward and reverse primer pairs were designed to anneal back to back by their 5' ends, whereas the forward primer carried the substitution, as represented in Table 23. The plasmids pGEX-4T-3 and pET28a (+), carrying the sequence of the catalytic domain of *amiC2* from *N. punctiforme*, were enriched and isolated using the Monarch Plasmid Miniprep Kit. Further purification included chloroform extraction and dialysis against water for 30 min at room temperature. The purified plasmids were amplified by PCR using the appropriate primer pairs. In that way, distinct nucleotides in the *amiC2*cat sequence were exchanged. The PCR product was digested overnight by DpnI and purified, as previously described in 2.8.4, by extraction and dialysis. The linear plasmid was transformed into electro-competent *E. coli* DH10 β cells (see chapter 2.8.6 for transformation). In an alternative way, the linear plasmid was circularized and transformed into chemical competent NEB *E. coli* DH5 α cells according to the Q5 Site-directed Mutagenesis Kit (New England BioLabs, Inc., Ipswich, USA).

2.8.6. Transformation of electro or chemical competent cells

Circular or linear plasmids were transformed into electro competent *E. coli* DH10 β or *E. coli* Lemo21 (DE3) cells (244). Electroporation cuvettes, with 2 mm gap size, were cooled on ice, and filled with 50 μ l electro-competent *E. coli* cells and 0.1 - 0.5 μ l of plasmids or 10 μ l of Gibson assembled plasmids. Electroporation was carried out with the following parameters: 2.5 kV, 25 μ F and 200 Ω . Subsequently, one millilitre LB-medium, pre-warmed at 37°C, was added. The cells were transferred into a reaction tube and incubated for about 1h at 37°C. The whole millilitre was streaked onto LB-agar plate, supplemented with the appropriate antibiotics, in the case of Gibson assembled plasmids. Otherwise, 50 or 100 μ l of freshly transformed cells in LB medium were plated onto LB-agar plates, supplemented with antibiotics.

Transformation of plasmids into chemical competent cells was performed as described in the manual for the Q5 Site-Directed Mutagenesis Kit (New England BioLabs, Inc., Ipswich, USA).

2.9. Biochemical methods

2.9.1. Protein determination

The purple complex formation of bicinchoninic acid (BCA) with Cu⁺-ions is widely used to determine protein concentrations. Cu²⁺ ions are reduced to Cu⁺ ions in the presence of proteins under alkaline conditions. BCA forms stable complexes with the reduced copper ions, which leads to an increase in absorbance at 562 nm. A calibration curve of BSA was used to calculate the protein concentration ranging from 0, 62.5, 125, 187.5 to 250 μ g/ml. Proteins were diluted in 40 μ l appropriate buffer or ddH₂O in triplicates. Subsequently, 800 μ l of a 1:50 mixture of BCA reagent (Thermo Fisher Scientific, Waltham, USA) and 4% (w/v) CuSO₄ were added to the calibration and protein samples. All samples were incubated at 60°C for 30 min. Absorbance was spectrophotometrically measured at 562 nm.

2.9.2. SDS-PAGE (Laemmli, 1970 (251))

A common procedure to determine the purity of protein fractions or to separate complex protein samples is the SDS-polyacrylamide gel electrophoresis (SDS-PAGE). In this work, proteins were

separated using a discontinuous gel electrophoresis under denaturing conditions according to Laemmli, 1970 (251). The proteins were first solubilized in SDS-sample buffer at 96°C for 5 min and subsequently applied onto a 5% SDS-polyacrylamide stacking gel. The separation of proteins occurred through a 15% SDS-polyacrylamide running gel, supplemented with 8 M urea where stated, in a TRIS-Glycine buffer system. SDS-PAGE ran for 30-60 min at 100V. The gel was stained for 15 min at room temperature or overnight at 4°C in a ready-to-use InstantBlue solution (Expedeon, 4basebio, Heidelberg, Germany) based on coomassie staining.

Table 31: SDS-PAGE sample buffer

Substance	amount
Tris-HCl pH 6.8	60 mM
SDS	2%
glycerol	10%
β-mercaptoethanol	5%
bromophenol blue	0.01%

Table 32: SDS-PAGE running buffer

Substance	M
Tris	0.125 M
Glycine	0.96 M
SDS	0.5%

Table 33: Composition of SDS-polyacrylamide gel

Components	15% running gel [10 ml]	5% stacking gel [5 ml]
H ₂ O	2.3 ml	3.4 ml
ROTIPHORESE®Gel 30 acrylamide/bisacrylamide (37.5:1)	5 ml	830 µl
1.5 M Tris/HCl pH 8.8	2.5 ml	-
1.0 M Tris/HCl pH 6.8	-	630 µl
10% (w/v) SDS	100 µl	50 µl
10% (w/v) APS	100 µl	50 µl
TEMED	10 µl	5 µl

2.9.3. Western blot

The detection of AmiC2cat proteins occurred through western blot analysis using polyclonal antibodies against the C-terminal part of AmiC2. Proteins were separated by SDS-PAGE, as described in the previous subsection, and transferred to a PVDF membrane (Immobilon®-P PVDF, Merck Millipore, Burlington, USA). Briefly, the PVDF membrane was activated for 10 min in pure ethanol or methanol and subsequently equilibrated for 10 min in Friendly-Towbin buffer (see chapter 2.5). Two thick and thin Whatman filter papers were as well separately soaked in Friendly-Towbin buffer for 10 min. The SDS-polyacrylamide gel was rinsed with ddH₂O and washed, for 10 min, in Friendly-Towbin buffer. A thick Whatman filter paper was placed onto the anode site of a semidry western blot system (PerfectBlue™, VWR PeqLab, Radnor, USA), followed by a thin Whatman filter paper, the PVDF membrane, the SDS-polyacrylamide gel, a thin and a thick Whatman filter paper. The semidry western blot apparatus was fully assembled and properly closed. Transfer of the proteins onto the PVDF membrane occurred at 30 V for 30 min. After blotting, the PVDF membrane was incubated for 1h in 1x PBS buffer (see chapter 2.5) supplemented with 0.1% (v/v) Tween20 and 5% (w/v) dry milk at room temperature. Subsequently, the PVDF membrane was transferred into a 50 ml Falcon tube and 3 ml 1x PBS buffer containing 0.1% Tween20, 0.5% dry milk and 1/500 polyclonal antibodies against AmiC2cat (242, 244) were added. Incubation was carried out at 4°C overnight. On the next day, the PVDF-membrane was washed three times in 10 ml 1x PBS buffer supplemented with 0.1%

Tween20 and 0.5% dry milk each for 20 min. Afterwards, 3 ml of the same buffer containing additionally (1/10000) horseradish peroxidase conjugated secondary antibody (Sigma-Aldrich, St. Louis, USA) was filled into the tube. After 2h at room temperature, the membrane was washed four times with 1x PBS supplemented with 0.1% Tween20 and twice with ddH₂O water. The PVDF membrane was put, protein side up, into a box and 1 ml Lumi-Light (1:1 mixture, Pierce ECL western blotting substrate, Thermo Scientific), sufficient for 10 lanes, was added. After 5 min, luminescence was recorded (Gel Logic 1500 Imaging System, Kodak MI , see chapter 2.3).

2.9.4. Determination of SDS (Hayashi, 1975 (252))

The Hayashi method is an experimental procedure to determine the concentration of the detergent sodium dodecyl sulfate (SDS). SDS forms a water insoluble complex with methylene blue, which is easily extracted by chloroform. One microliter of the sample is mixed with 495 μ l of 0.7 mM sodium phosphate buffer, pH 7.2 and 5 μ l methylene blue. The suspension is mixed for 30s and the aqueous and organic phases will immediately separate. SDS is present if the chloroform phase turns bluish. It is possible to determine absolute amounts of SDS by measuring the absorbance at 655 nm using a calibration curve of different SDS concentrations.

2.9.5. Protein-interaction assays

Microscale thermophoresis (MST)

Microscale thermophoresis (MST) detects biomolecular interactions by ligand induced changes in the directed movement and fluorescence of molecules in a temperature gradient. Fluorescently labelled molecules and putative ligands are filled into thin glass capillaries and a temperature gradient is induced by an infrared laser. The movement of the labelled molecule alongside the gradient, also termed thermophoresis, is altered by an interaction with the putative ligand. The temperature change also affects the fluorescence intensity of the labelled molecule. This effect is known as temperature related intensity change (TRIC) and depends on the chemical environment of the molecule that is changed upon ligand binding. Thermophoresis and TRIC determine the overall MST signal plotted against the ligand concentration. The resulting curve provides insights into the binding affinity of the ligand to the labelled molecule.

His-tagged proteins were fluorescently labelled using the Monolith His-Tag Labeling Kit RED-tris-NTA from Abcam. The fluorescent dye was added to a protein fraction and incubated for 30 min at room temperature. Protein aggregates and other non-soluble substances were removed by centrifugation (10 min, maximum speed). Peptidoglycan was digested by 10 U mutanolysin (Sigma-Aldrich, St. Louis, USA) for 16 h at 37°C. Soluble muropeptides were enriched by evaporation and titrated in sodium phosphate buffer, containing different supplements as stated elsewhere, until 16 dilutions were prepared. Fluorescently labelled protein was added to each muropeptide dilution and filled into a standard glass capillary. All capillaries were put into slots of a sample tray and the MST experiment was started using the following conditions:

Table 34: Parameters for MST-measurements. LED (%) indicates the power used for fluorescence excitation. MST (%) represents the infrared laser (IR)-laser power.

LED [%]	MST [%]	Fluor. Before [s]	MST on [s]	Fluor. After [s]	Delay [s]
60	40	5	30	5	5

The fluorophore was excited using the red LED colour from the Green/Red type of the Monolith NT.115 device (NanoTemper, Munich, Germany). The MST-measurement was performed at room temperature. Data analysis occurred through the software NT Analysis v.1.5.41.

Surface plasmon resonance based BIAcore X biosensor system

Putative Interactions between AmiC2cat and peptidoglycan were carried out using a surface plasmon resonance (SPR)-based BIAcore X biosensor system (GE Healthcare). His-tagged proteins (200 nM) were immobilized onto a Ni-NTA sensor chip in flow chamber 2, with a flow rate of 15 μ l/s, whereas chamber 1 (without Ni²⁺) was flushed exclusively with 50 mM sodium phosphate buffer supplemented with 150 mM NaCl. Peptidoglycan was digested by 10 U mutanolysin (Sigma-Aldrich, St. Louis, USA) for 16h at 37°C to release soluble muropeptides. These were captured by centrifugation and injected into both flow chambers, with a flow rate of 15 μ l/s. The difference between both flow cells represents a specific binding of muropeptides to the immobilized AmiC2cat.

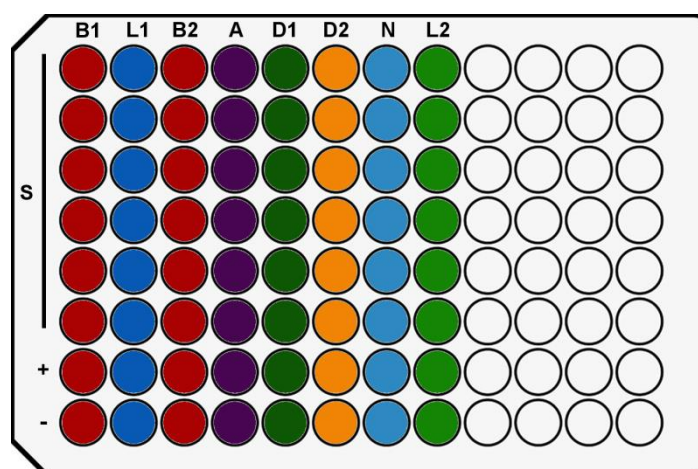
Biolayer interferometry by OctetK2

The OctetK2 (FortéBio, Fremont, USA) uses a label-free technique based on biolayer interferometry (BLI). It analyses the interference of white light reflected from two surfaces. The first layer represents the biosensor tip that harbours immobilized proteins. The second one functions as an internal reference layer. The biosensor is dipped into an aqueous solution containing the putative ligand. An interaction between the protein and the ligand changes the interference pattern of the measured white light. A shift in interference upon binding reflects the level of binding or interaction (illustrated in Fig. 36A). The experiment was carried out in 96 well plates (non-binding, black and flat bottomed chimney style microplates from Greiner Bio-One). The Ni-NTA biosensors were equilibrated for 10 min in 50 mM sodium phosphate buffer, pH 8 supplemented with 150 mM NaCl for at least 10 min, prior to each experiment. Peptidoglycan was homogenised in 50 mM sodium phosphate buffer, pH 8 supplemented with 150 mM NaCl by sonication until an optical homogenous suspension was reached. Subsequently, peptidoglycan was adjusted to an OD_{600nm} between 0.5 and 1, and used for the BLI-measurement.

The experiments started with a 100 s long baseline step in 50 mM sodium phosphate buffer, pH 8 supplemented with 150 mM NaCl. His-tagged proteins (50-200 nM) were loaded within 300 s onto the Ni-NTA biosensor tip and washed for 100 s in 50 mM sodium phosphate buffer, pH 8 supplemented with 150 mM NaCl. The protein-loaded biosensor subsequently dipped into wells containing peptidoglycan, which was dissolved in the same buffer as was used for the second baseline step. After 600 s of association, dissociation was carried out, for further 600 s, in 50 mM sodium phosphate buffer, pH 8 supplemented with 150 mM NaCl. The Ni-NTA biosensors could be recovered and reused 3-4 times by washing them 3 times first in glycine, pH 1.7 and then in 50 mM sodium phosphate buffer, pH 8 supplemented with 150 mM NaCl. The biosensors were loaded again with Ni²⁺ for 60s. All assay steps were performed at 30°C and 1000 rpm. Acquired data were analysed by Data Analysis HT software (see chapter 2.3).

Table 35: Octet measurement. The list below represents the sequence of all assay steps and their designated wells on a 96 well plate. + = positive control; - = negative control.

Step	Abbr.	code	Time [s]	Sample (S)
Baseline1	B1	Red	100	Buffer
Loading1	L1	Blue	300	Protein
Baseline2	B2	Red	100	Buffer*
Association	A	Purple	600	Peptidoglycan
Dissociation1	D1	Yellow	600	Buffer*
Dissociation2	D2	Dark Green	5	Glycine, pH 1.7
Neutralization	N	Light Blue	5	Buffer
Loading2	L2	Green	60	Ni ²⁺



Peptidoglycan-binding assay

SDS-PAGE analysis was performed to determine the binding between AmiCcat and its mutant variants to peptidoglycan. Purified peptidoglycan from *Anabaena* was adjusted to an OD_{600nm} of 1 in 50 µl 50 mM sodium phosphate buffer, pH 8 supplemented with 150 mM NaCl. Proteins were added up to an end concentration of 1-2 µM. Proteins were omitted for the negative control. Incubation occurred at room temperature for at least 30 min. Peptidoglycan was collected by centrifugation at maximum speed for 10 min and washed once in 50 µl 50 mM sodium phosphate buffer, pH 8 supplemented with 150 mM NaCl. The peptidoglycan pellet was dissolved in 60 µl SDS-sample buffer (see Table 31) and heated up at 96°C for 5 min. The supernatants from the first and second centrifugation step were as well adjusted to 60 µl with SDS-sample buffer and boiled for 5 min at 96°C. A total of 20 µl of each sample was loaded onto a 15% SDS-polyacrylamide gel (see Table 33). SDS-PAGE (see chapter 2.9.2) was carried out for 1-2h at 100V. The SDS-polyacrylamide gel was stained for 10 min at room temperature or overnight at 4°C in InstantBlue staining solution.

2.9.6. Monitoring AmiC2cat hydrolytic activity

Dye-release assay (DRA)

The influence of site-specific mutations on the hydrolytic activity of AmiC2cat was determined by the Dye-release assay according to Zhou et al. (253) with minor modifications. *E. coli* peptidoglycan was isolated and purified according to Büttner et al. (242). *E. coli* peptidoglycan was incubated with 20 mM Remazol Brilliant Blue (RBB, Sigma Aldrich, St. Louis, USA) in 250 M NaOH overnight at 37°C.

Excess RBB-dye was removed by several washes with ddH₂O water until the supernatant was colourless. The pH of the reaction solution was first neutralized by the addition of HCl and subsequently filled into ultracentrifuge tubes for the Ti45 rotor. Ultracentrifugation was performed with 30.000 rpm, or 30 min at room temperature.

The RBB-labelled *E. coli* peptidoglycan was adjusted to an OD_{600nm} of 2 in ddH₂O water. For each experimental approach, 50 µl of RBB-labelled *E. coli* peptidoglycan were washed with 50 mM sodium phosphate buffer, pH 8 supplemented with 150 µM NaCl and dissolved again in 50 µl 50 mM sodium phosphate buffer, pH 8 supplemented with 150 µM NaCl. Proteins were added to a final concentration of 0.5 to 4 µM. Incubation took place at 37°C and for 30 min or 1-2h (depending on the protein concentration). Protein was omitted for the negative control. The reaction was stopped by heating at 99°C for 10 min and protein was precipitated by addition of 50 µl 20% (w/v) TCA. Reaction mixture was incubated for 10 min at 4°C. Subsequently, the peptidoglycan was removed by centrifugation and the absorbance of the supernatant was measured at 595 nm.

Activity assay using OPA-derivatization

The fluorescent dye o-phthaldialdehyde (OPA) reacts with primary amines and is therefore widely used in the analysis of amino acids, peptides or proteins. The catalytic domain of AmiC2 releases peptide stems from the glycan backbone by hydrolysing the amide bond between MurNAc and alanine. The released peptide stems can be captured by OPA, which enables detection via fluorescence or absorbance at 340 nm. Here, the protocols according to Prigozhin et al. (254) and Darrouzet-Nardi et al. (255) were combined to detect OPA-derivatized PGN peptides by fluorescence.

Nostoc peptidoglycan was homogenized by sonication and adjusted to an OD_{600nm} of 2 in 50 mM sodium phosphate buffer, pH 8 supplemented with 150 mM NaCl. One millilitre of this peptidoglycan suspension was incubated with 1-4 µM enzymes at 37°C. Several samples were removed during 24h and first heat inactivated, at 95°C for 5 min, and subsequently centrifuged to remove undigested peptidoglycan, at maximum speed in a table centrifuge for 10 min. Thereafter, the supernatant was transferred into an Amicon Ultra 0.5 ml filter device with a cut off of 10 kDa. The supernatant was diluted in 50 mM sodium phosphate buffer pH 8, supplemented with 150 mM NaCl in a total volume of 50 µl and was mixed with 50 µl OPA-solution. The OPA reagent was prepared as described in Darrouzet-Nardi et al. (255). Briefly, 2.5 mg OPA (Thermo Fisher Scientific, Waltham, USA) were dissolved in 250 µl methanol p.A. and added to 10 ml 20 mM borate buffer pH 9 (see chapter 2.5) supplemented with 5 µl mercaptoethanol. Fluorescence was recorded by a Tecan reader in black 96 well plates (non-binding, black and flat bottomed chimney style microplates from Greiner Bio-One) with an excitation wavelength of 360 nm and an emission wavelength of 460 nm.

Alanine was titrated in 50 mM sodium phosphate buffer, pH 8 supplemented with 150 mM NaCl to obtain 10, 5, 2.5 and 1.25 µM concentrations for a calibration curve. The OPA reagent and the alanine solutions were mixed 1:1 and fluorescence was monitored as described previously.

2.10. Analytical methods

2.10.1. High Performance liquid chromatography (HPLC)

High performance liquid chromatography (HPLC) was used, on the one hand, to purify and separate mutanolysin released PGN fragments, and, on the other hand, to analyse amino acids derived from PGN.

Muropeptides were purified by an Infinity II HPLC device from Agilent, Santa Clara, USA, using a linear acetonitrile gradient (see Table 38 and Table 39 for LC method and solvents) with the following modification: Formic acid was used as ion pairing agent instead of TFA and a flow rate of 2.5 ml/min was used. The semi preparative, reversed-phase column Kinetex (5 μ m, C18, 100A, 250 x 10 mm) was used for muropeptide separation.

PGN derived amino acids were analysed by an HPLC HP1090 M device (Hewlett Packard, Palo Alto, USA) equipped with a diode array detector (detection: 340 nm, reference: 550 nm). OPA-derivatized amino acids (obtained by pre-column derivatization with o-phthalaldehyde from Dr. Maisch, Ammerbuch, Germany) were separated by a C18 reverse-phased ReproSil[®] OPA column (5 μ m, 150 x 4 mm, Dr. Maisch GmbH, Ammerbuch, Germany) connected to a pre-column (5 μ m, C18, 10 x 4 mm, Dr. Maisch GmbH, Ammerbuch, Germany) with a flow rate of 1.1 ml/min using a sodium phosphate gradient (see Table 36 for HPLC method and Table 37 for solvents). Data were analysed by ChemStation for LC 3D, Rev. A.08.03, Agilent Technologies.

Table 36: HPLC method.

Time [min]	Solvent B [%]
0 - 2.5	0
2.5 - 12	50
12 - 18	60
18 - 24	100
24 - 28	100
28 - 29	0

Table 37: Composition of HPLC solvents. THF = Tetrahydrofuran; ACN = acetonitrile; MeOH = Methanol

	A	B
25 mM sodium phosphate buffer pH 7.2	99.15%	50%
THF	0.75%	0%
ACN	0%	15%
MeOH	0%	35%

2.10.2. Mass spectrometry

Compositional analysis of peptidoglycan fragments was performed using an Acquity ultra performance liquid chromatography (UPLC) system coupled to Time-of-Flight mass spectrometry and electrospray ionization (SynaptG2, Waters) at the Core Facility from the Center for Plant Molecular Biology, University of Tübingen. A reversed-phase ACQUITY UPLC CSH C18 column was used for all measurements with the following dimensions: 130Å, 1.7 μ m, 2.1 mm X 100 mm. The mass spectrometer (MS) was set to positive electrospray ionization (ESI) mode with a scan range between 50 and 2000 Da. The column temperature was set to 52°C. Further MS settings corresponded to those from Kühner et al. (256).

Muropeptides were separated using a linear acetonitrile gradient with a flow rate of 0.176 ml/min according to the conditions described in the tables below.

Table 38: LC-MS method.

Time [min]	Solvent B [%]
0-2	2
2-70	15
70-72	100

The analysis of HPLC purified muropeptide fractions was performed by HPLC-HR-MS/MS (Dionex UltiMate 3000, Thermo Scientific and maXis, Bruker) coupled to ESI-QTOF and a HCD collision cell. The mass range was set from 45-1255 Da. The Nucleoshell column from Macherey-Nagel was used with the following dimensions: C18, 130 Å, 2.7 µm, 2.0 mm x 150 mm. Muropeptide fractions (3 µl) were loaded onto the column with a flow rate of 0.3 ml/min.

Table 40: LC-MS method.

Time [min]	Solvent B [%]
0-20	10-100

Table 39: Composition of LC-MS solvents. Trifluoroacetic acid (TFA) was use as ion pairing agent. ACN = acetonitril

	A	B
TFA	0.1% TFA	0.1% TFA
ACN	0%	100%

Table 41: Composition of LC-MS solvents. Formic acid (TFA) was use as ion pairing agent.

	A	B
FA	0.1% FA	0.1% FA
MeOH	0%	100%

Tryptic digests were analysed by Tandem mass spectrometry coupled to ESI in the Proteom Core Facility, University of Tübingen.

Table 42: LC-MS method.

Time [min]	Solvent B [%]
0	2
0-36	20
36-73	33
73-76	50
76-79	90
79-87	90

Table 43: Composition of LC-MS solvents. Formic acid (TFA) was use as ion pairing agent. ACN = acetonitril

	A	B
FA	0.1% TFA	0.1% TFA
ACN	0%	80%

2.11. Compositional analysis of peptidoglycan

2.11.1. Amino acid analysis

Isolated, pure peptidoglycan fractions were dissolved in 300 µl ddH₂O water in HPLC glass vials and 1 ml 6 M HCl (for amino acid analysis, Sigma-Aldrich) supplemented with 0.4% β-mercaptoethanol and 0.2% sodium azide were added. Reaction mixture was immediately flash frozen in liquid nitrogen and degassed with Argon. HPLC vials were closed with butyl stoppers and aluminium caps. Acid hydrolysis was carried out at 110°C for 24h. Afterwards, hydrolysates were transferred into reaction tubes in a vacuum desiccator over NaOH and evacuated for 1h with the help of a vacuum pump. HCl was evaporated under vacuum for 2 days. Neutralized hydrolysates were centrifuged and supernatants were transferred into new HPLC glass vials for HPLC analysis (2.10.1).

2.11.2. Release of mucopeptides for HPLC and LC-MS

Peptidoglycan was dissolved in 500 μ l 50 mM MES buffer, pH 6 supplemented with 1 mM $MgCl_2$ to an OD_{600nm} of 3 (higher OD values prevent mutanolysin digestion). Mutanolysin (40 U) was added to the peptidoglycan suspension and incubated for 16h at 37°C. Afterwards, reaction was heat inactivated at 95°C for 5 min and centrifuged for 10 min at maximum speed in a table centrifuge. Supernatant was transferred into a new reaction tube and 100 μ l 10 mg/ml sodium borohydride in 0.5 M tetraborate buffer, pH 9.0 was added. Incubation occurred at room temperature for 20 min and was stopped by the addition of 10 μ l phosphoric acid. The pH was adjusted between 2 and 3 with phosphoric acid. Reduced mucopeptides were transferred into HPLC vials and subjected to LC-MS or HPLC (2.10.1 and 2.10.2).

Measured m/z ratio and proposed sum formula for all ions measured by LC-MS were given by the software Data Analysis (Bruker Daltonics). Mucopeptide structures were drawn with the help of ChemDraw to obtain the sum formulas and m/z for each putative mucopeptide. The smaller the difference between measured and calculated m/z, the higher the likelihood of a true mucopeptide identification. MS/MS of fragmented parent ions was performed to verify the putative mucopeptide structure or composition.

2.12. Purification of AmiC2cat and its mutant variants

2.12.1. Protein expression and cell lysis

AmiC2cat and its mutant variants were produced using the T7 expression system (257). The gene *amiC2cat* was cloned under the control of the T7-promoter from the plasmid pET28a (+) or pGEX-4T-3. Both plasmids were introduced into *E. coli* Lemo21 (DE3), which carries a chromosomal copy of the T7-RNA polymerase gene under a *lac*-promoter. The addition of lactose or IPTG induces the expression of the T7-RNA-polymerase which in turn transcribes the *amiC2cat* gene. *E. coli* Lemo21 (DE3) transformed with pET28a His8-*amiC2cat* was grown in TB-medium until an OD_{600nm} between 0.6 and 0.8. Protein expression was induced by the addition of 0.5 mM IPTG and cultivation was continued at 30°C overnight. On the next day, cells were harvested (Ja-10 rotor, 6000 rpm, Beckman centrifuge, 4°C 30 min) and washed once in 50 mM sodium phosphate buffer supplemented with 150 mM NaCl. The cell pellet was stored at -20°C.

Lactose-derived autoinduction was used for the production of GST-tagged proteins. The highest yield of recombinant protein expression was obtained three days after inoculation at 20°C. Cells were harvested as described previously and stored as well at -20°C.

A total of 5 g cells (wet weight) were dissolved in 40 ml 50 mM sodium phosphate buffer containing additionally 150 mM NaCl, 1% Tween20, 5% glycerol and one tablet of protease inhibitors (cComplete™ Protease Inhibitor Cocktail, Roche). Cells were disrupted by sonication (3x 3 min, output 4, duty cycle 40, Branson Sonifier). Cell debris were removed by centrifugation (JA25.50 rotor, Beckman centrifuge) at 50.000xg for 1 h. DNase1 and 10 mM $MgSO_4$ were added to the supernatant and incubated on ice for 30 min. Subsequently, the supernatant was diluted twice in 50 mM sodium phosphate buffer supplemented with 150 mM NaCl and 5% glycerol and filtered through a PVDF membrane with a cut off of 0.22 μ M. The attachment of different tags on AmiC2cat and its mutant variants required different procedures for affinity chromatography, which are described in detail in the following subsection.

2.12.2. Affinity chromatography

Affinity chromatography using GSTrap HP columns and Benzamidin FF columns

Lysates were loaded onto GSTrap HP columns (GE Healthcare, Chicago, USA), equilibrated in GST-binding buffer (Table 17), with a flow rate of 0.5 ml/min at 4°C with the help of peristaltic pump. Protein loaded column was washed with 20 ml GST-binding buffers. Subsequently, 1 ml of a thrombin solution, containing 500 U thrombin (Sigma-Aldrich, St. Louis, USA), was subjected and on-column digestion occurred rotating at 4°C for 3 days. Alternatively, GST-tagged proteins were eluted with GST-binding buffer and digested by thrombin in solution for 3 days at 4°C. The thrombin digest was loaded onto a GSTrap column coupled to a Benzaminidase column, equilibrated in GST-binding buffer, with a flow rate of 0.5 ml/min. Protein fractions were stored in 50% glycerol at -20°C. Proteins were dialysed in dialysis tubes (cut off 3kDa) against buffer without glycerol for 24h for further use or treatment.

GSTrap columns were regenerated as described in the handbook “GST Gene Fusion System” (GE Healthcare) and Benzamidin FF columns were recovered according to the manual HiTrap Benzamidine FF (GE Healthcare). All columns were stored in 20% ethanol at 4°C.

Affinity chromatography using Zn²⁺-loaded Hitrap chelating columns or HisTrap columns

HiTrap chelating or HisTrap columns (GE Healthcare, Chicago, USA) were washed with 10 column volumes (CV) with buffer containing 20 mM sodium phosphate, pH 7.4, 0.5 M NaCl and 50 mM EDTA with a flow rate of 1 ml/min with the help of a peristaltic pump or using the ÄktaPurifier (GE Healthcare, Chicago, USA). Subsequently, 10 CV of HiTrap binding buffer (Table 19), without DTT, were loaded onto the column and rinsed afterwards with 10 CV ddH₂O water. The HiTrap column was charged with 0.5 ml ZnCl₂ whereas NiSO₄ was loaded onto HisTrap columns. Both metal loaded columns were immediately washed with 10 CV ddH₂O water and subsequently with 10 CV 20% ethanol for storage at 4°C.

Lysate was filled into a glass sample loop, connected to an ÄktaPurifier system, and automatically loaded onto a zinc or nickel loaded column, with a flow rate of 0.5 ml/min at 16°C. Column was washed with 10 CV HiTrap-binding buffer or until the UV signal, at 280 nm, was constant. An imidazole gradient, from 0-300 mM within 30 min and a flow rate of 0.5 ml/min, was applied and 1 ml elution fractions were collected. Protein fractions were stored in 50% glycerol at -20°C and dialysed in dialysis tubes (cut off 3kDa) against buffer, without glycerol, for 24h for further use or treatment.

2.12.3. Size exclusion chromatography

After dialysis, proteins were concentrated using VivaSpin50 centrifugal concentrators (PES membrane, MWCO = 10 kDa) to a volume of 500 µl and loaded onto a Superdex75 GL 10/300 column (GE Healthcare, flow rate 0.5 ml/min) equilibrated in 50 mM sodium phosphate buffer containing 150 mM NaCl and 5% glycerol using an ÄktaPurifier with detection at 280 nm (GE Healthcare). Proteins were eluted in the same buffer, diluted twice with glycerol and stored at -20°C.

2.13. Isolation and purification of peptidoglycan

The isolation of peptidoglycan was performed using three different protocols. The protocol according to dePedro et al. (258) was used by default for transmission electron microscopy and was optimized, in this work, to yield pure fractions of peptidoglycan for LC-MS-based analysis. The third protocol was developed by Kühner et al. (256) and results in a fast isolation and purification of peptidoglycan out of few cell material.

2.13.1. Modified dePedro et al protocol

Cyanobacterial cells were harvested for 10 min at 6000 rpm (JA10-rotor, Beckman Avanti), washed once in 5 M NaCl and stored at -20°C. Approximately 0.5 – 2 g cells (wet weight) were dissolved in 40 ml buffer containing 100 mM Tris-HCl, pH 6.8 and 150 mM NaCl. Suspension was dropped into 100 ml boiling 6% SDS in a 250 ml Schott flask that was put in a waterbath. After 4h boiling, the suspension was incubated at 37°C overnight and boiled again for 1h on the next day. Crude peptidoglycan was collected by ultracentrifugation at 30.000 rpm for 30 min (Ti45-rotor, Beckman ultracentrifuge, 40°C). The pellet was dissolved in 10 ml ddH₂O and dropped into 5 ml hot 6% SDS in a 100 ml Schott flask. After 2h, the crude peptidoglycan was again pelleted and dissolved in 8 ml ddH₂O. The suspension was again boiled for 2h in 6% SDS in a 100 ml Schott flask put into a water bath. Afterwards, SDS was removed by several washing steps with ddH₂O. Residual SDS in the peptidoglycan suspension was checked by the Hayashi method (described in chapter 2.9.4). The SDS-free PGN fraction was dissolved in 10 ml 100 mM Tris HCl pH 6.8, and 150 mM NaCl. Traces of DNase1 (Sigma-Aldrich, St. Louis, USA) and RNase (Carl Roth GmbH + Co, Karlsruhe, Germany) were added and incubated for 2h at 37°C. Trypsin (50 µg/ml, Carl Roth GmbH + Co, Karlsruhe, Germany) was added and reaction mixture was incubated overnight slightly shaking or stirring. On the next day, tryptic peptides were removed by boiling for 3 h in 5 ml 6% SDS. Extensive washing steps with ddH₂O followed to remove SDS from the peptidoglycan fraction. PGN pellet was stored at -20°C.

2.13.2. Optimized dePedro et al protocol

The isolation of peptidoglycan was optimized in the course of this work and is described here in detail: *Nostoc* cells were harvested for 10 min at 6000 rpm (JA10-rotor, Beckman Avanti), washed once in 5 M NaCl and stored at -20°C. Between 0.5 – 2 g cells (wet weight) were dissolved in 40 ml ice-cold buffer containing 100 mM Tris-HCl, pH 6.8 and 150 mM NaCl supplemented with 10 mM DTT. Cells were disrupted by sonication (burst 5, output 5) for 5 min and subsequently centrifuged for 30 min at 30.000 rpm (Ti45-rotor, Beckman ultracentrifuge, 4°C). The pellet was dissolved in 4 ml buffer consisting of 100 mM Tris-HCl, pH 6.8 and 150 mM NaCl supplemented with 10 mM DTT and 10 mM MgCl₂. A few crystals of DNase1 were added and the reaction mixture was incubated for 10 min on ice. Subsequently, the suspension was applied onto a sucrose density gradient harboring 60, 40, 30, 20 and 10% sucrose layers. The density gradient was run at 25.000 rpm in the swing bucket rotor SW 32 for 16h (Beckman ultracentrifuge, 4°C). Afterwards, the pellet and the two upper layers were collected and dissolved in 50 ml buffer containing 100 mM Tris-HCl, pH 6.8 and 150 mM NaCl supplemented with 10 mM DTT. The suspension was dropped into 100 ml hot 6% SDS and boiled for 4 h. The protocol was continued as described in 2.13.1.

2.13.3. Kühner et al. method

Less than 0.5 g *Nostoc* cells in a 2 ml reaction tube were dissolved in 1 ml 6% SDS and heated for 20 min in a heating block at 100°C. The cell suspension was centrifuged at maximum speed for 10 min. The supernatant was removed and the pellet washed twice in 1.5 ml ddH₂O. Afterwards, the pellet was dissolved in 1 ml ddH₂O and put in an ultrasonic bath for 30 min. The disrupted cells were spun down and dissolved in 1 ml 100 mM Tris HCl, pH 6.8 supplemented with 15 µg/ml DNase1 (Sigma-Aldrich, St. Louis, USA) and 60 µg/ml RNase (Carl Roth GmbH + Co, Karlsruhe, Germany). The suspension was incubated for 60 min at 37°C on a shaker. Subsequently, 50 µg/ml trypsin (Carl Roth GmbH + Co, Karlsruhe, Germany) was added and incubation was prolonged overnight. On the next day, incubation was stopped by boiling at 100°C in a heating block. The crude PGN was collected by centrifugation and washed once in ddH₂O. The PGN pellet was dissolved in 500 µl 1M HCl and incubated for 4H at 37°C. The PGN was washed several times with ddH₂O until the pH was neutral. The PGN pellet was stored at -20°C.

3. Results

3.1. The peptidoglycan composition of the filamentous cyanobacterium *Nostoc punctiforme*

Peptidoglycan is a mesh-like macromolecule in the periplasm of nearly all bacteria and fulfils various functions. In heterozygous cyanobacteria, it plays a special role in cell-cell communication. Septal peptidoglycan between neighbouring cells harbours numerous perforations to accommodate septal junctions (219, 220, 232) and thus enables intercellular communication (215, 221, 232). Nanopore formation is, to date, poorly understood. Amidases, like AmiC1 in *Anabaena* or AmiC2 in *N. punctiforme*, are necessary to drill the nanopores (222, 223). Mutation of both *amiC* genes has deleterious effects on the nanopore-array and the intercellular communication (221-223, 236). The regulation of these nanopore-forming enzymes remains still unclear. In order to get an idea of possible regulation mechanisms, it is beneficial to characterize the substrate of AmiC1 or AmiC2, the peptidoglycan.

In this section, a protocol for the isolation and purification of peptidoglycan from filamentous cyanobacteria is presented. The basic composition of peptidoglycan from *N. punctiforme* and a mutant lacking *amiC2* is described. This includes the determination of amino acids in the peptide stems and the elucidation of the muropeptide profile. The last subsection deals with peptidoglycan modifications and reveals that *N. punctiforme* contains covalently bound polysaccharides.

3.1.1. Isolation and purification of cyanobacterial peptidoglycan

The basic elucidation of cyanobacterial peptidoglycan was an important part of this work and required the isolation of pure peptidoglycan for analytical purposes. The modified protocol according to dePedro et al., which was used by default for electron microscopy in our laboratories, was established for the analysis of peptidoglycan by LC-MS (a detailed description of the protocol is in chapter 2.13.1 and represented in Fig. 13, upper panel). Electron micrographs of isolated sacculi from *Nostoc* sp. PCC 7120 showed long and empty filaments that indicate no larger contaminations with cellular components that would appear at higher electron density (Fig. 11A).

Proteomic analysis of the tryptic digest of the SDS insoluble PGN fraction derived from *N. punctiforme* identified more than 6000 peptides that were assigned to 1613 proteins (Fig. 12) and confirms previous results obtained by Josef Lehner (personal communication). The majority of these proteins belong to the photosynthesis apparatus, like phycobiliproteins, Psa- (photosystem I) or Psb- (photosystem II) proteins. A high abundance of cytosolic proteins, for example ribosomal proteins or membrane-embedded enzymes of the respiratory chain, was also detected. These proteins are not covalently linked to the peptidoglycan and were apparently resistant to the SDS treatment. This unspecific attachment represents a contamination risk and might cause false-positive interactions in protein-peptidoglycan binding assays when protein residues remain bound to the PGN due to an inefficient trypsin digestion.

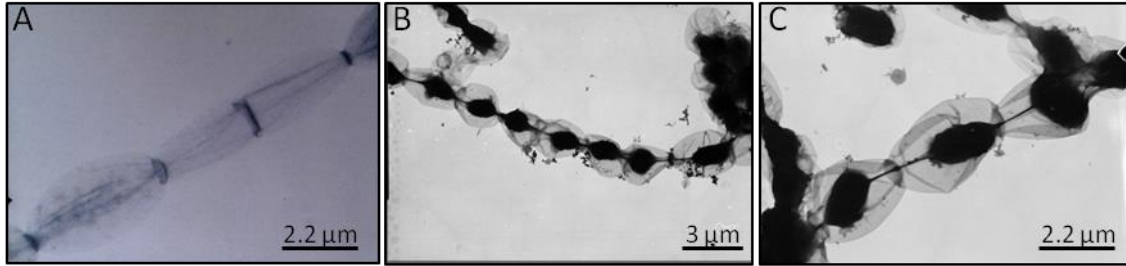


Fig. 11: Transmission electron micrographs of *Nostoc* sp. PCC 7120 PGN sacculi. A PGN was isolated according to the modified dePedro et al. protocol and imaged directly after the trypsin treatment. B and C display *Nostoc* sacculi isolated according to the Kühner et al. protocol.

For that, the protocol according to Kühner et al. (2014) was tested. The authors developed a time-saving method to yield pure peptidoglycan (protocol described in detail in chapter 2.13.3 and illustrated in Fig. 13, middle panel) (256).

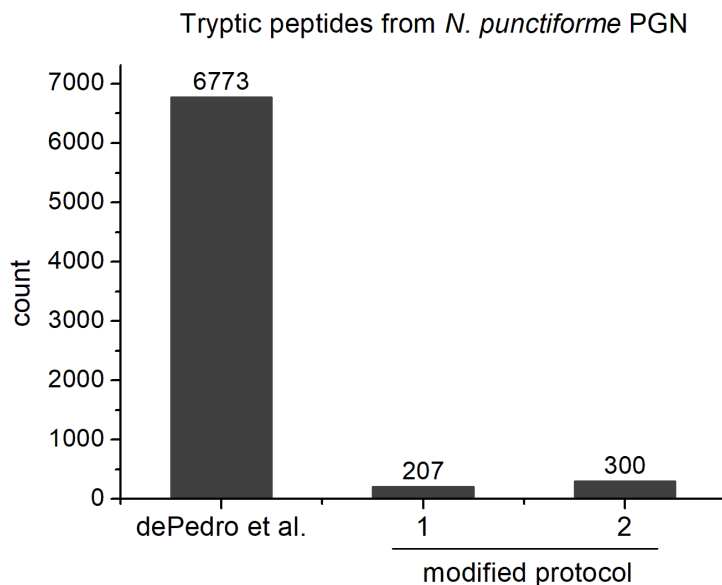


Fig. 12: Tryptic peptides derived from *Nostoc* peptidoglycan. PGN was isolated according to the dePedro et al protocol or according to the new modified protocol. Trypsin digests of both differently isolated PGNs were analysed by LC-MS. Identified peptides are displayed in the figure. Bar 1 and 2 represent biological replicates from PGN isolated according to the new modified protocol. Number of identified peptide ions plotted against the ion intensity (count)

Fig. 11 B and C display electron micrographs of peptidoglycan sacculi of *Nostoc* sp PCC 7120 isolated according to the modified protocol from Kühner et al. An electron dense component was visible, that reached through the whole filament. Apparently, the sacculi were not entirely pure and additional cellular components remained after the isolation procedure. This unidentified electron dense component demonstrated that this protocol is likely not suitable for the isolation of PGN from filamentous cyanobacteria.

Hereafter, a protocol was developed to prevent the previously detected carry-over of possible contaminations and to inhibit potential artificial crosslinking reactions between proteins during the extraction process. DTT addition creates reducing conditions and was aimed to prevent potential crosslinking reactions between the PGN and a broad range of proteins.

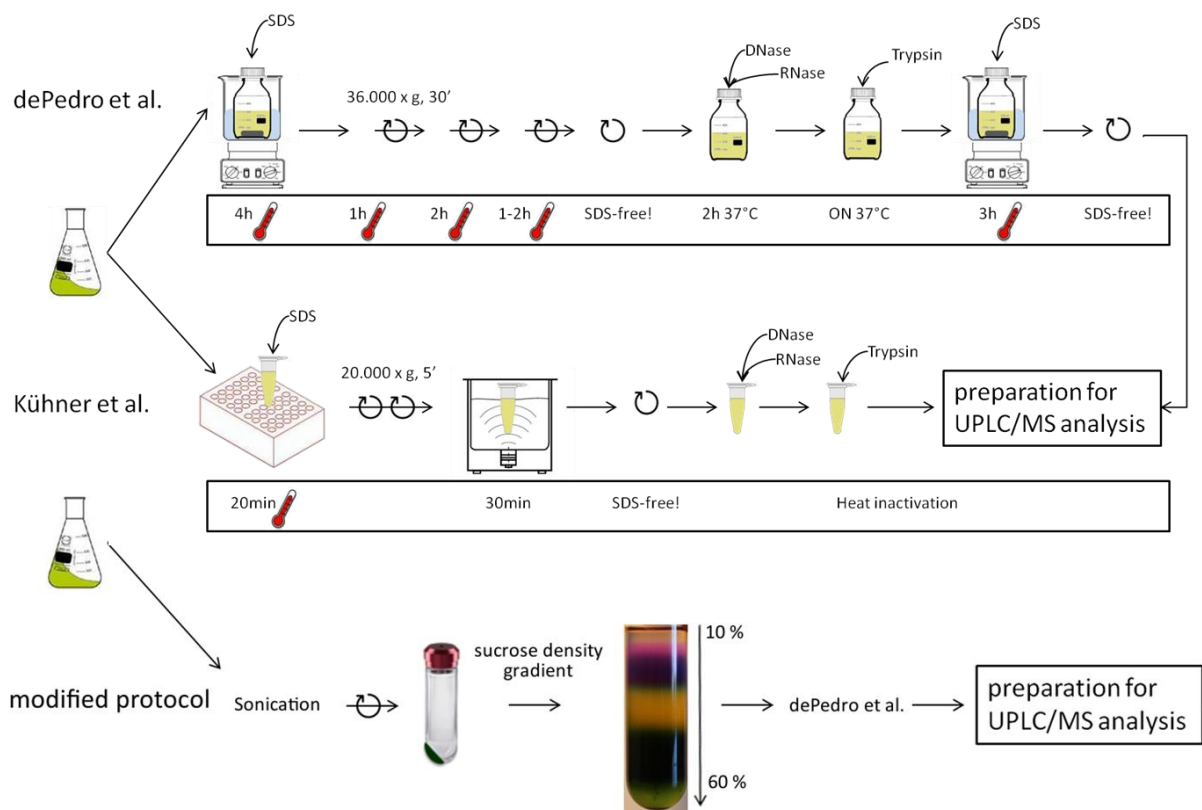


Fig. 13: Experimental design of three different peptidoglycan isolation protocols. Cyanobacteria were harvested and washed once in 5M NaCl. Peptidoglycan was isolated using to three different protocols. Upper panel describes the protocol according to Pedro et al. (2.13.1). Middle panel represents the method according to Kühner et al. (2.13.3). The lower panel shows the additional steps of a protocol developed in the course of this work (2.13.2) to yield pure peptidoglycan fractions for LC-MS analysis.

Furthermore, cytoplasmic proteins were removed by centrifugation and the resulting crude PGN extract was applied to a discontinuous sucrose density gradient. Afterwards, the crude PGN extract was treated according to the dePedro et al. protocol (this modified protocol is represented in Fig. 13, lower panel and described in detail in chapter 2.13.2). Afterwards, trypsin was added to the SDS-insoluble crude PGN to remove covalently linked proteins. The tryptic digest was subsequently analysed by LC-MS. A total of 207 and 300 tryptic peptides, assigned to 154 and 200 proteins, were identified in two biological replicas in contrast to more than 6000 identified peptides previously (Fig. 12). Resulting in a 95% reduction in the peptide background, the here presented protocol generates significantly purer PGN isolates compared to the modified dePedro et al protocol.

Therefore, the new protocol represents an appropriate basis for the isolation of pure sacculi from cyanobacteria for diverse biochemical approaches. A complete and detailed protocol is written in the Materials and Method section in chapter 2.13.2.

This section describes the isolation and purification of *Nostoc* peptidoglycan. A slightly modified protocol according to de Pedro et al. (see chapter 2.13.1) and Kühner et. al (see chapter 2.13.3) were tested. It was observed, that proteinaceous contaminations were carried over throughout the extraction procedure, using both protocols. The addition of DTT and the use of a sucrose-density ultracentrifugation diminished these contaminations and led to the optimized isolation protocol for *Nostoc* PGN, which is described in detail in chapter 2.13.2.

3.1.2. Determination of peptidoglycan derived amino acids

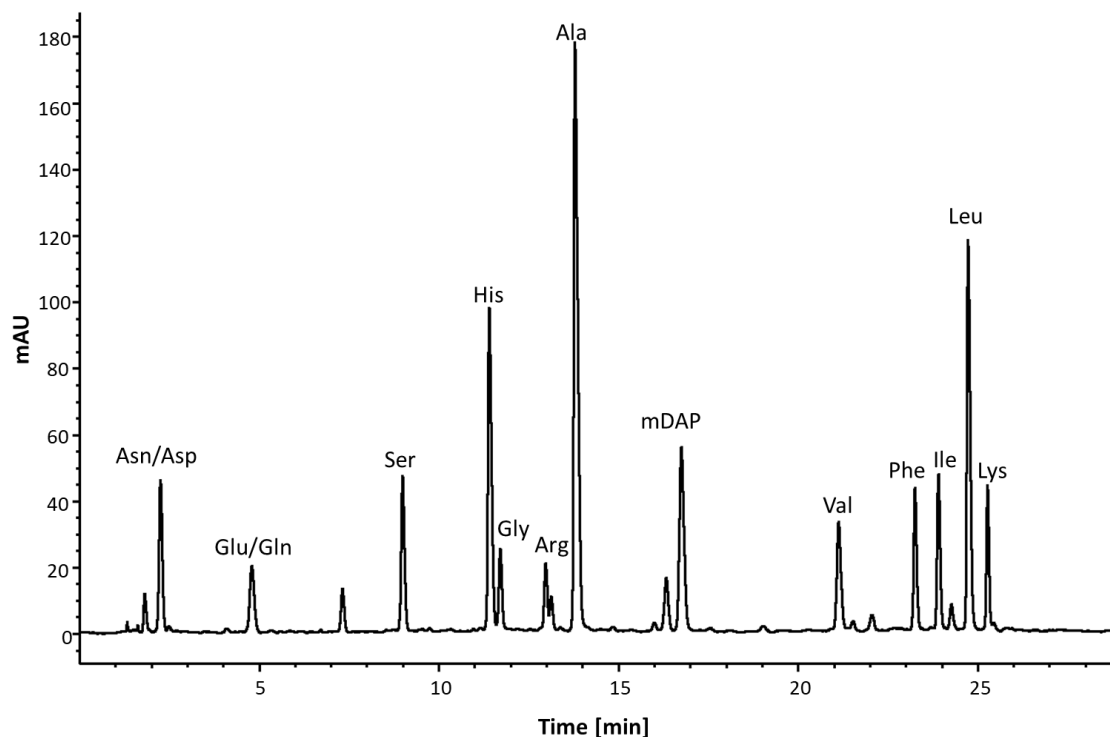
A first step in the characterization of the peptidoglycan from filamentous cyanobacteria was the identification of amino acids in the peptide stem. The peptide stem can undergo several modifications of the basic pentapeptide L-Ala-D-Glu-mDAP/L-Lys-D-Ala-D-Ala, as described in detail in chapter 1.2.2. The first amino acid analysis was based on peptidoglycan isolated according to the modified dePedro protocol. The amino acids were released by HCl hydrolysis, as described in chapter 2.11.1 and analysed as OPA derivatives by HPLC.

Fig. 14A shows the UV-chromatogram with all identified amino acids in the hydrolysate. The identification followed by the comparison of analyte retention times with those of the 21 standard amino acids. A total of 13 amino acids were detected with Ala being the most abundant. Glutamine and asparagine are converted to glutamate and aspartate due to the harsh HCl treatment and are not individually detectable. Proline carries a secondary amine and is therefore not identified in the chromatogram, as OPA only binds to primary amine groups. Furthermore, tryptophan is hydrolysed to completeness under the present acidic conditions and could not be detected. The non-proteinogenic diamino acid mDAP was identified in the HCl-hydrolysate of *N. punctiforme* PGN. It can elute multiple times during the HPLC separation due to its two primary amino groups that are either individually derivatized with OPA resulting in two peaks with different retention times, as can be seen in Fig. 14, or simultaneous, resulting in one peak.

In the previous section, it was described that the peptidoglycan isolated according to the modified dePedro et al. protocol might be contaminated with proteins that are potentially crosslinked to the PGN. A new protocol was developed to prevent such crosslinking reactions. The amino acid content of a PGN fraction obtained with the new protocol was determined. Surprisingly, all amino acids identified in the hydrolysate were also detected in the previous analysis using PGN isolated according to the modified dePedro et al. protocol (Fig. 14 A and B).

For the clear identification of amino acids, which are parts of the PGN peptide stem, muropeptides were specifically enriched, HPLC-purified, and used for the amino acid analyses. A muropeptide is a MurNAc-GlcNAc disaccharide with a peptide stem. Depending on the crosslinking degree, it occurs as a monomer, dimer, trimer or a higher oligomer. The peptidoglycan was digested by the muramidase mutanolysin, cleaving β -1,4 linkages between GlcNAc and MurNAc. The glycan chains are thereby disrupted and muropeptides are released. These soluble PGN fragments were separated by HPLC using an acetonitrile gradient (Fig. 15A). The most abundant peaks were collected. After hydrolyzation, derivatisation and HPLC analysis (Fig. 15B) the most abundant peaks were identified as alanine, arginine, mDAP and glutamine or glutamate. These amino acids constituted the peptide stem of muropeptides. The chromatogram also showed the elution of two components between 1 and 2 min. The retention time was not congruent with any of the 21 amino acids that were used as standards.

A. Amino acid analysis of PGN isolated according to dePedro et al



B. Amino acid analysis of PGN isolated according to the new protocol

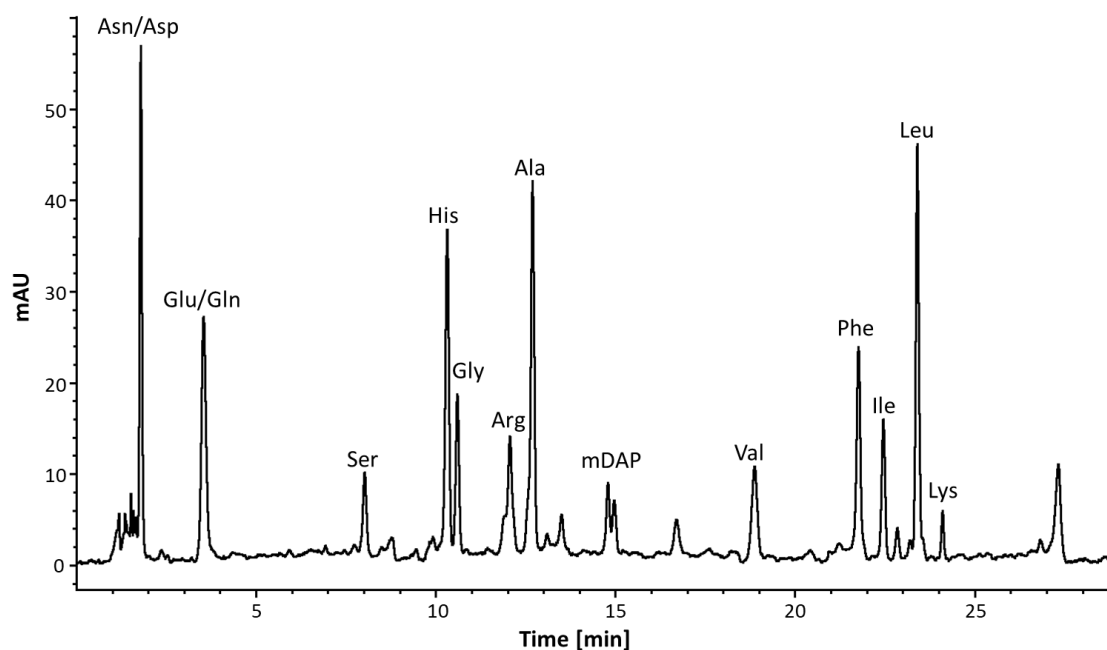
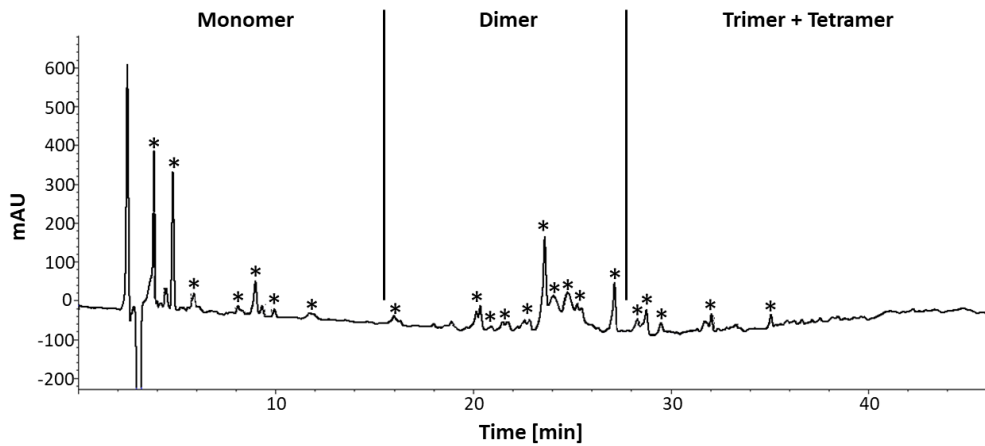


Fig. 14: OPA-derivatized amino acids in hydrolysates of PGN from *N. punctiforme*. PGN was isolated either according to the modified dePedro et al protocol (**A**) or the optimized protocol (**B**). Crude PGN was hydrolysed in 6 M HCl. Amino acids in acid hydrolysates were derivatized with OPA and analyzed by HPLC. Absorbance was measured at 340 nm. Identified amino acids are indicated.

A. HPLC-purification of muuropeptides from wildtype *N. punctiforme*



B. Amino acid analysis of muuropeptides from wild type *N. punctiforme*

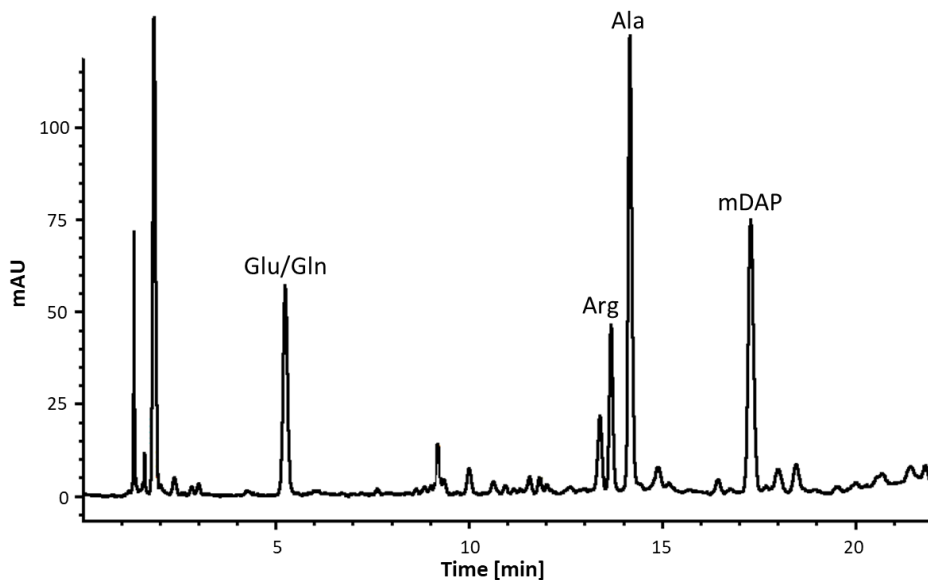


Fig. 15: Amino acid analysis of muuropeptides from *N. punctiforme*. A. Mutanolysin released PGN fragments were reduced by NaBH_4 and separated by HPLC on a reverse-phase C18 column. Absorbance was measured at 205 nm. Asterisks mark collected peaks for amino acid analysis. B. HPLC-purified muuropeptides were hydrolysed with 6M HCl and derivatized with OPA prior to HPLC. Identified amino acids are displayed in the chromatogram.

In the next step, the peptidoglycan from the *amiC2* mutant of *N. punctiforme* (229), in which the *amiC2* gene was interrupted by a C.K3 cassette, was analysed. The PGN was isolated and purified according to the new protocol as described in chapter 2.13.2 and hydrolysed in 6 M HCl. Hydrolysed components were derivatized with OPA and separated by HPLC. The chromatogram in Fig. 16 displays four highly abundant peaks that were assigned to the amino acids Ala, mDAP, Glu or Gln and Arg with a molar stoichiometry of 2:1:1:0.5 (Fig. 16). Lys, Ser, Leu and Ile, which were measured with high intensities in the PGN from wild-type *N. punctiforme* (Fig. 14) were only detected at background level as has been already seen in Fig. 15 for the muuropeptides from wild-type PGN. Two peaks appeared at retention times 6.5 and 13.5 min, but could not be identified.

Amino acid analysis of *N. punctiforme* *amiC2::ck3* PGN

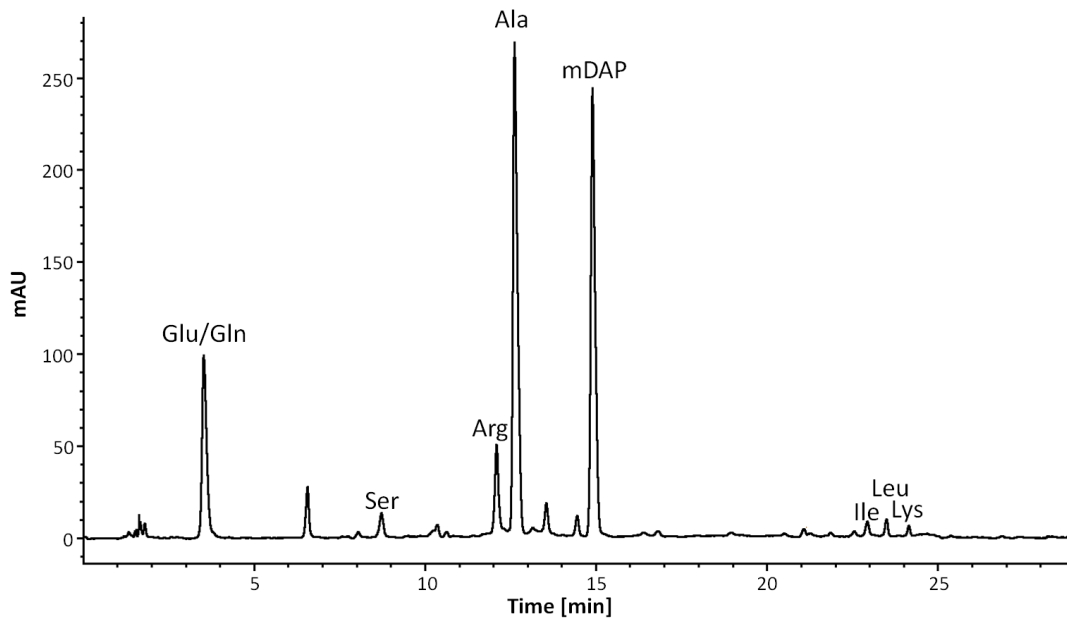


Fig. 16: Amino acid analysis of PGN derived from *N. punctiforme* *amiC2::ck3*. PGN was isolated and purified according to the new protocol described in 2.13.2. OPA-derivatized amino acids were analyzed by HPLC. Absorbance was measured at 340 nm. Identified amino acids are depicted

The peptidoglycan from wild-type *N. punctiforme* contains quite a number of amino acids, next to the PGN derived amino acids alanine, glutamate/glutamine and meso-diaminopimelic acid, whereas HPLC purified wild-type muuropeptides are exclusively assembled by the PGN derived amino acids and arginine. The amino acid composition is drastically changed upon the inactivation of the *amiC2* gene. The additional amino acids disappeared, almost completely, from the UV-chromatogram of HCL hydrolysed peptidoglycan fractions from the *amiC2* mutant variant except for arginine.

3.1.3. Muropeptide profile of *N. punctiforme* and its *amiC2* mutant

The amino acid analysis revealed that the peptide stem of *N. punctiforme* peptidoglycan is assembled of the amino acids alanine, glutamine or glutamate, meso-diaminopimelic acid and to a lesser extent arginine. Further experiments were made to determine the oligomeric state of these peptide stems and to identify the monosaccharides that form the glycan strands. HPLC coupled to mass spectrometry (MS) was used to provide more insights into PGN composition and structure. Therefore, muropeptides were released by mutanolysin and reduced by sodium borohydride to prevent mutarotation. MurNAc can undergo structural changes after mutanolysin digestion, due to its reducing end, and will form α - and β -anomers, which elute with different retention times from a C18 reverse phase column. The reduced muropeptides were separated by HPLC and subjected to LC-MS. Muropeptides were identified by the comparison of the measured mass-to-charge (m/z) ratio and sum formula of the detected ions with the theoretical m/z and sum formula.

The UV-chromatogram in Fig. 17 depicts the elution profile of *N. punctiforme* muropeptides and displays the muropeptide structure for each numbered peak. Monomeric muropeptides elute within 10 min from the C18 reverse phase column. Muropeptides in peak 1 generated two abundant ions with an m/z of 870.3954 and 698.3098. These measured m/z ratios correspond to a GlcNAc-MurNAc-disaccharide with an adjacent tripeptide (870.3954 m/z) or a dipeptide (698.3098 m/z) with amidated carboxyl side chains, respectively.

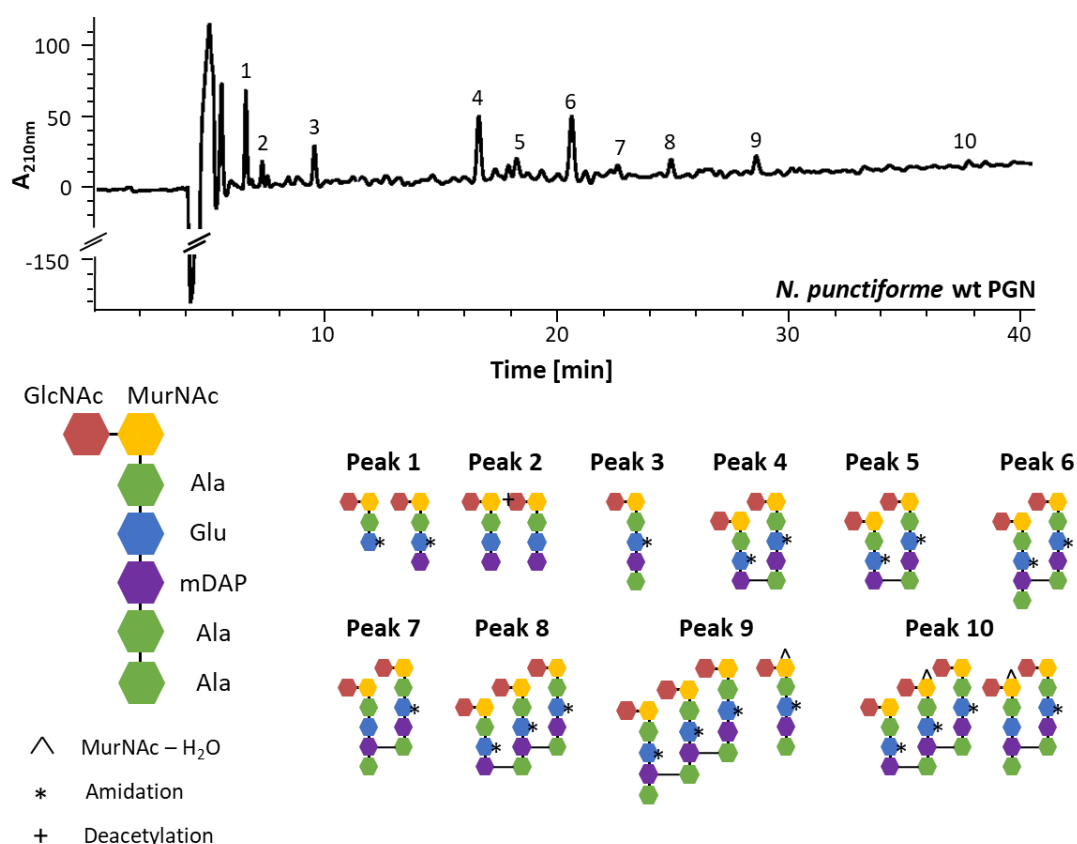


Fig. 17: HPLC analysis of muropeptides from *N. punctiforme*. Peptidoglycan from *N. punctiforme* was digested by mutanolysin. Released muropeptides were reduced by NaBH₄ and subjected to HPLC. Peak fractions marked by a number were collected and applied to LC-MS. Identified muropeptides with their referred structures are displayed.

Proposed sum formulas for these measured ions are in-line with the theoretical sum formulas with amidated tri- and dipeptides (Table 44). Furthermore, MS/MS-fragmentation identifies Ala, Glu and mDAP in the tripeptide as well as Ala and Glu in the dipeptide stem (5.10, supplementary information). The position of the additional amine group could not be determined, but for reasons of simplification, the additional amidation will be represented by glutamine, Gln. The position of the extra amine group will be discussed in chapter 4.1.2.










A less abundant ion with the m/z of 871.3814 was detected in peak 2. Fragmentation pattern of this measured ion reveals a GlcNAc-MurNAc disaccharide with an Ala-Glu-mDAP peptide (5.10, supplementary information). This is consistent with the theoretical mass and sum formula of a disaccharide with a tripeptide (Table 44). Another ion was measured in peak 2 with the m/z of 828.3837. The protonated mass of this ion matches with the theoretical mass of a deacetylated disaccharide with a tripeptide (Table 44). MS/MS fragmentation pattern revealed the fragment ion 162.0766 m/z (proposed sum formula $C_6H_{12}NO_4^+$) that corresponds to the theoretical m/z of glucosamine lacking its N-acetyl group whereas the fragment ion of GlcNAc (204.0872 m/z) could not be found (5.10, supplementary information). The MS/MS profile also demonstrated that the peptide linked to MurNAc consists of Ala, Gln and mDAP. It is possible that functional groups, such as acetyl groups or other fragments of the analyte, are cleaved off during the initial ionization. These ionization-induced cleavage products have the same retention time as the parent ions, but do not occur in that form in the original analyte. This is likely true for the deacetylated muropeptide, because the retention time between the deacetylated (828.3837 m/z) and the N-acetylated muropeptide (871.3814 m/z) was identical. In order to distinguish between fragment ions obtained from MS/MS fragmentation and those during the initial ionization, the former ones are termed fragment ions, whereas the latter ones are called ionization-induced cleavage products.





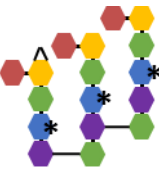
A high abundant double positively charged ion (471.2202 m/z) was measured in peak 3 with 10 min retention time on the C18 column (Fig. 17). The single protonated mass of these ions (941.4394 m/z) consists of a GlcNAc-MurNAc-disaccharide with an amidated tetrapeptide. The sequence of this tetrapeptide is Ala-Gln-mDAP-Ala according to the MS-MS profile (5.10, supplementary information). Several ionization-induced cleavage products of these ions were also detected in peak 3 such as ions with the respective m/z of 738.3526 (not shown). These ions were the result of the elimination of one GlcNAc molecule.

The first dimeric muropeptides eluted after 17 min from the HPLC column (peak 4). Mass spectrometric analysis of this fraction indicated the presence of ions (598.2756 m/z at $z = 3$ and 896.9090 m/z at $z = 2$), which correspond to a dimer of a GlcNAc-MurNAc-tripeptide and a GlcNAc-MurNAc-tetrapeptide with the single protonated mass of 1792.8128 Da (Table 44). The peptide stems are crosslinked by a peptide bond between mDAP from one peptide stem and the fourth Ala from the second peptide stem according to the MS/MS fragmentation (5.10, supplementary information). Besides, the carboxyl side chains of both peptide stems are amidated.

Peak 5 comprises muropeptides that eluted between 18 and 19 min from the HPLC column. The most abundant ions represented ionization-induced cleavage products of the aforementioned dimer (not shown). There were ions indicating the loss of an acetyl group (1750.8005 m/z) or the elimination of one disaccharide (1295.5874 m/z). The parental ions with the positively charged mass 1792.8080 were only low abundant (Fig. 17 and Table 44). Peak 6 contained a dimer between two GlcNAc-MurNAc-tetrapeptides (1863.8483 m/z , Fig. 17 and Table 44).

Table 44: LC-MS analysis of HPLC-purified mucopeptides from wild-type *N. punctiforme*. Mucopeptides were separated by HPLC and subsequently subjected to LC-(ESI-TOF)-MS analysis. Table summarizes all identified mucopeptides with measured m/z and proposed sum formula. Corresponding theoretical m/z and sum formula are as well represented. *= Amidation; ^ = anhydrous; + = Deacetylation

Wild-type mucopeptides						
	Theoretical			Measured		
Peak	species	m/z	sum formula	m/z	sum formula	Rel. abundance (%)
1		698.3091	C ₂₇ H ₄₈ N ₅ O ₁₆ ⁺	698.3098	C ₂₇ H ₄₈ N ₅ O ₁₆ ⁺	9.8
1		870.3938	C ₃₄ H ₆₁ N ₇ O ₁₉ ⁺	870.3954	C ₃₄ H ₆₁ N ₇ O ₁₉ ⁺	
2		871.3779	C ₃₄ H ₅₉ N ₆ O ₂₀ ⁺	871.3814	C ₃₄ H ₅₉ N ₆ O ₂₀ ⁺	3.5
2		828.3595	C ₃₂ H ₅₈ N ₇ O ₁₈ ⁺	828.3837	C ₃₂ H ₅₈ N ₇ O ₁₈ ⁺	
3		941.4310	C ₃₇ H ₆₆ N ₈ O ₂₀ ²⁺	941.4394	C ₃₇ H ₆₆ N ₈ O ₂₀ ²⁺	5
4		1792.8070	C ₇₁ H ₁₂₂ N ₁₅ O ₃₈ ⁺	1792.8128	C ₇₁ H ₁₂₂ N ₁₅ O ₃₈ ⁺	11.6
5		1792.8070	C ₇₁ H ₁₂₂ N ₁₅ O ₃₈ ⁺	1792.8080	C ₇₁ H ₁₂₂ N ₁₅ O ₃₈ ⁺	9.5
6		1863.8441	C ₇₄ H ₁₂₇ N ₁₆ O ₃₉ ⁺	1863.8483	C ₇₄ H ₁₂₇ N ₁₆ O ₃₉ ⁺	13.3
7		1864.8281	C ₇₄ H ₁₂₆ N ₁₅ O ₄₀ ⁺	1864.8326	C ₇₄ H ₁₂₆ N ₁₅ O ₄₀ ⁺	3.6

Wild-type muropeptides						
Peak	Theoretical			Measured		
	species	m/z	sum formula	m/z	sum formula	Rel. abundance (%)
8		2715.2201	$C_{108}H_{184}N_{23}O_{57}^+$	2715.2282	$C_{108}H_{184}N_{23}O_{57}^+$	5
9		2786.2572	$C_{111}H_{189}N_{24}O_{58}^+$	2786.2682	$C_{111}H_{189}N_{24}O_{58}^+$	5
9		921.4047	$C_{37}H_{61}N_8O_{19}^+$	921.4078	$C_{37}H_{61}N_8O_{19}^+$	
10		1843.8179	$C_{74}H_{123}N_{16}O_{38}^+$	1843.8242	$C_{74}H_{123}N_{16}O_{38}^+$	1
10		2695.1939	$C_{10}H_{180}N_{23}O_{56}^+$	2695.2014	$C_{10}H_{180}N_{23}O_{56}^+$	

Both peptide stems were additionally amidated and connected by a peptide bond formation between mDAP from one peptide stem and the fourth amino acid from the second peptide stem (5.10, supplementary information). The following peak represented the same dimeric muropeptides species and several ionization-induced cleavage products. However, the most abundant ions were generated by a dimeric muropeptide with two tetrapeptides with a single amidation in the carboxylic side chains (1864.8326 m/z, peak 7, Fig. 17 and Table 44). Another abundant ion was detected that could not be assigned to a known muropeptide structure (not shown). The double positively charged ion 683.8157 m/z, with the respective m/z of 1366.6244 had a mass difference of 498.2037 Da to the single amidated muropeptide dimer (1864.8181 m/z). This difference did not correspond to a

cleavage product where a GlcNAc residue (minus 204.0872 Da), an acetyl group (minus 43.0184 Da) or a disaccharide (minus 481.2033 Da) was eliminated.

Trimeric muropeptides with three additional amidations (2715.2282 m/z) were identified in peak 8. MS/MS-fragmentation of all multi charged ions, generated by the trimeric muropeptides, reveal two GlcNAc-MurNAc-tetrapeptides and one GlcNAc-MurNAc-tripeptide (5.10, supplementary information). The three peptide stems of this trimeric muropeptide are crosslinked via mDAP-Ala bond formation. A putative structure of this muropeptide is illustrated in Fig. 17 and Table 44. Another trimeric muropeptide species (2786.2682 m/z) was detected in peak 9. The MS/MS-profile indicates three GlcNAc-MurNAc-tetrapeptides crosslinked by a peptide bond between Ala and mDAP (5.10, supplementary information). The same peak also contained a highly abundant muropeptide with the m/z of 921.4078. This mass-to-charge ratio corresponds to a GlcNAc-MurNAc-tetrapeptide after elimination of a water molecule. The late retention time and the MS/MS-fragmentation indicated the presence of anhydrous MurNAc, the aminosugar with an intramolecular ring structure between the C1 and C6 atom. Fraction 10 contained mainly two muropeptide species with an m/z of 1843.8242 and 2695.2014. Fragmentation pattern revealed that 1843.8242 m/z was a dimer of two GlcNAc-MurNAc-tetrapeptides with one anhydrous MurNAc (5.10, supplementary information). The muropeptide with 2695.2014 m/z was a trimer of two GlcNAc-MurNAc-tetrapeptides and one GlcNAc-MurNAc-tripeptide with one anhydrous MurNAc (5.10, supplementary information).

The amino acid analysis indicated that disruption of the *amiC2* gene might affect the peptidoglycan composition. A first step in the verification of this assumption was the analysis of the muropeptide profile from this mutant. Muropeptides were separated by HPLC, collected and analysed by LC-MS likewise for the wild-type muropeptides. Fig. 18 shows the UV-chromatogram of muropeptides from the *amiC2* mutant with the referred structures. Based on this analysis, there were no major differences compared to the PGN from wild-type *N. punctiforme*.

Monomeric muropeptides with a dipeptide (698.3108 m/z), a tripeptide (870.396 m/z and 871.3814 m/z) or a tetrapeptide (941.4332 m/z) were identified in the peaks 1 to 3. The GlcNAc-MurNAc dipeptide from the *amiC2* mutant had a longer retention time on the C18 reverse phase column than that of the wild-type. Muropeptides of peak 4 are a dimer of an amidated GlcNAc-MurNAc-tripeptide and an amidated GlcNAc-MurNAc-tetrapeptide (1792.811 m/z, also see MS/MS-profile in 5.11, supplementary information). An isomer of this dimer was also found in peak 5 as well as several ionization-induced cleavage products (not shown) that indicated the elimination of an acetyl group (1750.802 m/z).

Peak 6 harboured a highly abundant muropeptide (1863.8504 m/z) consisting of a dimer between two GlcNAc-MurNAc-tetrapeptides, with each peptide carrying an additional amine group as confirmed by MS/MS-fragmentation (5.11, supplementary information). Next to cleavage products and adducts of this dimer, ions with an m/z of 850.3683 were identified. The MS/MS fragmentation of this ion with the m/z of 850.3683 demonstrated the fragment ion 329.1356 m/z that revealed the presence of an anhydrous MurNAc covalently bound to Ala ($C_{14}H_{21}N_2O_7^+$) and a dipeptide of Gln and mDAP (319.1611 m/z, $C_{12}H_{23}N_4O_6^{2+}$).

The base peak chromatogram of the equivalent peak fraction from the wild-type was screened for the m/z of 850.3683. Indeed, a molecule with this mass-to-charge was detected, but only the Gln-mDAP-peptide could be clearly identified (319.1609 m/z, $C_{12}H_{23}N_4O_6^{2+}$) by MS/MS fragmentation. The

fraction 7 harbours a dimer of two GlcNAc-MurNAc-tetrapeptides (1864.8341 m/z), that generated multi-charged ions, as it has been already shown for fraction 7 from the wild-type.

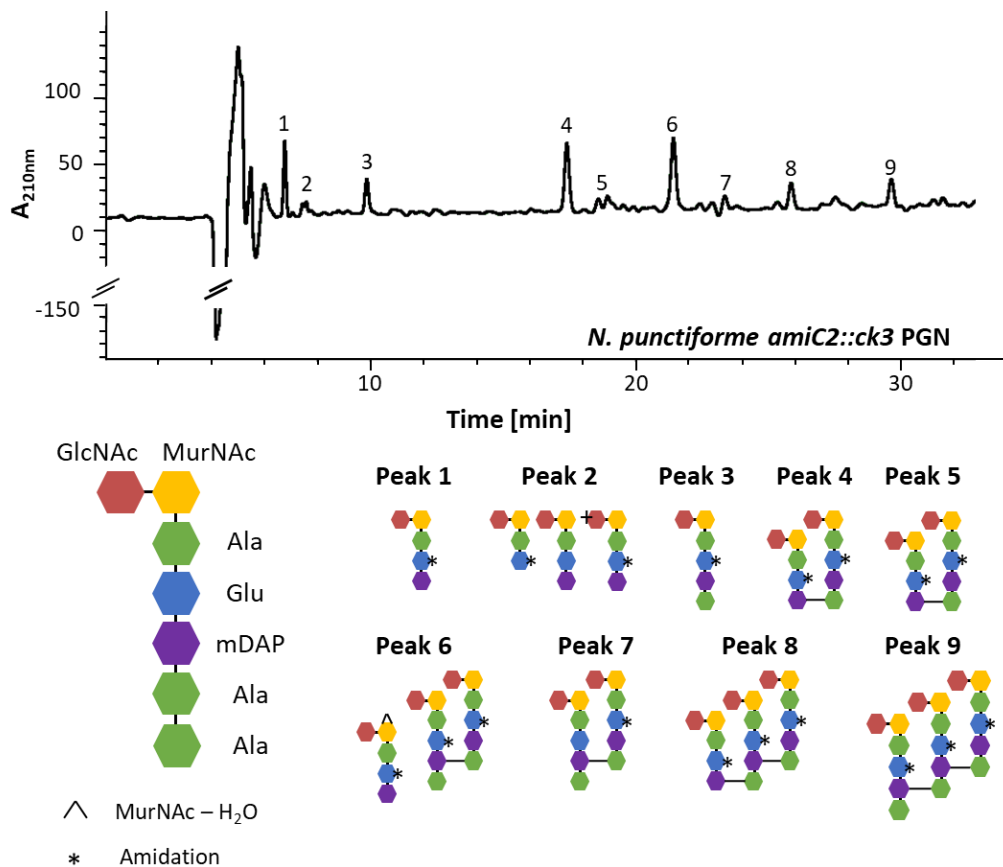











Fig. 18: Muropeptide profile of the *amiC2* mutant from *N. punctiforme*. Peptidoglycan was digested by the muramidase mutanolysin to yield soluble muropeptides. These were reduced by NaBH₄ and separated by HPLC. Abundant peaks were collected and subjected to LC-MS. Referred muropeptide structures and the corresponding peaks are displayed.




The trimeric muropeptides identified in the peaks 8 and 9 from the wild-type were also found in the same peak fractions from the *amiC2* mutant. But the anhydrous GlcNAc-MurNAc-tetrapeptide with the m/z of 921.4078 that was detected in the peak fraction 9 from the wild-type was not found in the corresponding fraction from the mutant. Moreover, the anhydrous oligomeric muropeptides from the wild-type that eluted in peak 10 could not be found in the *amiC2* mutant because no further components eluted after 32 min from the HPLC-column.

The comparison of the UV-chromatograms between the muropeptides from the wild-type and the *amiC2* mutant as well as the LC-MS analysis of all collected peak fractions showed minor differences and demonstrated that the most abundant muropeptides consisted of unmodified, basic PGN-building blocks. The disaccharide was formed by GlcNAc, MurNAc or anhydrous MurNAc covalently linked to a peptide of alanine, glutamate and meso-diaminopimelic acid. It was shown that the muropeptides were additionally amidated on a free carboxyl group and formed complex peptidoglycan structures ranging from monomers to trimers.

However, this analysis did not explain the presence of several atypical cell wall amino acids in the amino acid analysis of peptidoglycan from wild-type *N. punctiforme*. The LC-MS analysis of mutanolysin digests of PGN from wild-type *N. punctiforme* without prior HPLC-purification considered also less abundant muropeptides.

Table 45: LC-MS analysis of HPLC-purified mucopeptides from the *amiC2* mutant of *N. punctiforme*. Mucopeptides were separated by HPLC and subsequently subjected to LC-(ESI-TOF)-MS analysis. Table summarizes all identified mucopeptides with measured m/z and proposed sum formula. Corresponding theoretical m/z and sum formula are as well represented. *= Amidation; ^ = anhydrous; + = Deacetylation

<i>amiC2</i> mutant mucopeptides						
	Theoretical			Measured		
Peak	species	m/z	sum formula	m/z	sum formula	surface area (%)
1		870.3938	C ₃₄ H ₆₁ N ₇ O ₁₉ ⁺	870.396	C ₃₄ H ₆₁ N ₇ O ₁₉ ⁺	10.6
2		698.3091	C ₂₇ H ₄₈ N ₅ O ₁₆ ⁺	698.3108	C ₂₇ H ₄₈ N ₅ O ₁₆ ⁺	3.9
2		871.3779	C ₃₄ H ₅₉ N ₆ O ₂₀ ⁺	871.3814	C ₃₄ H ₅₉ N ₆ O ₂₀ ⁺	
2		870.3938	C ₃₄ H ₆₁ N ₇ O ₁₉ ⁺	870.396	C ₃₄ H ₆₁ N ₇ O ₁₉ ⁺	
3		941.4310	C ₃₇ H ₆₆ N ₈ O ₂₀ ²⁺	941.4332	C ₃₇ H ₆₆ N ₈ O ₂₀ ²⁺	5.9
4		1792.8070	C ₇₁ H ₁₂₂ N ₁₅ O ₃₈ ⁺	1792.811	C ₇₁ H ₁₂₂ N ₁₅ O ₃₈ ⁺	12.1
5		1792.8070	C ₇₁ H ₁₂₂ N ₁₅ O ₃₈ ⁺	1792.811	C ₇₁ H ₁₂₂ N ₁₅ O ₃₈ ⁺	6.9
6		1863.8441	C ₇₄ H ₁₂₇ N ₁₆ O ₃₉ ⁺	1863.8504	C ₇₄ H ₁₂₇ N ₁₆ O ₃₉ ⁺)	14.5
6		850.3676	C ₃₄ H ₅₆ N ₇ O ₁₈ ⁺	850.3683	C ₃₄ H ₅₆ N ₇ O ₁₈ ⁺	

<i>amiC2</i> mutant muropeptides						
Peak	Theoretical			Measured		
	species	m/z	sum formula	m/z	sum formula	surface area (%)
7		1864.8281	C ₇₄ H ₁₂₆ N ₁₅ O ₄₀ ⁺	1864.8341	C ₇₄ H ₁₂₆ N ₁₅ O ₄₀ ⁺	5.5
8		2715.2201	C ₁₀₈ H ₁₈₄ N ₂₃ O ₅₇ ⁺	2715.2285	C ₁₀₈ H ₁₈₄ N ₂₃ O ₅₇ ⁺	6.6
9		2786.2572	C ₁₁₁ H ₁₈₉ N ₂₄ O ₅₈ ⁺	2786.2658	C ₁₁₁ H ₁₈₉ N ₂₄ O ₅₈ ⁺	8

A total of 29 peaks could be identified in the Total Ion Current (TIC) chromatogram as represented in Fig. 19 (Table 51, supplementary information). Peak 1 to 6 comprised mainly monomeric muropeptides with a basic composition. The disaccharides GlcNAc and MurNAc were linked to peptides containing Ala, Glu/Gln and mDAP. A double and a single deacetylated dimer of a GlcNAc-MurNAc-tripeptide and a GlcNAc-MurNAc-tetrapeptide were detected in peak 3 and 5 although the majority of dimers eluted after 9.5 min. The loss of the acetyl group changed the polarity of this dimer that affected the elution on the C18 reverse phase column. The different retention times between the deacetylated and the N-acetylated muropeptides indicate that deacetylated muropeptides occurred in wild-type peptidoglycan and were not the result ionization-induced cleavage.

Peak 3 also contained an amidated MurNAc-tetrapeptide with an m/z of 738.349. This mass-to-charge ratio was probably not the result of an ionization-induced cleavage of GlcNAc (204.0872 m/z) because the m/z for the equivalent disaccharide tetrapeptide (calculated 941.4310 m/z) was not found. A tetrasaccharide (977.403 m/z) was identified in peak 7 that indicated a less efficient mutanolysin digestion that normally results in the formation of disaccharides.

Peak 8 to 10 comprised dimeric muropeptides that lost one acetyl group and peak 14 to 16 contained dimers that lacked one disaccharide or a GlcNAc-residue. The most abundant dimeric muropeptides were single and double amidated GlcNAc-MurNAc-tripeptide - GlcNAc-MurNAc-tetrapeptide dimers (peak 17 and 20) and double amidated GlcNAc-MurNAc-tetrapeptide dimers (peak 20). Isomers of the double amidated dimer between a GlcNAc-MurNAc-tripeptide and a GlcNAc-MurNAc-tetrapeptide were also detected in peak 13 and 18. Several ions with the m/z of 850.376 and 921.405 were measured that corresponded to monomeric muropeptides containing an anhydrous MurNAc. The intramolecular ring formation altered the interaction with the column and prolonged the elution.

Peak 11 and 12 contained an anhydrous disaccharide with a tripeptide while peak 18 comprised an anhydrous disaccharide with a tetrapeptide.

The majority of trimeric muropeptides was detected between 19 and 29 min. The most abundant trimers consisted of either two GlcNAc-MurNAc-tetrapeptides and one GlcNAc-MurNAc-tripeptide (2715.217 m/z, peak 25), or three GlcNAc-MurNAc-tetrapeptides (2786.283 m/z, peak 26). Deacetylated trimers eluted prior compared to unmodified trimers from the column and were measured in the peaks 19, 23 and 24.

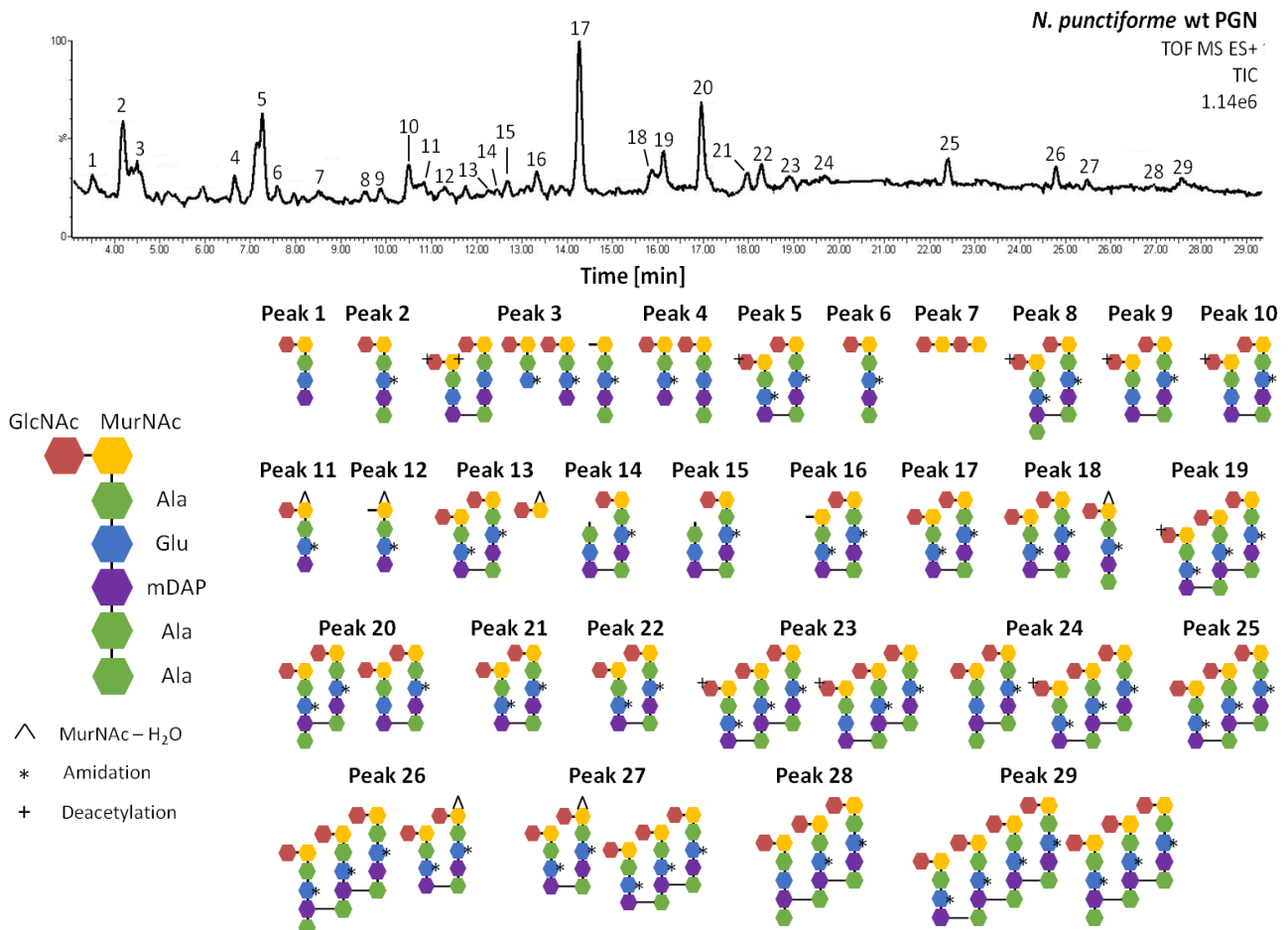


Fig. 19: LC-MS analysis of mutanolysin released muropeptides from *N. punctiforme*. A pure PGN fraction of wild type *N. punctiforme* was digested by mutanolysin. The released muropeptides were reduced by NaBH₄ and subjected to LC-MS. The total ion current (TIC) chromatogram represents all identified muropeptides with their referred structure.

Peak 27 to 29 contained isomers of trimers from previously eluting peaks. Dimeric muropeptides with an anhydrous MurNAc were also measured in peak 26 and 27, coeluting with trimeric muropeptides. It was also possible to identify a tetrameric muropeptide consisting of three GlcNAc-MurNAc-tetrapeptides and one GlcNAc-MurNAc-tripeptide in peak 29 with an m/z of 3637.688, characterized by four additional amidation events.

In summary, high as well as low abundant muropeptides from wild-type *N. punctiforme* consist of the typical PGN components GlcNAc, MurNAc, alanine, glutamate and meso-diaminopimelic acid. Several modifications, such as deacetylation of the disaccharide or amidation of carboxyl side chains from the peptide stem, were observed. However, no single muropeptide was found in mutanolysin digests, neither from the wild-type nor the *amiC2* mutant from *N. punctiforme*, which carries an

atypical amino acid. The amino acid analysis of wild-type muropeptides and the PGN from the *amiC2* mutant indicated the presence of arginine, as an atypical amino acid (Fig. 15 and Fig. 16). Unfortunately, arginine was not detected in any analyzed sample.

3.1.4. Differences between lateral and septal peptidoglycan of wild-type *N. punctiforme*

The septal peptidoglycan of *N. punctiforme* differs in size and quantity compared to the lateral cell wall. It appears thicker than the lateral wall in electron micrographs (Fig. 20) but display only a diameter of roughly 1.6 μm (259). Lateral peptidoglycan surrounds the overall surface of vegetative (diameter: 5 -6 μm) or specialized cells like heterocysts (diameter up to 10 μm) and contains the largest part of peptidoglycan. Turner et al. estimated that the cylindrical part of *E. coli* covers 75% of the total surface, whereas the cell pole covers 25% (260). The amount of septal peptidoglycan is therefore proportionally lower than the lateral cell wall and might be underrepresented in PGN analysis. Septal disks of *N. punctiforme* were isolated and enriched using harsh sonication cycles and filtration techniques (Fig. 20A) to find differences between lateral and septal cell walls.

Fig. 20B represents the base peak ion chromatogram (BPI) of muropeptides from septal or whole peptidoglycan. The designation "whole peptidoglycan" includes muropeptides of crude, unprocessed peptidoglycan. Accordingly, lateral and septal cell walls are still combined within this fraction and are not separated. Septal disks were enriched out of the whole peptidoglycan fraction and purified by diverse filtrations. Differences in the composition of septal disks will emerge upon the direct comparison of BPI-chromatograms between whole and septal peptidoglycan fragments.

Monomeric muropeptides obtained from both PGN samples eluted within 8 min from the C18 reverse phase column. A detailed list of all detected and identified muropeptides is given in Table 52 - Table 54 in the supplementary information. Two highly abundant peaks (peak 8 and 6 in both BPI-chromatograms) elute with a retention time of 3.5 and 6 min from the HPLC column loaded with septal muropeptides (Fig. 20B, green BPI-chromatogram). These two peaks could not be detected in the BPI-chromatogram obtained from the whole peptidoglycan sample (Fig. 20B, red BPI-chromatogram). Peak 8 comprises monomeric muropeptides with an adjacent tripeptide (Ala-Gln-mDAP) with the m/z of 870.4. Similar mass-to-charge ratios, 869.377 $[M+H]^+$ and 868.385 $[M+H]^+$ (see Table 52 - Table 54, supplementary information), were found in the peaks eluting after 4.5 min and 6.6 min in the BPI-chromatogram of whole peptidoglycan (peaks are not numbered). The difference to the corresponding calculated m/z for an amidated GlcNAc-MurNAc-tripeptide ($m/z = 870.3938$) is 1.017 and 2.009. The difference between calculated and measured m/z is therefore too large and indicates that these m/z ratios likely do not represent muropeptides.

The m/z found in peak 6 in both chromatograms contains an ion with the respective m/z of 206.1. This ion eluted after 6 min in the LC-MS run of septal cell walls. An identical ion, with the m/z of 206.1, was detected in the BPI-chromatogram of the whole PGN sample. But, instead of eluting within the monomeric fraction, as has been seen in the sample of septal muropeptides, the retention time delayed about 10 min, and this ion was detected within the dimeric fraction of muropeptides with a retention of 16 min. A shift in the retention time of corresponding m/z was observed multiple times. The first defined peak in the BPI-chromatogram of the whole PGN eluted after 4.2 min and was identified as a GlcNAc-MurNAc-tetrapeptide with the following sequence: Ala, Glu, mDAP and Ala (peak not numbered). The carboxylic side chain of this stem peptide was additionally amidated

(measured m/z 941.429). An identical ion was also found in the BPI-chromatogram of septal disks with a delayed retention time of 6.2 min.

The most abundant dimeric muropeptides ($m/z = 1792.8$ and 1863.8) in the sample, containing whole peptidoglycan, eluted after 14.3 and 17 min (peaks not numbered). The same muropeptide species had a delayed retention of 15.5 and 18.5 min in the BPI-chromatogram of the septal PGN.

The peaks in the BPI-chromatogram of septal disks show a general delay in retention compared to the BPI-chromatogram of whole PGN except for the ion $206.1 m/z$, which elutes 10 min earlier in the LC-MS run of septal muropeptides. This shift could explain the absence of amidated GlcNAc-MurNAc-tripeptides (m/z of 870.4) in the BPI-chromatogram of whole PGN. Highly abundant muropeptides from the whole PGN sample eluted apparently earlier from the HPLC column than the corresponding ones in the septal disk sample. Consequently, amidated GlcNAc-MurNAc-tripeptides (m/z of 870.4), as found in peak 8 in the BPI of septal cell walls, could have eluted within the injection peak (solvent peak including unretained material) of the whole PGN. This is the reason why there might be any defined peak for the amidated GlcNAc-MurNAc-tripeptide in the BPI-chromatogram of the whole PGN.

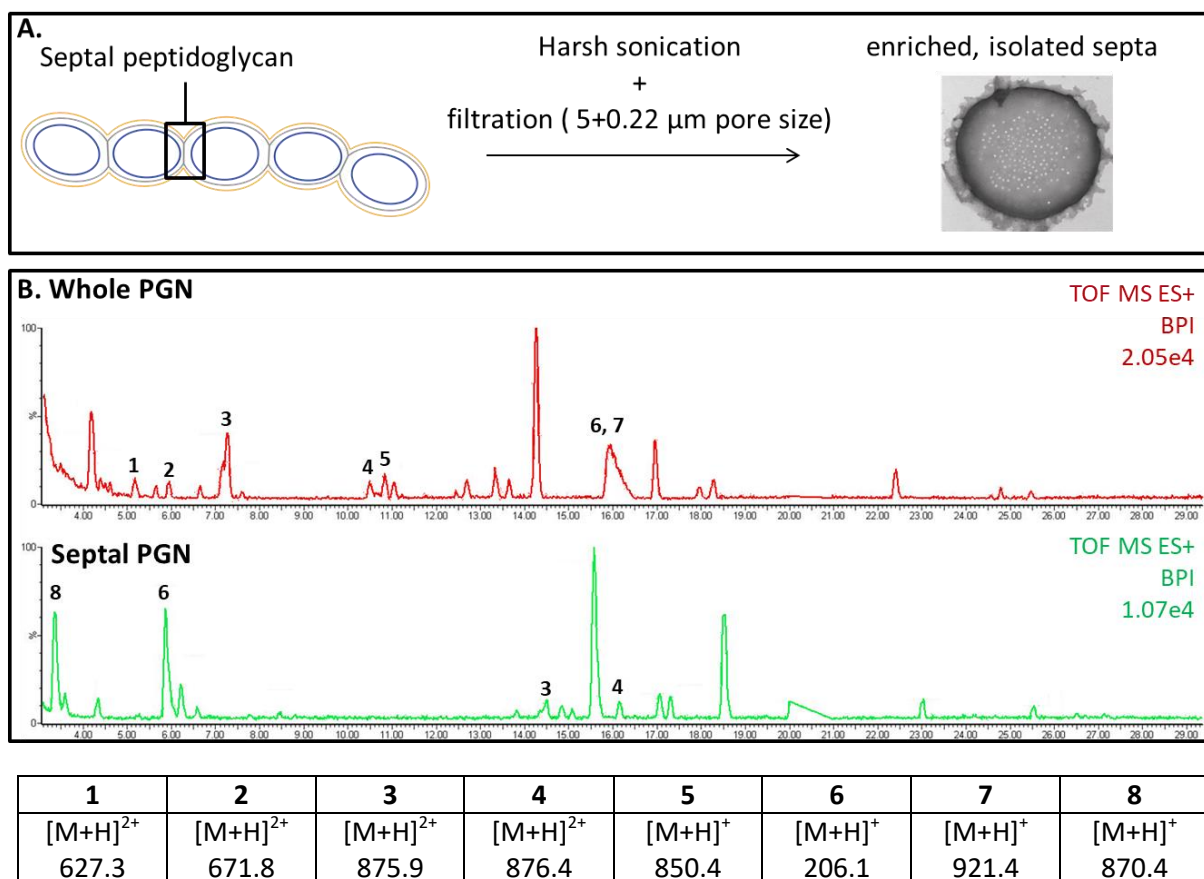


Fig. 20. Comparison between muropeptide elution profiles from crude and septal peptidoglycan. **A.** Experimental procedure for the isolation and enrichment of septal peptidoglycan. **B.** Reverse-phase LC-MS analysis of mutanolysin digested crude peptidoglycan (whole = septal and lateral cell wall) or exclusively septal peptidoglycan. Base peak ion chromatogram (BPI) represents elution profile of muropeptides in positive mode. Numbered peaks indicate differences between both BPI chromatograms. Table represents the mass-to-charge ratio of each numbered peak.

Less abundant double charged ions ($m/z=627.29$ and 671.81) were detected in peak 1 and 2 from the whole PGN fraction. These ions had a retention time of 5.2 and 6 min and were not identified in septal PGN. Furthermore, these mass-to-charge ratios could not be assigned to any known muropeptide structure. Peak 3 contained a highly abundant double charged ion with the measured m/z of 875.903 and showed a retention time of 7.2 min in the BPI-chromatogram of whole PGN. This ion could be identified as a deacetylated dimer of a GlcN-MurNAc-tripeptide and a GlcNAc-MurNAc-tetrapeptide, carrying two additional amidations. This muropeptide elutes within the monomeric fraction of whole PGN with a retention time of 7.2 min indicating that deacetylation did not occur through the ionization, as observed several times before. The same muropeptide species had a delayed retention of 14.5 min in the BPI-chromatogram of septal PGN. In this case, deacetylation might have occurred through the ionization. The muropeptide species, eluting in peak 4 with the m/z of 876.4, were identified as a deacetylated dimer of a GlcN-MurNAc-tripeptide and a GlcNAc-MurNAc-tetrapeptide with one additional amidation. The retention time of this muropeptide differs between the BPI-chromatograms of whole and septal PGN. This dimer eluted after 16.1 min from the HPLC column, loaded with septal muropeptides, while the same muropeptide species eluted approximately 6 min earlier in the LC-MS run of the whole PGN. Isomeric forms of this dimer were apparently detected, because this dimer was found in the peaks at retention time 9.9 min and 10.5 min in the BPI-chromatogram of whole PGN (peaks are not numbered). Anhydrous MurNAc-peptides were exclusively detected in the peaks 5 and 7 ($m/z = 850.368$ and 921.405) in the fraction containing the whole PGN but not in that of septal PGN.

Altogether, the qualitative LC-MS analysis revealed high similarity in the PGN composition of septal and lateral cell walls in *N. punctiforme*. The muropeptides of both PGN types are composed of basic PGN building blocks. However, a few differences were detected, such as the absence of the unknown compounds with $627.29 [M+H]^{2+}$ and $671.81 [M+H]^{2+}$ and the anhydrous MurNAc peptides with an m/z of 850.368 and 921.405 in septal peptidoglycan. Furthermore, two dimeric deacetylated muropeptides ($875.903 [M+H]^{2+}$ and $876.39 [M+H]^{2+}$), a molecule with the $m/z = 206.1$ showed different retention times in the LC-MS analysis of septal and whole PGN.

3.1.5. Polysaccharides are covalently bound to cyanobacterial peptidoglycan

The peptidoglycan from various bacteria can be modified by glycopolymers like polysaccharides or wall teichoic acids as described in chapter 1.2.1. These polymers are linked to the PGN mainly by phosphodiester bonds. The phosphate content of a PGN fraction reveals not only the presence of compounds that are linked via their phosphate groups to the PGN but also distinguishes between wall teichoic acids or other molecules. Wall teichoic acids are anionic sugars composed of long chains of glycerol phosphate or ribitol phosphate units (102, 103). Increased levels of phosphate in PGN fractions are a first hint for covalently bound wall teichoic acids.

The phosphate groups of *Nostoc* PGN were released by HCl and perchloric acid. Free phosphate was measured and quantified using a calibration curve with different concentrations of inorganic phosphate. About $0.45 \mu\text{mol}$ phosphate was measured per mg PGN in samples from *N. punctiforme* as displayed in Fig. 21. In comparison to *B. subtilis*, a wall teichoic acid producer, 37% less phosphate was detected, but 55% more than in *E. coli* samples, an organism that does not produce any wall teichoic acids.

The enhanced phosphate levels in acid hydrolysates indicated that the PGN might be modified by polysaccharides. Determination of covalently bound polysaccharides was performed by High Pressure Anionic Exchange Chromatography (HPAEC) at alkaline conditions. The retention times of PGN derived polysaccharides were compared to those of mono- and oligosaccharides in a mixed standard solution (Fig. 22A and B blue line). Fig. 22A displays seven abundant peaks in the chromatogram obtained from wild-type samples.

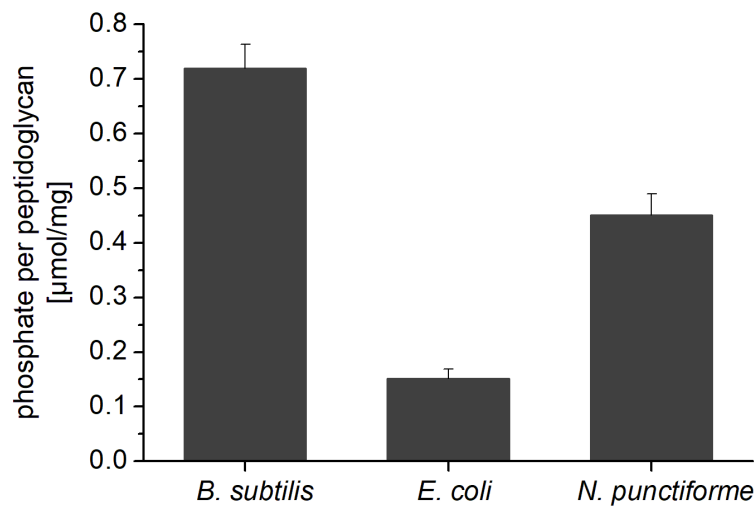


Fig. 21: Phosphate content in PGN fractions obtained from different bacterial species. Phosphate containing compounds were collected by acid treatment from PGN. Phosphate groups were removed by perchloric acid and measured using the phosphate assay kit (Abcam).

A total of 4 peaks could be assigned to arabinose, galactose, glucose and mannose or xylose. Peaks at retention times 1 and 3 min as well as the peak eluting after 17 min could not be identified. The four monosaccharides were also detected in samples derived from the *amiC2* mutant (Fig. 22B). Glucose generated the most abundant peak, whereas Gal, Man and Ara were less abundant and detected only slightly elevated from background levels.

In comparison to the chromatogram obtained from wild-type samples, glucose showed only a twofold higher intensity than the other three monosaccharides. Peaks eluting between 1 and 3 min as well as the peak with a retention time of 11 min could not be assigned to a mono- or oligosaccharide.

In summary, the peptidoglycan from wild-type *N. punctiforme* is not modified by anionic wall teichoic acids. However, HPAEC analysis revealed several monosaccharides and unidentified oligosaccharides which might assemble a covalently linked polysaccharide. Interestingly, the inactivation of the gene *amiC2* changes the composition of this presumptive polysaccharide, in such a way that the abundances of the detected sugars were altered.

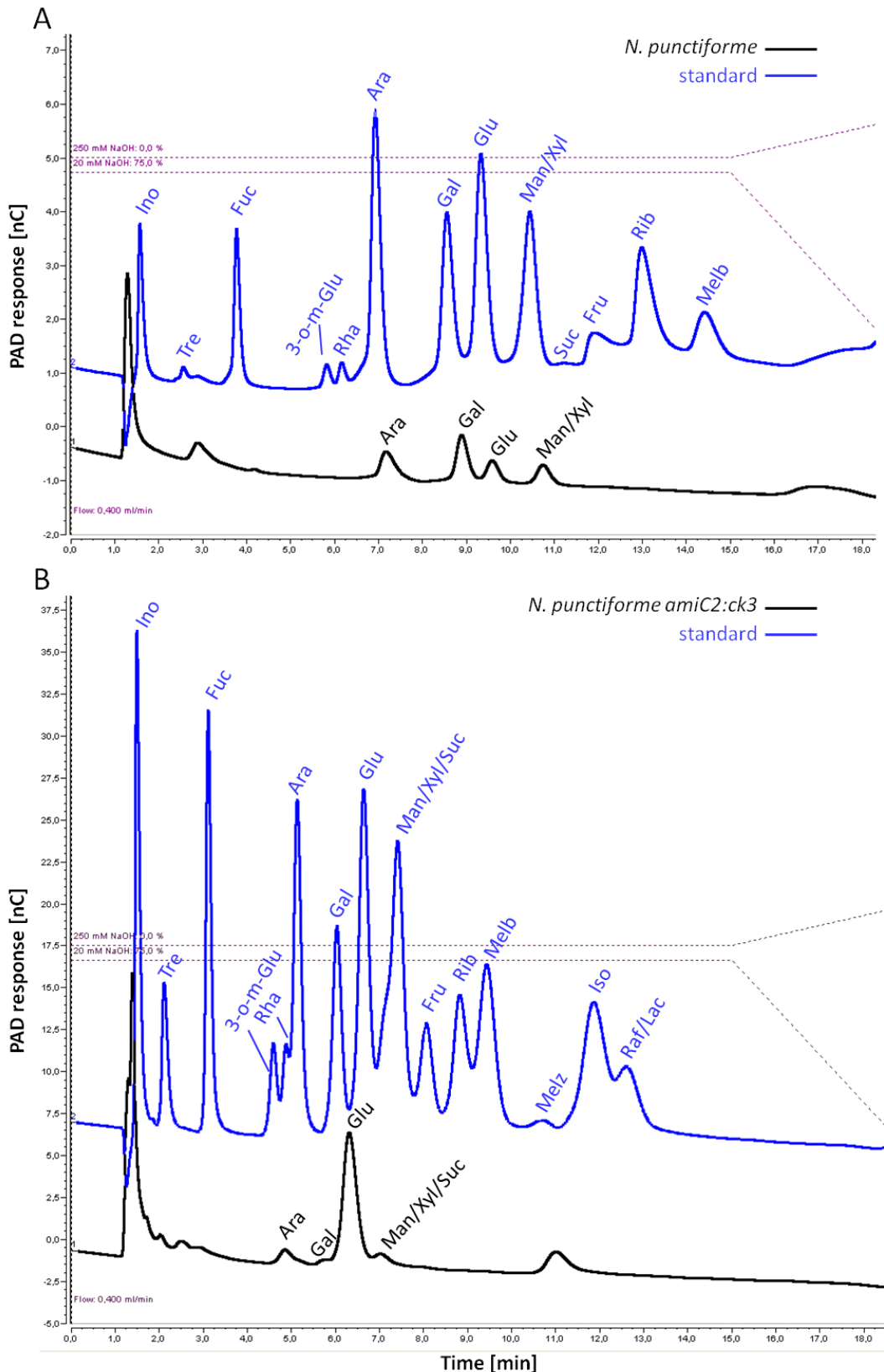


Fig. 22: Determination of covalently bound polysaccharides in acidic hydrolysates of PGN by HPAEC. PGN from wild-type (**A**) or the *amiC2* mutant of *N. punctiforme* (**B**) was treated with 1M HCl for 4h at 37°C and removed by centrifugation. Acidic hydrolysates were dried and dissolved in 6M NaOH. HPAEC analysis was performed using a stepwise NaOH gradient to separate monomeric and oligomeric carbohydrates. Black line = acid hydrolysate of *N. punctiforme* wild-type or *amiC2* mutant PGN; blue line = standard carbohydrate mixture.

3.1.6. Putative proteins associated or covalently bound to the peptidoglycan

Analysis of trypsin digested *N. punctiforme* peptidoglycan (in chapter in 3.1.1) revealed 172 and 248 peptides from two biological replicates (Fig. 12). These peptides could be assigned to 133 and 181 annotated proteins, respectively. More than 72% of these proteins in both samples comprised proteins that are not associated with the peptidoglycan and are therefore termed contaminants (Fig. 23). A detailed list in the supplementary information (Table 55 - Table 57) summarizes all identified proteins. The most abundant proteins are related to the phycobilisomes and the photosystem. Likewise, cytosolic proteins like chaperones, ribosomal proteins or metabolic enzymes are among these contaminations. The number of identified proteins could be reduced to 18 and 24 after subtraction of all contaminants and hypothetical proteins (Fig. 23 and Table 46).

Both replicates contained five common proteins (Table 46): Npun_F2686 is annotated as histidine kinase and displays complex domain architecture. The 2198 amino acid long protein comprises several transmembrane HAMP-like α -helices, the signalling module GAF, a histidine kinase domain mediating ATP-dependent autophosphorylation and dimerization, as well as three response regulator domains (Fig. 38, supplementary information). SecY (Npun_R4372) is part of the SEC-translocon that mediates protein secretion and membrane protein insertion. This membrane-spanning protein forms a multimeric complex with SecE and G in the cytoplasmic and thylakoid membrane (261). The channel likely opens upon ribosome binding (262) and translocates unfolded proteins in an ATP-dependant manner into the periplasm or the thylakoid lumen. *Nostoc* SecY reveals multiple interactions with ribosomal proteins that were highly abundant in tryptic digests of peptidoglycan (Table 55 - Table 57 supplementary information). The third protein is predicted as a transcriptional regulator (Npun_F5788) belonging to the WalR-like two-component system protein family. It contains proteins with an N-terminal receiver domain and a C-terminal DNA-binding domain.

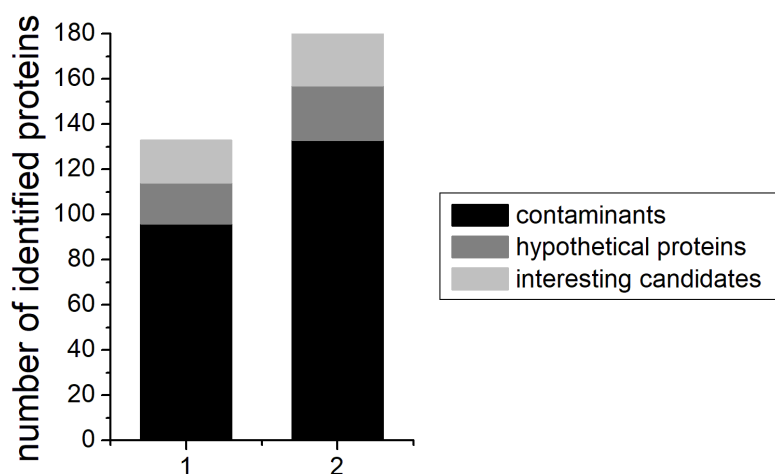


Fig. 23: LC-MS analysis of tryptic digests from *Nostoc* PGN representing identified proteins. Peptidoglycan was isolated and purified according to the protocol in chapter 2.13.2. Soluble fractions were collected after trypsin digestion of crude PGN and analyzed by mass spectrometry. Identified peptides were assigned to annotated proteins and classified into three groups: contaminants (not interacting with peptidoglycan), hypothetical proteins and interesting candidates (likely interacting with PGN).

Table 46: Proteins identified in tryptic digest of *Nostoc* PGN with a potential to interact or associate with PGN. Soluble peptides were analysed after trypsin digestion of *Nostoc* PGN by LC-MS. Identified peptides were assigned to annotated proteins (listed based on a decreasing relative intensity). Contaminants (proteins not interacting with PGN) as well as hypothetical proteins were removed. Proteins exclusively found in one of the two and those found in both replicates are listed below.

Interesting candidates in tryptic peptidoglycan digests		
	Identifier	Annotation
Both replicates	Npun_F2686	GAF sensor hybrid histidine kinase
	Npun_R4372	preprotein translocase, SecY subunit
	Npun_F5788	two component transcriptional regulator
	Npun_F3787	transport-associated
	Npun_F4881	ATP-dependent metalloprotease FtsH
Only in biological replicate 1	Npun_F1740	ATP-dependent metalloprotease FtsH
	Npun_F4615	urea ABC transporter, extracellular ligand-binding receptor UrtA
	Npun_F4649	NUDIX hydrolase
	Npun_R1355	ATP-dependent metalloprotease FtsH
	Npun_F4749	putative iron transport system substrate-binding protein
	Npun_F5536	periplasmic phosphate-binding protein of phosphate ABC transporter
	Npun_F2285	extracellular solute-binding protein
	Npun_R5086	extracellular ligand-binding receptor
	Npun_F1883	putative GAF sensor protein
	Npun_F5842	RND family efflux transporter MFP subunit
	Npun_F3826	inner-membrane translocator
	Npun_R4804	cell division protein FtsZ
	Npun_R5246	peptidoglycan binding domain-containing protein
Only in biological replicate 2	Npun_R0781	biopolymer transport protein ExbD/TolR
	Npun_R5324	inner-membrane translocator
	Npun_R1448	response regulator receiver sensor signal transduction histidine kinase
	Npun_F0354	multi-sensor hybrid histidine kinase
	Npun_F5285	acriflavin resistance protein
	Npun_F3299	phosphonate ABC transporter, periplasmic phosphonate-binding protein
	Npun_F0459	lipopolysaccharide biosynthesis protein
	Npun_F0891	phosphate ABC transporter, periplasmic phosphate-binding protein
	Npun_F4220	carbohydrate-selective porin OprB
	Npun_R2770	extracellular ligand-binding receptor
	Npun_R4325	TM helix repeat-containing protein
	Npun_R5326	periplasmic binding protein/LacI transcriptional regulator
	Npun_R1108	putative serine/threonine kinase
	Npun_F3850	protein-export membrane protein SecD
	Npun_R5647	lytic transglycosylase, catalytic
	Npun_R1548	glycoside hydrolase family protein
	Npun_R2022	ATP-dependent metalloprotease FtsH
	Npun_R3901	putative sensor protein
	Npun_R4162	NmrA family protein

Table 47: Hypothetical proteins in tryptic digests of *N. punctiforme*. Soluble tryptic peptides obtained after digestion on *Nostoc* PGN were analysed by LC-MS and assigned to proteins. Hypothetical proteins were removed and only annotated proteins are listed based on their relative intensity (decreasing). Domain features were obtained from Interpro, TMHMM, SignalP - 5.0 and COILS.

Identifier	UniProt - annotation	AA length	Domain / Region	
Npun_R4646	uncharacterized protein	75	1-19 20-42 43-75	non-cytoplasm transmembrane cytoplasm
Npun_F3932	uncharacterized protein	160	1-29 30-160	Lipo-SP non-cytoplasm
Npun_R3785	uncharacterized protein	1033	35-54 89-111 118-140 354-374 469-493 562-614 779-799 957-999 1004-1026	transmembrane transmembrane transmembrane coiled - coil coiled - coil coiled - coil coiled - coil coiled - coil transmembrane
Npun_R1321	uncharacterized protein	1038	42-60 95-117 130-152 575-595 691-711 967-1009 1014-1036	transmembrane transmembrane transmembrane coiled - coil coiled - coil coiled - coil transmembrane
Npun_F0289	ABC-1 domain protein	573	132-251 144-516 516-538 542-564	UBI Protein kinase transmembrane transmembrane
Npun_R4472	ALP_N domain-containing protein	389	53-204	ALP-domain

The fourth common protein is poorly characterized and annotated as transport-associated. It carries an N-terminal 20 amino acid long signal peptide, predicted by SignalP-5.0 as a lipoprotein signal peptide with a likelihood of 0.9986 (Fig. 41B, supplementary information). The C-terminus contains a 69 amino acid long BON (bacterial OsmY and nodulation) domain (Fig. 41A), presumably relevant in phospholipid-binding (263). The last common protein in Table 46 is a homologue of the membrane-embedded ATP-dependant metalloprotease FtsH. Npun_F4881 displays transmembrane regions in the N-terminus (Interpro prediction: FtsH extracellular domain), necessary for membrane anchorage (Fig. 43B, supplementary information). Furthermore, it contains a C-terminal domain specific for peptidases of the M41 family, a protein group comprising zinc metalloproteases, and the conserved H-E-X-X-H motif for zinc ion binding. An AAA+-domain resides in the central part of the putative metalloprotease and consists of the ATPase module, catalysing ATP hydrolysis, and the AAA+-lid

domain. The latter domain comprises α -helices forming a bundle which represents the nucleotide binding site blocking “lid”.

Both analysed replicates contained tryptic peptides from *Nostoc* PGN that were assigned to six common hypothetical proteins summarized in Table 47: Npun_F3932 carries a 31 amino acid long N-terminal sequence, most likely a lipoprotein signal peptide (Fig. 42, supplementary information). Furthermore, CELLO analysis predicts a periplasmic localization; however transmembrane α -helices or β -barrel motifs are missing. Npun_F0289 is a putative protein kinase with a domain commonly found in ABC1 proteins from yeasts or in homologous bacterial UbiB protein kinases required for ubiquinone biosynthesis (264). It contains transmembrane α -helices and is likely anchored in the cytoplasmic membrane and protruding into the cytoplasm, as predicted by CELLO. Another hypothetical protein is only partially described, Npun_R4472. This protein belongs to the family plasmid segregating ParM-like proteins with an N-terminal ALP domain (Actin-like protein). The other three proteins in Table 47 comprise one or several transmembrane α -helices and are likely membrane-embedded proteins with unknown function.

Other potentially peptidoglycan interacting proteins were found in only one biological replicate (Table 46): Periplasmic binding proteins Npun_F5536 and Npun_F4749 work in concert either with ABC transporter or iron-acquisition systems, as well as the MFP subunit of the RND-multidrug efflux pump, which connects the cytoplasmic and the outer membrane. These proteins are directly connected to the peptidoglycan due to their subcellular localization.

Interestingly, also a protein with a peptidoglycan binding domain (Npun_R5246) was identified, however based on a low identification score. The score reflects the correlation between experimental and theoretical MS/MS data. It combines all observed mass spectra that can be matched to an amino acid sequence within the putative protein. The higher the score, the more reliable the peptide/protein identification.

Several proteins were identified in supernatants of trypsin treated peptidoglycan with a potential to interact with peptidoglycan. Among these, a homologue of the membrane integral biopolymer transporter ExbD/TolR (Npun_R0781) was identified in replicate 2. As characterized in *E.coli*, TolR is part of the Tol/Pal system and essential for membrane invagination during cell division (148), whereas ExbD is involved in TonB dependent transports (265) and protrudes with the C-termini into the periplasm for an interaction with the peptidoglycan. Furthermore, two periplasmic binding proteins, Npun_F0891 and Npun_F3299, were detected and are likely involved in phosphate or phosphonate import via ABC transporters. The membrane anchored protein Npun_F5285 was also identified and is part of a putative multidrug efflux pump, homologous to the AcrA/B pump of *E. coli*. Interestingly, a putative lytic transglycosylase (Npun_R5326) was also detected. Lytic transglycosylases are peptidoglycan remodelling enzymes and cleave the β -1,4 linkage between GlcNAc and MurNAc thereby producing a 1,6-anhydro MurNAc peptide.

Taken all together, numerous peptides were detected in tryptic digests of *Nostoc* PGN, which could be assigned to several annotated proteins. The overlay of two biological replicates results in five proteins, which belong to transport or two-component systems. Furthermore, common hypothetical proteins with a probable lipoprotein signal peptide were found, which might potentially interact with the peptidoglycan.

3.2. The amidase AmiC2 and its substrate peptidoglycan

The peptidoglycan hydrolase AmiC2 has a pivotal role in the formation of a nanopore array in septal disks of *N. punctiforme* (223). The molecular mechanism underlying this action remains still unclear. AmiC2 lacks an important regulatory α -helix in the catalytic domain (242), but possesses a proline rich upstream region affecting PGN hydrolysis *in vitro* (244). Furthermore, the autoproteolytic cleavage of one AMIN domain, the mode of translocation into the periplasm or interacting NlpD homologues might regulate AmiC2 activity (242, 244). A further regulation mechanism should be considered as an additional possibility. The septal peptidoglycan itself can harbour cleavage sites for AmiC2 and target the amidase directly and specifically to the sites of future nanopores.

This section focuses on the enzymatic activity and substrate binding capacity of the catalytic domain from AmiC2 (AmiC2cat). Hydrolysis of *Nostoc* PGN was determined by labelling peptidoglycan released peptides with a fluorescent dye. Subsection 3.2.2 elucidates the substrates of AmiC2cat by a mass spectrometric approach. The last subsection deals with mutational analysis of site-specific amino acid residues, and the establishment of appropriate peptidoglycan binding assays.

3.2.1. AmiC2cat hydrolyses *amiC2* mutant PGN but not wild-type PGN

Zhou et. al developed a method to monitor the enzymatic degradation of peptidoglycan using the dye Remazol Brilliant Blue (RBB) that binds to hydroxyl groups of the sugar backbone under alkaline conditions (257). Crude peptidoglycan is usually insoluble and needs enzymatic digestion to release soluble fragments. Patterns of PGN breakdown by peptidoglycan hydrolases and the subsequent release of RBB-labelled soluble PGN fragments is displayed in Fig. 24A. The higher the peptidoglycan hydrolases activity the more RBB-labelled components are enriched in the supernatant. This enrichment results in an increase of the OD_{595nm}.

This principle was applied to measure the hydrolytic activity of AmiC2 on RBB-labelled *E. coli* PGN (Fig. 24B). AmiD is a N-acetylmuramoyl-L-alanine amidase anchored in the outer membrane of *E. coli* with a broad substrate specificity (266). A truncated version lacking the lipid moiety was used as a positive control. A second control was introduced in the experimental set up. Lysozyme cleaves the β -1,4-glycosidic bond between GlcNAc and MurNAc generating soluble muropeptides. This action was considered as a gold standard for the Dye-Release-Assay (DRA).

The catalytic domain of AmiC2 from *N. punctiforme* was able to cleave RBB-labelled *E. coli* PGN due to an increase of OD_{595nm} 30 min after incubation. In comparison to AmiD that exhibits a broad substrate specificity and is also able to cleave anhydrous peptidoglycan fragments (266), samples digested by AmiC2cat showed an approximately twice as high OD_{595nm}. Similar observations were made with lysozyme treated samples that demonstrated a 45% less hydrolytic activity of lysozyme on RBB-labelled *E. coli* PGN than those digested by AmiC2cat.

It was not possible to stain *Nostoc* PGN with RBB, instead a new method based on OPA fluorescence was used to monitor AmiC2cat activity (described in detail in chapter 2.9.6). Amidases cleave the covalent amide bond between L-alanine and MurNAc, thereby releasing the amine group of alanine. This amine group can be captured by ortho-phthalaldehyde (OPA), which can be monitored by a change in absorbance or fluorescence.

The Dye-Release-Assay demonstrated that the catalytic domain of AmiC2 is able to digest *E. coli* peptidoglycan (Fig. 24B). That is why *E. coli* PGN was used to set up the experimental procedure for the OPA derivatization of PGN released peptides. The amidase domain AmiE from the autolysin AtlE exhibits N-acetylmuramoyl-L-alanine amidase activity and was used as positive control. Aliquots were sampled at different time points and released peptides were derivatized with OPA. A calibration curve using different concentrations of the amino acid alanine was used for the quantification of amines in the samples (Fig. 25B). Amine groups were released over time by AmiC2cat or AmiE indicating that both enzymes cleave peptides from the glycan backbone (Fig. 25C). A huge initial increase of amines during the first 60 min of incubation with AmiC2cat was observed, whereas the amount of free amine groups in samples supplemented with AmiE increased steadily. This finding confirms that OPA-derivatization is an appropriate, sensitive method to detect PGN released peptides.

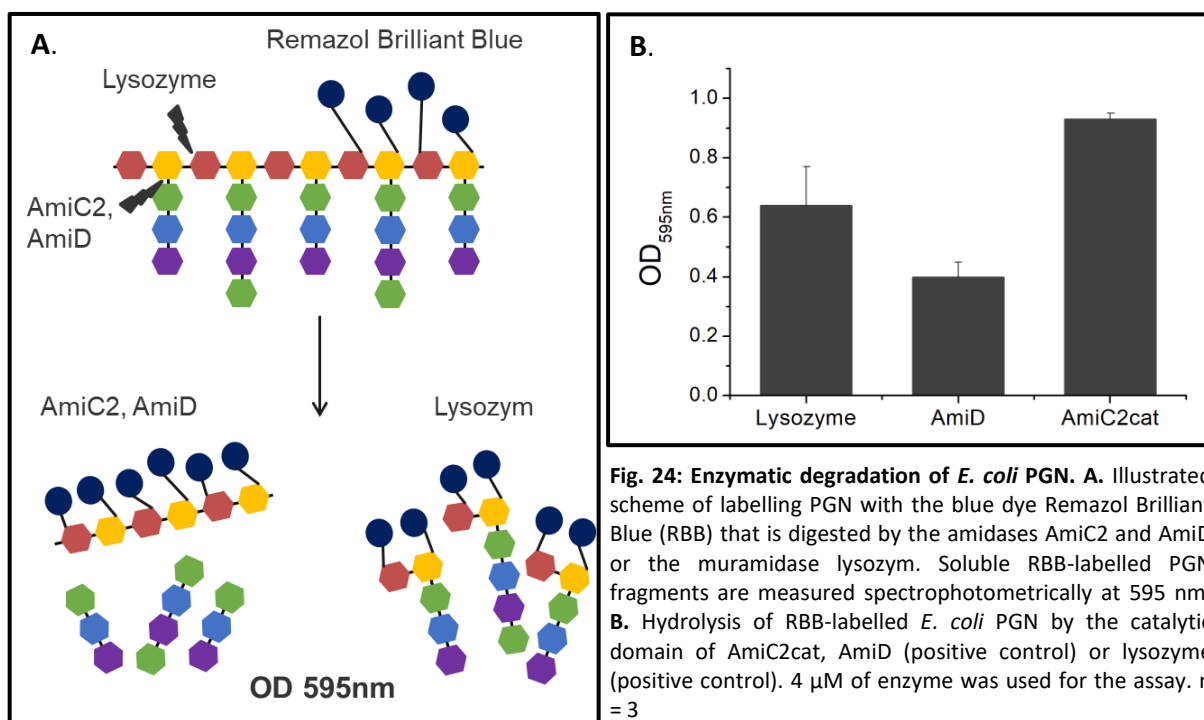


Fig. 24: Enzymatic degradation of *E. coli* PGN. A. Illustrated scheme of labelling PGN with the blue dye Remazol Brilliant Blue (RBB) that is digested by the amidases AmiC2 and AmiD or the muramidase lysozym. Soluble RBB-labelled PGN fragments are measured spectrophotometrically at 595 nm. B. Hydrolysis of RBB-labelled *E. coli* PGN by the catalytic domain of AmiC2cat, AmiD (positive control) or lysozyme (positive control). 4 μ M of enzyme was used for the assay. n = 3

Nostoc peptidoglycan was isolated, purified and adjusted to an OD_{600nm} of 2. Each experimental approach was supplemented with 1 μ M enzyme and incubated over 24 h at 37°C. Several samples were taken during the course of incubation and derivatized with OPA. Background fluorescence resulting from buffer components was subtracted. Amines were quantified using a calibration curve of different alanine concentrations and normalized to the PGN input yield.

Almost no increase of NH_2 -groups in any sample containing wild-type peptidoglycan could be detected (Fig. 26B). Neither AmiC2cat nor AmiE degraded wt PGN during 24 h indicated by constant low levels of free amine groups. The detected amount of amine groups in the samples incubated with the amidases did not differ from that incubated with BSA, serving as a negative control, at any given time point. In contrast, samples containing *amic2* mutant PGN revealed an increase of amine groups over time when incubated either with AmiC2cat or AmiE (Fig. 26C). In PGN samples digested with AmiE, 70% more amine groups were detected after 24 compared to PGN degraded by AmiC2cat. No increase of amines and therefore no catalytic activity on PGN was measured in samples containing BSA at any time point.

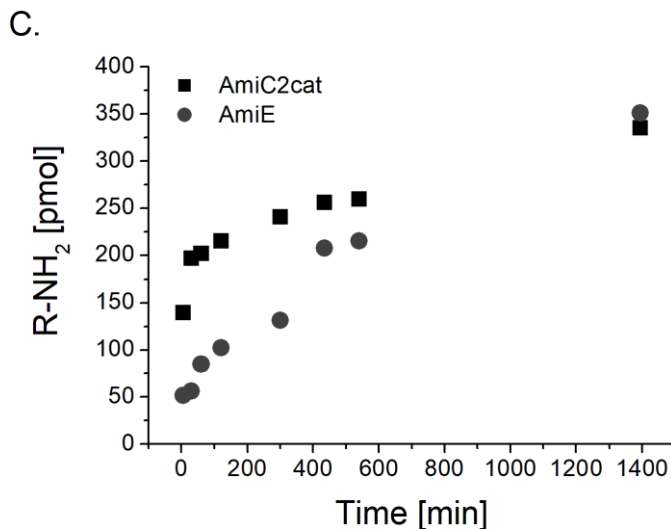
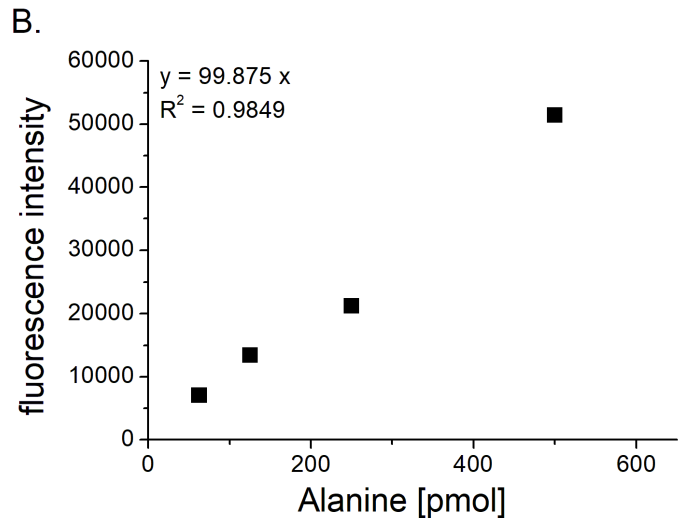
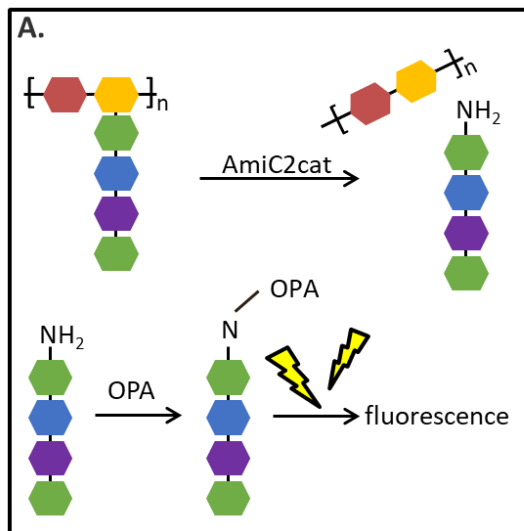


Fig. 25: Degradation of *E.coli* peptidoglycan. **A.** Schematic illustration of the experimental procedure. **B.** Calibration curve of OPA-derivatized alanine. **C.** Crude *E. coli* PGN was digested by 4 μ M AmiC2cat or AmiE. Samples were taken at different time points and derivatized by OPA. Fluorescence (excitation = 360 nm and emission = 460 nm) was immediately recorded using a Spark multimode microplate reader (Tecan). Background fluorescence was subtracted. Amine was quantified using the alanine calibration curve.

The catalytic domain of AmiC2 hydrolyses the peptidoglycan derived from *E. coli* (Fig. 24) and the *amiC2* mutant from *N. punctiforme*. Degradation of wild-type *N. punctiforme* peptidoglycan by AmiC2cat could not be detected in the assay.

All in all, the catalytic domain of the cell wall amidase AmiC2 hydrolyses Remazol-Brilliant Blue (RBB) labelled and unlabelled *E. coli* peptidoglycan. Since *Nostoc* PGN cannot be stained by RBB, a protocol was established to detect amidase released PGN-peptides by OPA-derivatization. Interestingly, the amidase is able to digest crude, unprocessed peptidoglycan from the *amiC2* mutant, but not from wild-type PGN.

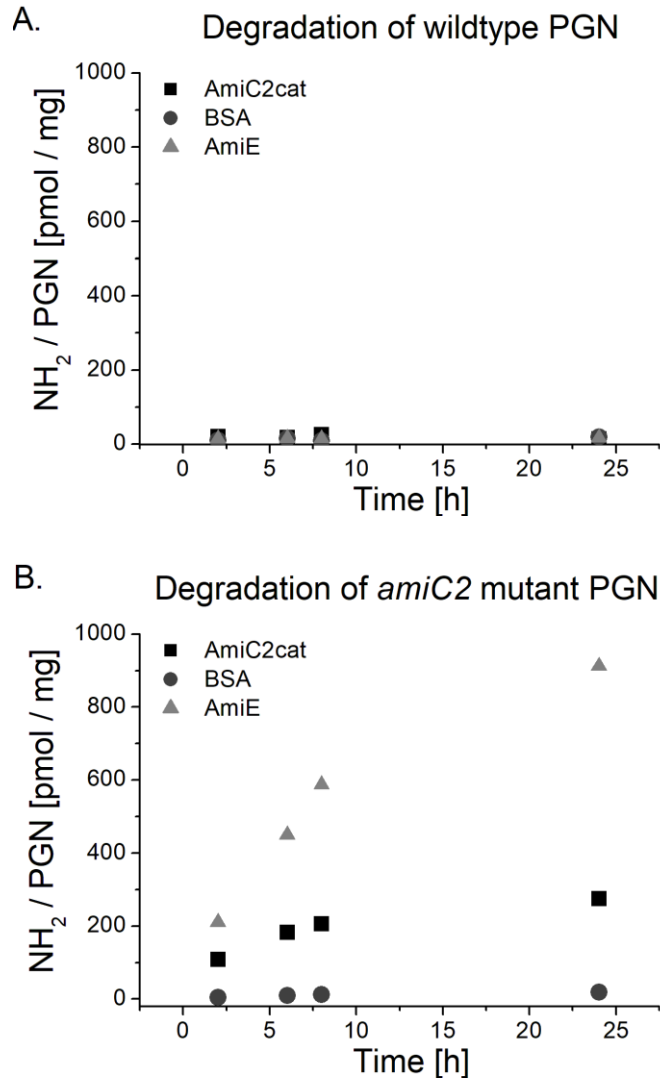


Fig. 26: Enzymatic hydrolysis of *Nostoc* PGN. Crude PGN of wild-type *N. punctiforme* (A) or the *amiC2* mutant (B) were digested with 1 μ M of AmiC2cat or AmiE (positive control) for 24 h at 37°C. Samples were removed at different time points and derivatized with OPA. Fluorescence (excitation at 360 nm and emission at 460 nm) was directly recorded using a Spark multimode microplate reader (Tecan). Background noise resulting from buffer constituents was subtracted from raw data. Amine groups of PGN peptides were quantified using a calibration curve of different alanine concentrations and normalized to the PGN amount. Equimolar amounts of BSA were used as negative control.

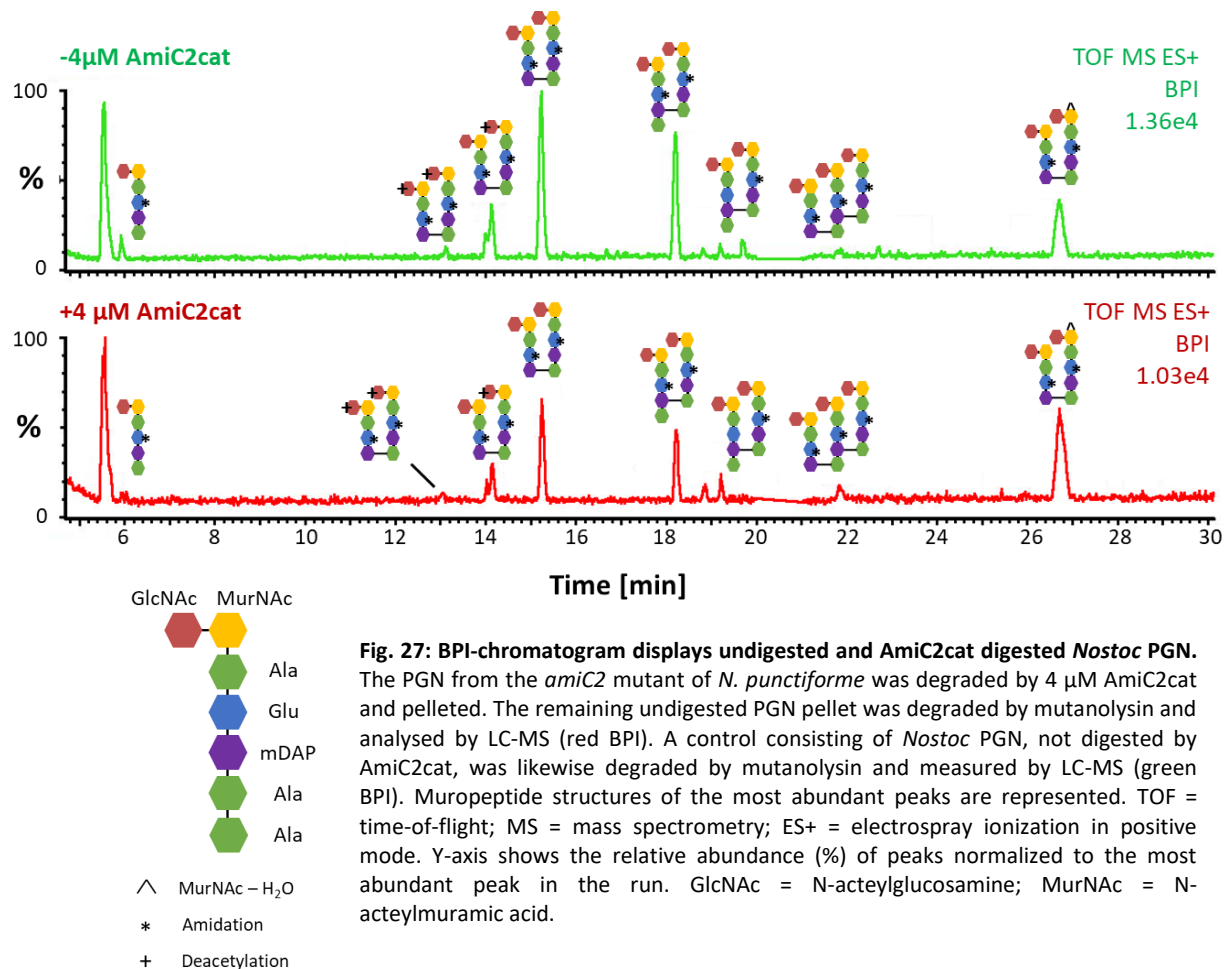
3.2.2. AmiC2cat prefers complex peptidoglycan fragments

The Dye-Release-Assay and the OPA-derivatization of released peptides are fast-screening methods to test if an enzyme can digest peptidoglycan in general. Detailed information about enzyme specificity is not obtained by these methods. Hence, two qualitative mass spectrometry approaches were applied for substrate profiling. The first method is for the detection of AmiC2cat released peptides by determining the mucopeptide profile before and after AmiC2cat digestion. Differences in the PGN fragment patterns are caused by AmiC2cat and will identify indirectly AmiC2cat substrates. The second procedure includes the analysis of AmiC2cat digests by two different mass-spectrometric methods.

Crude PGN from the *amiC2* mutant of *N. punctiforme* was used in both experimental approaches because AmiC2cat fully degrades the mutant PGN, as shown in Fig. 26B. Amidase released peptides were directly subjected to LC-(ESI-TOF)-MS in positive mode. The remaining, undigested PGN was further degraded by mutanolysin. The released soluble mucopeptides were subsequently analysed by LC-MS analysis. The resulting base peak chromatogram (BPI) was compared to a control in which the AmiC2cat digestion was omitted. The BPI- chromatograms from the control (green BPI) and the amidase treated sample (red BPI) are represented in Fig. 27. Both BPI-chromatograms revealed monomeric and highly crosslinked mucopeptides that are amidated, partially deacetylated or contained an anhydro-MurNAc residue. Evidently, both samples harboured the same mucopeptide species. There was no difference in the number of peaks or the type of mucopeptides. Differences could only be detected in the overall peak intensity, however, the peak intensity patterns were similar. An indirect detection of AmiC2cat substrates was not possible. Therefore, supernatants were collected after AmiC2cat digestion and analysed by LC-MS.

Three biological replicates were prepared using PGN from wild-type *N. punctiforme* and the *amiC2* mutant, respectively, as substrate for the amidase AmiC2cat. The LC-(ESI-Q-TOF)-MS provides a highly sensitive method for the detection of low amounts of PGN derived fragments. This was the reason why the PGN from the wild-type was used as well in the experiments, although the OPA-derivatization experiments in chapter 3.2.1 revealed that the amidase hardly hydrolysed wild-type *Nostoc* PGN.

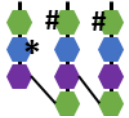
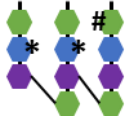
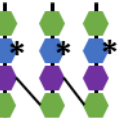
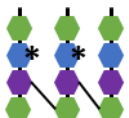
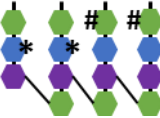
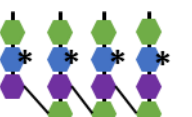
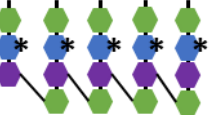
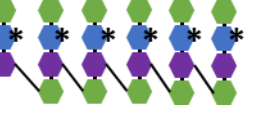
Table 48 summarizes all common mass-to-charge ratios in samples containing either the mutant or the wild-type derived PGN-peptides. PGN-peptide structures could be assigned to all detected mass-to-charge ratios. The difference of measured and calculated m/z for each PGN-peptide ranged between the second or third decimal place. The measurements were performed with a high-resolution LC-MS that provides high mass accuracy and deviations in the ppm range. The difference between the calculated and the measured m/z had therefore to be minimal. The identified putative PGN-peptides were highly cross-linked and additionally amidated. Even a hexamer might be the substrate for the amidase AmiC2cat. But further analyses had to be done, to verify all those m/z in AmiC2cat digested PGN samples and to confirm the presence of these highly cross-linked peptides by MS/MS fragmentation.



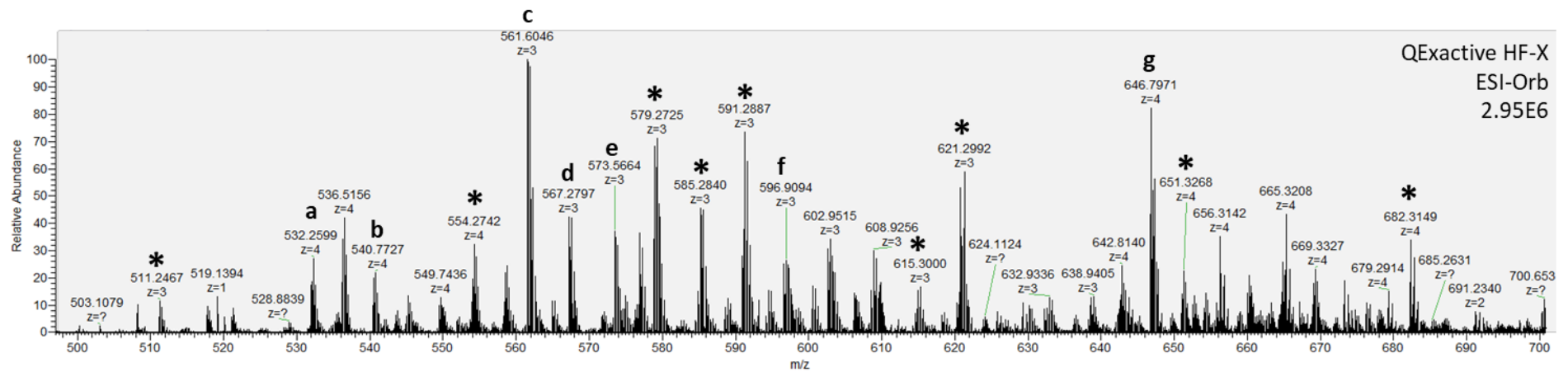
For this analysis, individual steps in the preparation were adapted to LC-MS/MS sample requirements. The desalted and concentrated PGN derived peptides were analysed by a high-resolution hybrid mass spectrometer (QExactive HF-X, Thermo Scientific). Fig. 28 and Fig. 29 display the MS₁-spectra of all PGN derived peptides from the wild-type PGN and the *amiC2* mutant PGN, eluting between 12 and 36 min. Relevant ions were detected in the range from 500 to 900 m/z. Abundant ions were chosen for fragmentation in the integrated HCD collision cell and subsequently measured in MS/MS mode. The HCD-fragmentation usually breaks the peptide bond between amino acids and generates fragments of different lengths. The fragmentation occurs randomly and not sequential but is designated by a serial loss of amino acids. The pattern of the fragment ions was used to identify AmiC2cat released peptides (Fig. 30). The m/z for each PGN-peptide is indicated by a letter (a - g) on top of the corresponding peak in the MS₁-spectrum (Fig. 28 and Fig. 29). The fragmentation pattern of each putative PGN-peptide is summarized in chapter 5.13.1 in the supplementary information.

The MS/MS fragmentation will be exemplarily explained for 1718.868 [M+H]⁺ (Fig. 31). The hypothetical peptide structure of 1718.868 [M+H]⁺ corresponds to a tripeptide connected to three monomers of a tetrapeptide. Each monomer of this highly crosslinked peptide consists of Ala, Glu and mDAP. There was a mass difference between the calculated m/z of this tetrameric structure (m/z 1720.7872) and the measured m/z (1718.868) of 1.919. This difference corresponds to two additional amidations, either on Glu or mDAP.

Table 48: PGN peptides cleaved by AmiC2cat. PGN derived from the *amiC2* mutant or the wild-type *N. punctiforme* were digested by AmiC2cat. Released PGN fragments were analysed by LC-MS. Presumable peptide structures are illustrated with their respective m/z. The difference between the calculated and measured m/z is displayed at the list below in ppm (parts per million). * = amidation; # = -H₂O

Oligomer	PGN-released peptide		from wild-type PGN	from <i>amiC2</i> PGN
	Species	Calculated m/z	m/z deviation	m/z deviation
Trimer		1240.5804	✓ (16.6 ppm)	✓ (-5 ppm)
Trimer		1257.607	✓ (-4 ppm)	✓ (38 ppm)
Trimer		1345.6706	✓ (6 ppm)	✓ (6.4 ppm)
Trimer		1346.6546	✓ (-1.6 ppm)	✓ (-2 ppm)
Tetramer		1682.798	✓ (45 ppm)	✓ (21 ppm)
Tetramer		1716.8511	✓ (5.9 ppm)	✓ (6 ppm)
Pentamer		2159.0687	✓ (3.4 ppm)	✓ (-9 ppm)
Hexamer		2601.2863	✓ (-38.3 ppm)	✓ (40 ppm)

A. MS1-spectrum of AmiC2cat released peptides from wild-type PGN with m/z between 500 and 700



B. MS1-spectrum of AmiC2cat released peptides from wildtype PGN with m/z between 700 and 900

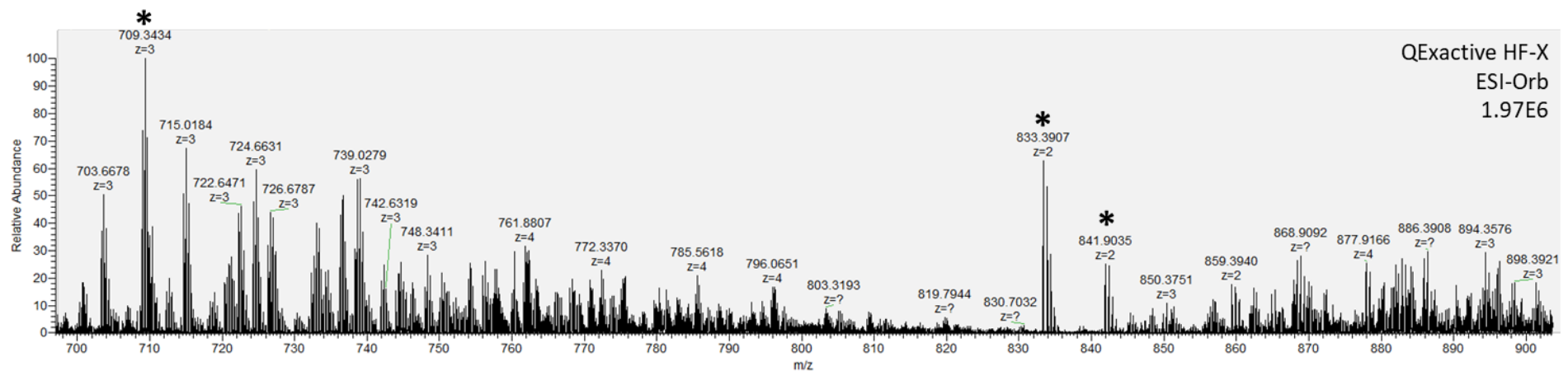
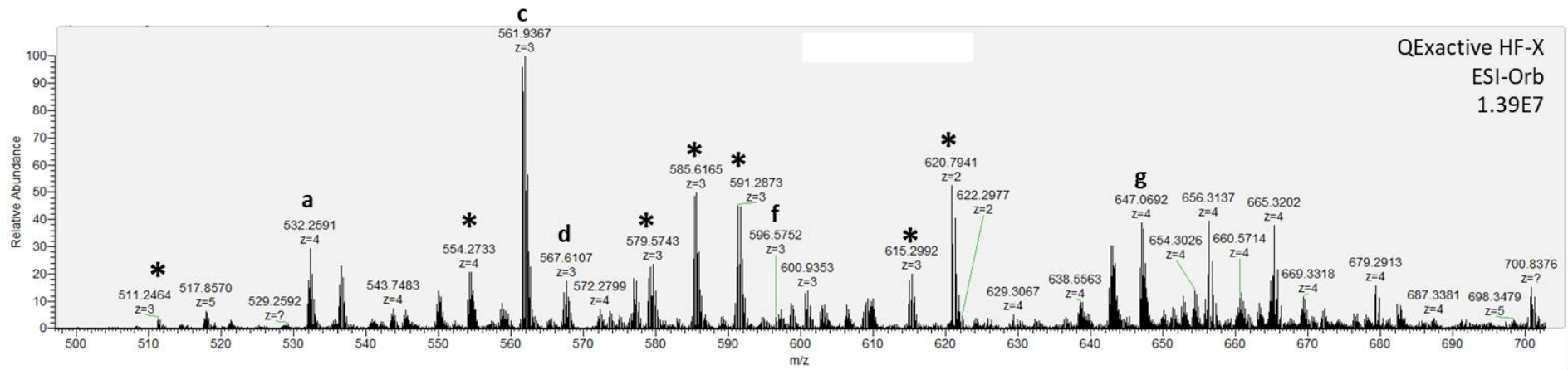


Fig. 28: MS1 spectra of AmiC2cat released peptides from *N. punctiforme* PGN. *Nostoc* PGN was incubated with 4 M AmiC2cat and released peptides were enriched and purified. The analysis of PGN derived peptides was performed by a QExactive HF-X equipped with an ESI source and an Orbitrap mass analyser. The peptides were separated by a 90 min linear acetonitrile gradient. Letters on top of the peaks represent PGN-peptides whose compositional structure was confirmed by MS/MS fragmentation. PGN-peptide structures could also be assigned to peaks, marked with a star, but MS/MS fragmentation could only partially confirm the structure.

A. MS1-spectrum of AmiC2cat released peptides from *amiC2* mutant PGN with m/z between 500 and 700



B. MS1-spectrum of AmiC2cat released peptides from *amiC2* mutant PGN with m/z between 700 and 900

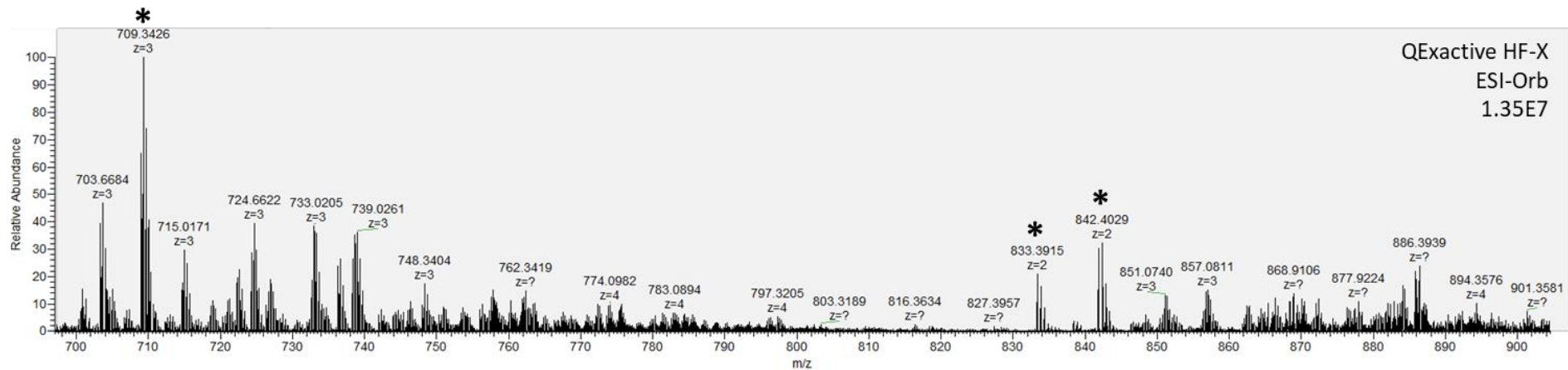


Fig. 29: MS1 spectra of an AmiC2cat digest from *amiC2* mutant PGN. The PGN was incubated with 4 M AmiC2cat and collected by centrifugation. The released peptides in the supernatant were enriched and purified. The analysis of PGN derived peptides was performed by a QExactive HF-X equipped with an ESI source and an Orbitrap mass analyser. The peptides were separated by a 90 min linear acetonitrile gradient. Letters on top of the peaks represent PGN-peptides whose compositional structure was confirmed by MS/MS fragmentation. PGN-peptide structures could also be assigned to peaks marked with a star but MS/MS fragmentation could only partially confirm the structure

Table 49: LC-MS analysis of AmiC2cat digests from *Nostoc* PGN. PGN from *amiC2* mutant or wild-type *N. punctiforme* were digested by AmiC2cat. Released peptides were analysed by LC-MS and a possible peptide structure was assigned to all numbered peaks. MS/MS fragmentation confirmed structural composition. A = amidation

Peak	m/z		Z	measured [M+H] ⁺		calculated [M+H] ⁺	modification	MS2
	wt	<i>amiC2</i>		Wt	<i>amiC2</i>			
A	532.259	532.259	4	2126.015	2126.036	2160.052	4A, -2H ₂ O	✓
B	540.769	-	4	2160.055		2160.052	4A	✓
C	561.604	561.637	3	1682.798	1682.911	1718.819	2A, -2H ₂ O	✓
D	567.616	567.611	3	1700.834	1700.833	1718.819	2A, -H ₂ O	✓
E	573.566	-	3	1718.684		1718.819	2A	✓
F	596.905	596.875	3	1788.701	1788.625	1788.872	3A	✓
G	646.796	646.769	4	2584.163	2584.076	2602.270	5A, -H ₂ O	✓

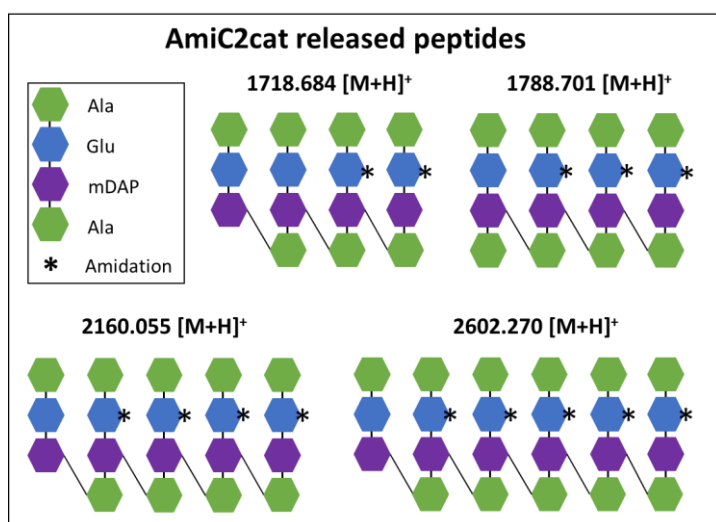


Fig. 30: Identification of AmiC2cat released PGN-peptides. PGN of wild-type *N. punctiforme* and its *amiC2* mutant were incubated with 4 μ M AmiC2cat. Soluble components, including PGN derived peptides, were purified and enriched. The sample was subjected to LC-MS and the MS1-spectra were screened for appropriate m/z corresponding to PGN-peptides. MS2-fragmentation confirmed the structural composition of four PGN derived peptides.

The amidation is represented by a star on the glutamate residue in Fig. 31B. As previously mentioned in chapter 3.1.3, the position of the amide group will be discussed in chapter 4.1.2 and hereafter always associated with glutamate.

The MS2-spectrum of the identified PGN tetramer, with the parental mass of 1718.868 [M+H]⁺, revealed a double charged fragment ion with the m/z = 673.751 (m/z of the single charged mass: 1346.495) (Fig. 31A). This mass-to-charge ratio matches to a peptide with the theoretical m/z of 1346.6308, which was generated by the loss of Ala, Gln and mDAP (m/z of 373.1959) from the parental ion with the calculated m/z of 1718.8191. The difference between the measured m/z of the fragment ion (1346.495 m/z) and the measured m/z of the parental ion (1718.868 m/z) corresponds to the loss of this tripeptide of Ala, Gln and Glu. Intermediate fragment ions revealing the sequential elimination of either Ala, Gln or mDAP were not identified. The MS/MS-profile of 1718.868 [M+H]⁺ is represented in different colours to better follow the degradation of each monomer.

Another double charged ion with m/z = 573.767 (1146.527 [M+H]⁺) was detected in the MS2-spectrum (Fig. 31A) indicating the simultaneous loss of Ala (-72.045) and Gln (-128.059) from the fragment ion with the m/z of 1346.495 (see black line in Fig. 31). Following, a monoisotopic fragment peak with m/z of 904.413 was identified. Its mass difference to the fragment ion with the m/z of

1146.527 is 242.114 Da. The simulated fragmentation of the parental ion with the m/z of 1718.8191 revealed that this difference of 242.114 Da is equivalent to a further loss of mDAP and Ala. A serial elimination of Ala (-72.045), Glu (129.043) and mDAP-Ala (-242.114) generated the fragment ions 832.364 [M+H]⁺, 703.326 [M+H]⁺ and 461.212 [M+H]⁺, respectively (see red lines in the MS2 spectrum in Fig. 31). Subsequently, ions (373.1713 m/z and 301.1389 m/z) were detected matching to an elimination of two alanine residues from the fragment ion with m/z of 461.212 (see pink lines in the MS2-spectrum in Fig. 31). Neutral loss of water (-18.01 Da) was frequently observed during the MS7MS fragmentation. This was also matching to a Gln-mDAP dipeptide was further cleaved into single amino acids.

The MS1-spectra (Fig. 28 and Fig. 29) obtained from the AmiC2cat digests of wild-type or *amiC2* mutant PGN revealed each two double charged ions, 561.604 m/z (c) and 567.616 m/z (d) for the wild-type and as well as 561.937 m/z (c) and 567.611 m/z (d) for the *amiC2* mutant. These ions resulted from the parental peptide ion 1718.868 [M+H]⁺ with a neutral loss of one or two water molecules (see MS2-spectra for c and d in chapter 5.13.1, supplementary information). A loss of water during ESI-ionization has to be considered, since the parental ion with 1718.868 [M+H]⁺, for example, could not be found in the sample derived from the *amiC2* mutant (Fig. 28 and Table 49). However, the presence of the double charged ions 561.937 m/z and 567.611 m/z and the MS/MS fragmentation of these ions (described in chapter 5.13.1, supplementary information) suggests the presence of this peptide also in the *amiC2* mutant sample.

Furthermore, an ion with the m/z of 1682.798 (Table 48) could be identified in previous LC-MS-analysis of AmiC2cat digests from wild-type and *amiC2* mutant PGN. This mass-to-charge ratio was equivalent with those detected in the optimized peptide analysis (Table 49, peak c). In contrast, a putative PGN-peptide with the m/z of 1716.851 was detected in the initial LC-MS measurements. This peptide was not found in the subsequent LC-MS/MS measurement.

Two highly crosslinked PGN-peptides were further identified in wild-type and *amiC2* mutant samples (Fig. 28 and Fig. 29, peak a, b and g). In the wild-type, a pentamer with 2160.055 [M+H]⁺ was detected. This oligomeric PGN fragment consists of four additional amidated tetrapeptide monomers and a tripeptide. This putative composition of the peptide was confirmed by MS/MS-fragmentation (see peak b in chapter 5.13.1, supplementary information). Ionization-induced cleaved ions were measured in both samples, with the m/z of 532.259. These ions correspond to the parent ion 2160.055 m/z (= 540 [M+H]⁴⁺) with the loss of two water molecules (see peak a in chapter 5.13.1, supplementary information). A corresponding ion was also detected in the dataset from the previous LC-MS analysis (Table 48). The mass-to-charge ratios of the equivalent ions differed by the mass of an amide group (0.987 Da).

Another highly crosslinked PGN derived peptide was found in Table 48 and Table 49 (calculated 2601.2863 [M+H]⁺ and 2602.270 [M+H]⁺). The mass-to-charge ratios differed again by an amide group (\pm 0.984 Da), but the general composition of the detected hexamer was identical. This comprises five tetrapeptide monomers and one tripeptide monomer. Each monomer consists of Ala, Glu and mDAP. The corresponding peptide analysis by hybrid mass spectrometry revealed only two ions with neutral loss of water in wild-type and *amiC2* mutant samples: 646.796 m/z and 646.769 m/z. The MS2-profile confirmed the hexameric composition and the presence of five amide-groups (see peak g in chapter 5.13.1, supplementary information).

In peak f from wild-type and the *amiC2* mutant PGN digests, a peptide with a tetrameric structure could be identified. The MS/MS fragmentation revealed an additional amidation of three of the four tetrapeptide monomers (see peak f in chapter 5.13.1, supplementary information). This tetramer was not detected in the previous LC-MS measurement (Table 48).

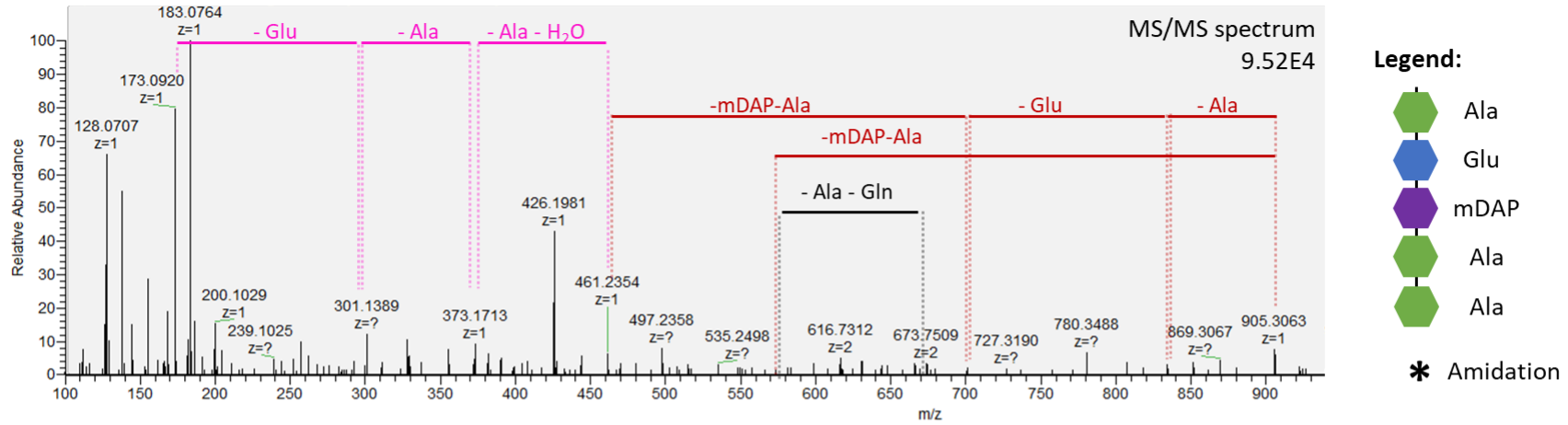
Table 48 represents four additional PGN-derived peptides in samples of the wild-type and the *amiC2* mutant variant. All these peptides revealed a trimeric composition. The ions 1240.5804 m/z and 1257.607 m/z comprised two tetrapeptide monomers and one tripeptide monomer whereas 1345.6706 m/z and 1346.6546 m/z consisted of four tetrapeptide monomers. The former ions were probably cleavage products of 1276.601 m/z and 1275.616 m/z under elimination of two or one water molecule, respectively. The ions 1345.6706 m/z and 1346.6546 m/z differed by an amide group. Equivalent ions were also found in the MS1-spectra of the subsequent peptide analysis of the wild-type and *amiC2* mutant sample.

Triple charged ions 414.30 m/z and 419.87 m/z were measured in both samples that corresponded to 1240.5804 m/z and 1257.607. No corresponding MS2-spectra were generated leaving the oligomeric structure of these peptides unconfirmed. The same was true for 1345.6706 m/z and 1346.6546 m/z. Ions were detected in both samples indicating a loss of two water molecules (437.18 [M+H]³⁺ and 437.50 [M+H]³⁺) but MS2-spectra were not obtained.

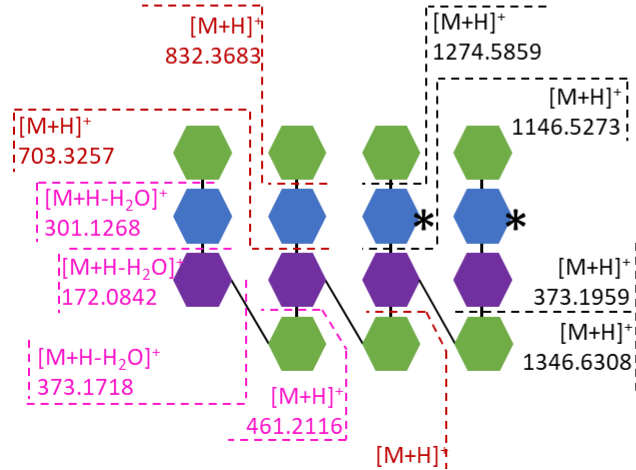
Moreover, the MS1-spectra from the wild-type and *amiC2* mutant samples (Fig. 28 and Fig. 29) demonstrated many highly abundant ions marked by a star. Overall, a putative PGN-peptide structure could be assigned for the majority of all these m/z, but the MS/MS fragmentation confirmed only parts of these structures (see Table 58, in the supplementary information, for a list of all these peptides).

In conclusion, the amidase AmiC2cat is able to hydrolyse wild-type and *amiC2* mutant PGN because released peptides from both peptidoglycans were detected by tandem mass spectrometry. The intensity of both MS1-spectra differed about the factor 10, whereby the MS1-spectrum from the *amiC2* mutant displayed the higher intensity. This might indicate that AmiC2cat likely released more peptides from the *amiC2* mutant PGN than from the wild-type PGN. This issue will be discussed in chapter 4.2.2 in the discussions part. MS/MS fragmentation identified tetrameric, pentameric and hexameric structures of the released peptides. These highly crosslinked peptides represent the substrate for the amidase AmiC2cat.

A. MS2-spectrum of 1718. 8684 [M+H]⁺



B. MS/MS fragmentation pattern:



C. Detailed MS/MS fragmentation:

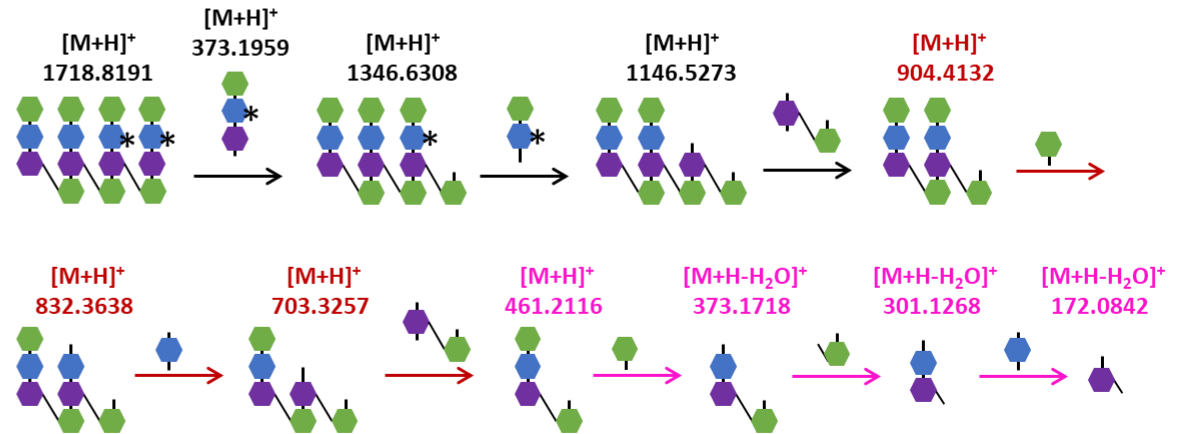


Fig. 31: MS/MS fragmentation of 1718.8684 [M+H]⁺. A. MS2 profile of 1718.8684 [M+H]⁺ displaying the stepwise dissociation of amino acids or peptides from the parental ion. B. Putative composition of the PGN-peptide with 1718.8684 [M+H]⁺. The serial fragmentation of each monomer is represented by different colours and displays the m/z for each intermediate fragment ion. C. Detailed illustration for MS/MS fragmentation of 1718.8684 [M+H]⁺.

3.2.3. Putative catalytic residues: F564, E529 and L576

The amidase AmiC2 was characterized to hydrolyse highly cross-linked peptidoglycan fragments. This finding is in line with crystallographic data obtained from the catalytic domain of AmiC2. The wide and shallow cavity allows the binding of peptidoglycan with different orientations or oligomerization (242). Mutational analysis of amino acid residues in the substrate binding-groove elucidates how AmiC2 accommodates PGN. Fig. 32A represents the catalytic domain of AmiC2 in complex with a putative PGN molecule. Amino acid residues that are potentially involved in substrate binding are highlighted in magenta. S518, D520, E529 and V519 are predicted to interact with the glycan backbone of the peptidoglycan, whereas F564 and L576 likely form a hydrophobic pocket for the peptide stem (F. Büttner, personal communication). Arginine residues at position 568 and 563 might stabilize the complex by the formation of a salt bridge with mDAP.

The role of these amino acid residues in PGN-binding was analysed by site-directed mutagenesis. The catalytic domain of AmiC2, carrying different site-specific mutations (see Table 50 for type of substitution) was expressed in *E. coli* as GST fusion protein. The mutant variants were purified using affinity and size-exclusion chromatography. The GST-tag was subsequently removed by enzymatic cleavage. Table 50 represents the list of all site-specific mutant variants of AmiC2cat and indicates if the variants could be purified successfully. Unfortunately, it was not possible to express and purify each mutant variant of AmiC2cat due to decreased protein stability in specific cases. A total of eight site-specific mutants could be purified and were subsequently applied to Dye-Release-Assays (DRA) for the examination of their hydrolytic activity on RBB-labelled *E. coli* PGN (Fig. 33B).

The catalytic activity of AmiC2cat on *E. coli* PGN was significantly decreased upon specific point mutations. The substitution of glutamate and leucine at positions 529 and 576 had deleterious effects on the catalytic activity. More than 65% less RBB-labelled peptidoglycan fragments were released by AmiC2cat, when the physicochemical properties of glutamate were changed due to a substitution by an alanine residue. The exchange of the hydrophobic and unipolar leucine residue at position 576 to the polar amino acid serine decreased the PGN hydrolysis by 73%.

The phenylalanine replacement at position 564 affected as well the hydrolytic activity, albeit lower than E529A and L576S mutants. Approximately 43% or 40% less RBB-labelled PGN fragments were detected when phenylalanine was exchanged to serine or threonine, respectively. The exchange by serine or threonine decreases the distance to the mDAP residue and prevents an interaction. A minor effect was observed for the alanine substitutions of D520 or S518. Both sites are predicted to interact with the glycan chain of peptidoglycan. The single and double mutant variants V519T and R563DR568D of AmiC2cat revealed similar hydrolytic activity as the wild-type AmiC2cat. Threonine is a polar amino acid, whereas valine is aliphatic and hydrophobic. Both positively charged arginine residues are predicted to be involved in a salt bridge formation with mDAP. Aspartate is a negative charged amino acid and is hypothesized to interrupt salt bridge formation.

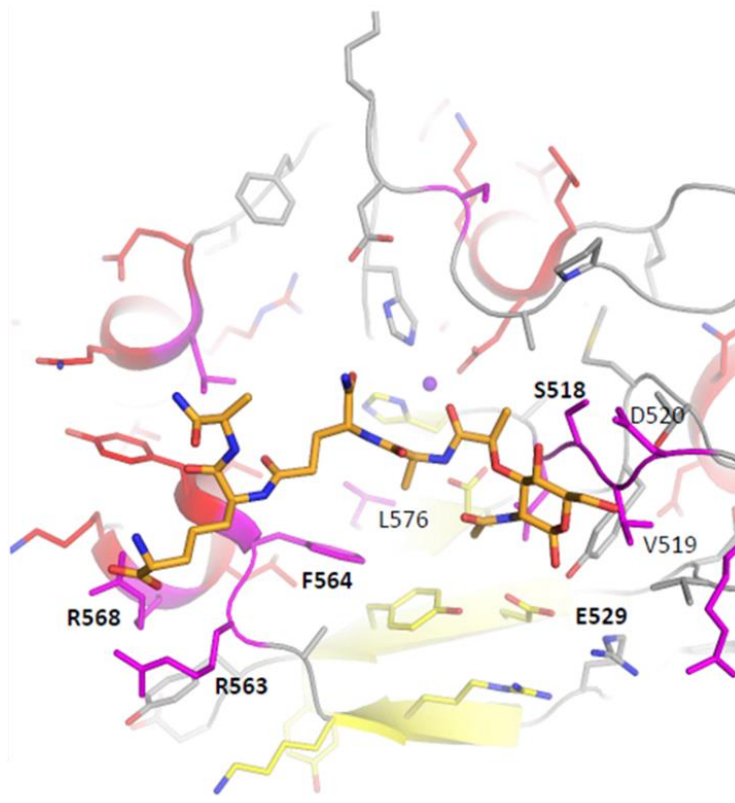


Fig. 32: AmiC2 in complex with PGN. The binding cavity of AmiC2 from *N. punctiforme* in complex with a MurNAc-tetrapeptide is represented. Amino acid residues involved in PGN binding are labelled magenta. PGN/AmiC2 binding model was done by F. Büttner.

A PGN-binding experiment was performed to answer the question if the substrate-binding capability was affected upon site-specific mutations. Each purified mutant variant or wild-type AmiC2cat were incubated with *Nostoc* PGN and subjected to SDS-PAGE after enzymatic cleavage. Soluble fragments in the supernatants were loaded as well onto a 15% SDS-polyacrylamide gel (Fig. 33C). Peptidoglycan-binding proteins are found in the fraction containing the washed peptidoglycan pellet (P), whereas non-binding proteins are found in the fraction containing the supernatant from the first centrifugation (S1). The supernatant from the washing step (S2) will harbour proteins that were unspecifically bound to the peptidoglycan.

The SDS-PAGE analysis revealed protein bands in lanes containing the PGN pellet (P) and the supernatant obtained from the first centrifugation (S1) (Fig. 33B). There was no protein detected in any lane containing the supernatant from the washing step (S2). Apparently, D520A, E529A, L576S and F564S were found exclusively in the S1-fraction. However, the intensity of these protein bands was very weak compared to those obtained from the wild-type AmiC2cat or the mutants S518A and R563DR568D.

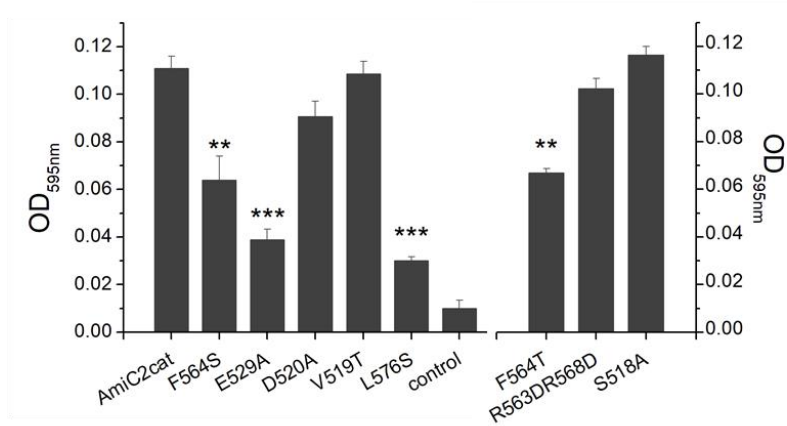
It is questionable if the substitutions of glutamine, glutamate, leucine or phenylalanine really abolish the PGN binding of AmiC2 due to low protein intensities found in the SDS-polyacrylamide gel. The wild-type version of AmiC2cat was present in the PGN and to a much higher extent in the S1-fraction. A similar pattern was observed for the site-specific mutants S518A and R563DR568D. Only faint

bands were detected in lanes obtained from the F564T mutant. It was impossible to predict an influence of the threonine substitution on the PGN-binding capability of AmiC2cat regarding the SDS-PAGE analysis. Besides this, it is challenging to observe slight alterations in the binding behaviour of AmiC2cat caused by amino acid substitutions. Although, equimolar protein amounts were utilized in each experimental approach and subsequently loaded onto the SDS-polyacrylamide gel, strong variations in the intensity of the protein bands became visible.

Table 50: Amino acid replacements in the substrate-binding site of AmiC2 from *N. punctiforme*. Conserved amino acid residues in the putative PGN-binding site of AmiC2 were analysed by site-directed mutagenesis. Table summarizes amino acid position, substitution and a successful purification of the mutant variant indicated by a checkmark. AA = amino acid; Pos. = position; Pred. = predicted Sub. = substitution

AA	Pos.	Assumed function	Nucleotide change	Sub.	Assumed function	Label	Purification
F	564	Hydrophobic interaction with mDAP	TTC -> TCT	S	Prevents hydrophobic interaction with mDAP	F564S	✓
			TTC -> GCG	A		F564A	-
			TTC -> GTG	V		F564V	-
			TTC -> ACC	T		F564T	✓
R	563	Salt bridge formation with mDAP	AGA -> GCG	A	Prevents salt bridge formation	R563A/	-
R	568		AGG -> GCG			R568A	
R	563	Salt bridge formation with mDAP	AGA -> GAT	D	Prevents salt bridge formation	R563D/	✓
R	568		AGG -> GAT			R568D	
L	576	Hydrophobic pocket for PGN-peptide stem	TTA -> AGC	S	Interrupts interaction with glycan chain	L576S	✓
			TTA -> GCG	A		L576A	-
S	518	Interaction with glycan chain	TCT -> GCG	A	Interrupts interaction with glycan chain	S518A	✓
V	519	Interaction with glycan chain	GTT -> ACC	T	Interrupts interaction with glycan chain	V519T	✓
D	520	Interaction with glycan chain	GAC -> GCG	A	Interrupts interaction with glycan chain	D520A	✓
E	529	Interaction with glycan chain	GAA -> GCG	A	Interrupts interaction with glycan chain	E529A	✓
			GAA -> CAG	Q		E529Q	-

A. PGN hydrolytic activity of AmiC2cat site-specific mutants



B. PGN-binding capability of AmiC2cat mutant variants

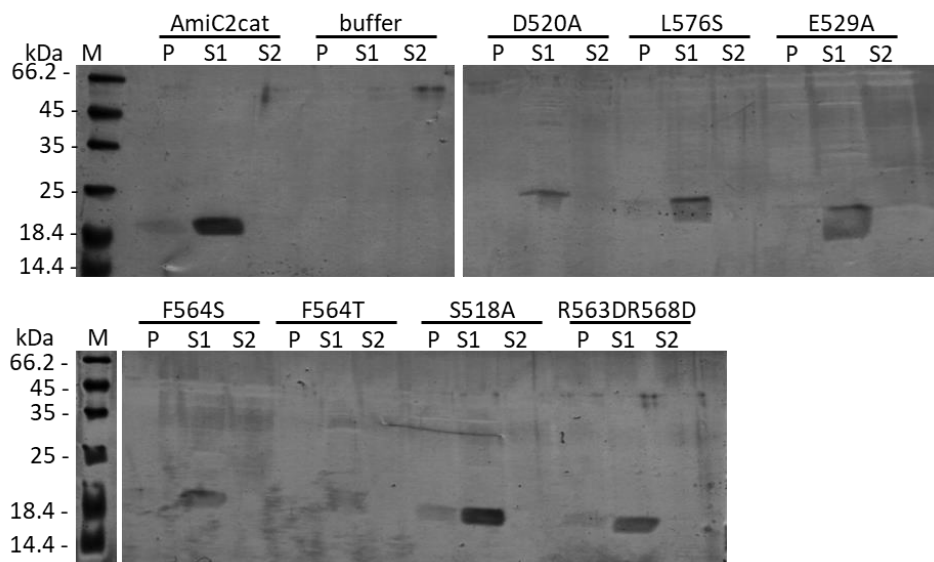


Fig. 33: Influence of site-specific mutations on AmiC2cat hydrolytic activity and binding capability. **A.** Hydrolytic activity of AmiC2cat and its site-specific mutants on RBB-labelled *E. coli* PGN. 50 μ l RBB-labelled *E. coli* PGN were incubated with 4 μ M enzymes for 30 min at 37°C. PGN was removed by centrifugation and absorbance of supernatants was measured at 595 nm. $p = 0.1$ (*); $p = 0.01$ (**) and $p = 0.001$ (***); $n = 3$. **B.** Binding of AmiC2cat and site-specific mutants on *Nostoc* PGN analysed by SDS-PAGE. *Nostoc* PGN (50 μ l adjusted to $OD_{600nm} = 1$) were incubated with 2 μ M enzymes for 1h at room temperature. PGN was pelleted, washed once and subjected to SDS-PAGE. Supernatants were collected and loaded onto SDS-polyacrylamide gel. P = PGN pellet; S1 = supernatant after first centrifugation; S2 = supernatant after second centrifugation; M = protein marker.

Due to these limitations, a more sensitive method was needed to detect the impact of site-specific mutations. A system based on surface plasmon resonance (SPR) was used to determine the interaction between AmiC2cat and peptidoglycan. A N-terminal His-tag was fused to AmiC2cat and its mutant variants to immobilize the enzymes on a Ni-NTA surface. The purification of the His-tagged metalloenzyme AmiC2cat required specific changes in the protocol due to its tendency to precipitate at various tested conditions (see chapters 2.12.2 and 2.12.3 for expression and purification of His-tagged enzymes).

As an initial step, the influence of the attached His-tag on the hydrolytic activity of AmiC2cat was tested using the DRA. Indeed, the substitution of F564, E529 and L576 decreased the PGN hydrolytic activity of AmiC2cat significantly (Fig. 34A). This finding was in line with the previous experiment using the non-tagged proteins (Fig. 33A). Unexpectedly, increased absorbance was detected with the histidine tag fused site-specific mutants compared to the non-tagged mutants. Especially the mutant variant E529A exhibited a 44% higher PGN hydrolytic activity with a His8-tag. Likewise, an increase in released RBB-labelled PGN fragments were observed for the tagged mutant variants F564S and L576S. The mutant F564S hydrolysed the double amount of RBB-labelled PGN compared to L567S. The same effect was already observed without the His8-tag (Fig. 33A). The replacement of S518, D520 and V519 did not significantly affect the catalytic activity of His8-AmiC2cat, as previously shown in Fig. 33A without affinity tag.

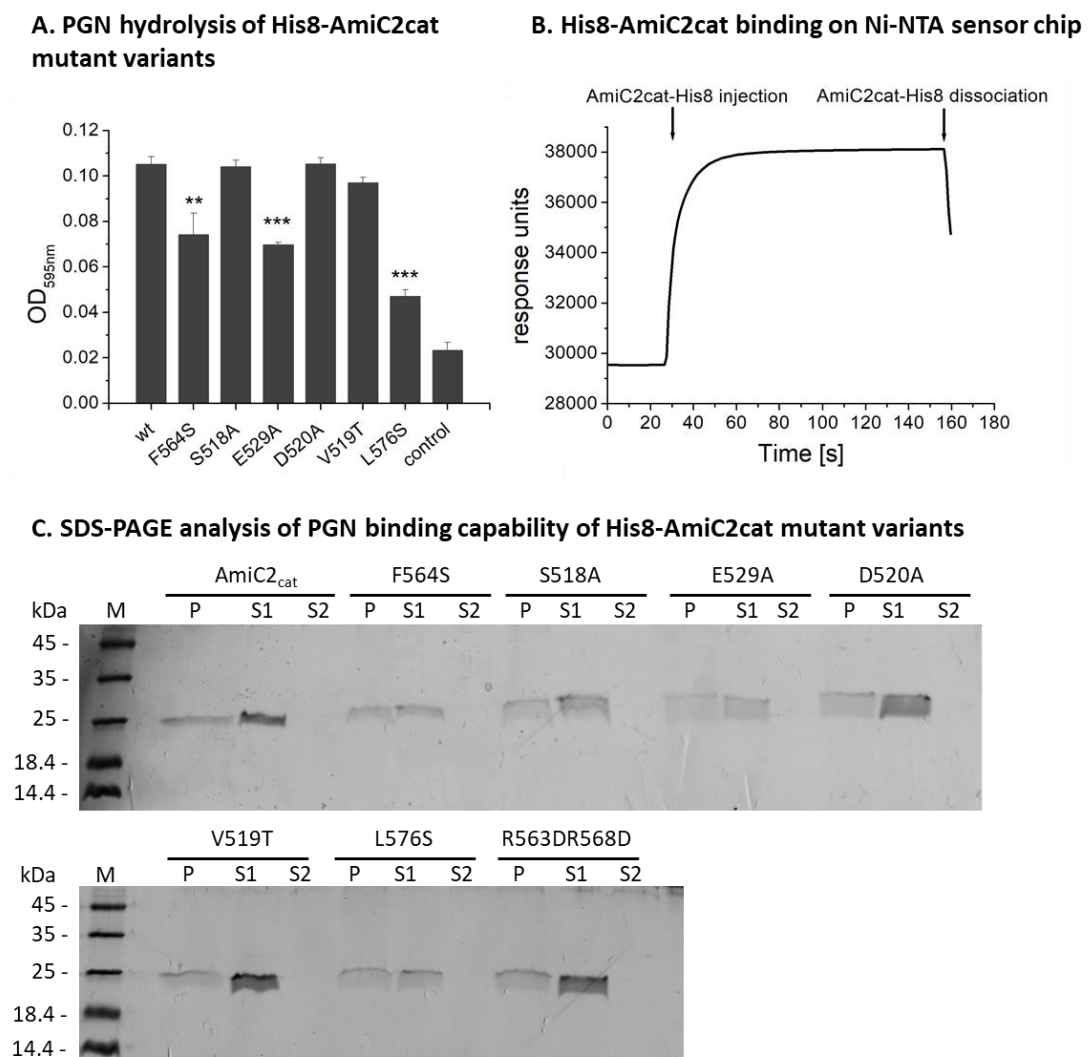


Fig. 34: PGN binding and hydrolysis of His8-tagged AmiC2cat mutant variants. **A.** Dye-release assay using 4 μM of His8-AmiC2cat and its site-specific mutants for the hydrolysis of RBB-labelled *E. coli* PGN. Absorbance was measured at 595 nm. $p = 0.1$ (*); $p = 0.01$ (**) and $p = 0.001$ (***); $n = 3$ **B.** 200 nM His8-AmiC2cat were immobilized onto Biacore Ni-NTA biosensor chips. Injection time and dissociation of His8-AmiC2cat are represented. **C.** SDS-PAGE analysis of the PGN binding behaviour of His8-AmiC2cat and site-specific mutants on *Nostoc* PGN. *Nostoc* PGN (50 μl adjusted to $\text{OD}_{600\text{nm}} = 1$) were incubated with 1 μM enzymes for 1h at room temperature. PGN was pelleted, washed once and subjected to SDS-PAGE. Supernatants were collected and loaded onto SDS-polyacrylamide gel. P = PGN pellet; S1 = supernatant after first centrifugation; S2 = supernatant after second centrifugation; M = protein marker.

The PGN-binding experiment, using the SDS-PAGE analysis, was repeated with the tagged variants (Fig. 34C). Reduced enzyme concentrations (1 μM) were applied to the reaction mixture with the aim to enhance the probability to detect PGN-AmiC2cat complexes. Indeed, protein bands were detected in all lanes containing the PGN pellet, indicating a binding of AmiC2cat and its mutant variants to *Nostoc* PGN. Besides this, all site-specific mutants and the wild-type His8-AmiC2cat were present in the S1-fraction. It was not possible to observe slight alterations in the PGN binding of His8-AmiC2cat upon mutation as previously observed in the PGN-binding experiment (Fig. 33B). To overcome this limitation, the high sensitive Biacore-SPR technique was applied to measure the interaction between His8-AmiC2cat and PGN. A solution of 200 nM His8 AmiC2cat was injected to load the Ni-NTA biosensor chip. However, a dissociation of His8-AmiC2cat from the Ni-NTA biosensor chip, soon after the injection, could be monitored (Fig. 34B). Neither a higher protein concentration nor a slower injection procedure could abolish the following dissociation from the chip. Therefore, an alternative Microscale Thermophoresis based method was selected to determine the PGN binding of His8-AmiC2cat.

Microscale Thermophoresis (MST) detects changes in the movement and the fluorescence of molecules in a temperature gradient upon ligand binding. His8-AmiC2cat was labelled with a red fluorescent dye to measure extrinsic fluorescence changes upon binding to mutanolysin released muropeptides. Mutanolysin digestion is usually performed under acidic conditions due to its catalytic optimum, whereas AmiC2cat reveals a pH optimum at mild alkaline condition. First experiments were performed to define if specific ingredients in the MST reaction buffer or the acidic pH affect the MST measurement (see chapter 5.4 in the supplementary information). Strong variable fluorescence intensities were observed when the MST-experiment was started under acidic pH conditions (Fig. 44 and Fig. 46 in the supplementary information). Such fluorescence fluctuations led to a false-positive result in the MST analysis (Fig. 46C, supplementary information). A constant pH during the MST measurements revealed no such implications (Fig. 45, supplementary information).

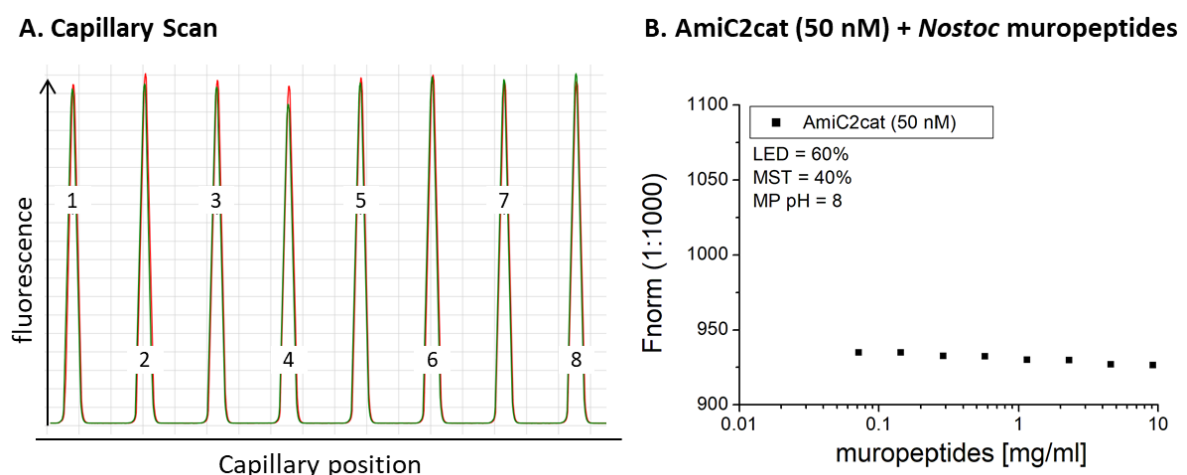


Fig. 35: MST measurement of AmiC2cat and soluble PGN fragments. **A.** Initial fluorescence intensity in each capillary just before the experiment started. **B.** Dose-responsive curve of His8-AmiC2cat and *Nostoc* muropeptides. His8-AmiC2cat was labelled with a red fluorescent dye and 50 nM were used in the experiment. *Nostoc* muropeptides were adjusted to pH8 and serial diluted in sodium phosphate buffer (1:1). LED: fluorophore excitation; MST: Infrared laser power; MP: muropeptides; Fnorm: normalized fluorescence.

Fig. 35A represents the fluorescence scan of each capillary containing the amidase and the muopeptides with an adjusted pH. The samples in the capillaries exhibited the same fluorescence intensity and the fluorescence peaks appeared symmetrical. Fig. 35B demonstrates the dose-responsive curve for AmiC2cat and *Nostoc* muopeptides and no dose-dependent increase could be observed.

There are several findings indicating a binding of AmiC2cat to peptidoglycan. The Dye-Release-Assays represented in Fig. 24, Fig. 33A and Fig. 34A, demonstrated the hydrolysis of *E. coli* PGN by AmiC2cat. This implies a binding of AmiC2cat to *E. coli* PGN. AmiC2cat-released peptides from *Nostoc* PGN were detected by LC-MS (Fig. 28 - Fig. 30), which involves an interaction between AmiC2cat and *Nostoc* PGN. Furthermore, the PGN-binding experiment in Fig. 34B revealed the presence of His8-AmiC2cat in pellets containing *Nostoc* PGN indicating a binding between the amidase and the peptidoglycan. The Biolayer interferometry was used in the next to detect the binding between the amidase and the peptidoglycan (illustrated in Fig. 36A).

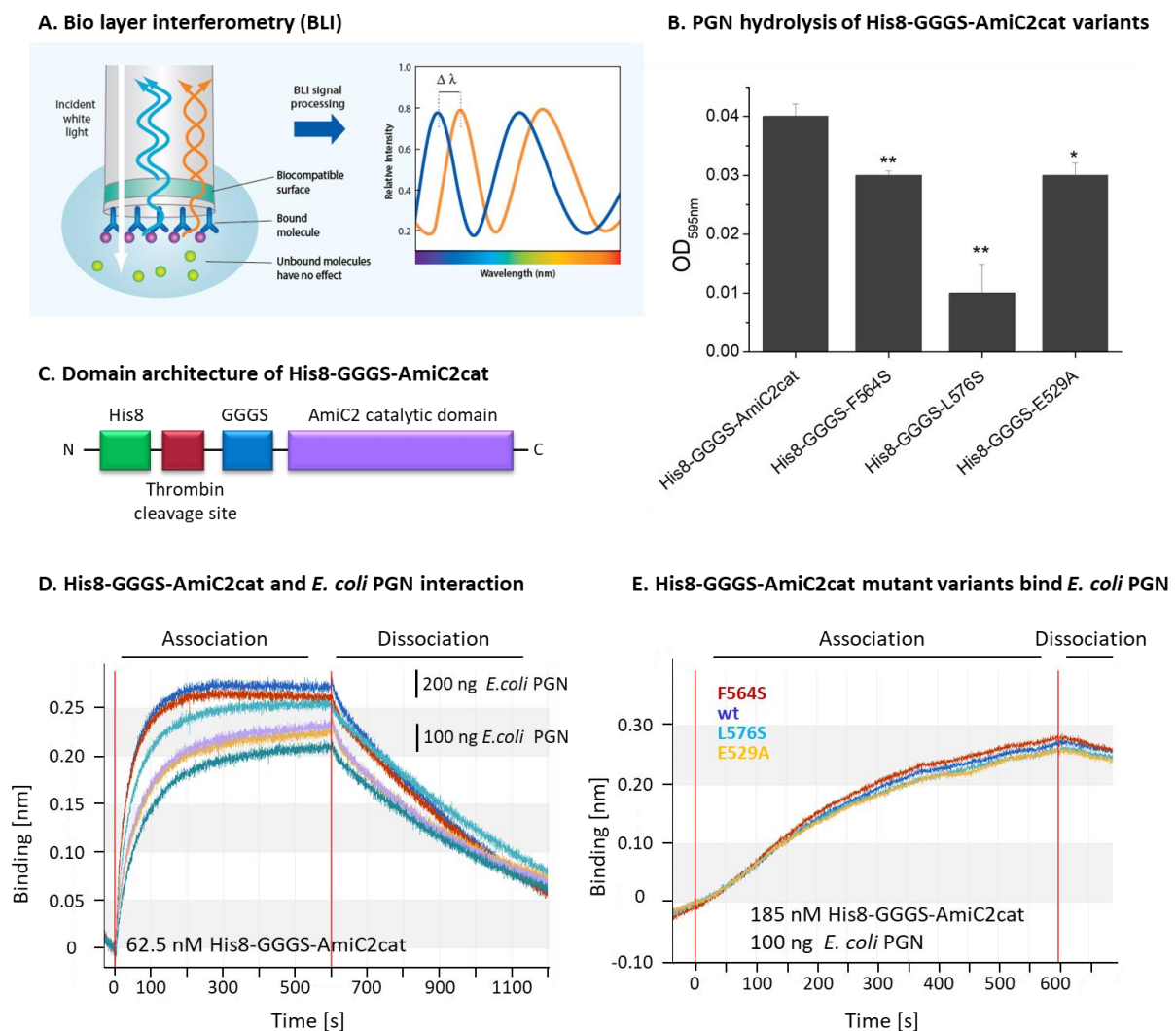


Fig. 36: A flexible linker enables detection of AmiC2cat/PGN interaction. **A.** Bio layer interferometry (BLI). This technique is based on the interference pattern of white light that is reflected from two surfaces. The first one represents the surface of the biosensors and the second one is an internal reference layer. A molecule is bound to the surface of the biosensor and a binding event shifts the interference of white light. Binding affinities and kinetics can be thereby deduced. **B.** Domain architecture of AmiC2cat harbouring a flexible linker between the His8-tag and the catalytic domain. **C.** GGGs-linker affects hydrolytic activity of wild-type and AmiC2cat mutant variants on RBB-labelled *E. coli* PGN. **D.** Interaction between His8-GGGS-AmiC2cat and *E. coli* PGN analysed by OctetK2. Reaction was performed in phosphate buffer supplemented with 1% BSA and 0.01% Tween20. Signals obtained from unspecific binding of PGN to Ni-NTA biosensors were subtracted. $n = 3$. **E.** Impact of site-specific mutations on PGN binding capability of AmiC2cat. Ni-NTA sensors were loaded with 123 nM protein and reaction was performed in phosphate buffer supplemented with 1% BSA and 0.01% Tween20. Signals obtained from unspecific binding of PGN to Ni-NTA biosensors were subtracted.

The binding of His8-AmiC2cat on Ni-NTA sensors was stable and unspecific interactions between the biosensors and the sodium phosphate buffer could be eliminated (Fig. 47, supplementary information). It was noticed, that the peptidoglycan binds to the Ni-NTA biosensors (Fig. 49, supplementary information). This unspecific interaction could be reduced by the addition of BSA and Tween20 in the buffer. Nevertheless, there was no interaction detected between His8-AmiC2cat and *Nostoc* PGN (Fig. 48, supplementary information). One reason for this effect could depend on a changed conformation of the amidase upon Ni-NTA biosensor binding, and thus inhibited the accessibility of the substrate binding site.

In order to enable a correct conformation of the enzyme on the Ni-NTA biosensors the effect of a flexible linker between the His8-tag and the catalytic domain was tested (Fig. 36B). It was observed that the polyglycyl-serine-linker decreased the PGN hydrolysis of wild-type and site specific AmiC2cat mutants (Fig. 36C), whereas an interaction between the wild-type His8-GGGS-AmiC2cat and *E. coli* PGN was detected by BLI-analysis (Fig. 36D). The interaction between PGN and His8-GGGS-AmiC2cat was recorded for about 10 min (association). A fast binding was detected within the first 3 min between the amidase and the peptidoglycan. An increased BLI signals was obtained by increasing the *E. coli* PGN from 100 ng to 200 ng in the binding assay, indicating that the interaction is dependent on the PGN concentration. The dissociation of His8-GGGS-AmiC2cat from PGN occurred slower than the association. The influence of site-specific mutations on the PGN binding capability of AmiC2cat was analysed using the mutants F564S, E529A and L576S. Those mutations affected the PGN hydrolysis most efficiently in previous experiments (Fig. 33A and Fig. 34A) and were therefore chosen for the binding assays. The mutants were generated as described for the wild-type His8-GGGS-AmiC2cat version. A flexible linker was introduced between the histidine-tag and the catalytic domain. The Dye-Release-Assay demonstrated that the hydrolytic activity was impaired by the GGGS-Linker (Fig. 36B), but increased the protein stability.

Fig. 36E represented the BLI sensogram obtained from the site-specific mutants F564S, E529A and L576S with *E.coli* PGN. A fast binding was also detected within the first 3 minutes as already observed for the wild-type in the previous experiment (Fig. 36D). No difference in the association or dissociation pattern between the site-specific mutants and the wild-type could be detected. The site-specific mutations did apparently not alter the PGN binding capability of AmiC2cat.

This chapter initially addressed the question which amino acids, in the putative binding cleft of AmiC2, are necessary to bind the peptidoglycan. Site-directed mutagenesis identified three amino acid residues (F564, E529 and L576), which affected the hydrolytic activity of AmiC2cat upon mutation. It was challenging to detect the interaction between the amidase and the peptidoglycan. However, the introduction of a flexible GGGS-amino acid linker between the His-tag and the catalytic domain of AmiC2cat enabled the detection of PGN-binding by Biolayer interferometry. It could be excluded that the decreased hydrolytic activity of AmiC2cat by the mutations F564S, E529A and L576S were caused by an altered PGN binding capability. Those amino acid residues might be relevant for the catalytic activity, and will be discussed in chapter 4.2.

4. Discussion

Bacteria pioneered successfully in the colonization of all conceivable niches on earth. This global thriving requires the ability to survive occasionally harsh and hostile conditions through multiple survival strategies and defence mechanisms. In the domain of bacteria, cyanobacteria are an outstanding phylum of morphologically diverse, photosynthetic active organisms. Their predecessors not only likely shaped the world by oxygen enrichment (11-13), but were substantially involved in the evolution of a multicellular lifestyle (27). Especially differentiation was one of the most successful innovations, providing an exceptional advantage regarding the colonization of new ecological habitats under various environmental conditions. Intercellular communication is crucial in a multicellular organism capable of differentiation. Regarding this, a recent study uncovered the fundamentals of cell-cell-communication in *Anabaena* (232). There, neighbouring cells in the filament are connected by septal junctions that can be actively opened and closed to allow the exchange of small molecules such as metabolites. The structure consists of a tube, traversing the septal peptidoglycan, and cap and plug structures on both ends of the tube. The framework for these septal junctions is the nanopore array in the septal peptidoglycan. It harbours numerous, regularly formed perforations in the central part of the septal disk between adjacent cells (222, 223). Nanopore drilling and septal junction formation rely on interdependent processes and mutually influence each other (221-223, 225, 226, 236, 240). A functional intercellular communication in the filament depends finally on both processes.

The peptidoglycan hydrolase AmiC2 from the heterocyst-forming cyanobacterium *N. punctiforme* is indispensable for nanopore drilling (223). The inactivation of the N-acetylmuramyl-L-alanine amidase not only impairs cell-cell communication and abolishes the nanopore array; it also affects cell morphology (223, 229). These wide ranging consequences address to one of the most important issues: "How is the amidase AmiC2 regulated?" There are some indications that point to possible regulation mechanisms, including post-translational autoprocessing and translocation of the inactive nascent polypeptide chain into the periplasm (242, 244). The modulatory region, a proline rich protein domain of AmiC2, affects the catalytic activity *in-vitro* (244) and a NlpD homologue (*aln3353*) activates the nanopore-forming AmiC1 in *Anabaena* (246). However, the interaction with the natural substrate of AmiC2, the peptidoglycan, remains so far elusive.

This work focused on the elucidation of the overall peptidoglycan composition of *N. punctiforme* to identify AmiC2 substrates. The peptidoglycan of *N. punctiforme* consists of highly amidated and crosslinked peptidoglycan fragments. The glycan backbone is composed of alternating N-acetylglucosamine and N-acetylmuramic acid disaccharides that are interconnected by short peptides consisting of alanine, glutamate and meso-diaminopimelic acid (Fig. 15, Fig. 17 and Fig. 19). The peptide stem contains highly amidated carboxyl side chains belonging to either glutamate or mDAP. The position of this extra amide group will be discussed in the first part of this section as well as other features like the presence of 1,6-anhydro-N-acetylmuramic acid or covalently bound polysaccharides (Fig. 22). Several atypical amino acids detected in acid hydrolysates of wild-type *N. punctiforme* (Fig. 14) might have originated from covalently bound or peptidoglycan associated proteins. Tryptic digests from wild-type PGN revealed PGN associated proteins or hypothetical proteins that are potentially linked to the peptidoglycan. These findings will be discussed in chapter 4.1.3. The last part focuses on the subtle differences between the lateral and septal cell walls of wild-type *N. punctiforme* (Fig. 20).

Inactivation of *amiC2* in *N. punctiforme* prevents the perforation of septal disks and possibly preserves the cleavage sites for the amidase AmiC2 in the septal disks. Atypical amino acids or specific muropeptides were assumed to be integrated in the septal peptidoglycan, representing the cleavage sites of the amidase AmiC2. The amino acid analysis of *amiC2* mutant PGN showed that the peptide stem consists of the PGN-typical amino acids Ala, Glu/Gln and mDAP, as has been shown for the wild-type PGN, and does not harbour any diverging amino acids, serving as putative cleavage sites for the amidase AmiC2 (Fig. 15). Moreover, mutanolysin digested PGN fragments of wild-type *N. punctiforme* (Fig. 17 and Fig. 19) and its *amiC2* mutant variant (Fig. 18) were compared, but no specific muropeptide species could be identified exclusively among the muropeptides of the *amiC2* mutant. Overall, the LC-MS analysis revealed an almost identical PGN composition of wild-type and mutant PGN.

Furthermore, the catalytic domain of AmiC2cat fully hydrolysed the peptidoglycan from the *amiC2* mutant (Fig. 26B) but hardly degraded any wild-type PGN (Fig. 26A). The LC-MS/MS analysis of AmiC2cat digests from the mutant or the wild-type PGN demonstrated highly crosslinked peptides (Fig. 28 - Fig. 30). This finding indicates that the amidase was in general able to degrade both types of PGN, but with a strongly different efficiency. Two possible reasons can be assumed for this, either the PGN from the *amiC2* mutant is crosslinked to a higher extend between peptides and therefore fully hydrolysed, or the PGN from the wild-type is modified in a way that inhibits enzymatic digestion. So far unidentified PGN bound proteins and their tryptic peptides, as identified in LC-MS measurements of trypsin digested PGN samples, could have also prevented AmiC2cat digestion. These hypotheses will be discussed in chapter 4.2.

The last subsection in chapter 4.2.3 addresses the role of the putative catalytic residues F56S, E529 and L576 in the binding cleft of AmiC2. Initially, mutational analysis was aimed to identify relevant amino acids for the binding of peptidoglycan, but revealed three catalytic amino acid residues (Fig. 33, Fig. 34 and Fig. 36).

4.1. *Nostoc punctiforme* and its Gram-negative type peptidoglycan

The peptidoglycan protects the bacterial cell from external influences and rupture at high turgor pressure. The functional properties of PGN are mediated by its mesh-like polymer structure, consisting of peptide linked glycan chains. This macromolecule is located in the periplasm and is shared with its universal composition by almost all bacteria with only a few exceptions. Early studies revealed the structure of the multi-layered cell envelope of cyanobacteria and highlighted the unique character with a combination of Gram-positive and Gram-negative features. Cyanobacteria are surrounded by a LPS - containing outer membrane (67, 68) and a phospholipid bilayer enclosing the cytoplasm. The space between these layers, the periplasm, contains the peptidoglycan (178, 179) which has an increased thickness in most cyanobacterial species (175, 186). Overall, cyanobacteria resemble Gram-positive bacteria based on their thick peptidoglycan layer, but also have an outer membrane, which is an exclusive feature of Gram-negative bacteria. A detailed analysis of the peptidoglycan from *N. punctiforme* was performed primarily to identify AmiC2 substrates, but was further helpful to reveal other Gram-positive and Gram-negative attributes. These are the amidation of carboxyl groups, the identification of covalently linked polysaccharides or proteins and the high degree of crosslinking.

4.1.1. The general composition of *Nostoc* peptidoglycan

In this work, LC-(ESI-TOF)-MS based techniques were used to identify the composition of the *N. punctiforme* peptidoglycan. The acetylated aminosugars, N-acetylglucosamine (204.087 m/z) and N-acetylmuramic acid (278.124 m/z), were detected in peptidoglycan fractions of *N. punctiforme* (see chapters 3.1.3 and 3.1.4). These two sugars are repetitively incorporated in the glycan backbone of almost all so far investigated Gram-positive and Gram-negative bacteria. Previous studies of the peptidoglycan from *Synechocystis* sp. strain PCC 6714 (183), *Phormidium uncinatum* (178), *Anacystis nidulans* or *Chlorogloea fritschii* (179) revealed these two acetylated amino sugars as main constituents in the glycan chains. Concerning the glycan backbone, cyanobacteria are no exception from other bacteria.

Concerning the peptidoglycan peptide stem, the archetypical structure is L-alanine (Ala) linked to D-glutamate, followed by a diamino acid in the third position and two adjacent D-alanine residues in position four and five. This peptide is subjected to many alterations, as already described in chapter 1.2.2. Usually, Gram-positive bacteria, except for *Mycobacteria* and *Bacilli*, incorporate lysine into the peptide stem, whereas meso-diaminopimelic acid (mDAP) is incorporated in Gram-negative (72). NMR-analysis of the UDP-MurNAc-pentapeptide of *Anabaena cylindrica* revealed the presence of lysine in the peptide stem (189), whereas the aforementioned analyses of cyanobacterial peptidoglycan demonstrated clearly the presence of mDAP (178, 179, 183). This analytical discrepancy required a clear identification of the amino acid at the third position in the peptide stem from *N. punctiforme*. To this end, amino acid analysis of HPLC purified *Nostoc* peptidoglycan fragments (Fig. 15) clearly identified meso-diaminopimelic acid at the third position. MS/MS fragmentation of *Nostoc* muropeptides (see MS/MS fragmentation profiles in chapter 5.10 in the supplementary information) gave further evidence for alanine in the first position in the peptide stem, followed by glutamate and again alanine in the fourth position. Interestingly, the fifth position could not be determined, since no pentapeptides could be detected in the samples.

Usually, the peptidoglycan precursor, consisting of a disaccharide-pentapeptide with D-alanine in the fourth and fifth position, is synthesized in the cytoplasm and subsequently translocated into the periplasm. Accordingly, pentapeptides are found at places where peptidoglycan synthesis takes place. Information about peptidoglycan synthesis and growth pattern in cyanobacteria is rare, but the presence of homologous Mur-ligases or the detection of the UDP-MurNAc-pentapeptide in *Anabaena* (189, 190) point to similar peptidoglycan synthesis machineries than already detected in other organisms. Moreover, HADA incorporation in cell walls of *Anabaena* uncovered peptidoglycan synthesis at division sites *in-vivo* (267). Peptidoglycan synthesis was only observed at the cell periphery when FtsI, involved in septal peptidoglycan synthesis, was inhibited by the antibiotic aztreonam. *N. punctiforme* might also possess similar peptidoglycan synthesis pattern because pentapeptides were imaged at the septum (223). A fluorescent derivative of vancomycin was successfully used in *N. punctiforme* and specifically stained septal cell walls (223). The antibiotic vancomycin binds to D-Ala-D-Ala of pentapeptides and thus enables peptidoglycan imaging when vancomycin is coupled to a fluorescent tracer (268). These findings postulate the presence of pentapeptides in the peptidoglycan of *N. punctiforme*.

The LC-(ESI-TOF)-MS data of septal disks was therefore screened for the presence of a disaccharide, attached to a pentapeptide. Indeed, a very low abundant peak with the 1012.437 [M+H]⁺ was identified, corresponding to a disaccharide with an adjacent pentapeptide. One possible explanation

for the relatively low abundance of pentapeptides in *Nostoc* samples is the respective growth phase of the sampled cells. The *in-vivo* imaging of septal peptidoglycan in *N. punctiforme* was performed with exponentially growing cells (223), whereas the cells used for peptidoglycan isolation and subsequent LC-(ESI-TOF)-MS analysis were from stationary grown cells in this work. The peptidoglycan is continuously subjected to alterations during bacterial growth. Growth conditions, cell cycle or environmental factors influence the dynamics and the plasticity of peptidoglycan. The peptidoglycan of heterozygous cyanobacteria underlies also great changes during nanopore formation. Several electron micrographs, depicting different levels of septum maturation in *Anabaena*, demonstrate a complete synthesis of the septum during growth before nanopores were drilled (246). Nanopore formation requires the enzymatic activity of N-acetylmuramyl-L-alanine amidases like AmiC1 from *Anabaena* or AmiC2 from *N. punctiforme*. Since AmiC2 preferably degrades highly crosslinked peptidoglycan (see chapter 3.2.2), the septal peptidoglycan must be remodelled, in parallel or directly after its synthesis, to include cleavage sites for AmiC2. The energy for crosslinking events originates from the cleavage of the D-Ala-D-Ala bond, which in turn explains the low abundance of pentapeptides in stationary grown *N. punctiforme* cells.

Muropeptide profiles from stationary *E. coli* strain Nisle 1917, *S. aureus* SA113 or *Staphylococcus carnosus* TM300 cultures demonstrated, in contrast, abundant pentapeptides in monomeric and oligomeric muropeptides (256, 269). A potential explanation for the discrepancy to the analysed *N. punctiforme* could be due to a rapid processing of pentapeptides in the stationary growth phase by L,D-transpeptidases or D,D-carboxypeptidases, because pentapeptide side chains were also not detectable in the LC-(ESI-TOF)-MS analysis of crosslinked muropeptide species. It was shown, that the levels of pentapeptides drastically increased in *E. coli* upon mutation of the D,D-carboxypeptidase PBP5 (270). Similar observations were obtained for *H. pylori* lacking the endo- and carboxypeptidase action of a putative metallopeptidase (271). *N. punctiforme* encodes seven putative class A PBPs, three class B PBPs and four presumptive LMW PBPs (192). This genetic repertoire might enable *N. punctiforme* to quickly trim pentapeptides into shorter peptide stems or use them as energy source for transpeptidation processes. There are also other systems, which coordinate or influence the amount of pentapeptide side chains. The peptidoglycan of the rhizobium *Sinorhizobium meliloti* does not harbour any detectable pentapeptides, similar to *N. punctiforme* (272). However, the inactivation of either the seven-transmembrane receptor RgsP or the membrane anchored peptidoglycan peptidase RgsM led to an accumulation of pentapeptides. The interplay between both proteins coordinates peptidoglycan maturation at polar zones. However, it is not clear whether the peptidase RgsM exhibits hydrolytic activity or inhabits a regulatory role. A BLAST search on NCBI using the sequences of *S. meliloti* RgsP and RgsM identified similar proteins in *N. punctiforme* with more than 50% sequence identity. Npun_AR143 is annotated as diguanylate cyclase/phosphodiesterase lacking the seven transmembrane helices and Npun_F4637 is described as a zinc-dependent endopeptidase in the peptidase M23B-family. Both proteins are structurally and functionally uncharacterized. Nevertheless, a similar system could exist in *N. punctiforme* considering the fact that *N. punctiforme* comprises more than 258 two-component and 146 one-component-systems (273). Tryptic digests of crude peptidoglycan from *N. punctiforme* revealed Npun_F5788, a part of a two component system (Table 46). This protein belongs to the WalR-like family. *B. subtilis* uses the WalRK - two component system to regulate the hydrolytic activity of two D,L-endopeptidases, CwlO and LytE, during cell elongation. Accumulation of peptidoglycan cleavage products inhibits the phosphorylation of the DNA-binding protein WalR by the membrane-embedded sensor kinase Walk. Consequently, transcription of *cwlO* and *lytE* decreases (274). This example

demonstrates how a two component system influences peptidoglycan composition, remodelling or maturation.

The peptidoglycan of *E. coli* contains 20-33% crosslinked peptidoglycan (275), whereas Gram-positive bacteria like *S. aureus* reveal higher crosslinking levels at up to 90% (72). The early studies of Jürgens and colleagues with peptidoglycan from the unicellular *Synechocystis* sp. strain PCC 6714 reported a high degree of crosslinking at 56 to 63% (183). The filamentous cyanobacterium *N. punctiforme* shares this typical Gram-positive feature of a highly crosslinked peptidoglycan since muropeptide profiles demonstrated 78.5% crosslinked species which include 59.2% dimers and 19.3% trimers (see Fig. 17 for muropeptide profile). The crosslinking crucially determines the cell shape. *Helicobacter pylori*, for example, hydrolyses crosslinks during growth to achieve a helical cell shape which is indispensable for infection (276). Crosslinking also influences the mechanical properties of the peptidoglycan. *S. aureus* highly crosslinks the peptidoglycan using the non-essential transpeptidase PBP4 (277). This action increases not only the β -lactam antibiotic resistance but also the overall stiffness of the peptidoglycan. The elasticity and robustness of peptidoglycan is directly related to the crosslinking degree since *S. aureus* mutants lacking *pbp4* had a more pliable peptidoglycan. Furthermore, these mutants were more susceptible towards β -lactam antibiotics. *N. punctiforme* is a non-pathogenic, terrestrial organism and usually not exposed to antibiotics. What is therefore the reason for its thick and highly crosslinked peptidoglycan layer? Studies using cold atmospheric-pressure plasma to inhibit biofilm formation demonstrated a correlation between the efficacy of the antimicrobial activity and the peptidoglycan thickness. The thicker the peptidoglycan layer, the higher the resistance of the bacteria towards the plasma treatment (278). *N. punctiforme* occurs in diverse ecological habitats like desert soil crusts, forest-steppes, forest soils in temperate climate regions or soils with higher salt concentrations (279). A thicker and more robust peptidoglycan layer protects the filamentous cyanobacteria from harsh environmental conditions. Terrestrial Gram-positive bacteria are more resistant towards drought and desiccation presumably due to a thick peptidoglycan layer (280).

The crosslinking varies greatly between different organisms. The majority of bacteria possess 3-4 crosslinks between mDAP and D-Ala residues, whereas others connect the peptide stems via the mDAP residues resulting in 3-3 crosslinks (72). Depending on different factors the peptidoglycan can also consist of 3-4 and 3-3 crosslinks. *E. coli* increases 3-3 crosslinks when it enters stationary growth phase (281) or to survive a defective outer membrane synthesis (282). Whereas *Coxiella burnetii* uses this strategy to enhance physical resistance during transition into small-cell variants (283). However, no such phenomenon was observed in *N. punctiforme*. Furthermore, interpeptide bridges as the glycine bridge in *S. aureus* or the aspartate bridge in *E. faecium* were not detected in *N. punctiforme*.

4.1.2. Modifications of *Nostoc* peptidoglycan

The LC-(ESI-TOF)-MS analysis of peptidoglycan from stationary grown *N. punctiforme* revealed fully or partially amidated carboxyl side chains of peptide stems. This type of modification occurs often in cyanobacteria (178, 179, 183). The first detailed peptidoglycan analysis of *Synechocystis* sp. strain PCC 6714 demonstrated as well partial amidation of carboxyl side chains but did not indicate if mDAP or Glu represented the amidation site (183). *N. punctiforme* contains glutamate and mDAP in the peptide stem, both of which have a free carboxyl group. The amidation of mDAP or Glu is associated with different functions. *Streptococcus pneumoniae* or *S. aureus* requires amidated α -carboxyl groups of glutamate to efficiently crosslink the glycan chains or to establish antibiotic resistance (284,

285). *M. tuberculosis* depends on mDAP amidation for the enzymatic activity of the D,L-transpeptidase Ldt_{Mt2} (286). Whereas *B. subtilis* uses the amidation of mDAP to modulate the action of peptidoglycan hydrolases (287).

The Gram-positive *B. subtilis* converts the free carboxyl group of mDAP into an amide with the help of the amidotransferase AsnB (287). A mutant lacking *asnB* had severe morphological defects and was unable to grow in the absence of Mg²⁺. Furthermore, muropeptides contained only non-amidated carboxyl side chains. Peptidoglycan hydrolysis in *B. subtilis* is dependent on the amidation of mDAP and the concentration of Mg²⁺-ions. Usually, *B. subtilis* reduces mDAP amidation in response to high Mg²⁺ concentrations to enhance peptidoglycan hydrolysis and counteract the hampering effect of Mg²⁺ ions on specific peptidoglycan hydrolases. This modulatory mechanism is impaired in the *asnB* mutant due to the absent amidation of mDAP residues. *N. punctiforme* might also modify the mDAP residue by amidation to modulate AmiC2 activity. The muropeptide profile of the *amiC2* mutant was the same as in the wild-type concerning detected amidated muropeptide species (see muropeptide profiles in Fig. 17 and Fig. 18). The amidation of *Nostoc* peptidoglycan plays potentially a role in crosslinking reactions rather than in the regulation of peptidoglycan hydrolases. As outlined above, there are some indications that *N. punctiforme* enzymatically amidates the free carboxyl group of glutamate instead of mDAP.

Recently, the *gatD/murT*-operon, encoding the enzymes for glutamate amidation, was identified in *S. aureus* (285, 288). GatD is a glutaminase and releases ammonia from glutamine. The NH₃-moiety is transferred to MurT, where it is used in an ATP-dependant step for the amidation of iso-glutamate of lipid II (289). The glutamine availability is highly important for glutamate amidation. Disruption of the *femC* operon in *S. aureus*, more precisely of *glnR* encoding a repressor of the glutamine synthetase operon, had polar effects on the transcription of *glnA*, the gene for the glutamine synthetase (79). The *femC* mutants showed 48% less amidated carboxyl groups and a decreased methicillin resistance. Morlot et al. determined the occurrence of the *gatD/murT* operon and observed that it is ubiquitous in cyanobacteria (289). The LC-(ESI-TOF)-MS data obtained from *N. punctiforme* revealed a highly abundant muropeptide with an adjacent dipeptide (Fig. 17). The comparison of the measured mass with the theoretical mass of a muropeptide with Ala and Glu in its peptide stem differed around 0.98 Da. This difference corresponds to an amidation and indicates that the carboxyl group of glutamate is amidated. However, the specific role of glutamate amidation in *N. punctiforme* needs to be further investigated.

The highly crosslinked and amidated peptidoglycan macromolecule of *N. punctiforme* contained anhydrous MurNAc residues in the glycan backbone (Fig. 17). *E. coli* strains terminate glycan chains consisting of 25 to 40 disaccharides with a ring-like structure of MurNAc (275). This modification is common amongst Gram-negative bacteria (290). It is hypothesized that lytic transglycosylases release the nascent peptidoglycan chain from undecaprenol-pyrophosphate or trim the nascent glycan chains by an intramolecular ring formation (1,6-anhydro) of the C1 and C6-atom of MurNAc (291, 292).

The most prominent protection mechanisms confer lysozyme resistance to many pathogenic bacteria. *S. pneumoniae* (109) or *B. subtilis* (110) remove the acetyl group from GlcNAc, whereas *N. gonorrhoeae* acetylates the OH-moiety on the C6-atom (111). The muropeptide profiles of the wild-type revealed deacetylation of GlcNAc residues (Fig. 17 - Fig. 19). A general role of this modification in the biogenesis of peptidoglycan seems likely. The extent of deacetylation could

control the action of lytic transglycosylases or other peptidoglycan hydrolases, as it was observed for the O-acetylation of peptidoglycan in many Gram-positive and Gram-negative species (293). Peptidoglycan-deacetylases in *B. anthracis* contribute as well to the attachment of neutral polysaccharides (294). Anionic polysaccharides and wall teichoic acids interfere with lysozyme and the glycyl-glycine endopeptidase lysostaphin in *S. aureus* (295, 296).

Acid hydrolysates of *Nostoc* peptidoglycan demonstrated several monosaccharides indicating the presence of a covalently linked polysaccharide. Polysaccharides are often associated with the cell wall of Gram-positive bacteria and are involved in many cellular processes. HPAEC analyses identified arabinose, galactose, glucose and mannose/xylose as main constituents of this presumptive polysaccharide (Fig. 22A). A phosphodiester might link the polysaccharide to the glycan backbone of peptidoglycan, using either the phosphate group of GlcNAc or MurNAc. Elevated phosphate levels were measured in HCl-hydrolysates, confirming this type of linkage (Fig. 21). Phosphate rich wall teichoic acids (WTA) do likely not modify *Nostoc* cell walls, since measured phosphate levels were much lower in acid hydrolysates compared to *B. subtilis*. In addition, no glycerol or ribitol alditols, the repeating units of WTAs (297), could be detected (Fig. 21). Identical sugars were also detected in hydrofluoric acid released components of cell walls from *Synechococcus* sp. PCC 6307 (298) and *Gloeobacter violaceus* (299). Hence, polysaccharides covalently bound to the peptidoglycan, occur more frequently in cyanobacteria (69).

The HPAEC analysis of acid hydrolysates of *N. punctiforme* cell walls revealed further peaks in the chromatogram that could not be identified. There were even more peaks at late retention times, indicating the presence of oligosaccharides. The putative peptidoglycan polysaccharide might be more complex. Obviously, the analysis requires further optimization to separate so far overlaying peaks of the injected sample and the standard mixtures for the elucidation of the polysaccharide composition. A GC-MS analysis of the peptidoglycan derived polysaccharide would provide potentially more insights and could help to distinguish between single components with identical retention times on HPAEC. Cryo-electron tomographic images of *Anabaena* cells indicate an electron dense layer between the peptidoglycan and the outer membrane (Fig. 50A, supplementary information). Acid hydrolysates of *Anabaena* cell walls revealed a peptidoglycan-polysaccharide consisting of glucose, mannose, raffinose, maltose and potentially more sugars. The analysis was not fully optimized but nevertheless indicates that this unknown, electron dense layer might consist of polysaccharides, which are covalently linked to peptidoglycan.

4.1.3. *Nostoc* PGN and its putative associated proteins

One of the most abundant proteins in *E. coli* is the Braun lipoprotein (101). This triacylated trimer occurs at every tenth to twelfth mDAP residue in the peptidoglycan and is linked via its C-terminal lysine to the carboxyl group of mDAP (97). Pronase E digested peptidoglycan of *E. coli* retains the C-terminal lysine and arginine residues of the Braun lipoprotein Lpp (300) while trypsin treatment leaves only lysine at the mDAP residue (97). This is a distinctive mark for the presence of the Braun Lpp in muropeptide profiles of other organisms. The extensive analysis of *N. punctiforme* peptidoglycan revealed mDAP at the third position of the peptide stems. According to this, and regarding the general occurrence of the Braun lipoprotein in Gram-negative bacteria (96, 100), the chances are quite high that *N. punctiforme* might contain the Braun lipoprotein, as well. However, the muropeptide profile of *Nostoc* did not show a muropeptide, which is modified by a lysine residue (Fig. 17 and Fig. 19). Considering the low peak intensity of all LC-(ESI-TOF)-MS measurements in the

measuring range between 1e3 and 1e6 cps (Fig. 15, Fig. 17 and Fig. 19), one might assume that modified muropeptides could have disappeared in the background noise. Furthermore, it was observed, that mutanolysin hydrolysed only 40% of wild-type peptidoglycan, whereas nearly 80% of *B. subtilis* or *E. coli* peptidoglycan was degraded by the muramidase (Fig. 52, supplementary information). Accordingly, fewer muropeptides were released and measured by LC-(ESI-TOF)-MS leading to the generally low peak intensity. On the other hand, all modified peptidoglycan fragments might have remained in the insoluble PGN-pellet and were not considered for LC-(ESI-TOF)-MS measurements. This might also explain why the amino acid analysis of *Nostoc* muropeptides did not demonstrate highly abundant amounts of lysine (Fig. 15). However, BLAST searches on NCBI using the sequence of *E. coli* Lpp revealed no hits indicating the presence of a homologue of the Braun lipoprotein in *N. punctiforme* or other species in the order of *Nostocales*.

Interestingly, arginine, the only atypical amino acid in high abundance, was found in the amino acid analysis of muropeptides from *N. punctiforme* (Fig. 15). This observation might be a hint for a covalently bound protein although muropeptides with an arginine residue were not detected in muropeptide profiles (Fig. 17 and Fig. 19). The tryptic digest of *Nostoc* peptidoglycan contained peptides assigned to proteins harbouring a lipoprotein signal peptide (Npun_F3787 and Npun_F3932). Npun_F3787 contains a BON-domain. This domain is found in phospholipid binding proteins, for example in OsmY from *E. coli* (263). This periplasmic or outer membrane protein is expressed during stationary growth or under osmotic stress conditions to prevent the wrinkling of the cytoplasmic membrane (301). Npun_F3787 possesses a C-terminal arginine residue, which was enriched in acid hydrolysates of wild-type muropeptides and the crude PGN from the *amiC2* mutant of *N. punctiforme* (Fig. 15 and Fig. 16). A partial acid hydrolysis of *Nostoc* peptidoglycan will retain peptides with varying lengths on the peptidoglycan that can be subsequently removed by trypsin and determined by mass spectrometry. This experimental procedure could verify and elucidate whether Npun_F3787 is covalently bound or not. Interestingly, the Braun lipoprotein is the only known lipoprotein, so far, which is covalently linked to the peptidoglycan (101). Other outer membrane proteins, such as PAL or OmpA, interact with the peptidoglycan in a non-covalent manner (101). The presence of arginine in acid hydrolysates of *Nostoc* peptidoglycan needs to be further investigated.

Many motifs and protein domains are known to interact with and bind to peptidoglycan. The Lysin Motif (LysM) comprises approximately 40 amino acids and was originally found in bacterial lysins (302). It was identified in the transglycosylase MltD from *E. coli* (303), the N-acetylglucosaminidase AcmA of *Lactococcus lactis* (304) and the autolysin of *Enterococcus faecalis* (305). The cell-wall sorting LPXTG-motif is widely distributed and represents the signal for the covalent peptidoglycan anchorage by membrane-embedded transpeptidases, so called sortases (306). Non-covalent binding is mediated through GW-modules (307), choline residues of lipoteichoic or teichoic acids (308) or the S-layer homology (SLH) domains via polysaccharides (309). A common protein with any of these motifs or domains was not found in both biological replicates containing tryptic peptides of *N. punctiforme* cell walls (see chapter 3.1.6 and chapter 5.12 in the supplementary information). Interestingly, a putative lytic transglycosylase (Npun_R5326) was detected in replicate 2 and a peptidoglycan binding domain protein (Npun_R5246) was identified in replicate 1. The common overlap of both replicates comprised two-component systems, SecY and an unknown protein annotated to be transport-associated. Two-component systems fulfil various functions in signalling and sensing. The previously mentioned WalRK-system modulates peptidoglycan hydrolysis by sensing the cleavage products of endopeptidases (274). In this way, the hydrolytic activity of endopeptidases

is monitored and can be specifically adjusted. The role of two-component systems in peptidoglycan synthesis or remodelling in cyanobacteria remains to be investigated. SecY is an integral membrane protein and a core component of the Sec-Translocon. A homologue (Npun_R4372) was detected in both replicates. Navarre et al. described the difficulty to remove membrane proteins or membrane-spanning proteins from *S. aureus* peptidoglycan by SDS-boiling (310). The presence of SecY could represent insufficient solubilisation of membranes. On the other hand, SecY translocates nascent peptide chains into the periplasmic space and is in contact with peptidoglycan, either directly or indirectly. The same is true for components of peptidoglycan-spanning transporters like AcrB (Npun_F5285), MFP (Npun_F5842) or TolR/ExbD (Npun_R0781).

More than 72% of all detected peptides in both replicates were assigned to contaminating proteins. The most abundant proteins were phycobiliproteins or belonging to the photosystem (Table 55 - Table 57, supplementary information). Unspecific crosslinking events might have occurred and might be responsible for the carry-over of contaminations. DTT could efficiently reduce the amount of contamination, from nearly 7000 detected peptides to 200, but not completely abolish unspecific crosslinking events (Fig. 12). Braun and Rehn demonstrated ten atypical amino acids in hydrolysates of the SDS-insoluble peptidoglycan fraction of *E. coli*, that disappeared after trypsin treatment, except for lysine (97). In contrast, the peptidoglycan from *N. punctiforme* revealed ten atypical amino acids after trypsin treatment (Fig. 14). These originated from amino acids or peptides that were left associated with the peptidoglycan after trypsin treatment. Quantitative analysis of amino acids in enzymatically digested peptidoglycan from diverse cyanobacteria demonstrated several other atypical amino acids, albeit in lower amounts than peptidoglycan derived amino acids (179). These additional amino acids or tryptic peptides, still bound to the peptidoglycan, could also have blocked the cleavage site for mutanolysin leading to the low hydrolytic activity of mutanolysin on wild-type peptidoglycan compared to peptidoglycan from other organisms (Fig. 52, supplementary information). Non-specific proteinases like pronase E, proteinase K or chymotrypsin could be included into the isolation protocol, substituting trypsin. Although this treatment would result in pure peptidoglycan fractions, unspecific crosslinking would not be abolished. Exposure to oxygen likely represents one of the main causes for unspecific crosslinking. The use of a stronger reducing agent during cell disruption or already during the washing of harvested cells could help to minimize or even prevent oxidative crosslinking.

The analysis of tryptic digests from wild-type peptidoglycan was aimed to examine the level of contaminations. The use of DTT and including further experimental steps into the isolation protocol reduced the amount of contaminations. However, the identification of proteins or peptides, which are covalently linked to the peptidoglycan, requires further optimization of the isolation procedure to efficiently remove contaminations. A good starting point for optimized experiments comprises cell synchronization and the usage of identical sample amounts for the isolation of peptidoglycan for all biological replicates. Besides, unspecific crosslinking has to be prevented to bypass the carry-over of contaminating proteins.

4.1.4. Minor differences in the septal and lateral cell wall of *N. punctiforme*

Septal peptidoglycan is only a minor part of the overall peptidoglycan and might be underrepresented in a LC-MS analysis, as previously described in chapter 3.1.4. For this purpose, an enriched fraction of septal peptidoglycan was compared to a fraction containing unchanged ratios of septal and lateral cell walls (Fig. 20). Indeed, minor differences were observed between both samples. Two components were exclusively detected in the whole peptidoglycan fraction with the m/z ratios 627.29 $[M+H]^{2+}$ and 671.81 $[M+H]^{2+}$. Putative muropeptide structures could not be assigned to these components, which were furthermore not found in any previous LC-(ESI-TOF)-MS measurements. Considering the overall high purity of the samples, it is possible that these components are rather fragments originating from specific muropeptide species generated by ESI-ionization process, than contaminations. A confirmation of this hypothesis was not possible due to missing MS2-spectra. Besides, these two components were not identified in previous LC-MS measurements of *Nostoc* PGN.

Anhydro-muropeptides with 850.368 $[M+H]^+$ and 921.405 $[M+H]^+$ were not detected in septal disks. The peak intensity of the whole peptidoglycan sample was twice as high as that containing the septal peptidoglycan. The anhydro-muropeptides might be underrepresented or under the detection limit and could therefore not be reported. Another difference was the shifted retention time of two muropeptide species with 875.903 $[M+H]^{2+}$ and 876.39 $[M+H]^{2+}$. Isomeric forms have different retention times and form several peaks on the LC-MS chromatogram. *Streptomyces coelicolor*, for example, increases 3-3 crosslinks of a dimer during sporulation. The presence of 3-3 and 3-4 crosslinked dimers resulted in two peaks in the chromatogram (311). However, *N. punctiforme* contained exclusively 3-4 crosslinks. Diastereomers of 2,6-diaminopimelic acid can also cause multiple peaks on LC-MS-chromatograms (312). *Myxococcus xanthus* incorporates LL-DAP and meso-DAP into the peptidoglycan sacculus and generates multiple peaks in the muropeptide profile (313). The OPA-derivatization of hydrolyzed muropeptides from *N. punctiforme* identified meso-diaminopimelic acid as the only diamino acid in the peptidoglycan (Fig. 15). Hence, the muropeptides were rather stereo-isomers as similarly observed in *S. aureus* (256).

Previous HPLC and LC-MS analyses of *Nostoc* peptidoglycan (Fig. 17 and Fig. 19) detected the GlcNAc-MurNAc-tripeptide with 870.394 $[M+H]^+$. A general shift in the retention times of all peaks was observed between the measurements. This caused the absence of 870.394 $[M+H]^+$ in the whole peptidoglycan sample. Presumably, this muropeptide eluted within the injection peak of the whole peptidoglycan sample and could not be recorded as a defined ion species. This effect was also visible on another highly abundant analyte with the m/z ratio of 206.06, which is expected to originate from a double protonated GlcNAc-residue.

4.1.5. The peptidoglycan model of *N. punctiforme*

All the information obtained throughout the first part this work is summarized in the figure below and represents the general peptidoglycan composition and its modifications:

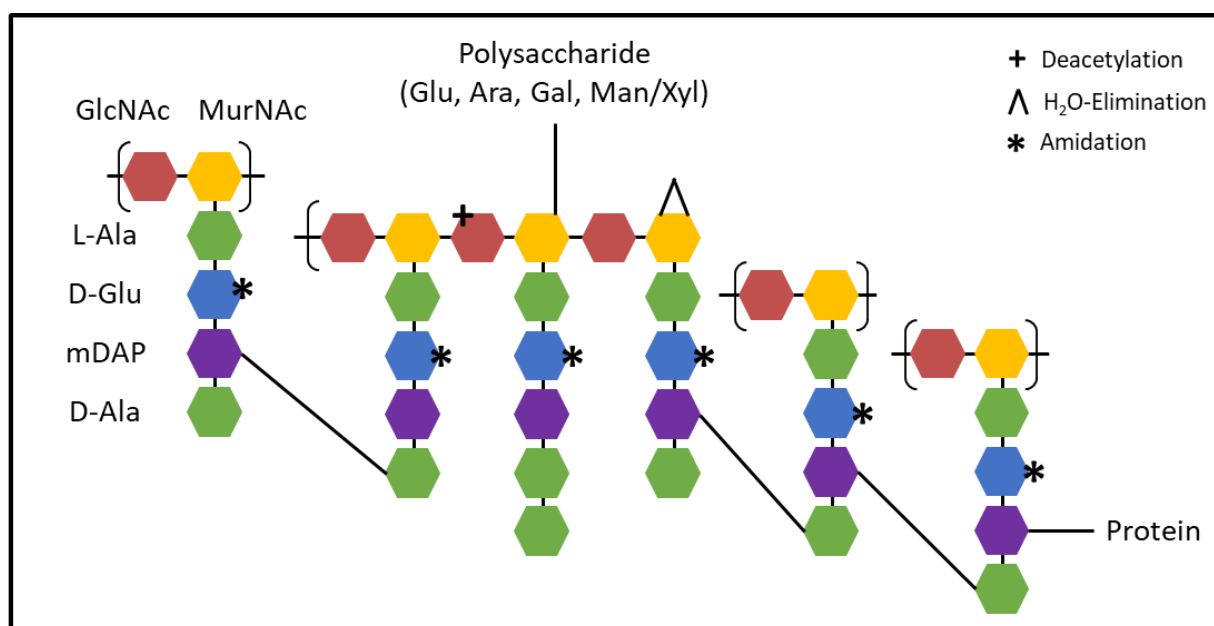


Fig. 37: Peptidoglycan composition of *N. punctiforme*. The filamentous, heterocyst-forming cyanobacterium forms a complex mesh-like network of carbohydrates and amino acids in the periplasm. The glycan backbone consists of alternating units of N-acetylated disaccharides composed of N-acetylglucosamine (GlcNAc) and N-acetylmuramic acid (MurNAc). A peptide is covalently linked to MurNAc and undergoes crosslinking reactions with other peptide stems. By doing this, highly crosslinked muropeptide species, from dimers, trimers and up to hexamers, are formed. The carboxyl side chains of the peptide stems, mainly through the carboxyl group of glutamate, are highly amidated (marked by a star). Proteins might be covalently linked to the peptide stem (exemplarily shown on mDAP). It is not known, if these proteins are linked to mDAP or another amino acid in the peptide stem. A polysaccharide is attached to the glycan chain and consists of glucose, galactose, arabinose and mannose/xylose. The exact anchorage site of this polysaccharide needs to be investigated and is exemplarily shown on MurNAc. The end of a glycan chain is characterized by an anhydrous MurNAc residue.

4.2. The amidase AmiC2 and its substrate, the peptidoglycan

The nanopore array in septal disks between neighbouring cells in heterozygous cyanobacteria harbours regularly formed pores with a diameter of around 15-20 nm (222, 223). N-acetylmuramyl-L-alanine amidases have a central role in nanopore formation (222, 223, 236), but the regulation mechanism is still unknown. There are a few attempts in previous studies to find an appropriate explanation for the nanopore drilling mechanism of the amidases AmiC1 from *Anabaena* or AmiC2 from *N. punctiforme* (242, 244, 246). The natural substrate of these amidases, the peptidoglycan, has however not been targeted for many years.

Peptidoglycan amidases cleave the amide bond between MurNAc and alanine. This bond specificity enables a rather broad substrate specificity which differs enormously amongst peptidoglycan amidases. *E. coli* AmpD prefers anhydro-muropeptides with a tri- or a tetrapeptide side chain (314) whereas AmiD exhibits a broader specificity, cleaving also monomeric and oligomeric muropeptides without an anhydro-MurNAc-residue (315). The amidase domain of the autolysin AtIA of *S. aureus* degrades only peptidoglycan substrates with a pentaglycin-bridge (316). The substrate specificity of amidases indirectly unravels compositional features of peptidoglycan. Heterocyst-forming cyanobacteria might incorporate preferred substrates of the nanopore-drilling amidases at specific sites in the septal disk to mark the position or form of future nanopores.

The characterization of the amidase AmiC2 from *N. punctiforme* was the main focus of this work. The first subsection addresses the alternation of peptidoglycan modifications in response to the inactivation of *amiC2*. The second subsection addresses the peptidoglycan crosslinking levels as a potentially critical factor for the amidase binding and activity, as well as three putative catalytic residues and their influence on peptidoglycan binding and hydrolysis.

4.2.1. Disruption of *amiC2* altered peptidoglycan modification

Inactivation of *amiC2* in *N. punctiforme* has been reported to cause deleterious effects on different cellular levels such as cell morphology, intercellular communication or differentiation (229). As a first step to systematically study these profound effects, peptidoglycan from the *amiC2* mutant was isolated and analysed by LC-(ESI-TOF)-MS with the aim to define, if this mutation affects peptidoglycan composition. The analysis of mutanolysin released muropeptides revealed almost no differences in the peptidoglycan composition compared to the wild-type (Fig. 17 and Fig. 18). The crosslinking degree is almost identical with 78.5% crosslinked species, but the ratio between trimers and dimers was slightly different. The peptidoglycan of the *amiC2* mutant contains 54.8% dimeric and 23.7% trimeric muropeptides. The relative abundance of the two most abundant trimeric muropeptides (Fig. 18, peak 8 and 9) is doubled compared to the wild-type. This relative quantification occurred through peak-area-quantitation on HPLC-chromatograms. Several things have to be considered using a standardless method: Anhydro-muropeptides have a longer retention on rp-HPLC than their hydrous counterparts and will elute within the fraction of higher oligomers. Isomers of all muropeptide species also retain longer on the C18-column and elute with different retention times. Consequently, single defined peaks on HPLC-chromatograms can contain different muropeptide species. Stereo-isomers of muropeptides are frequently formed throughout the sample preparation and elute at different retention times (256). Reduction with NaBH₄ prevented the formation of α/β -anomers but not of stereo-isomers. Therefore, it might happen that some species are over- or underrepresented using this type of quantification. The development of a mass spectrometric based quantitation strategy would be advantageous in this case. However, the basic composition and the crosslinking were identical between the *amiC2* mutant and the wild-type peptidoglycan. Overall, the basic composition was unaffected due to *amiC2* disruption, but not the level of peptidoglycan modification.

Amino acid analysis of the mutant peptidoglycan demonstrated only the amino acid Arg next to the peptidoglycan-derived amino acids Ala, Gln/Glu and mDAP (Fig. 16). There were no other atypical amino acids detected, as it was observed for the wild-type peptidoglycan (Fig. 14). *N. punctiforme* might modify the peptidoglycan by the attachment of proteins, peptides or amino acids to protect this mesh-like structure from the hydrolytic activity of enzymes, like AmiC2. Modification of peptidoglycan is a common procedure amongst Gram-positive and Gram-negative bacteria to prevent enzymatic digestion (72). O-acetylation of MurNAc, N-deacetylation of GlcNAc or MurNAc or the amidation of mDAP represent the most prominent examples of peptidoglycan modifications (108-111, 287). The incorporation of atypical amino acid into the peptide stem could be excluded because all highly and low abundant muropeptides from the wild-type peptidoglycan consisted of Ala, Gln/Glu and mDAP (Fig. 15, Fig. 17 and Fig. 19). However, the presence of additional amino acids on the glycan backbone or peptide cannot be excluded, as previously outlined in chapter 4.1.3. Tryptic digests of wild-type peptidoglycan revealed several proteins that are presumably associated or attached to the peptidoglycan (Table 46). Numerous, abundant hypothetical proteins were

identified, which potentially play a role in the regulation of peptidoglycan hydrolases. The amidases AmiC2cat and AmiE hardly hydrolysed the crude wild-type peptidoglycan (Fig. 26A). The tryptic remainings of these assumed peptidoglycan associated proteins might have blocked the cleavage sites of the amidases and prevented degradation. This type of modification might no longer be required in a mutant lacking *amiC2* because AmiC2cat and AmiE almost fully hydrolysed the peptidoglycan of the *amiC2* mutant (Fig. 26B).

There are other possibilities to explain the absence of atypical amino acids in *amiC2* mutant muropeptides. Unspecific crosslinking, as discussed previously, affects the level of contamination in peptidoglycan fractions. Each amino acid between the peptidoglycan and the first tryptic cleavage site will remain PGN associated and enters the subsequent analysis. Prevention of unspecific crosslinking may reduce contamination and alongside the amount of atypical amino acid residues. The tryptic digest of wild-type peptidoglycan revealed at least 72% contaminating proteins (Fig. 23) besides proteins that are associated or presumably covalently bound to the peptidoglycan. This suggests that atypical amino acids did not exclusively originate from contaminations. The tryptic peptides of these proteins associated with the peptidoglycan could have blocked enzymatic digestion, and disruption of *amiC2* somehow affected the modification of peptidoglycan by proteins, peptides or amino acids.

Wild-type *N. punctiforme* produced polysaccharides which are likely connected to the glycan backbone of peptidoglycan (Fig. 22A). Interestingly, inactivation of *amiC2* altered the composition of a putative, covalently linked polysaccharide (Fig. 22B). Analysis of the composition revealed glucose as the most abundant monosaccharide, whereas arabinose, galactose and mannose/xylose/sucrose decreased drastically in their abundance. Polysaccharides have ubiquitous functions such as virulence factors, protective barriers against phagocytosis or as receptors for phages (317). Recently, another component of the polysaccharide pellicle of *Lactococcus lactis* was identified (317). The polysaccharide consists of repetitive units of rhamnan trisaccharides which are covalently linked to MurNAc via a GlcNAc residue. The inactivation of essential rhamnan biosynthesis genes affected cell division and septation. These results make it easy to speculate about similar functions in *N. punctiforme*, suggesting a link between the altered polysaccharide composition and the severe morphological defects monitored in the *amiC2* mutant.

4.2.2. Highly crosslinked peptidoglycan is the substrate of AmiC2

The identification of AmiC2 substrates resulted from LC-MS analysis of muropeptide profiles from wild-type *N. punctiforme* before and after AmiC2cat digestion (Fig. 51, supplementary information). This approach is the standard to characterize the substrate specificity of amidases or to determine the peptidoglycan hydrolytic activity (314-316). There is hardly any difference between the TIC-chromatograms obtained before and after AmiC2cat digestion (Fig. 51, supplementary information). As a unique difference between the muropeptide profiles of digested samples of the wild-type and the AmiC2cat mutant, a GlcNAc-MurNAc disaccharide with 8.5 min retention time was detected, displaying a clear sign for hydrolytic activity of AmiC2. Thereafter, OPA-derivatization of AmiC2cat released peptides demonstrated that AmiC2cat as well as AmiE were mainly inactive towards wild-type peptidoglycan (Fig. 26A). Instead, the enzymes degraded the peptidoglycan from a mutant lacking *amiC2* (Fig. 26B). Peptidoglycan associated peptides or amino acids might have blocked the cleavage sites and thus inhibited hydrolysis. The *amiC2* mutant could have also preserved the cleavage sites for AmiC2 in the non-perforated septal disks. These enriched cleavage sites might have

contributed to the detected NH_3 -level increase in AmiC2cat treated *amiC2* mutant peptidoglycan. Interestingly, the relative abundance of two trimeric muropeptide species was twice as high in the *amiC2* mutant compared to the wild-type (Fig. 17 and Fig. 18, peak 8 and 9). So far, trimeric muropeptides were thought to be the substrates for the amidase AmiC2. In contrast, a repetition of the digestion experiment, using the peptidoglycan from the *amiC2* mutant (Fig. 27) revealed barely any differences between the LC-MS chromatograms of AmiC2cat digested and undigested muropeptides. This was partly a result from the low peak intensity. Especially, the peaks for the trimeric muropeptides were hardly visible in both TIC-chromatograms. It was even difficult to observe a decrease in abundance of trimeric muropeptides.

The OPA derivatization revealed the presence of AmiC2cat released peptides (Fig. 26B). Therefore, supernatants containing AmiC2cat cleaved peptides were directly measured by nanoLC-MS (Fig. 28 and Fig. 29). The analysis of AmiC2cat released peptides revealed highly crosslinked peptidoglycan peptides ranging from tetramers to pentamers, and even hexamers could be identified (Fig. 28, Fig. 30 and 5.13.1, supplementary information). This finding is consistent with crystallographic data of the catalytic domain from AmiC2, predicting highly crosslinked muropeptides with different orientations as substrates (242). The first analysis of supernatants, obtained after AmiC2cat digestion, by LC-(ESI-TOF)-MS demonstrated also the presence of trimeric peptides (see Table 48). Corresponding peaks were obtained by the QExactive HF-X analysis using the optimized method for the separation of peptidoglycan derived peptides. The MS1-spectrum of the *amiC2* mutant sample displayed abundant peaks of triply charged parental ions (425.549 $[\text{M}+\text{H}]^{3+}$ and 449.228 $[\text{M}+\text{H}]^{3+}$) and their counterparts with a neutral loss of water (Fig. 55, supplementary information). These triply charged ions were also detected in the MS1-spectrum from the wild-type sample but to a much lower extent. The theoretical mass-to-charge ratios corresponding to the measured single protonated counterparts with 1274.634 $[\text{M}+\text{H}]^+$ and 1345.671 $[\text{M}+\text{H}]^+$, contain fully amidated carboxyl side chains. The former molecule with 1274.634 $[\text{M}+\text{H}]^+$ is a trimer of tetrapeptides, whereas the latter molecule with 1345.671 $[\text{M}+\text{H}]^+$ is a dimer of two tetrapeptides and one tripeptide. Due to missing MS2 spectra, the putative peptidoglycan peptide structure could not be verified.

However, if these trimers constitute the substrate of the amidase, why were constant levels detectable after AmiC2cat digestion? In the case of *E. coli*, anhydro-muropeptides disappeared from the TIC-chromatogram after digestion by AmpD (314). AmiD treated *E. coli* peptidoglycan or AmiA digested *S. aureus* cell walls did not show any comparable peaks in TIC chromatograms (315, 316). This suggests that the amidase AmiC2cat prefers muropeptides with higher levels of crosslinking over trimers or is dependent on the substrate concentration or configuration. Having a closer look on the activity assays, one might assume that AmiC2cat requires an activating or enhancing factor when digesting *N. punctiforme* peptidoglycan. While AmiC2cat degraded *E. coli* peptidoglycan as fast as AmiE (Fig. 25C), it drastically decreased hydrolytic activity on *amiC2* mutant peptidoglycan from *N. punctiforme* (Fig. 26B) by about 68% compared to AmiE. Hydrolysis of RBB-labelled *E. coli* peptidoglycan by AmiC2cat was enhanced in the presence of an NlpD-homologue (Alr3353) of *Anabaena* (246). Based on this observation, it seems possible that the catalytic activity of AmiC2 has to be further enhanced by an external factor to reach the full capacity of peptidoglycan hydrolysis. Furthermore, decreased AmiC2-levels in the *amiC1* mutant of *Anabaena* affected the size of nanopores, suggesting a regulatory role of AmiC2 (221). A knock out mutation of the gene encoding for AmiC1 in *N. punctiforme* could not yet be successfully established (229, 244). Elevated levels of

amiC1 transcripts were prevalent in developmental stages of *N. punctiforme* (318). AmiC2 localizes as well to the cross walls of maturing heterocysts under nitrogen depleting conditions (223). AmiC1 could have an essential role in guiding or coordinating AmiC2 hydrolysis. A recently characterized amidase (RC0497) from obligate, intracellular *Rickettsia conorii* dimerizes upon zinc-binding and is transformed into a biologically active form (319). The catalytic domain of AmiC2 from *N. punctiforme* is active in its monomeric form and elutes as a monomer during size-exclusion chromatography.

Muropeptides with a higher order of crosslinking, exceeding trimers, were not found in the HPLC or LC-MS measurements of mutanolysin digested *amiC2* mutant or wild-type peptidoglycan (Fig. 18 and Fig. 27). The OPA-derivatization and peptide-release assays (Fig. 26, Fig. 28 and Fig. 29) were performed with crude, undigested peptidoglycan, while mutanolysin-digested fragments were standardly used for LC-(ESI-TOF)-MS-measurements. It seems possible, that mutanolysin was not able to hydrolyse the glycosidic bond of these highly crosslinked muropeptide species, as already hypothesized for modified peptidoglycan fragments. Accordingly, tetrameric and higher oligomeric muropeptides were not detected by LC-MS before AmiC2cat treatment, and a disappearance of these peaks could as well not be observed after AmiC2cat digestion. Several reports from Gram-positive species, like *Enterococcus faecalis*, demonstrated abundant, well resolved peaks harbouring tetrameric and pentameric muropeptides, which were released by mutanolysin from the peptidoglycan (85). These results demonstrate that mutanolysin is able to cleave the glycan chains of higher oligomers.

Disruption of *amiC2* does not necessarily lead to a huge increase of highly crosslinked peptidoglycan. It is not clear how many cleavage sites a future nanopore for AmiC2 has and how this influences the total amount of crosslinked peptidoglycan. An increase of highly crosslinked peptidoglycan influences the mechanical properties of peptidoglycan and represents an energy-consuming process. It is doubtful whether *N. punctiforme* highly crosslinks septal peptidoglycan in the absence of AmiC2. On the other hand, not much is known about the structural architecture of septal peptidoglycan in general. New strategies and technologies were developed in the last years to image the peptidoglycan architecture. Recently, Turner et al. uncovered the arrangement of glycan chains in the rod-shaped bacterium *E. coli* (260). The glycan chains are long and circumferentially oriented in the cylindrical part as well as at the cell poles. This architecture changes to a reduced ordered structure when a spheroid form is induced. *B. subtilis* shows a similar circumferentially ordered structure in the cylindrical part, but displayed concentric rings at the cell poles (320). The architecture of peptidoglycan in *B. subtilis* changed during exponential to stationary growth, from a less ordered to a cable-like structure, accompanied by an increase of the overall thickness (321). The appearance of septal disks from *B. subtilis* in AFM images differed strongly, some had a smooth surface while others had the aforementioned concentric structure (321). A higher crosslinking increases the rigidity of septal peptidoglycan (277), displaying potentially a mechanism to support the stress-bearing function of the peptidoglycan. Hence, *N. punctiforme* might crosslink the septal peptidoglycan in the absence of AmiC2. However, highly crosslinked peptidoglycan would only appear at specific points in the septal disk. A quantitative analysis of an enriched fraction of septal disks from the *amiC2* mutant, in comparison to wild-type septal disks, would indicate whether there is an increase of highly crosslinked muropeptides or not.

It can be speculated if the area of a future nanopore harbours also cleavage sites for other amidases, carboxy- or endopeptidases. The loss of AmiC2 might block the nanopore-formation machinery in an early stage and inhibits subsequent steps. The attachment of a glycine bridge in *S. aureus* depends on

Fem-proteins that sequentially add five glycine residues on lysine. FemB, catalysing the binding of the fourth and fifth glycine, is dependent on FemA, which is adding the second and third glycine residue (322). *S. aureus* strains lacking *femA* incorporate monoglycine bridges instead of pentaglycine interpeptide bridges and display pleiotropic defects such as an overall reduction of crosslinked muropeptides. Nanopore formation might result from a combined action of peptidoglycan hydrolases, which depend on the groundwork of AmiC2. AmiC2 could remove highly crosslinked peptides to enable the access for other peptidases as well as glycosidases. The cross walls of *Anabaena* lacking *amiC1* display few nanopores in the very central part (221), in contrast to *N. punctiforme* lacking any nanopores in the absence of *amiC2* (223). There has to be a minimum of enzymatic activity to perforate the septal disks in the *amiC1* mutant of *Anabaena*. Furthermore, a third amidase, AmiC3, was found to be encoded in the genome of *Anabaena* (323). This putative amidase is located at the septal disks and is presumably involved in cell-cell communication by expanding the nanopores.

4.2.3. Site-specific mutations alter hydrolytic activity but not peptidoglycan binding

The catalytic domain of AmiC2 is characterized by a broad and shallow binding groove (242). Distinctive features, like the presence of an α -helix or a β -hairpin, which obstruct the active site and represent autoregulatory mechanisms, are found in various members from Amidase_2 and Amidase_3 families (149, 151, 245, 324), but are missing in the catalytic domain of AmiC2 from *N. punctiforme* (242). This apparently offers a freely accessible binding site to peptidoglycan and addresses to the question how the amidase interacts and binds highly crosslinked peptidoglycan. A MurNAc-tetrapeptide was remodelled into the binding site of AmiC2cat to identify relevant amino acid residues, which potentially interact with this muropeptide (Fig. 32). Mutational analysis of these residues should elucidate the specific role of each amino acid in peptidoglycan binding. The initial experiment was performed to reveal if amino acid substitutions affect peptidoglycan hydrolysis. Accordingly, the exchange of residues F564, L576 and E529 significantly decreased the release of RBB-labelled *E. coli* peptidoglycan and had the greatest impact on the hydrolytic activity of AmiC2cat, compared to all other tested site-specific mutants (Fig. 33A and Fig. 34A).

A phenylalanine residue at position 564 was assumed to stabilize the position of the peptide stem by a hydrophobic interaction with mDAP. Hydrophobic amino acid residues, like Leu, Ile, Val, Phe and Tyr, are conserved at this position in homologous amidases (estimated by F. Büttner). Substitution of phenylalanine by the polar amino acid threonine or serine decreased the hydrolytic activity of AmiC2cat by approximately 40% (Fig. 34A). This mutation not only affected the hydrophobic character, but also the side chain length and increased thereby the distance to mDAP which might have also contributed to the decreased hydrolytic activity of AmiC2cat. The replacement by another hydrophobic amino acid with a shorter side chain could have verified the importance of side chain length, but unfortunately, the AmiC2cat mutants carrying F564A or F564V were not stable and precipitated after affinity chromatography. The binding capability of AmiC2cat was apparently not affected upon mutation of F564. The F564S mutant did not alter the binding behaviour to crude *E. coli* peptidoglycan, compared to the wild-type, neither during the association, nor during the dissociation phase (Fig. 36E). This finding suggests an important role of F564 in the catalysis rather than in the substrate binding process.

Similar observations were made for the mutants with E529A and L576S substitutions. The glutamate residue was ascribed to bind the glycan chain, whereas the leucine residue might have been involved

in the formation of a hydrophobic pocket for the peptide stem. Both mutant variants showed a decreased hydrolytic activity on RBB-labelled *E. coli* peptidoglycan (Fig. 33A and Fig. 34A). The attachment of a His-tag clearly enhanced peptidoglycan hydrolysis of the three mutant variants F564S, E529A and L576S, in accordance with previous descriptions (Fig. 34A). F564S hydrolysed almost twice as much RBB-labelled *E. coli* peptidoglycan as L576S, independent from an affinity tag. Only the E529A mutant showed a differential effect with and without a tag. The E529A mutant hydrolysed 25% more RBB-labelled *E. coli* peptidoglycan than F564S, and 10% less than L576S without any tag. But when a His-tag was attached to the N-terminus of the E529A mutant, it released 21% less and 5% more RBB-labelled fragments into the supernatant than L576S and F564S. It was observed that especially this mutant showed a reduced molecular weight compared to other mutant variants in a Western blot assay, using polyclonal antibodies against the C-terminal part of AmiC2, (Fig. 54, supplementary information). Apparently, removal of the GST-tag decreased the stability of the E529A mutant, and caused degradation. This presumably affected the catalytic activity of E529A. His-tagged E529A enzymes or those carrying additionally a flexible GGS-linker did not show any signs of degradation. However, mutation of E529 impaired peptidoglycan hydrolysis, but not peptidoglycan binding (Fig. 36E). The same result was obtained for the L576S mutant. Consequently, F564, L576 and E529 seem to be part of the catalytic mechanism.

The positively charged arginine residues at positions 563 and 568 were predicted to form salt bridges with the free carboxyl group of mDAP (Fig. 32). Aspartate residues often participate in the formation of salt bridges with the amino-groups of lysine, arginine or meso-diaminopimelic acid. Highly crosslinked peptides with 4-3 crosslinks between the amine group of mDAP and the carboxyl-group of Ala were detected as cleavage products from AmiC2cat (see chapter 5.13.1, supplementary information). The amino group of mDAP could therefore not be used for the formation of a salt bridge with aspartate. Accordingly, the exchange of both arginine residues, R563 and R568, by aspartate should have impaired peptidoglycan binding and consequently hydrolysis, as long as both residues were essential for substrate binding. The hydrolytic activity of AmiC2cat was unaffected upon mutation of R583 and R568 (Fig. 33A and Fig. 34A). Either, both arginine residues are not involved in substrate binding or the interaction with other peptidoglycan derived amino acid residues, by yet unknown amino acids in the binding site, might have compensated the loss of both arginine residues and enabled the binding of peptidoglycan.

It is also unknown which conformation trimeric and peptidoglycan oligomers of higher order adopt upon binding to AmiC2 and whether the whole or only parts of these highly crosslinked peptidoglycan structures occupy the binding site. The N-terminal amidase domain of the major autolysin LytA from *S. pneumoniae* binds nascent peptidoglycan with at least four saccharides and two adjacent pentapeptides (325, 326). Structural data reveal that one pentapeptide is bound deeply into the binding crevice of LytA, whereas the other pentapeptide stem resides outside the binding cleft. This pentapeptide-tetrasaccharide undergoes conformational changes upon binding, whereas the amidase domain remains structurally almost unchanged (326). Interestingly, the LytA amidase requires long glycan chains of more than four saccharides because it does not hydrolyse mono- and disaccharides (325). The catalytic domain of AmiC2 acts on crude, enzymatically unprocessed peptidoglycan (Fig. 24 - Fig. 26, Fig. 33, Fig. 34). This requires the ability to recognize and bind intact, long glycan chains. The mutation of three putative MurNAc interacting residues (S518, V519 and D520) in the binding site of AmiC2cat did not alter peptidoglycan hydrolysis (Fig. 33A and Fig. 34A). Single site-specific mutations in the putative glycan binding site, exclusively involving one MurNAc

residue, might not necessarily affect the binding behaviour or hydrolytic activity of Ami2cat when several saccharides are still bound. Moreover, more than 21 amino acids were identified in the amidase domain of LytA to interact with the tetrasaccharide-pentapeptide substrate (326). Ami2cat released highly crosslinked, complex peptides in the range of tetramers to hexamers with an unknown conformation (5.13.1, supplementary information). Exactly those fragments must be kept in the binding groove of Ami2cat as long as the catalysis takes place, indicating an involvement of numerous site-specific residues of Ami2cat. The question remains open how Ami2cat accommodates highly crosslinked peptidoglycan substrates. It is necessary to crystallize the catalytic domain in complex with its natural substrate to identify relevant amino acids for the binding of peptidoglycan and to understand the catalytic mechanism.

Little is known about the catalytic mechanism of AmiC2. Büttner et al. were able to crystallize the catalytic domain of AmiC2 and identified the highly conserved zinc-binding residues H447, H515 and E462 (242). Another glutamate residue (E578), in close proximity to the catalytic zinc ion, might be involved in peptidoglycan hydrolysis, because mutation of this residue abolished the hydrolysis of RBB-labelled *E. coli* peptidoglycan almost completely (242). The inactive mutant E578A was purified with a His-tag in this work to analyse its influence on the peptidoglycan binding ability. The Dye-release assay demonstrated high hydrolytic activity comparable to wild-type levels (Fig. 53, supplementary information). In contrast to Büttner et al., a total of 4 μM enzymes, instead of 0.08 μM , were used in the assay. Sequencing of the plasmid carrying the His-tagged Ami2cat clearly confirmed the substitution of glutamate, at position 578, by alanine. The amidase AmiC2 reveals some differences to homologous AmiC proteins. The domain architecture comprises a SEC-signal sequence, two AMIN domains, separated from the catalytic domain by a proline rich modulator. The catalytic domain misses structural elements, which block the active site, and releases exclusively highly crosslinked peptides from *N. punctiforme* peptidoglycan. A different catalytic mechanism, distinctive from that of homologous amidases and other peptidoglycan hydrolases, might therefore not be far-fetched. This would fit to a unique function of AmiC2 in drilling nanopores.

5. Supplementary information

5.1. LC-MS analysis of *Nostoc* muropeptides

Table 51: LC-(ESI-TOF)-MS analysis of *Nostoc* muropeptides. Mutanolysin released muropeptides from *N. punctiforme* were analysed by LC-(ESI-TOF)-MS using a 80 min linear acetonitrile gradient in positive mode. Identified muropeptides with retention time, m/z and composition are listed below. A = amidation; Ac = acetylation

Retention time	GlcNAc-MurNAc residues	Peptide length	calculated [M+H] ⁺	measured [M+H] ⁺	Modifications
3.5	1	3	871.3779	871.389	
4.2	1	4	941.431	941.429	+ A
4.5	1	3	870.3938	868.385	+ A
	1 - GlcNAc	4	738.3516	738.349	+ A
	1	2	698.3091	698.32	+ A
	2	4 + 3	1709.7699	1709.768	- 2 Ac
6.6	1	4	942.415	942.409	
	1	3	870.3938	869.377	+ A
7.2	2	3 + 4	1750.796	1750.799	+ 2 A, - Ac
7.6	1	4	941.431	939.419	+ A
8.5	2	0	977.393	977.403	
9.5	2	4 + 4	1821.8335	1821.847	+ 2 A, - Ac
9.9	2	3 + 4	1751.7804	1751.773	+ A, - Ac
10.5	2	3 + 4	1751.7804	1751.799	+ A, - Ac
10.8	1	3	850.3676	850.368	+ A, - H ₂ O
11.3	1 - GlcNAc	3	647.2883	647.283	+ A, - H ₂ O
12.3	1	0	479.1872	479	- H ₂ O
	2	3 + 4	1792.807	1792.825	+ 2 A
12.5	1	3 + 4	1295.5849	1295.585	+ A, - H ₂ O
12.7	1	3 + 4	1295.5849	1295.585	+ A, - H ₂ O

Retention time	GlcNAc-MurNAc residues	Peptide length	calculated [M+H] ⁺	measured [M+H] ⁺	Modifications
13.3	2 - 2 GlcNAc	3 + 4	1384.6802	1384.635	+ 2 A
14.3	2	3 + 4	1792.807	1792.799	+ 2 A
15.9	1	4	921.4047	921.405	+ A, - H ₂ O
	2	3 + 4	1790.8389	1792.807	+ 2 A
16.1	3	4 + 4 + 3	2673.2095	2673.175	+ 3 A, - Ac
17	2	4 + 4	1863.8441	1863.841	+ 2 A
	2	3 + 4	1793.791	1793.795	+ 1 A
18	2	3 + 4	1790.8389	1792.807	+ 2 A
18.3	2	3 + 4	1790.8389	1792.807	+ 2 A
18.9	3	4 + 4 + 3	2673.2095	2671.208	+ 3 A, - Ac
	3	4 + 4 + 3	2674.1953	2674.223	+ 2 A, - Ac
19.7	2	4 + 4	1864.8281	1864.829	+ A
	3	4 + 4 + 3	2653.1833	2653.193	+ 3 A, Ac, - H ₂ O
22.4	3	4 + 4 + 3	2715.2201	2715.217	+ 3 A
24.8	3	4 + 4 + 4	2786.2572	2786.283	+ 3 A
	2	3 + 4	1772.7808	1772.783	+ 2 A, - H ₂ O
25.5	2	3 + 4	1772.7808	1772.799	+ 2 A, - H ₂ O
	3	4 + 4 + 3	2715.2201	2713.22	+ 3 A
27	3	4 + 4 + 4	2787.2412	2787.215	+ 2 A
27.6	4	4 + 4 + 4 + 3	3637.6332	3637.688	+ 4 A
	3	4 + 4 + 4	2784.2892	2784.527	+ 3 A
30.9	3	4 + 4 + 3	2695.1939	2695.22	+ 3 A, - H ₂ O

5.2. Muropeptides in septal and lateral cell wall fractions

Table 52: Muropeptide species in mutanolysin digested peptidoglycan fractions. *Nostoc* PGN was harshly sonified to remove lateral cell wall and isolate septal disks. These were enriched and purified by filtration using different cut-offs. Mutanolysin released soluble PGN fragments were analysed by LC-MS and compared to untreated PGN containing both, lateral and septal PGN. * = amidation; + = deacetylation; # = -H₂O; \wedge = anhydrous. Part 1










Muropeptide		Whole PGN		Septal PGN	
species	m/z	Rt	ppm	Rt	ppm
	871.378	3.5	0.011	4.3	0.011
	941.431	4.2	-0.002	6.2	-0.002
		7.6	-2.012	6.6	0.012
	870.394	4.5	-2.009	3.3	0.002
		6.6	-1.017		
	698.309	4.5	0.011	4.3	-0.001
	738.352	4.5	-0.003	5.3	0.009
	942.415	6.6	-0.006	7.8	0.007
	1012.468			7.8	-0.031
	1750.796	7.2	0.003	14.5	-0.007
	1751.799	9.9	-0.007	16.1	-0.007
		10.5	0.019		

Table 53: Muropeptide species in mutanolysin digested PGN fractions. Septal disks were isolated by harsh sonication of crude *Nostoc* PGN and enriched by filtration. Mutanolysin released soluble PGN fragments were analysed by LC-MS and compared to untreated PGN containing lateral and septal PGN. * = amidation; + = deacetylation; # = -H₂O; Δ = anhydrous. Part 2












Muropeptide		Whole PGN		Septal PGN	
species	m/z	Rt	ppm	Rt	ppm
	850.368	10.8	0		
	1295.585	12.5	0	13.8	-0.045
	1792.807	12.3	0.018	13.5	0.01
		13.3	-0.008	15.1	-0.008
		14.3	-0.008	15.5	-0.008
		15.9	-0.994		
		18	-0.994		
	921.405	15.9	0		
	2673.21	16.1	-0.034	22	-0.034
	1863.844	17	-0.003	18.5	0.025
	1793.791	17	0.004	17.1	0.03
				17.3	0.004
	2716.204	22.4	0.02	23	0.02

Table 54: Muropeptide species in mutanolysin digested peptidoglycan fractions. *Nostoc* PGN was harshly sonified to remove lateral cell wall and isolate septal disks. These were enriched and purified by filtration

using different cut-offs. Mutanolysin released soluble PGN fragments were analysed by LC-MS and compared to untreated PGN containing both, lateral and septal PGN.
 * = amidation; + = deacetylation; # = -H₂O; λ = anhydrous. Part 3

Muropeptide		Whole PGN		Septal PGN	
species	m/z	Rt	ppm	Rt	ppm
	2786.257	24.8	0.026	25.5	-0.022
	1772.781	24.8 25.5	0.002 0.018	27.2	-0.008
	1864.282	19.7	0.001	20	0.029

5.3. Domain organization and *in-silico* interactions of putative PGN-interacting proteins

Npun_F2686: GAF sensor hybrid histidine kinase

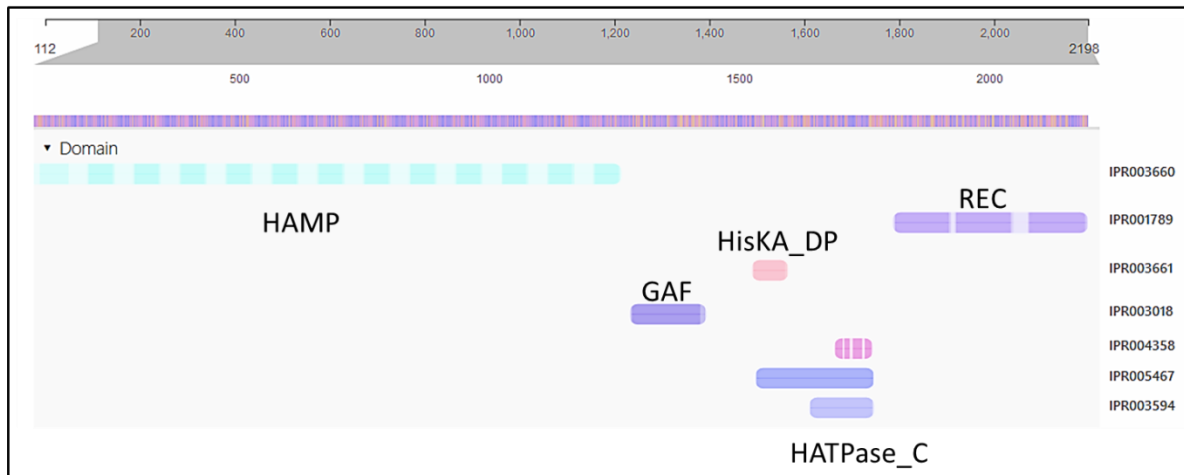


Fig. 38: Domain architecture of Npun_F2686. The uncharacterized protein is a predicted histidine kinase consisting of several HAMP domains, a GAF signalling module, the dimerization and autophosphorylation unit (HisKA_DP), the ATPase domain (HATPase_C) and three response and receiver domains (REC).

Npun_R4372: Protein translocase subunit SecY

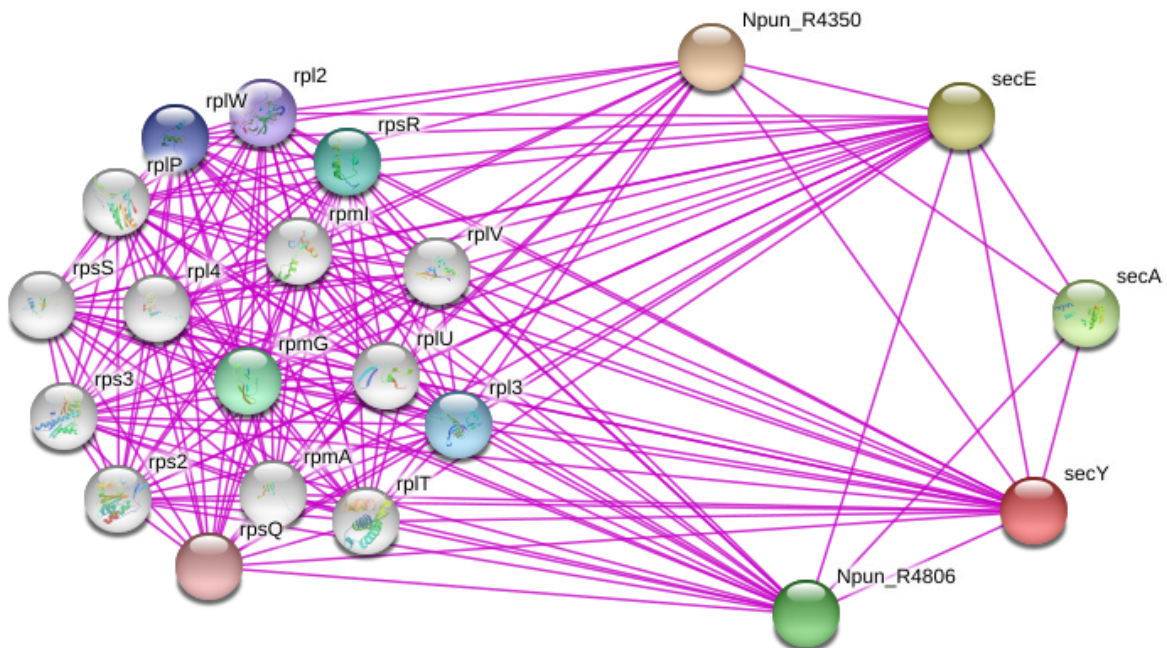
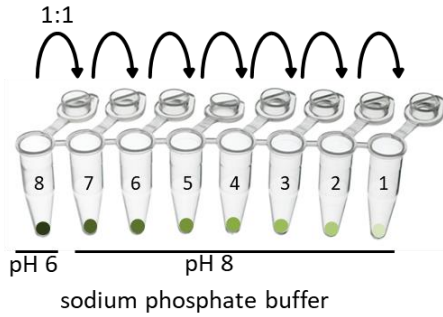


Fig. 39: SecY (Npun_R4372) interactome obtained from experimental data summarized by STRING database. SecY forms a transmembrane channel with SecE and SecG (NpunR4350). SecA is a cytoplasmic protein that binds to unfolded preproteins and interacts with the SecYEG complex. The latter complex has multiple interactions with ribosomal proteins (Rps, Rpl and Rpm proteins). FtsQ (Npun_R4806) was also shown to interact with SecY, A and E.

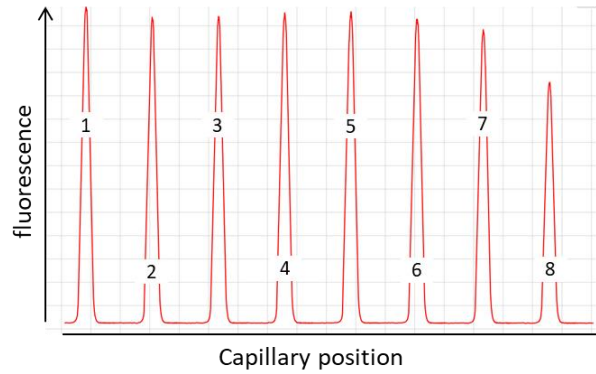
5.4. Factors affecting MST measurements

Influence of pH on MST analysis

A. Serial dilution of buffer pH6 -> pH8



B. CapScan of 50 nM AmiC2cat + buffer pH 6-8



C. Dose-responsive curve for AmiC2cat + buffer pH 6-8

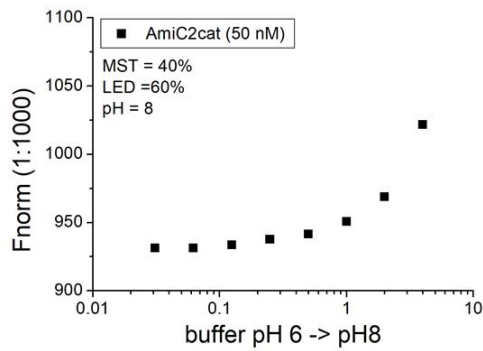
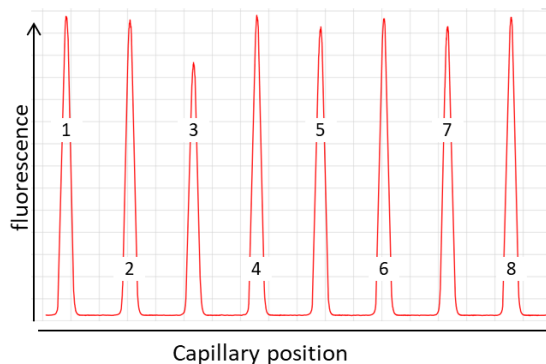


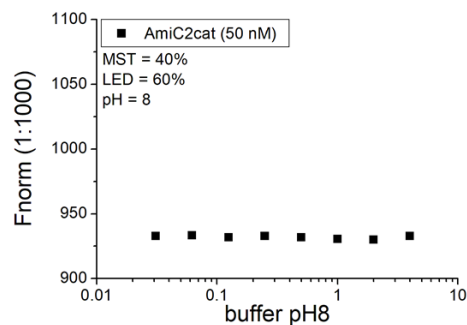
Fig. 44: Influence of pH changes on the MST analysis.
A. Serial titration of sodium phosphate buffer pH6 in phosphate buffer pH8 (1:1). **B.** Capillary Scan (CapScan) of 50 nM His8-AmiC2cat in phosphate buffer with different pH values. Fluorescence of each capillary was recorded. **C.** MST measurement of His8-AmiC2cat in sodium phosphate buffer with different pH values. LED: fluorophore excitation; MST: Infrared laser power; Fnorm: normalized fluorescence

Influence of phosphate buffer on the MST analysis

A. CapScan of 50 nM AmiC2cat + buffer pH8



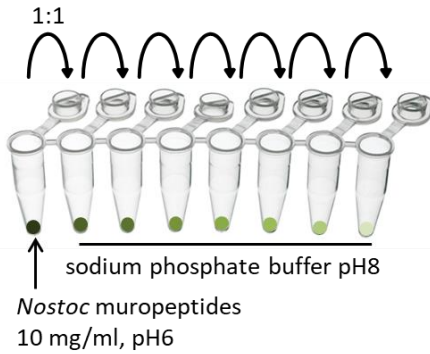
B. Dose-responsive curve for AmiC2cat + buffer pH8



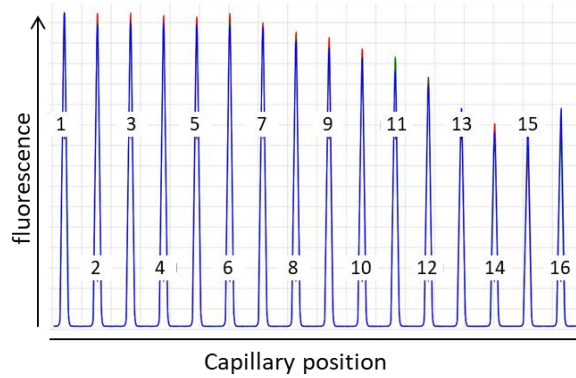
Influence of pH changes on the interaction between AmiC2cat and *Nostoc* muropeptides

Fig. 45: Influence of phosphate buffer on the MST analysis. **A.** Capillary Scan (CapScan) of 50 nM His8-AmiC2cat in phosphate buffer with the pH8. **B.** Binding curve of His8-AmiC2cat in phosphate buffer pH8. LED: fluorophore excitation; MST: Infrared laser power; Fnorm: normalized fluorescence

A. Serial dilution of muropeptides



B. Capillary Scan of AmiC2cat + MP pH6-8



C. Interaction between AmiC2cat + MP pH6-8

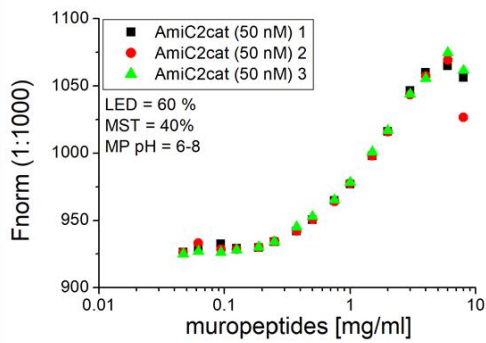


Fig. 46: MST analysis of AmiC2cat and *Nostoc* muropeptides with differentiated pH values **A.** Serial titration muropeptides (stored in pH6) in phosphate buffer pH8 (1:1). **B.** Capillary Scan (CapScan) of 50 nM His8-AmiC2cat and muropeptides with different pH values. Fluorescence of each capillary was recorded. **C.** Dose responsive curve for His8-AmiC2cat and *Nostoc* muropeptides with different pH values. LED: fluorophore excitation; MST: Infrared laser power; Fnorm: normalized fluorescence; MP = muropeptides. Numbers 1 – 16 = muropeptides from low to high concentration.

5.5. BLI-measurements

His8-AmiC2cat loading on Ni-NTA biosensors

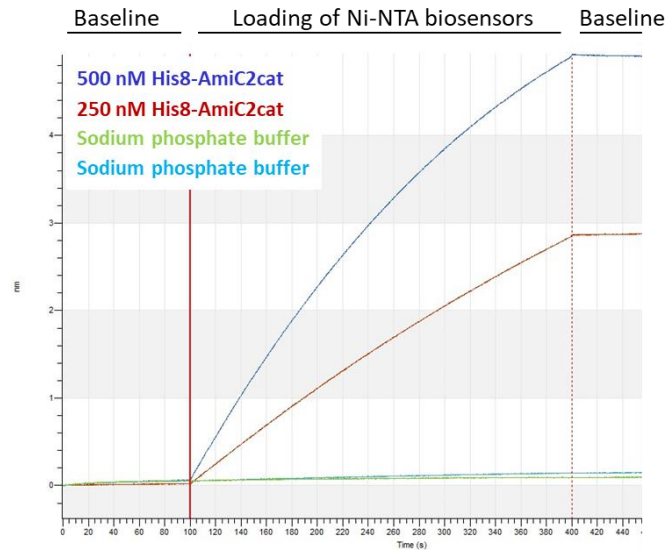


Fig. 47: His8-AmiC2cat loading on Ni-NTA biosensors. Ni-NTA biosensors were equilibrated in sodium phosphate buffer (baseline) and loaded with 500 nM (blue) or 250 nM (red) His8-AmiC2cat. Another pair of sensors (green and light blue) were not loaded with His8-AmiC2cat.

Supplementation of 1% BSA and 0.1% Tween20 to BLI-measurement

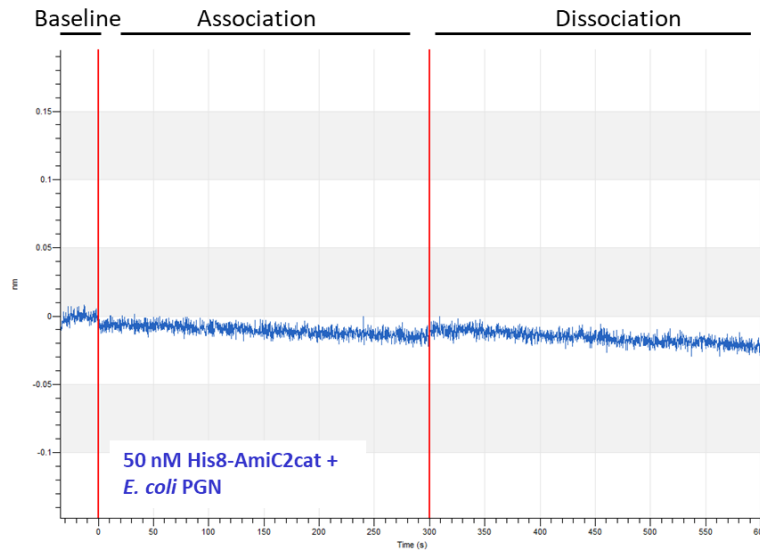
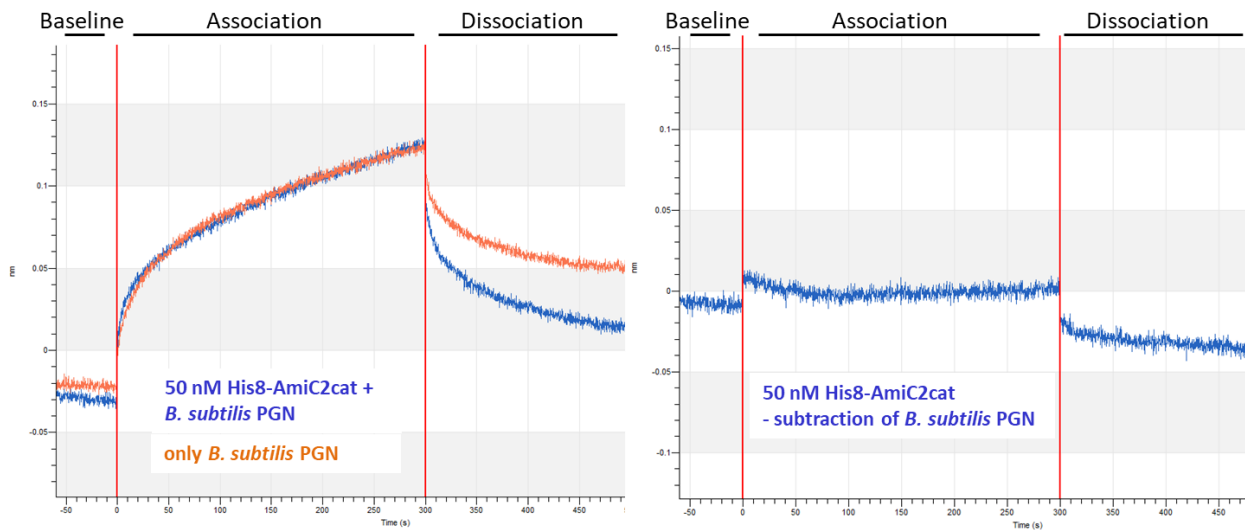


Fig. 48: BLI-measurement of *E. coli* PGN and 50 nM AmiC2cat in the presence of BSA and Tween 20. Sensor was equilibrated in 0.1 M Tris-HCl buffer pH 8, containing 150 mM NaCl and loaded with 50 nM His8 AmiC2cat (blue). Subsequently the sensor was washed in the same buffer supplemented with 1% BSA and 0.1% Tween20 (baseline). Binding to (association) and dissociation from *E. coli* PGN (adjusted to $OD_{600nm} = 0.5$ in buffer + additives) was recorded. Reference sensor was not loaded with His8-AmiC2cat and subtracted from curve obtained from AmiC2cat and *E. coli* PGN.

Unspecific interaction between peptidoglycan and Ni-NTA biosensors

A. Unspecific interaction between *B. subtilis* peptidoglycan and Ni-NTA biosensors



B. Unspecific interaction between *Nostoc* peptidoglycan and Ni-NTA biosensors

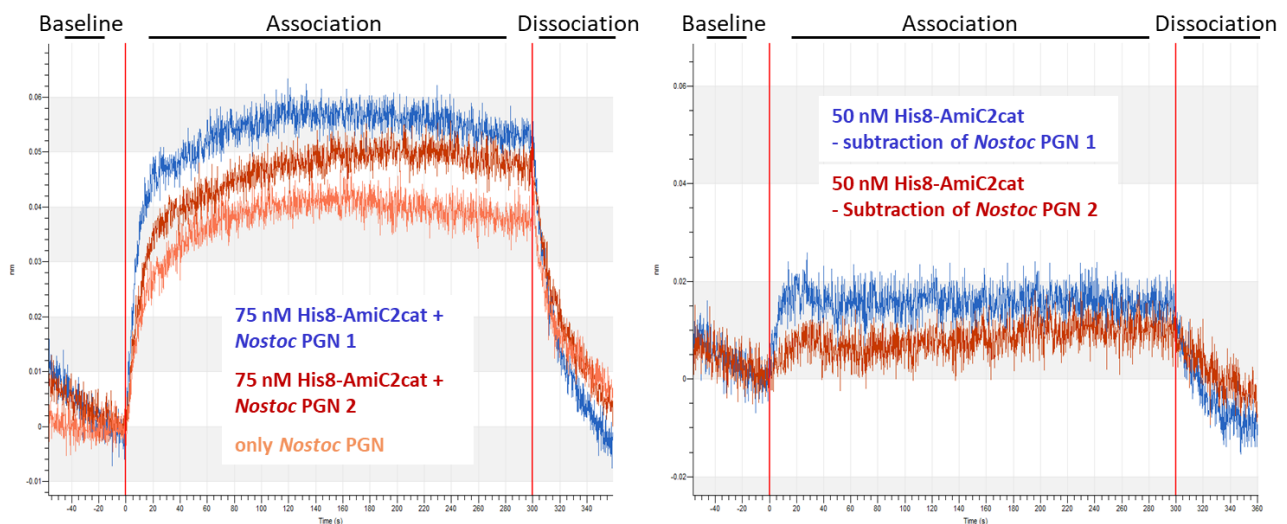


Fig. 49: Unspecific peptidoglycan binding on Ni-NTA biosensors. **A.** BLI-analysis of His8-AmiC2cat and *B. subtilis* PGN. Sensors were equilibrated in sodium phosphate buffer, loaded with 50 nM His8 AmiC2cat (blue) and equilibrated again in the same buffer (baseline). Binding to (association) and dissociation from *B. subtilis* PGN (adjusted to $OD_{600nm} = 0.5$) was analysed by BLI. Reference sensor (orange) was not loaded with His8-AmiC2cat and subtracted from curve obtained from AmiC2cat and *B. subtilis* PGN. **B.** Interaction between His8-AmiC2cat and *Nostoc* PGN. Ni-NTA biosensors were equilibrated in sodium phosphate buffer, loaded with 75 nM His8-AmiC2cat (blue and red) and equilibrated again buffer (baseline). Interaction between His8-AmiC2cat loaded Ni-NTA biosensors with *Nostoc* PGN (adjusted to $OD_{600nm} = 0.5$) was analysed. Reference Ni-NTA biosensor was not loaded with Hi8-AmiC2cat and subtracted from curves obtained from AmiC2cat and *Nostoc* PGN.

5.6. Peptidoglycan-polysaccharide of *Nostoc* sp. PCC 7120

A.

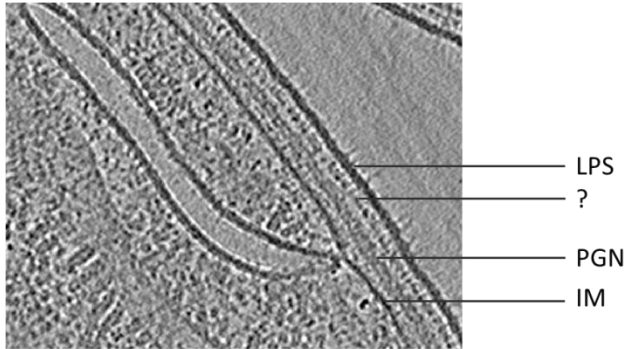
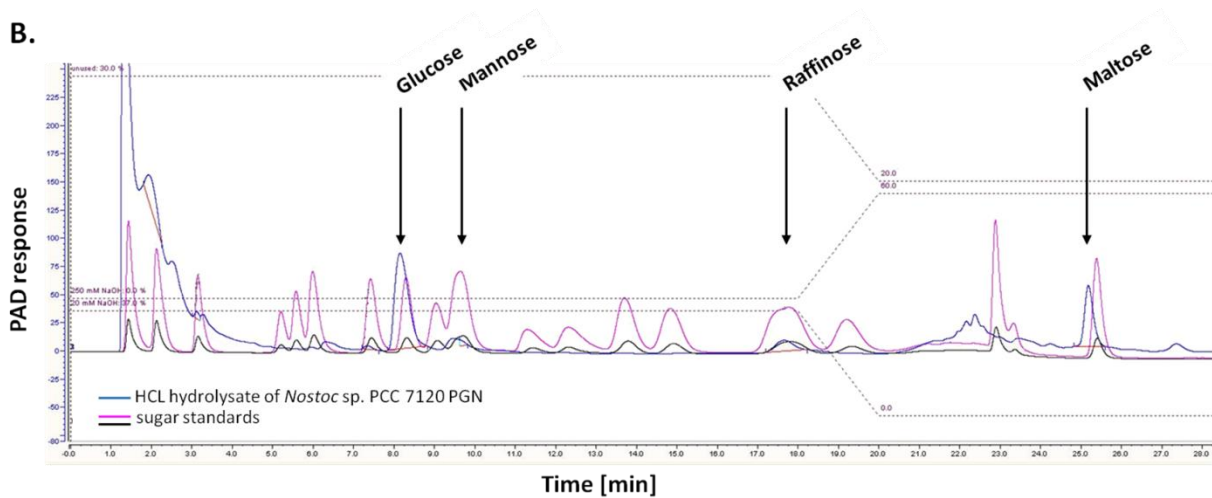


Fig. 50: Peptidoglycan-polysaccharide of *Nostoc* sp. PCC 7120. A. Cryo-electron tomograph of a *Nostoc* sp. PCC 7120 cell. LPS = lipopolysaccharide; PGN = peptidoglycan; IM = inner membrane; question mark represents electron-dense, unknown layer. Courtesy of Gregor Weiss. B. HPAEC - analysis of acid hydrolysates of *Nostoc* sp. PCC 7120 cell walls. Pink and black lines = standard carbohydrate mixture; blue line = *Nostoc* sample.

B.



5.7. AmiC2cat digestion of wild-type peptidoglycan

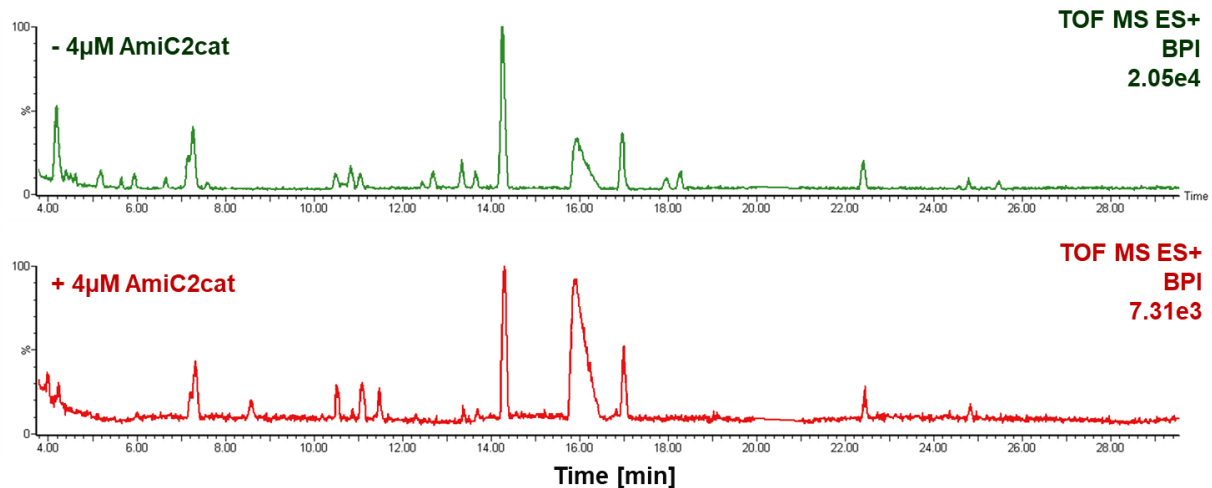


Fig. 51: Basepeak ion chromatogram of AmiC2cat undigested (upper panel) and digested (lower panel) wild-type peptidoglycan. The PGN from wild-type *N. punctiforme* was degraded by 4 μM AmiC2cat and pelleted. The remaining undigested PGN pellet was degraded by mutanolysin and analysed by LC-MS (red BPI). A control consisting of *Nostoc* PGN, not digested by AmiC2cat, was likewise degraded by mutanolysin and measured by LC-MS (green BPI).

5.8. Efficiency of mutanolysin cleavage

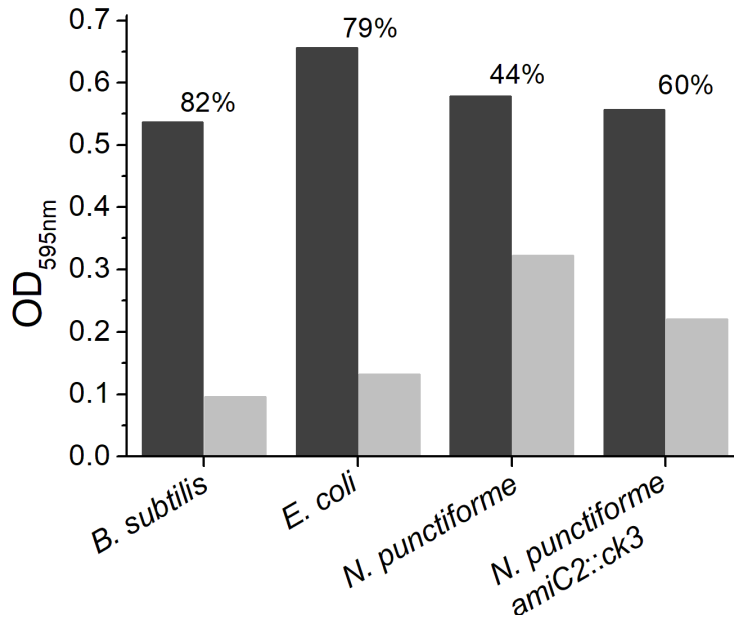


Fig. 52: Mutanolysin digestion of peptidoglycan from different organisms. Mutanolysin hydrolytic activity corresponds to a decrease in absorbance at 595nm after 16h incubation at 37°C. PGN hydrolysis is represented in %. Dark grey = before digestion; light grey = after digestion.

5.9. Site-specific AmiC2 mutants

Influence of E578A on the hydrolytic activity of AmiC2

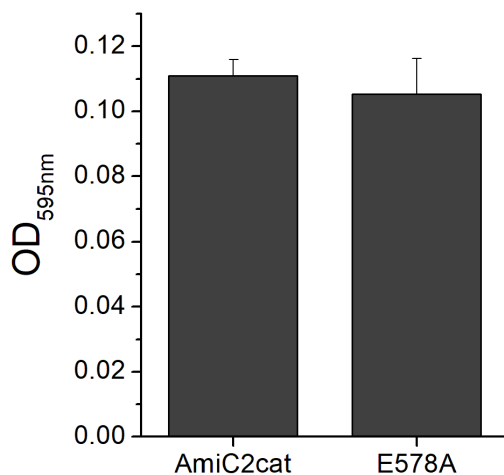


Fig. 53: DRA of AmiC2cat and its E578A mutant. RBB-labelled *E. coli* PGN was hydrolysed by 4 μ M of either AmiC2cat or E578A for 30 min at 37°C. Optical density was measured at 595nm after removal of undigested RBB-labelled PGN.

Western blot analysis of AmiC2cat mutant variants

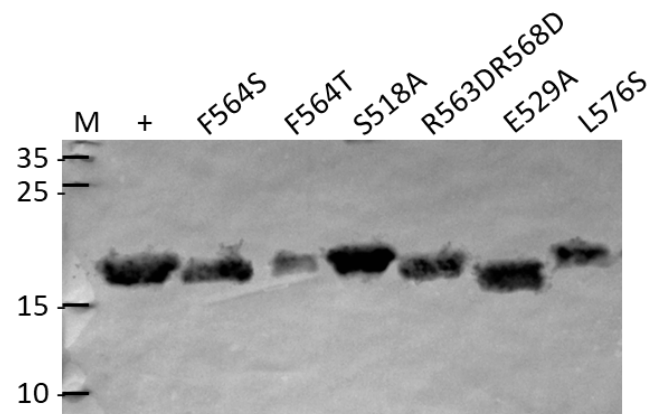
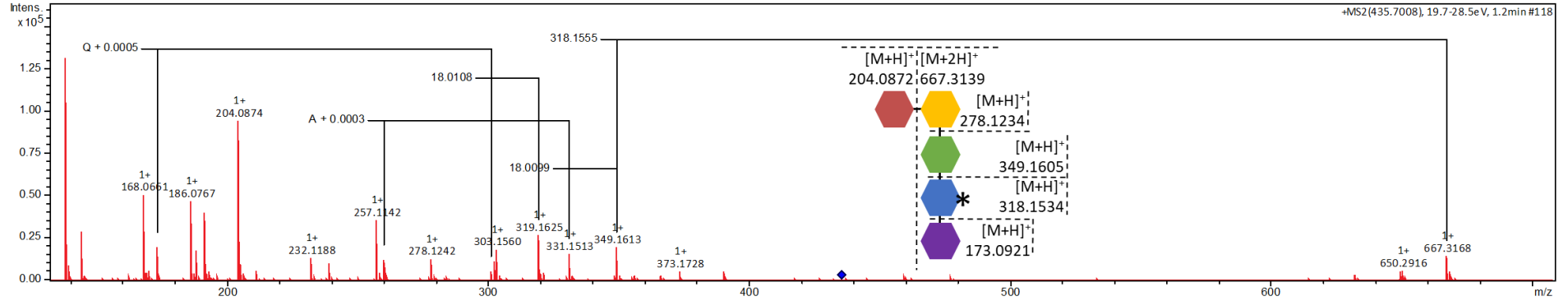


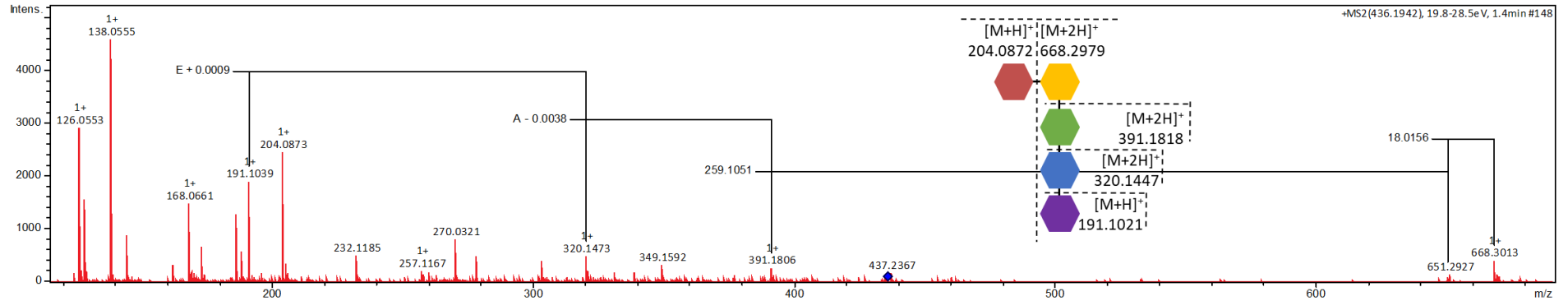
Fig. 54: Western blot of AmiC2cat mutants. Mutant variants were recombinantly expressed with a GST-tag in *E. coli* and purified via affinity and size-exclusion chromatography. GST-tag was removed and 1 μ M proteins were subjected to Western blot analysis using polyclonal antibodies against the C-terminal part of AmiC2. M= protein marker; += wild-type AmiC2cat

5.10. MS/MS fragmentation of mucopeptides derived from wild-type *N. punctiforme* PGN

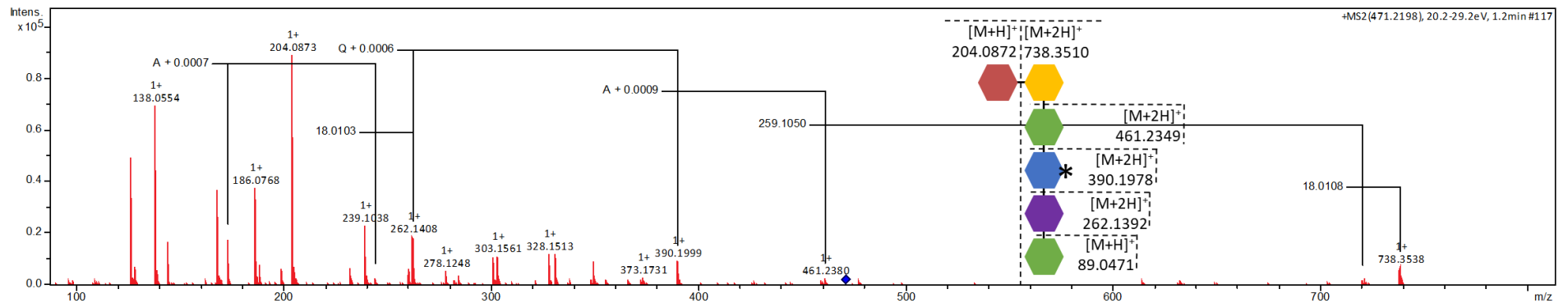
870.3954 [M+H]⁺



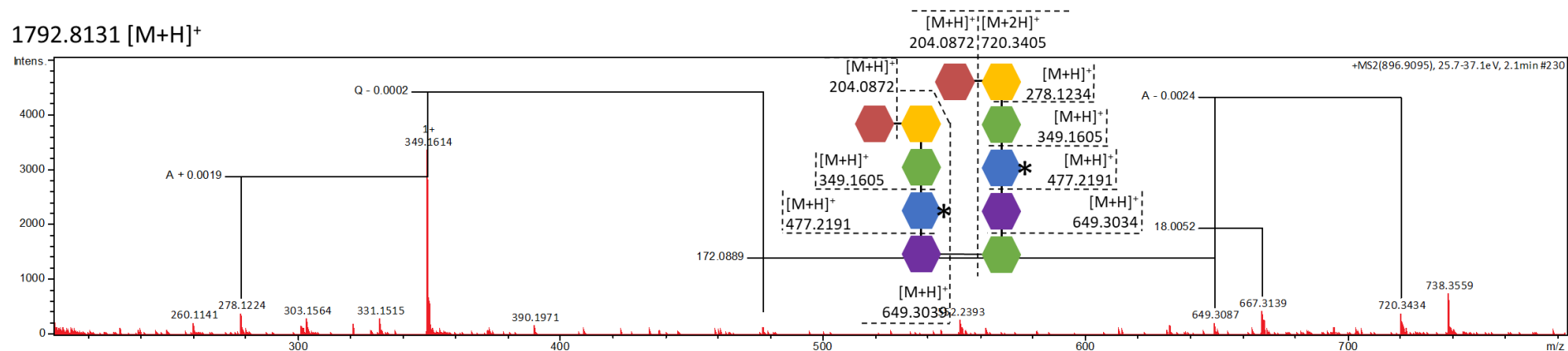
871.3814 [M+H]⁺



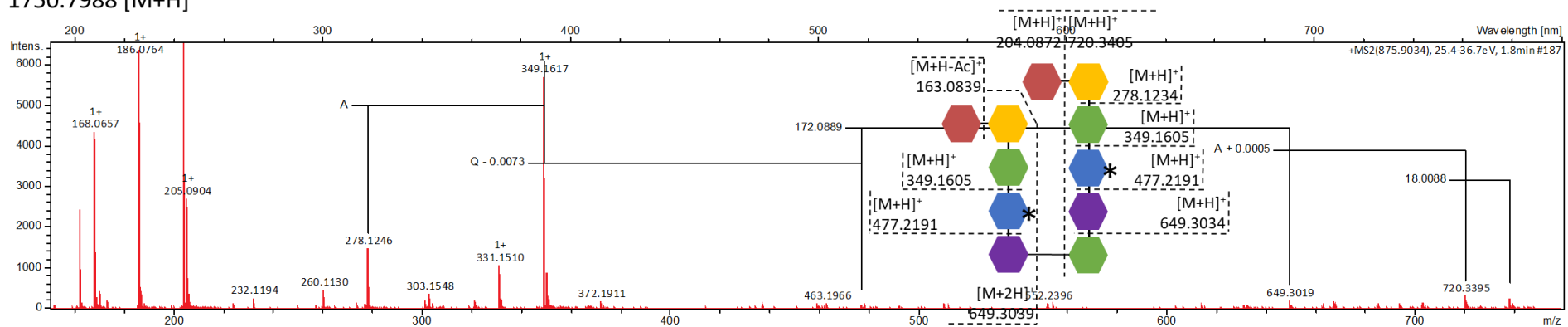
941.4326 [M+H]⁺



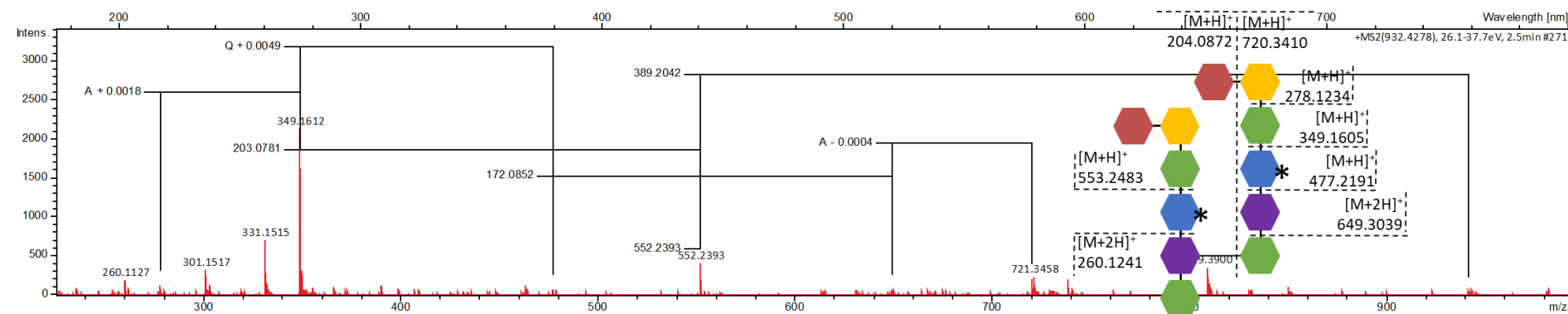
1792.8131 [M+H]⁺



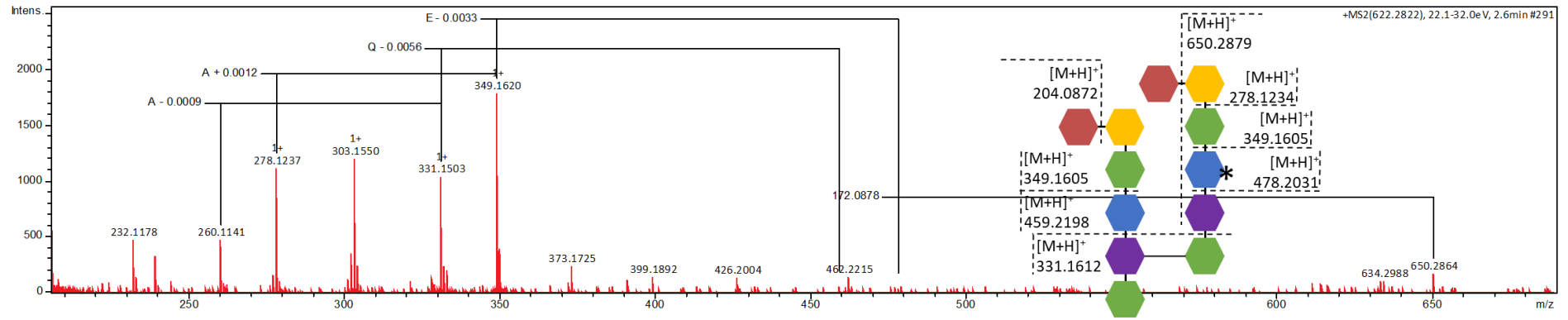
1750.7988 [M+H]⁺



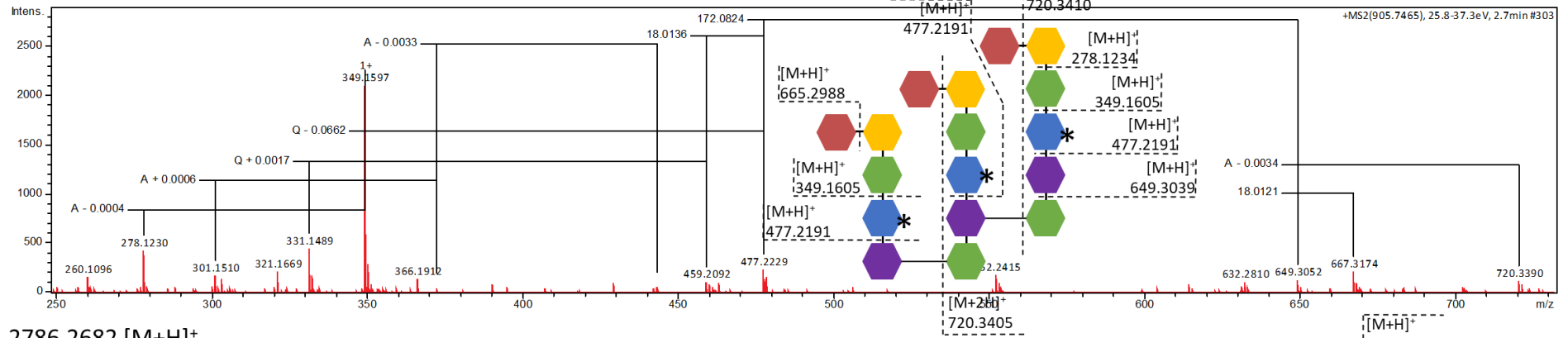
1863.8483 [M+H]⁺



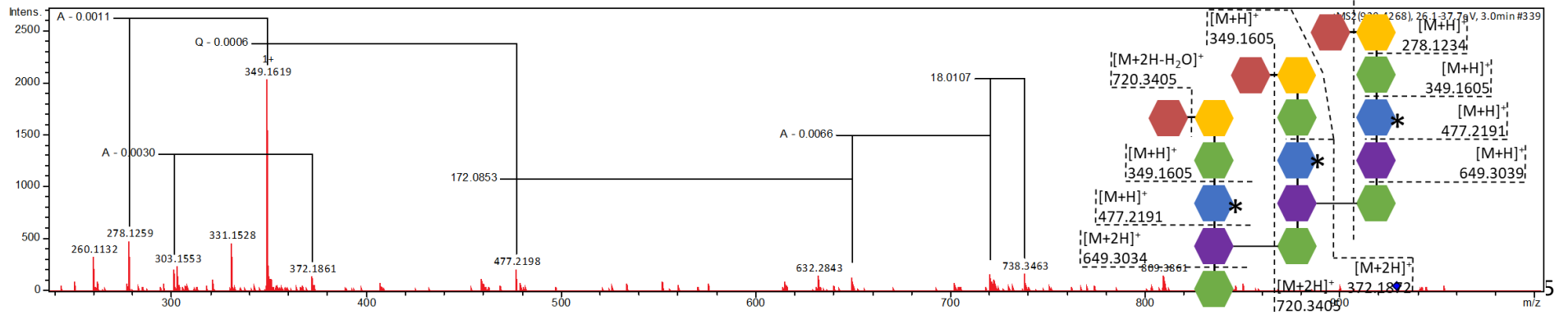
1864.8326 [M+H]⁺



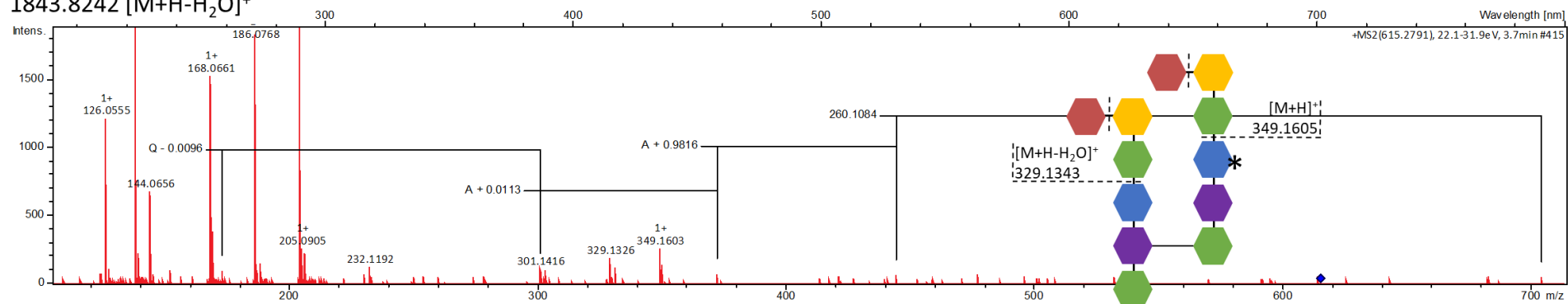
2715.2278 [M+H]⁺



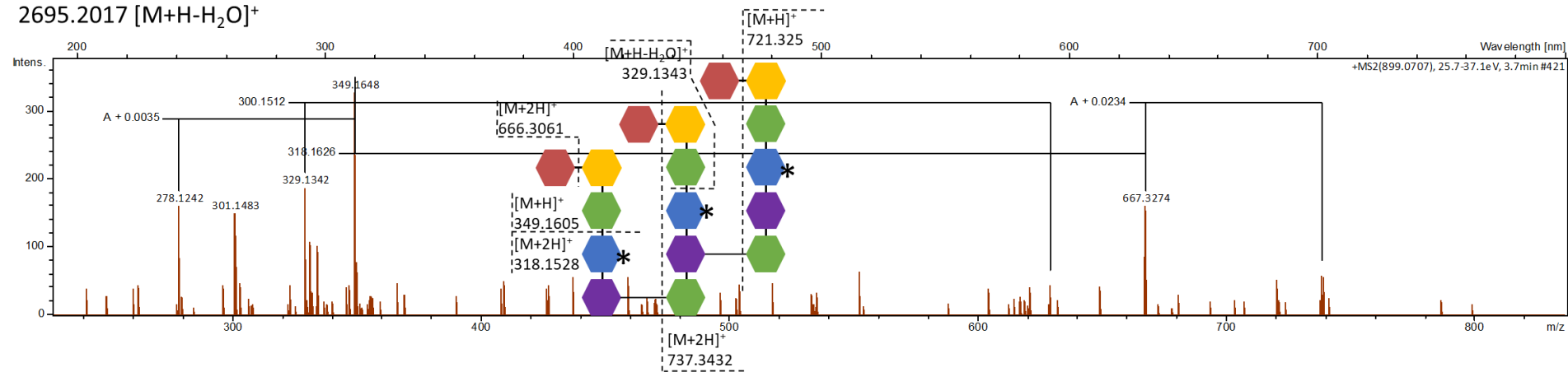
2786.2682 [M+H]⁺



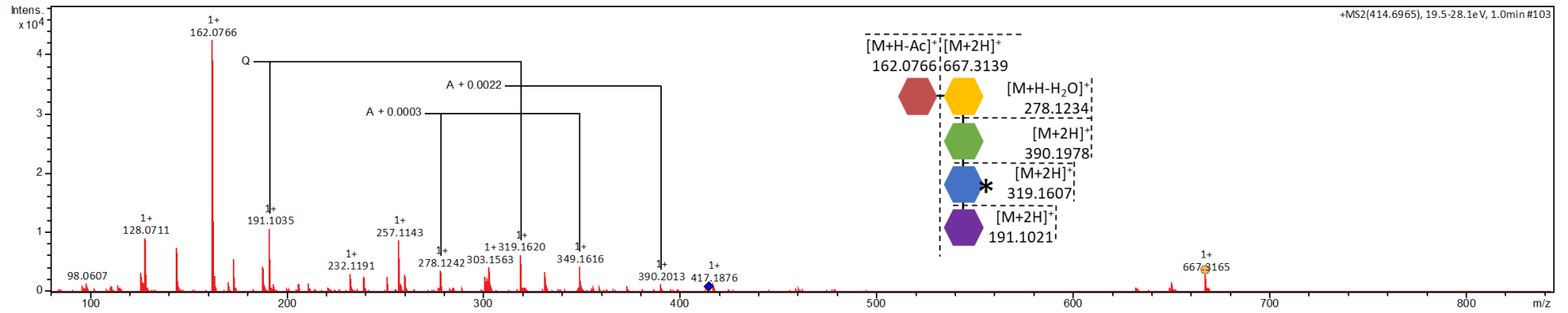
1843.8242 [M+H-H₂O]⁺



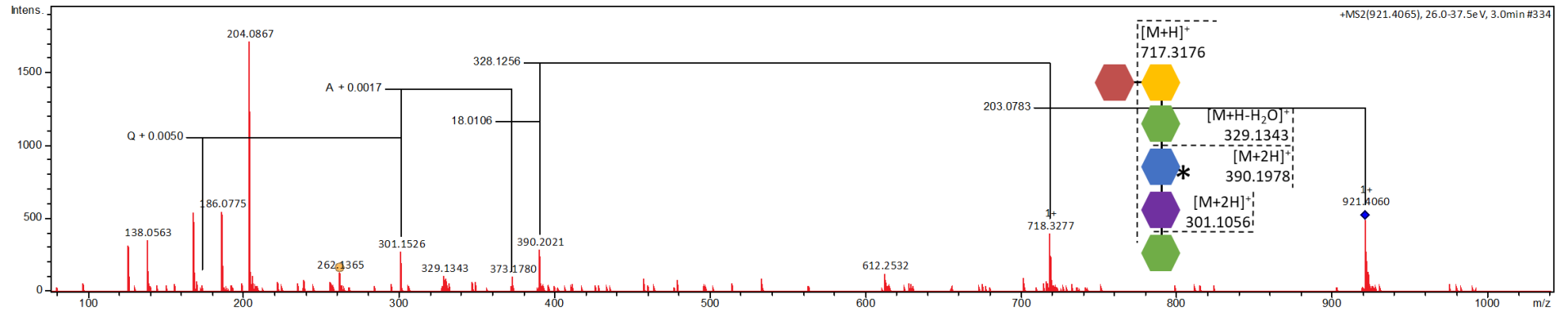
2695.2017 [M+H-H₂O]⁺



828.3837 [M+H]⁺

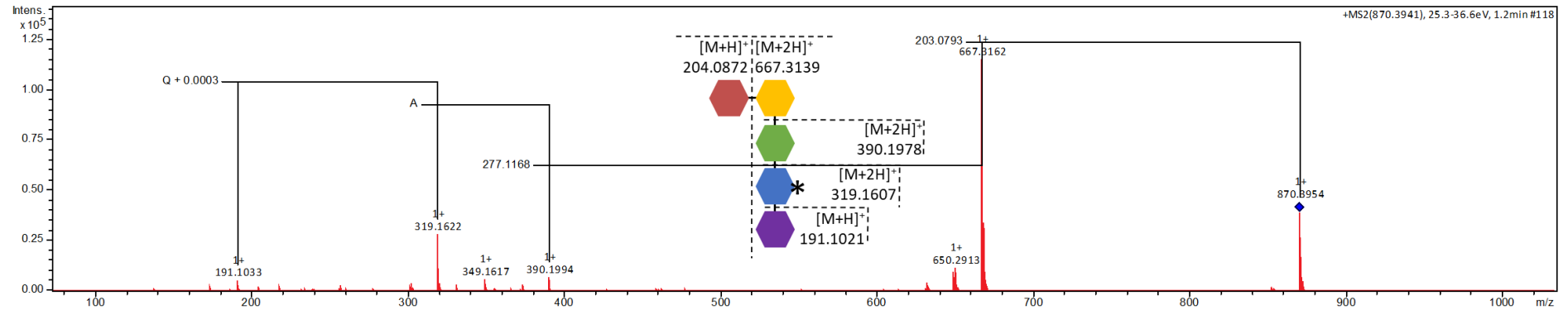


921.4078 [M+H]⁺

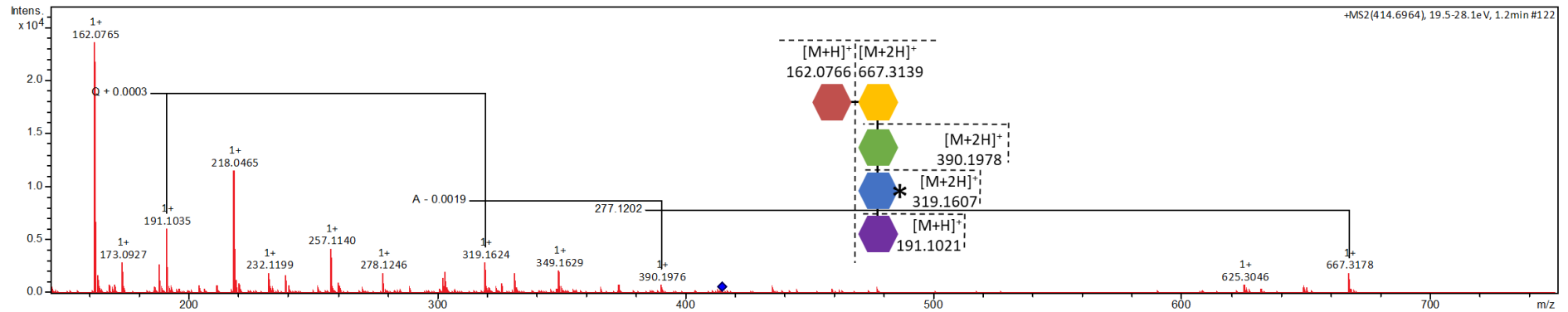


5.11. MS/MS profiles of muuropeptides from *N. punctiforme* amiC2::ck3 PGN

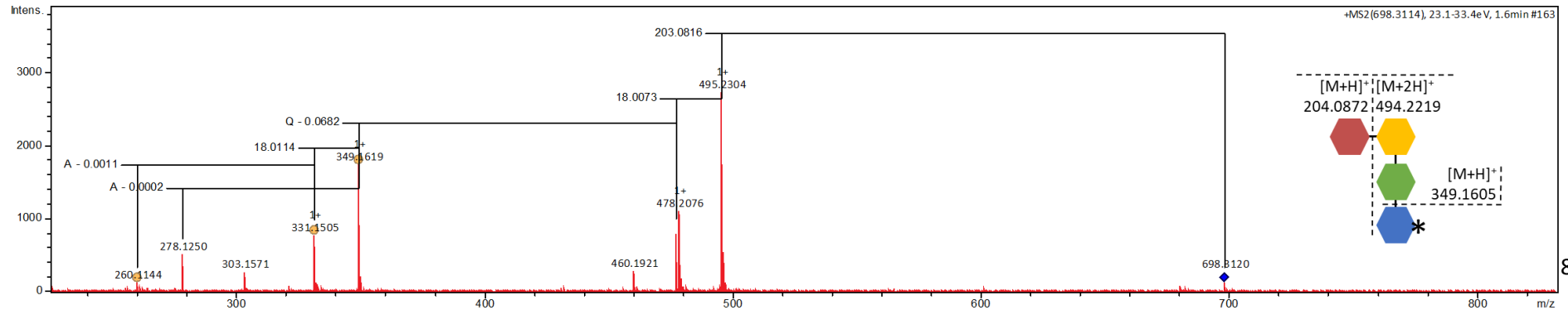
870.396 [M+H]⁺



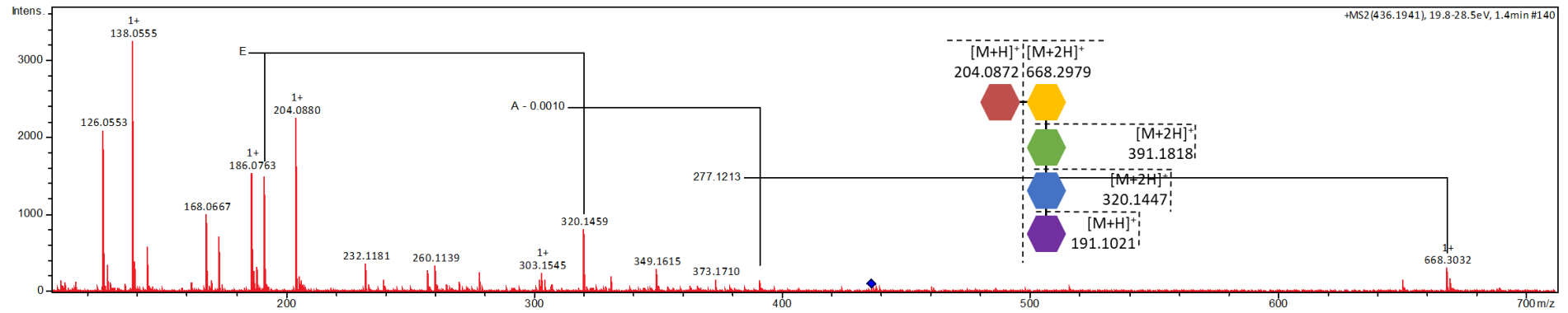
828.386 [M+H]⁺



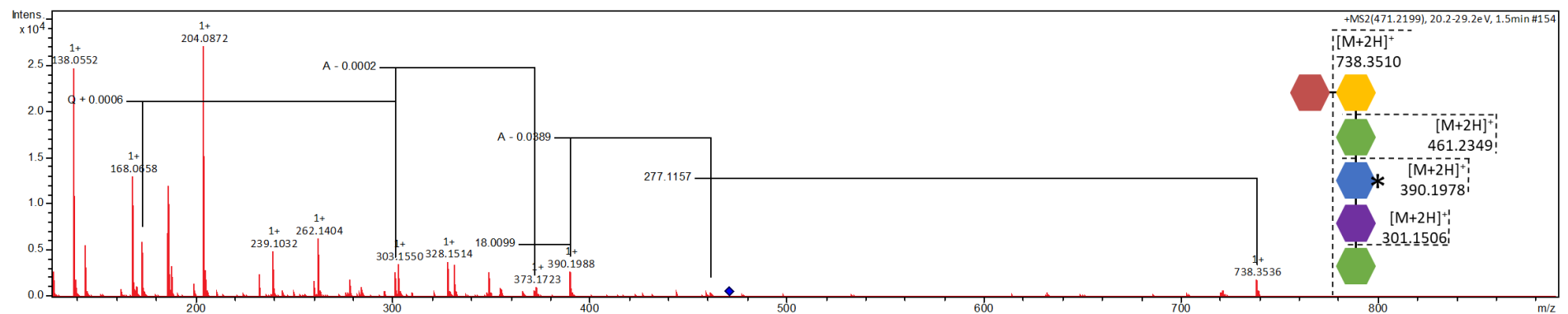
698.3108 [M+H]⁺



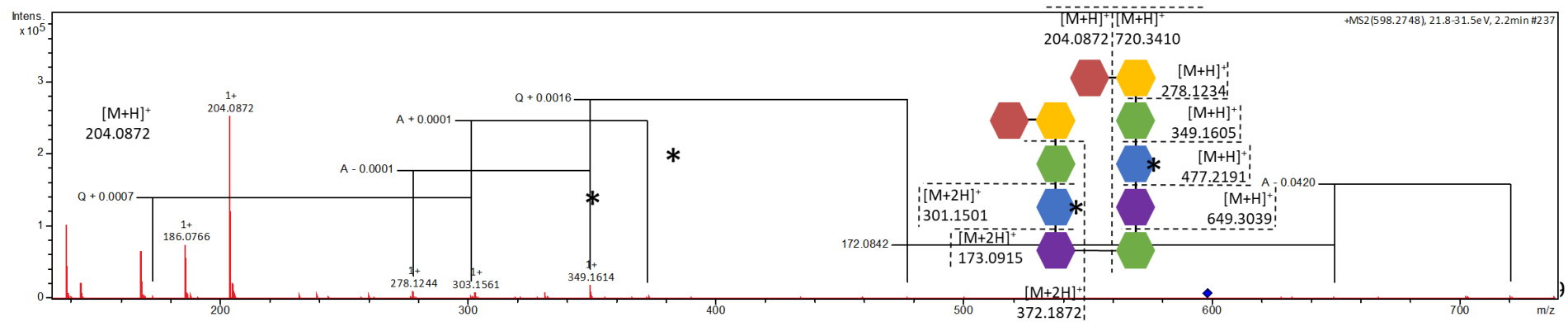
871.3812 [M+H]⁺



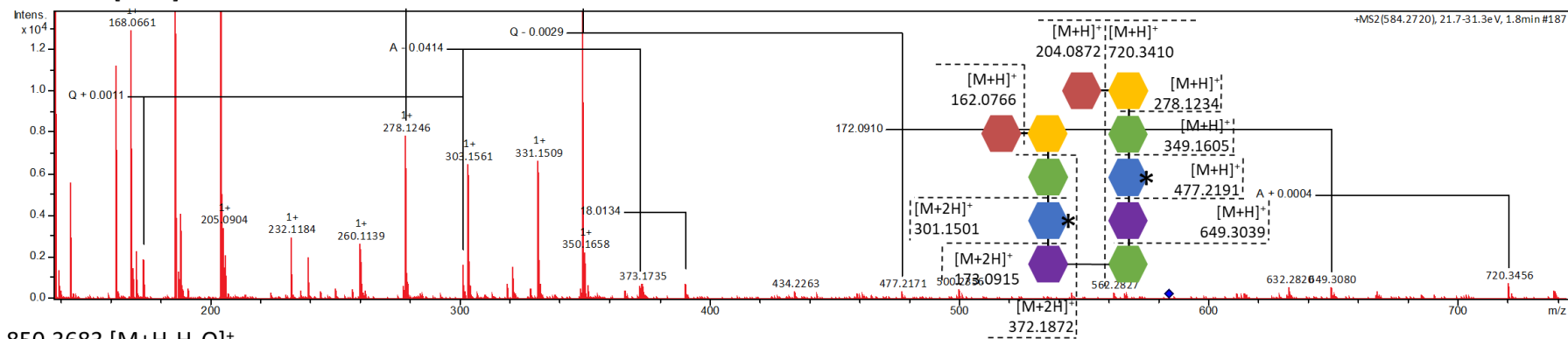
941.4332 [M+H]⁺



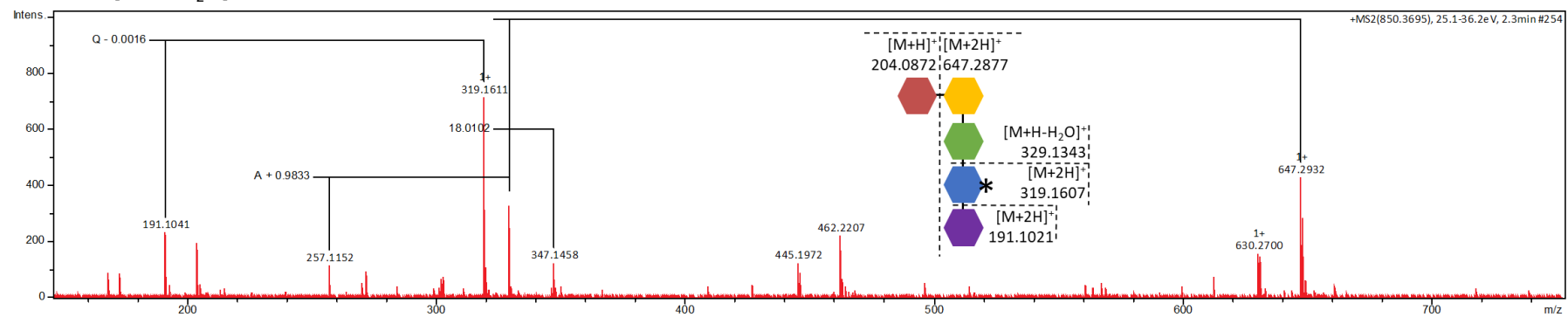
1792.811 [M+H]⁺



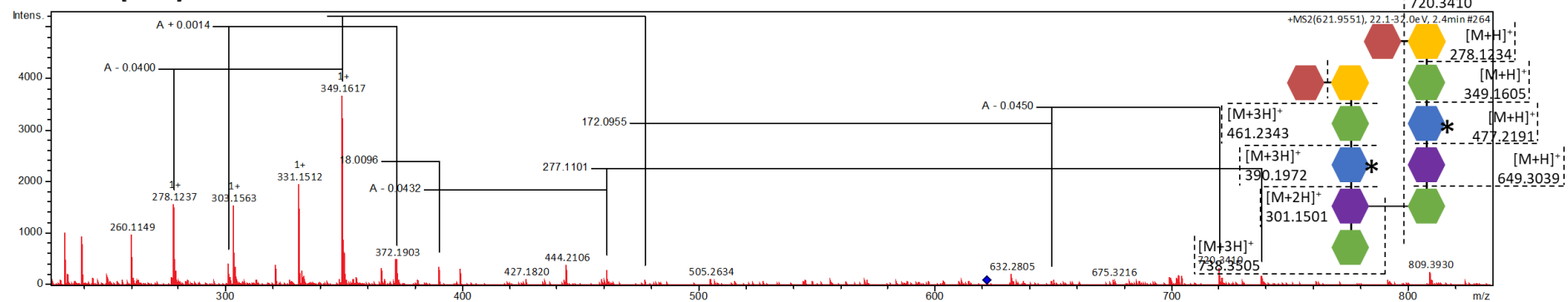
1750.802 [M+H]⁺



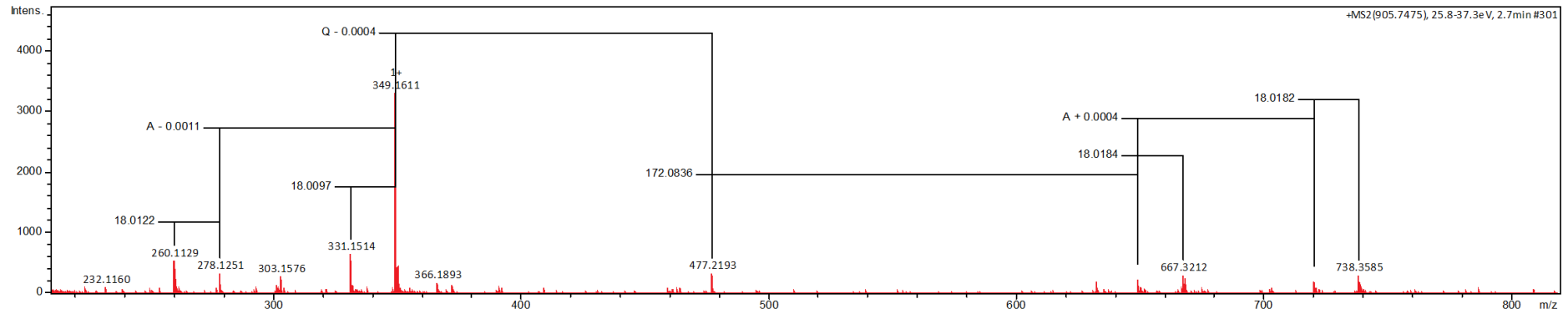
850.3683 [M+H-H₂O]⁺



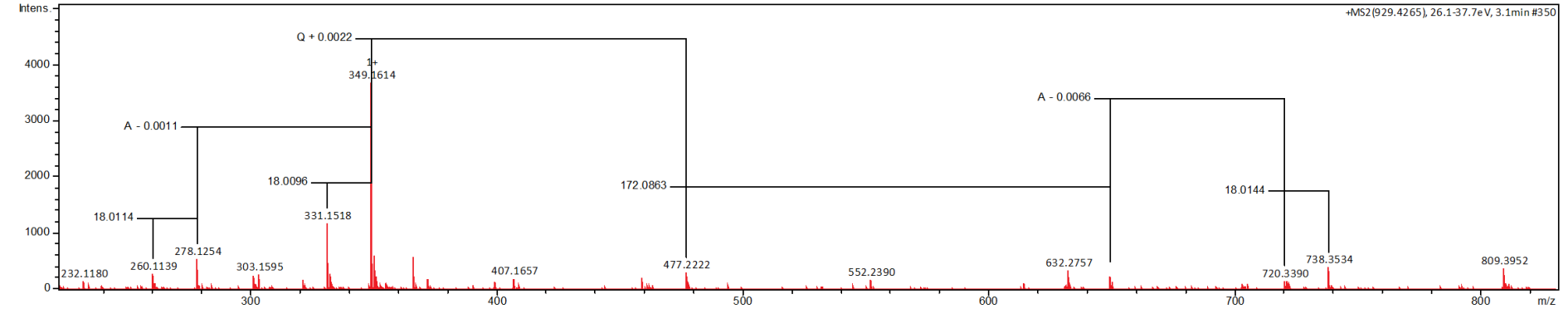
1863.8504 [M+H]⁺



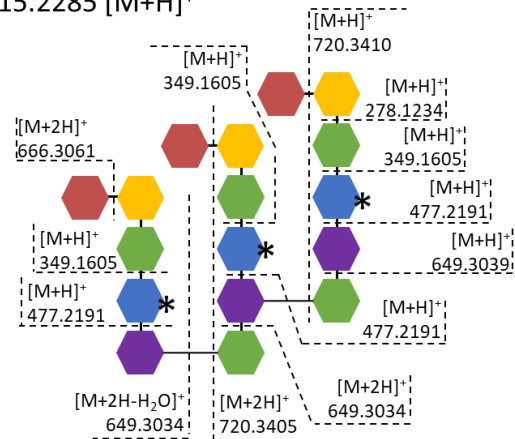
2715.2285 [M+H]⁺



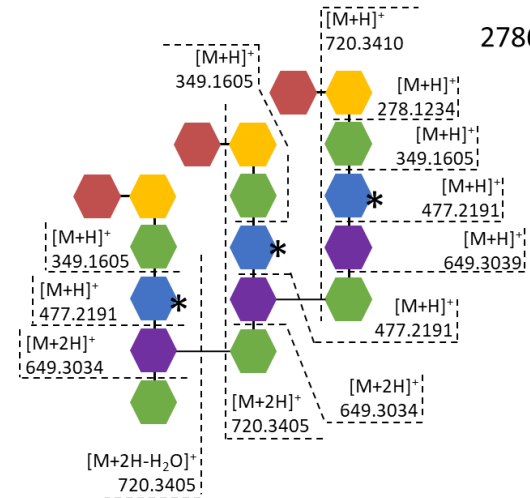
2786.2658 [M+H]⁺



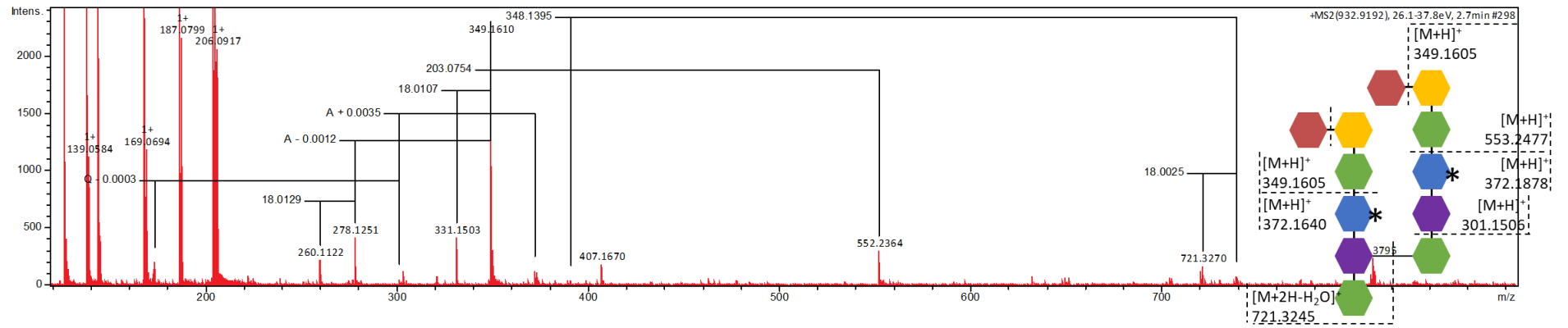
2715.2285 [M+H]⁺



2786.2658 [M+H]⁺



1864.8341 [M+H]⁺



5.12. Proteins identified in tryptic digests from *Nostoc* PGN

Table 55: Proteins in tryptic digests from *Nostoc* PGN. *Nostoc* PGN was digested by trypsin and soluble components were analyzed with a QExactive HF-X mass spectrometer. Tryptic peptides were assigned to proteins using the Uniprot databank for *Nostoc punctiforme* (strain ATCC 29133 / PCC 73102). List contains all identified proteins that were exclusively found in replicate 1.

Identified proteins in replicate 1				
	Identifier	Annotation	Sequence coverage [%]	Peptides
Ribosomal proteins	Npun_F3882	ribosomal protein S7	10.9	1
	Npun_F0963	ribosomal protein S21	12.9	1
	Npun_R2873	sigma 54 modulation protein/ribosomal protein S30EA	4.7	1
	Npun_R4937	ribosomal protein L20	8.5	1
RNA/DNA metabolism	Npun_F0080	NusB antitermination factor	7	1
	Npun_F2298	RNA methyltransferase	4.1	1
	Npun_R4571	DNA topoisomerase I	1.1	1
Glycan metabolism	Npun_F5214	glucosamine--fructose-6-phosphate aminotransferase, isomerizing	1.8	1
	Npun_F3917	GlpX family protein	3.5	1
	Npun_R1027	alpha amylase, catalytic region	1.6	1
	Npun_F4951	sucrose synthase	1.4	1
Amino acid/protein synthesis	Npun_F3884	protein synthesis factor, GTP-binding	7.6	3
	Npun_F5989	diaminopimelate decarboxylase	1.5	1
	Npun_R0899	aminotransferase, class I and II	3.9	1
	Npun_F5056	carboxyl-terminal protease	2.6	1
	Npun_F3458	aspartyl-tRNA synthetase	3.4	1
	Npun_R3312	lanthionine synthetase C family protein	0.8	1
	Npun_R6463	gamma-glutamyl phosphate reductase	1.8	1
Photosystem	Npun_F3863	photosystem I reaction centre, subunit IX / PsaI	24.5	1
	Npun_F5290	phycocyanin, alpha subunit PcyA	15.3	2
	Npun_F3864	photosystem I reaction centre, subunit XI PsaL	4.6	1

Identified proteins in replicate 1				
	Identifier	Annotation	Sequence coverage [%]	peptides
Photosystem	Npun_F4277	pyruvate kinase	2.9	1
	Npun_F5002	photosystem II protein PsbY	19.5	1
Transport	Npun_R1355	ATP-dependent metalloprotease FtsH	4.9	3
	Npun_R1585	60 kDa inner membrane insertion protein	1.8	1
	Npun_F5842	RND family efflux transporter MFP subunit	1.9	1
	Npun_F3826	inner-membrane translocator protein	3.5	1
	Npun_F1740	ATP-dependent metalloprotease FtsH	1.1	1
Signalling	Npun_F1883	putative GAF sensor protein	2.2	1
Periplasmatic proteins	Npun_F5536	periplasmic phosphate-binding protein of phosphate ABC transporter	4.5	1
	Npun_F4749	putative iron transport system substrate-binding protein	3.6	1
	Npun_F2285	extracellular solute-binding protein	1.5	1
	Npun_R5086	extracellular ligand-binding receptor	1.9	1
	Npun_F4615	urea ABC transporter, extracellular ligand-binding receptor UrtA	3.2	1
Chaperons	Npun_F0567	chaperone protein DnaK	4.6	2
	Npun_R3439	FkbH like protein	2.5	1
	Npun_R5915	Dyp-type peroxidase family protein	2.3	1
Energy metabolism	Npun_F5758	polyphosphate kinase	1.5	1
Protein degradation	Npun_R0382	UBA/THIF-type NAD/FAD binding protein	6.3	1
	Npun_R0987	peptidase S14, ClpP	5.4	1
Glycolysis	Npun_F5938	phosphoglycerate kinase	3	1
Defense	Npun_R0514	abortive infection protein	4	1
	Npun_F6498	alkyl hydroperoxide reductase/ Thiol specific antioxidant/ Mal allergen	4.2	1
Pyrimidine metabolism	Npun_F4226	uracil phosphoribosyltransferase	4.2	1
Carbohydrate metabolism	Npun_F1309	pyruvate phosphate dikinase, PEP/pyruvate-binding	1	1
Purine metabolism	Npun_F2438	phosphoribosylamine--glycine ligase	2.1	1

Identified proteins in replicate 1				
	Identifier	Annotation	Sequence coverage [%]	peptides
Protoheme biosynthesis	Npun_F2510	Ferrochelatase	2.6	1
Pyrophosphates	Npun_F4649	NUDIX hydrolase	3.8	1
Sulfur metabolism	Npun_F4803	glutathione synthetase	3.4	1
Glycogen metabolism	Npun_R6087	glucose-1-phosphate adenylyltransferase	2.8	1
Cofactor	Npun_R5587	Thioredoxin	9.3	1
PGN metabolism	Npun_R5246	peptidoglycan binding domain-containing protein	4.3	1
Cell division	Npun_R4804	cell division protein FtsZ	3	1
Transferases	Npun_R4093	glutathione S-transferase domain-containing protein	6.4	1
hypothetical proteins	Npun_F6211	hypothetical protein	3.2	1
	Npun_R2397	hypothetical protein	6.5	1
	Npun_F0870	hypothetical protein	9.1	1
	Npun_F1638	hypothetical protein	3.2	1
	Npun_F6444	hypothetical protein	5.3	1
	Npun_F4184	hypothetical protein	6.8	1
	Npun_F1013	hypothetical protein	7.6	1
	Npun_F6540	hypothetical protein	2.4	1
	Npun_R2760	hypothetical protein	7.2	2
	Npun_R6438	hypothetical protein	2.1	1
	Npun_R2867	hypothetical protein	6.6	1

Table 56: Proteins in tryptic digests from *Nostoc* PGN. *N. punctiforme* PGN was digested by trypsin and soluble components were subjected to QExactive HF-X mass spectrometer. Tryptic peptides were assigned to proteins using the Uniprot databank for *Nostoc punctiforme* (strain ATCC 29133 / PCC 73102). List contains all identified proteins that were exclusively found in replicate 2.

Identified proteins in replicate 2				
	Identifier	Annotation	Sequence coverage [%]	Peptides
Ribosomal proteins	Npun_F5851	ribosomal protein L11	7.2	1
	Npun_R4390	ribosomal protein L3	6.2	1
	Npun_F3881	ribosomal protein S12/S23	7.1	1
	Npun_R5570	ribosomal protein S2	8	2
	Npun_F5848	ribosomal protein L19	16.7	2
	Npun_R4373	ribosomal protein L15	22.4	2
RNA/DNA metabolism	Npun_F4987	DNA-directed RNA polymerase, beta subunit rpoC2	1.1	2
	Npun_R0751	phage integrase family protein	2.8	1
	Npun_F6355	helicase domain-containing protein	0.7	1
	Npun_F2857	signal recognition particle protein	1.4	1
	Npun_F6188	LysR family transcriptional regulator	2.7	1
Glycan metabolism	Npun_R0029	Transaldolase	5.1	2
	Npun_R4557	Transketolase	3.1	2
	Npun_F1876	sucrose synthase	2.1	1
	Npun_F1951	D-xylulose 5-phosphate/D-fructose 6-phosphate phosphoketolase	1.3	1
	Npun_R6073	alpha amylase, catalytic region	1.4	1
	Npun_R6280	nucleotidyl transferase	2.1	1
	Npun_R1548	glycoside hydrolase family protein	0.9	1
	Npun_F4024	transaldolase, Tal	2.1	1
	Npun_F5705	malto-oligosyltrehalose trehalohydrolase	1.1	1
Amino acid/protein synthesis	Npun_R5218	D-3-phosphoglycerate dehydrogenase	8.4	4
	Npun_F1315	3-phosphoshikimate 1-carboxyvinyltransferase	1.6	1

Identified proteins in replicate 2				
	Identifier	Annotation	Sequence coverage [%]	peptides
Amino acid/protein synthesis	Npun_R5147	anthranilate synthase component I	1.4	1
	Npun_R3615	aminotransferase, class I and II	1.7	1
	Npun_F0065	methionine synthase	0.9	1
	Npun_F6279	arginine decarboxylase	1.2	1
Photosystem	Npun_F3818	photosystem I core protein PsaA	2.4	2
	Npun_R3636	photosystem II 44 kDa subunit reaction center protein	5	2
	Npun_F3862	photosystem I reaction center protein PsaF, subunit III	7.9	2
	Npun_F5289	phycocyanin, beta subunit	8.1	2
	Npun_F5551	cytochrome b559, alpha subunit	8.5	1
	Npun_R5740	PRC-barrel domain-containing protein	2.4	1
	Npun_R4841	allophycocyanin, beta subunit ApcB	10.5	1
	Npun_R5148	photosystem I protein PsaD	6.4	1
Npun_R0210	photosystem I core protein PsaB	1.1	1	
Transport	Npun_R2022	ATP-dependent metalloprotease FtsH	3.1	2
	Npun_F0949	preprotein translocase, SecA subunit	1.1	1
	Npun_R0781	biopolymer transport protein ExbD/TolR	7.5	1
	Npun_F5285	acriflavin resistance protein	1.1	1
	Npun_R5324	inner-membrane translocator	3	1
	Npun_F4220	carbohydrate-selective porin OprB	1.8	1
	Npun_F3850	protein-export membrane protein SecD	3.6	1
Redox homeostasis	Npun_R4179	dihydrolipoamide dehydrogenase	1.5	1
	Npun_R1623	FAD-dependent pyridine nucleotide-disulphide oxidoreductase	2.5	1
	Npun_R3470	pyridine nucleotide-disulphide oxidoreductase dimerisation region	2.7	1
	Npun_F0920	pyridine nucleotide-disulphide oxidoreductase dimerisation region	1.8	1
	Npun_F6301	oxidoreductase domain-containing protein	2.5	1

Identified proteins in replicate 2				
	Identifier	Annotation	Sequence coverage [%]	peptides
Redox homeostasis	Npun_R3653	amine oxidase	1.6	1
Phycobilisome	Npun_R3807	phycobilisome protein CpeB	8.1	2
	Npun_F3811	phycobilisome linker polypeptide	3.1	1
Signalling	Npun_R4162	NmrA family protein	2.4	1
	Npun_R1448	response regulator receiver sensor signal transduction histidine kinase	2.4	1
	Npun_F0354	multi-sensor hybrid histidine kinase	0.6	1
	Npun_R3901	putative sensor protein	2.1	1
	Npun_R1108	putative serine/threonine kinase	1.1	1
Periplasmatic proteins	Npun_F0891	phosphate ABC transporter, periplasmic phosphate-binding protein	3.8	2
	Npun_F3299	phosphonate ABC transporter, periplasmic phosphonate-binding protein	2.6	1
	Npun_R2770	extracellular ligand-binding receptor	2.3	1
	Npun_R5326	periplasmic binding protein/LacI transcriptional regulator	2.6	1
Chaperons	Npun_R5998	chaperone protein DnaK	2.6	2
	Npun_F3575	ATPase	2.8	2
	Npun_F5907	chaperone protein DnaK	1.3	1
	Npun_F3510	ATPase	1.5	1
Energy metabolism	Npun_F4970	NADH-ubiquinone oxidoreductase, chain 49kDa	4.3	2
	Npun_F4860	H ⁺ -transporting two-sector ATPase, B/B subunit	5.6	1
	Npun_F5838	flavin reductase domain-containing protein	1.4	2
	Npun_F6553	NADH:ubiquinone oxidoreductase complex I intermediate-associated protein 30	3	1
Protein degradation	Npun_F4427	ATPase	2.6	2
	Npun_R6632	peptidase S1 and S6, chymotrypsin/Hap	2.3	1
	Npun_R3609	peptidase M16 domain-containing protein	2	1

Identified proteins in replicate 2				
	Identifier	Annotation	Sequence coverage [%]	peptides
Glycolysis	Npun_R4631	aldehyde dehydrogenase	2	1
CO ₂ fixation	Npun_F4201	ribulose biphosphate carboxylase, small chain	3.5	2
Defense	Npun_F6082	alkyl hydroperoxide reductase/ Thiol specific antioxidant/ Mal allergen	3.4	1
Lipid metabolism	Npun_F0459	lipopolysaccharide biosynthesis protein	2.3	2
	Npun_R5951	acetyl-CoA carboxylase, biotin carboxylase	2	1
Purine metabolism	Npun_F0612	adenylosuccinate synthetase	1.6	1
Repair mechanism	Npun_R3963	phage shock protein A, PspA		
Fatty acid metabolism	Npun_F2349	3-oxoacyl-(acyl-carrier-protein) reductase		
Glycogen metabolism	Npun_F3799	glycogen/starch synthase	3.1	1
Cofactor	Npun_R3506	3,4-dihydroxy-2-butanone 4-phosphate synthase	1.3	1
PGN metabolism	Npun_R5647	lytic transglycosylase, catalytic	1.2	1
Transferases	Npun_R5019	glycosyl transferase family protein	2.8	1
TCA-cycle	Npun_F1921	aconitate hydratase 2	1.4	1
Porphyrin biosynthesis	Npun_F3848	delta-aminolevulinic acid dehydratase	4	1
Unknown	Npun_F1205	aldehyde dehydrogenase	4.8	2
	Npun_F0409	band 7 protein	1.4	1
	Npun_R0033	radical SAM domain-containing protein	1.7	1
Hypothetical proteins	Npun_R3257	hypothetical protein	5.5	2
	Npun_F2787	hypothetical protein	1.4	1
	Npun_R3866	hypothetical protein	15.9	1
	Npun_F4335	hypothetical protein	3.3	1
	Npun_F0885	hypothetical protein	3.4	1
	Npun_F1415	hypothetical protein	3.2	1
	Npun_F5453	hypothetical protein	2.3	1
	Npun_R2396	hypothetical protein	3.7	1

Identified proteins in replicate 2				
	Identifier	Annotation	Sequence coverage	peptides
			[%]	
hypothetical protein	Npun_F0077	hypothetical protein	4.3	1
	Npun_F4818	hypothetical protein	7.1	1
	Npun_R3817	hypothetical protein	1.8	1
	Npun_R5166	hypothetical protein	2.5	1
	Npun_R1240	hypothetical protein	3.3	1
	Npun_R3177	hypothetical protein	6	1
	Npun_F4021	hypothetical protein	0.6	1
	Npun_F0468	hypothetical protein	4.6	1
	Npun_R5683	hypothetical protein	2.3	1

Table 57: Common proteins identified in replicate 1 and 2. *N. punctiforme* PGN was digested by trypsin and soluble components were subjected to QExactive HF-X mass spectrometer. Tryptic peptides were assigned to proteins using the Uniprot databank for *Nostoc punctiforme* (strain ATCC 29133 / PCC 73102). List contains all identified proteins that were exclusively found in replicate 2.

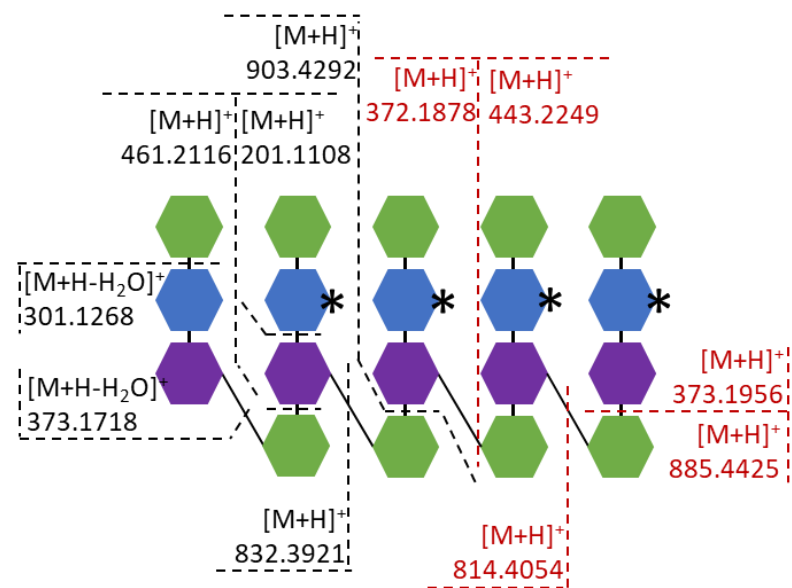
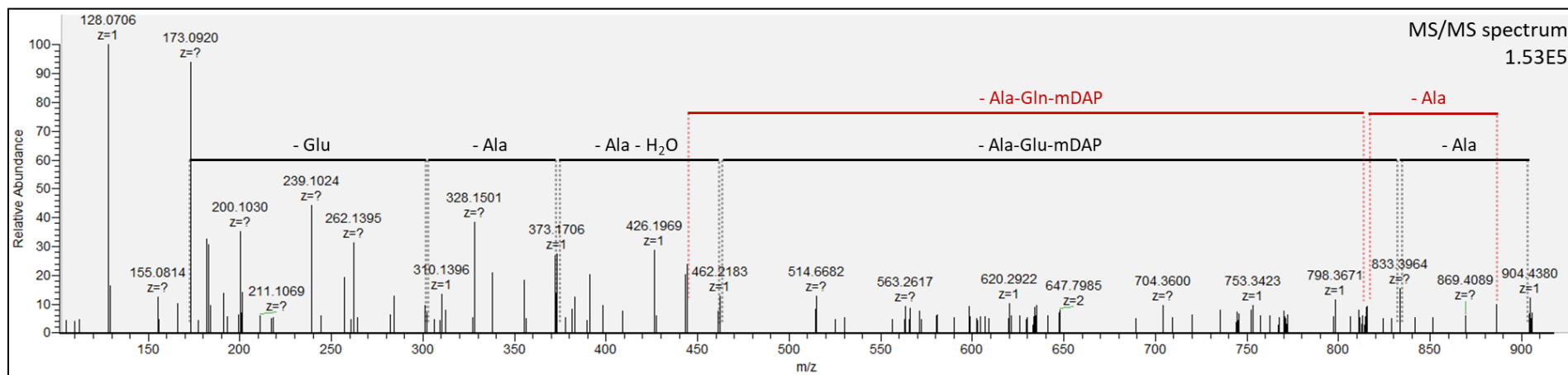
Identified proteins in both replicates								
	Identifier	Annotation	Sequence coverage		Peptides		Intensity	
			[%]		1	2	1	2
			1	2	1	2	1	2
Ribosomal proteins	Npun_R4387	ribosomal protein L2	8.4	8.4	2	2	3.6518E8	2.0959E7
	Npun_F2858	ribosomal protein S16	15.1	15.1	2	2	5.8923E7	1.5303E8
	Npun_R4367	ribosomal protein S11	9.9	19.8	1	2	4.8947E7	9.5671E7
	Npun_R4380	ribosomal protein L14	7.4	29.5	1	3	3.7789E7	2.7771E8
	Npun_R4378	ribosomal protein L5	5.5	5.5	1	1	3.694E7	8.9049E6
	Npun_R4362	ribosomal protein S9	10.1	15.2	1	2	3.2212E7	5.5888E7
	Npun_R4368	ribosomal protein S13	6.3	6.3	1	1	3.2115E7	6.0015E7

Identified proteins in both replicates								
	Identifier	Annotation	Sequence coverage [%]		peptides		Intensity	
			1	2	1	2	1	2
Ribosomal proteins	Npun_R4377	ribosomal protein S8	9	24.1	1	2	2.899E7	9.0398E7
	Npun_R1720	ribosomal protein S4	7.9	5	2	2	2.5366E7	2.3535E7
	Npun_R4361	ribosomal protein L31	8.8	8.8	1	1	1.5152E7	1.3855E7
	Npun_R4374	ribosomal protein S5	5.1	33.1	1	5	1.2874E7	1.2292E8
	Npun_F5852	ribosomal protein L1	3	6.3	1	1	3.7585E6	4.0907E6
	Npun_F3885	ribosomal protein S10	9.5	23.8	1	2	3.6671E6	1.4686E8
	Npun_R4384	ribosomal protein S3	3.8	15.4	1	4	1.5974E6	3.9404E8
	Npun_R4373	ribosomal protein L15	10.2	22.4	1	2	n.d	6.9237E7
	Npun_R4385	ribosomal protein L22	11.9	17.8	1	2	9.5954E5	2.3613E8
RNA/DNA metabolism	Npun_F2381, Npun_R5840	RNP-1 like RNA-binding protein, RNP-1 like RNA-binding protein	6.7	6.7	1	1	1.0884E8	3.4562E7
	Npun_F5010	histone family protein DNA-binding protein	22.3	25.5	3	2	4.945E7	4.914E7
	Npun_F5349	type III restriction enzyme, res subunit	1.2	1.2	1	1	3.7394E7	1.4506E7
	Npun_F4985	DNA-directed RNA polymerase, beta subunit RpoB	2.8	3.5	3	4	2.0332E7	7.0718E7
	Npun_R2469	RNA-binding S1 domain-containing protein	7.7	8.8	3	3	1.203E7	1.3715E8
	Npun_F4986	DNA-directed RNA polymerase, gamma subunit RpoC1	3.4	3.2	2	2	7.3057E6	6.7437E7
	Npun_F3515	ATPase domain-containing protein	2.4	1.1	2	1	7.1285E6	8.5315E6
	Npun_R2707	exodeoxyribonuclease III	3.1	3.1	1	1	5.2831E6	3.6761E8
RNA/DNA metabolism	Npun_R5944	transcriptional regulator AbrB	4.8	6.9	1	1	4.3336E6	3.5158E7
Amino acid/protein synthesis	Npun_R4982	histidinol dehydrogenase	3.9	1.8	2	1	3.622E7	8.0123E6
	Npun_F3883	protein synthesis factor, GTP-binding	2	2	1	1	6.6433E9	2.365E6
	Npun_F5451	PRC-barrel domain-containing protein	3.5	3.5	1	1	9.9912E6	4.3856E7
	Npun_R1308	glutamyl-tRNA(Gln) amidotransferase, A subunit	2.1	2.3	1	1	4.9415E6	1.3367E7
	Npun_F4034	seryl-tRNA synthetase	1.9	1.9	1	1	2.655E6	3.7968E6

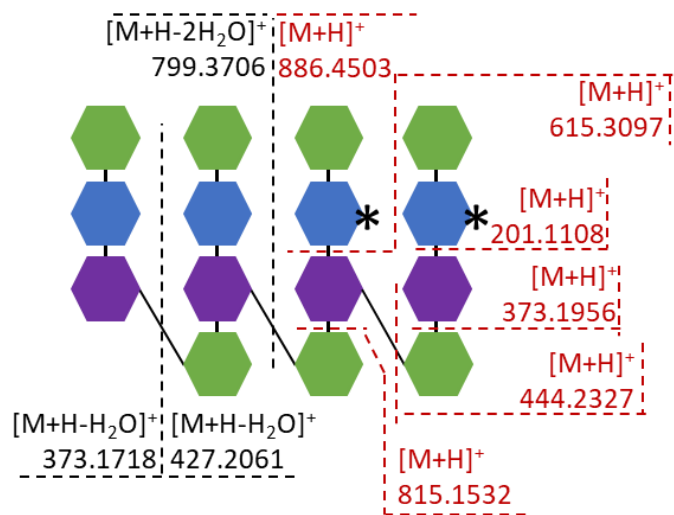
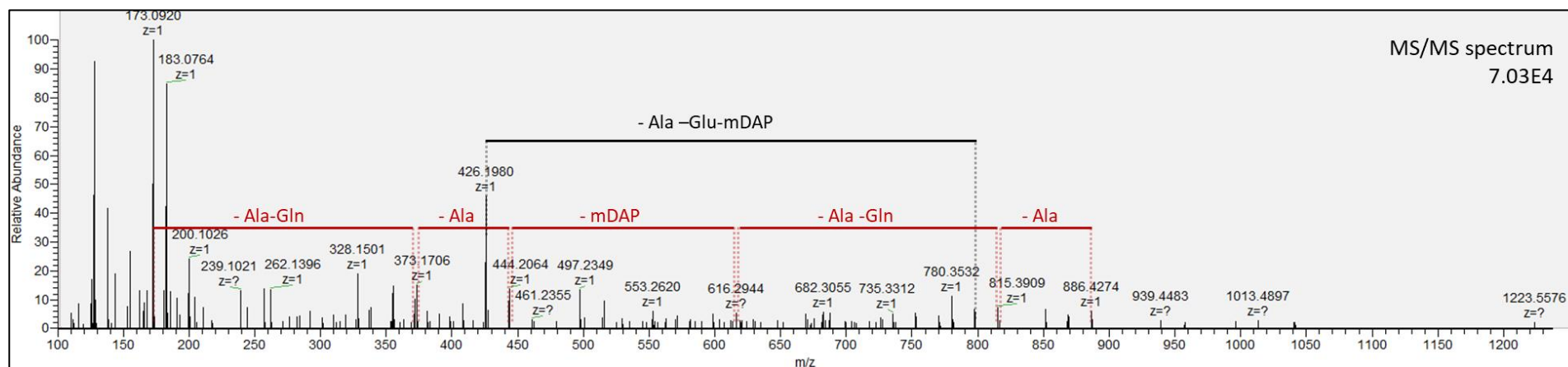
Identified proteins in both replicates								
	Identifier	Annotation	Sequence coverage [%]		peptides		Intensity	
			1	2	1	2	1	2
Photosystem	Npun_F3819	photosystem I core protein PsaB	1.6	2.7	1	2	1.693E8	2.365E8
	Npun_F5452	PRC-barrel domain-containing protein AvaK	10.4	5.4	4	3	9.0936E7	1.0169E8
	Npun_F3638	photosystem I assembly Ycf4	4.2	7.9	1	2	1.4481E7	3.4961E7
	Npun_R2471	photosystem antenna family protein	2	2	1	1	4.7355E6	1.4532E7
	Npun_R3637, Npun_F4553	photosystem II D2 protein (photosystem q(a) protein)	2.8	2.8	1	1	2.679E6	3.858E7
Transport	Npun_R4372	preprotein translocase, SecY subunit	1.6	1.8	1	2	2.2758E7	1.2461E7
	Npun_F4881	ATP-dependent metalloprotease FtsH	6	6	2	2	1.8839E7	4.9266E7
	Npun_F3787	transport-associated	4.6	5.2	1	1	2.5644E6	n.d.
Redox homeostasis	Npun_R6327	cytochrome P450	2.1	2.1	1	1	1.6567E7	n.d.
	Npun_F1887	aldo/keto reductase	2.9	2.4	1	1	3.1195E6	1.0986E9
Phycobilisome	Npun_R4842	phycobilisome protein ApcA	5.6	14.3	1	2	4.3641E8	5.2279E8
	Npun_R4843	phycobilisome linker polypeptide ApcE	4.3	2.8	6	4	1.7738E8	1.6327E8
	Npun_R4840	phycobilisome linker domain-containing protein ApcC	14.7	20.6	1	2	4.5806E7	2.1412E8
	Npun_F5292	phycobilisome linker polypeptide CpcC	12.5	5.5	4	2	1.691E7	3.921E8
	Npun_F5291	phycobilisome linker polypeptide CpcC2	2.6	7.4	1	2	1.0177E6	3.059E6
Signalling	Npun_F2686	GAF sensor hybrid histidine kinase	1.1	0.7	3	2	1.3559E7	3.7343E7
	Npun_F5788	two component transcriptional regulator	4.5	4.5	1	1	4.3493E6	1.9885E7
Chaperons	Npun_F1230	chaperonin GroEL	3.9	5.2	2	3	6.7279E6	1.6147E8
	Npun_R0829	chaperonin GroEL	2	3.7	2	2	5.9081E6	4.6027E7
Energy metabolism	Npun_F4863	ATP synthase F1, alpha subunit	3.8	6.1	2	3	5.504E7	2.0411E8
Glycolysis	Npun_R0031	glyceraldehyde-3-phosphate dehydrogenase, type I	4	2.9	1	1	2.7275E6	2.1453E6
	Npun_R0444	glyceraldehyde-3-phosphate dehydrogenase, type I	5.6	2.4	2	1	1.1496E7	6.1979E6
	Npun_F5584	fructose-bisphosphate aldolase, class II	2.2	2.2	1	1	3.0475E6	4.4088E7

Identified proteins in both replicates								
	Identifier	Annotation	Sequence coverage [%]		peptides		Intensity	
			1	2	1	2	1	1
CO ₂ fixation	Npun_F4195	ribulose biphosphate carboxylase, large chain RbcL	3.6	3.8	2	2	7.5332E7	2.004E7
	Npun_F4294	ribulose biphosphate carboxylase, small chain	1.2	4	1	1	5.2787E6	n.d.
Sulfur metabolism	Npun_F5448	sulfate adenylyltransferase	1.8	2	1	1	6.1255E6	8.0409E6
Vitamin metabolism	Npun_F6516	pyridoxal-5-phosphate-dependent enzyme, beta subunit	4.6	4.6	1	1	3.898E7	2.6343E8
TCA-cycle	Npun_R5474	isocitrate dehydrogenase, NADP-dependent	1.7	2.5	1	1	3.0462E6	1.1108E7
Unknown	Npun_R1898	alcohol dehydrogenase	3.9	3.9	1	1	4.6606E6	1.6945E8
	Npun_F6411	AMP-dependent synthetase and ligase	2	2	1	1	4.5112E6	3.6931E6
	Npun_R5987	ATPase	1	2.4	1	2	2.0649E6	8.9394E7
hypothetical proteins	Npun_R4646	hypothetical protein	17.3	17.3	1	1	2.1861E8	1.0296E7
	Npun_F3932	hypothetical protein	8.1	8.1	1	1	1.1669E8	6.7759E6
	Npun_R3785	hypothetical protein	2.8	0.8	2	1	5.9915E7	7.4238E6
	Npun_R1321	hypothetical protein	2	4.4	2	4	9.1459E6	9.269E7
	Npun_F0289	hypothetical protein	1.4	1.4	1	1	8.9234E6	5.9421E6
	Npun_R4472	hypothetical protein	2.3	4.1	1	2	7.8498E6	6.4514E7

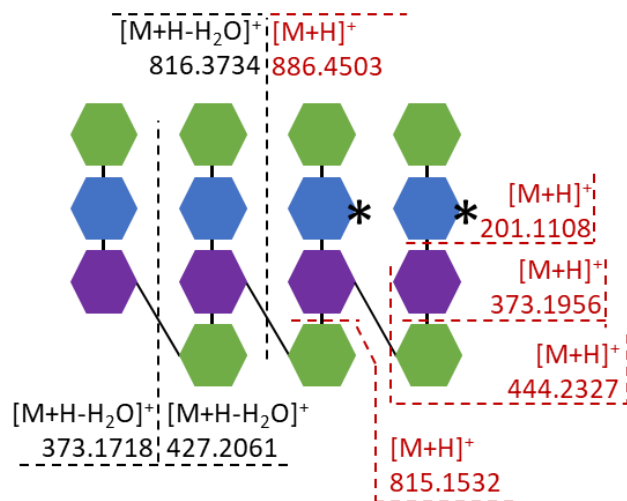
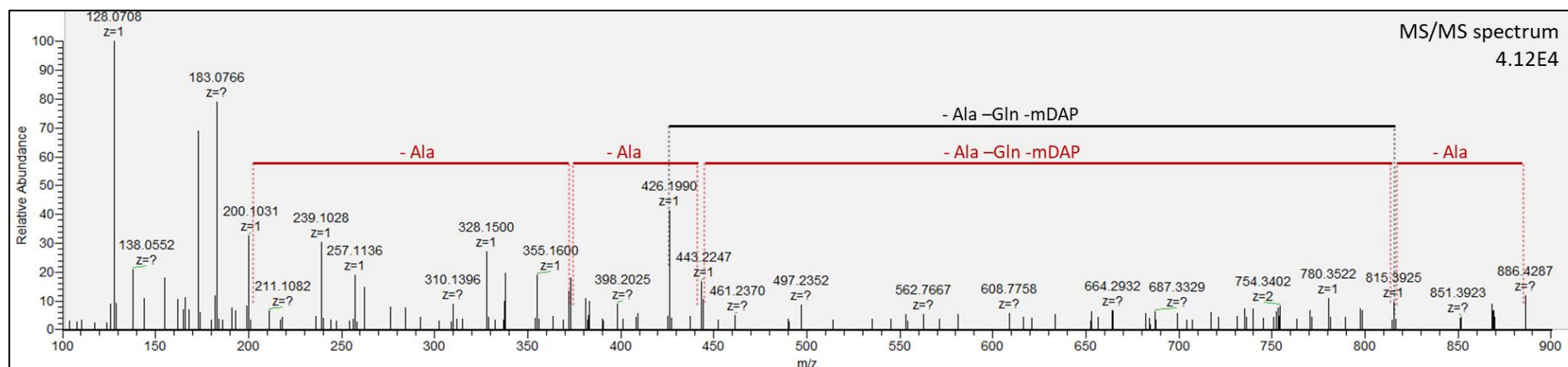
b) $m/z = 540.769, z = 4, 2160.056 [M+H]^+$



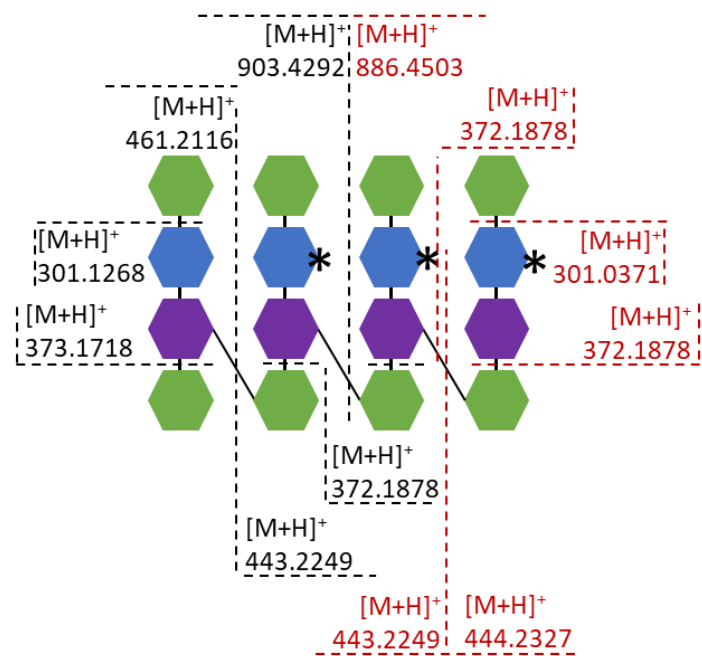
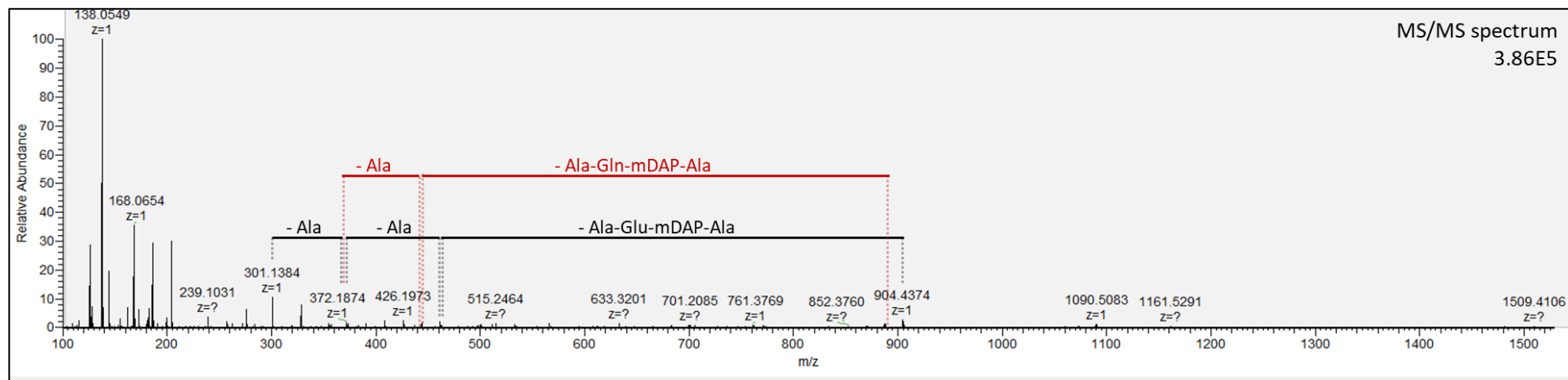
c) $m/z = 561.6046, z = 3, 1682.7998 [M+H-2H_2O]^+$



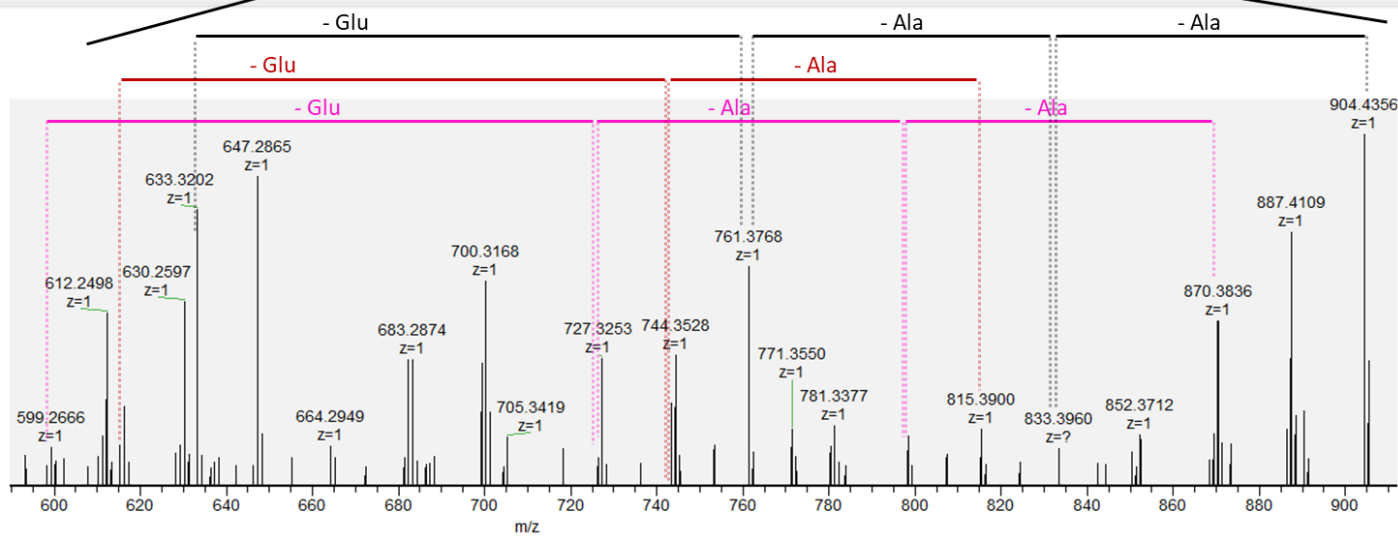
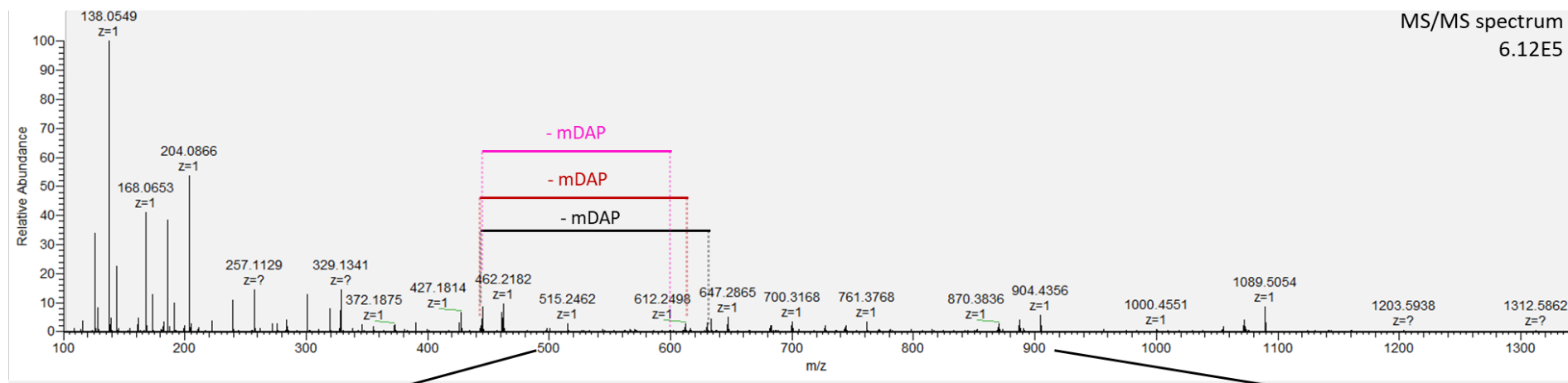
d) $m/z = 567.616, z = 3, 1700.833 [M+H-H_2O]^+$



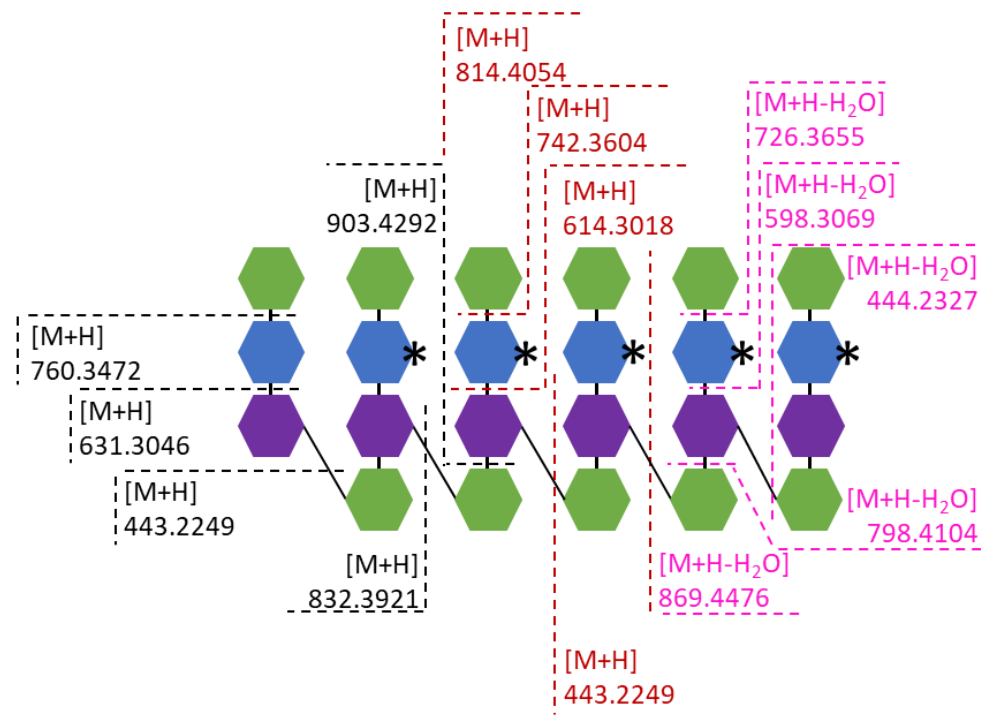
f) $m/z = 596.9052, z = 3, 1788.7016 [M+H]^+$



g) $m/z = 646.7959, z = 4, 2584.1626 [M+H-H_2O]^+$

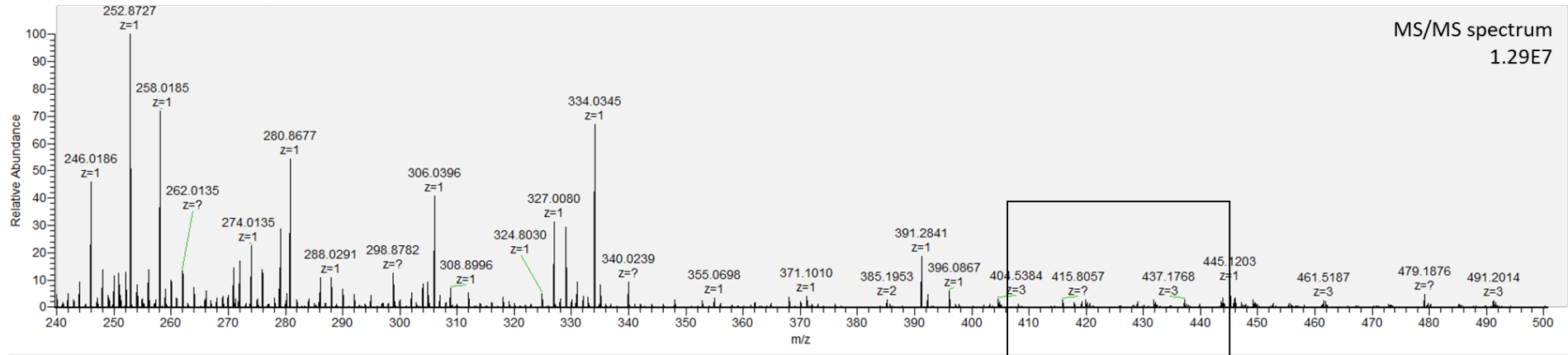


g) $m/z = 646.7959, z = 4, 2584.1626 [M+H-H_2O]^+$



5.13.2. MS1-spectra of wild-type and *amiC2* mutant PGN derived peptides in the range between 200 and 500 m/z

A. MS1 spectrum of wildtype PGN derived peptides



B. MS1 spectrum of *amiC2* mutant PGN derived peptides

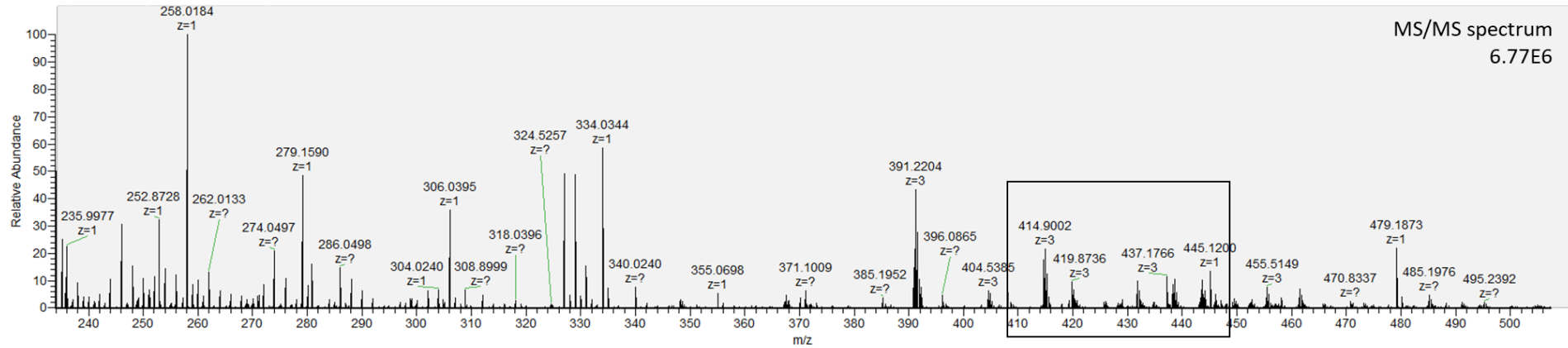


Fig. 55: MS1-spectra of wild-type and *amiC2* derived peptidoglycan peptides in the range of 200 and 500 m/z. Wild-type (A) and *amiC2* mutant (B) *Nostoc* PGN was incubated with 4 M Ami2cat and released peptides were enriched, purified and analysed by LC-MS. Box represents

5.13.3. Further m/z detected in wild-type and *amiC2* mutant PGN samples digested by AmiC2cat

Table 58: LC-MS analysis of AmiC2cat digests from *Nostoc* PGN. PGN from *amiC2* mutant or wild-type *N. punctiforme* were digested by AmiC2cat. Released peptides were analysed by LC-MS and a putative peptide structure was assigned to all peaks. MS/MS fragmentation confirmed partially the structural composition. A = amidation

Peak	m/z		z	measured [M+H] ⁺		calculated [M+H] ⁺	modification	MS/MS
	wt	<i>amiC2</i>		wt	<i>amiC2</i>			
*	511.247	511.246	3	1531.726	1531.717	?	A; fragment	✓
*	554.274	554.273	4	2214.076	2214.065	2231.0898?	4A, -H ₂ O; fragment	✓
*	579.273	579.574	3	1735.804	1736.702	?	A; fragment	✓
*	585.617	585.617	3	1754.836	1754.829	1718.8191?	2A, -2H ₂ O	-
*	591.289	591.287	3	1771.852	1771.841	1788.872?	3A, -H ₂ O?	-
*	621.299	620.794	3	1861.884	1860.361	1861.8774?	A; fragment	✓
*	651.327	-	4	2602.286		2602.270	5A	-
*	682.321	-	4	2726.265		3116.5091?	5A, -H ₂ O; fragment	-
*	709.673	709.343	3	2127.006	2126.007	2160.0522?	A, -2H ₂ O; fragment	✓
*	833.391	833.392	2	1665.776	1665.769	1718.8191?	2A, -3H ₂ O; fragment	✓
*	841.9035	841.903	2	1682.800	1682.792	1718.8191?	2A, -2H ₂ O; fragment	-
*	615.300	615.299	3	1843.886	1843.877	1861.854	-H ₂ O; fragment	✓

6. Literature

1. Muro-Pastor AM & Maldener I (2019) Cyanobacterial Heterocysts. *In eLS, John Wiley & Sons, Ltd.*
2. Wang M, Fang C, Ma B, Luo X, & Hou Z (2019) Regulation of cytokinesis: FtsZ and its accessory proteins. *Current Genetics*.
3. Taguchi A, Kahne D, & Walker S (2019) Chemical tools to characterize peptidoglycan synthases. *Current Opinion in Chemical Biology* 53:44-50.
4. Dion MF, *et al.* (2019) *Bacillus subtilis* cell diameter is determined by the opposing actions of two distinct cell wall synthetic systems. *Nature Microbiology* 4(8):1294-1305.
5. Silhavy TJ, Kahne D, & Walker S (2010) The bacterial cell envelope. (Translated from eng) *Cold Spring Harb Perspect Biol* 2(5):a000414-a000414 (in eng).
6. Des Marais DJ (2000) When Did Photosynthesis Emerge on Earth? *Science* 289(5485):1703.
7. Demoulin CF, *et al.* (2019) Cyanobacteria evolution: Insight from the fossil record. *Free Radical Biology and Medicine*.
8. Holland HD (2006) The oxygenation of the atmosphere and oceans. *Philos Trans R Soc Lond B Biol Sci* 361(1470):903-915.
9. Holland HD (2002) Volcanic gases, black smokers, and the great oxidation event. *Geochimica et Cosmochimica Acta* 66(21):3811-3826.
10. Lyons TW, Reinhard CT, & Planavsky NJ (2014) The rise of oxygen in Earth's early ocean and atmosphere. *Nature* 506(7488):307-315.
11. Dismukes GC, *et al.* (2001) The origin of atmospheric oxygen on Earth: The innovation of oxygenic photosynthesis. *Proceedings of the National Academy of Sciences* 98(5):2170.
12. Hamilton TL, Bryant DA, & Macalady JL (2016) The role of biology in planetary evolution: cyanobacterial primary production in low-oxygen Proterozoic oceans. *Environmental Microbiology* 18(2):325-340.
13. Schirmer BE, Gugger M, & Donoghue PC (2015) Cyanobacteria and the Great Oxidation Event: evidence from genes and fossils. *Palaeontology* 58(5):769-785.
14. Demoulin CF, *et al.* (2019) Cyanobacteria evolution: Insight from the fossil record. *Free Radic Biol Med*.
15. Rasmussen B, Fletcher IR, Brocks JJ, & Kilburn MR (2008) Reassessing the first appearance of eukaryotes and cyanobacteria. *Nature* 455:1101.
16. Hofmann HJ (1976) Precambrian Microflora, Belcher Islands, Canada: Significance and Systematics. *Journal of Paleontology* 50(6):1040-1073.
17. Golubic S & Abed RMM (2010) Entophysalis Mats as Environmental Regulators. *Microbial Mats: Modern and Ancient Microorganisms in Stratified Systems*, eds Seckbach J & Oren A (Springer Netherlands, Dordrecht), pp 237-251.
18. Green JW, Knoll AH, Golubic S, & Swett K (1987) Paleobiology of distinctive benthic microfossils from the upper proterozoic limestone-dolomite "series," Central East Greenland. *American Journal of Botany* 74(6):928-940.
19. Barghoorn ES & Tyler SA (1965) Microorganisms from the Gunflint Chert: These structurally preserved Precambrian fossils from Ontario are the most

- ancient organisms known. (Translated from eng) *Science* 147(3658):563-575 (in eng).
20. Lepot K, *et al.* (2017) Iron minerals within specific microfossil morphospecies of the 1.88 Ga Gunflint Formation. (Translated from eng) *Nature communications* 8:14890-14890 (in eng).
 21. Tomitani A, Knoll AH, Cavanaugh CM, & Ohno T (2006) The evolutionary diversification of cyanobacteria: molecular-phylogenetic and paleontological perspectives. (Translated from eng) *Proceedings of the National Academy of Sciences of the United States of America* 103(14):5442-5447 (in eng).
 22. Golubic S, Sergeev VN, & Knoll AH (1995) Mesoproterozoic Archaeoellipsoides: akinetes of heterocystous cyanobacteria. (Translated from eng) *Lethaia* 28:285-298 (in eng).
 23. Pang K, *et al.* (2018) Nitrogen-Fixing Heterocystous Cyanobacteria in the Tonian Period. *Current Biology* 28(4):616-622.e611.
 24. Edelman M, Swinton D, Schiff JA, Epstein HT, & Zeldin B (1967) Deoxyribonucleic Acid of the blue-green algae (cyanophyta). (Translated from eng) *Bacteriol Rev* 31(4):315-331 (in eng).
 25. Palinska KA & Surosz W (2014) Taxonomy of cyanobacteria: a contribution to consensus approach. *Hydrobiologia* 740(1):1-11.
 26. Rippka R, Deruelles J, Waterbury JB, Herdman M, & Stanier RY (1979) Generic Assignments, Strain Histories and Properties of Pure Cultures of Cyanobacteria. *Microbiology* 111(1):1-61.
 27. Schirrmester BE, Antonelli A, & Bagheri HC (2011) The origin of multicellularity in cyanobacteria. (Translated from eng) *BMC evolutionary biology* 11:45-45 (in eng).
 28. Rossetti V, Schirrmester BE, Bernasconi MV, & Bagheri HC (2010) The evolutionary path to terminal differentiation and division of labor in cyanobacteria. *Journal of Theoretical Biology* 262(1):23-34.
 29. Meeks JC & Elhai J (2002) Regulation of cellular differentiation in filamentous cyanobacteria in free-living and plant-associated symbiotic growth states. (Translated from eng) *Microbiology and molecular biology reviews : MMBR* 66(1):94-121 (in eng).
 30. Kumar K, Mella-Herrera RA, & Golden JW (2010) Cyanobacterial heterocysts. (Translated from eng) *Cold Spring Harb Perspect Biol* 2(4):a000315-a000315 (in eng).
 31. Berman-Frank I, Lundgren P, & Falkowski P (2003) Nitrogen fixation and photosynthetic oxygen evolution in cyanobacteria. (Translated from eng) *Res Microbiol* 154(3):157-164 (in eng).
 32. Fay P (1992) Oxygen relations of nitrogen fixation in cyanobacteria. (Translated from eng) *Microbiol Rev* 56(2):340-373 (in eng).
 33. Nicolaisen K, Hahn A, & Schleiff E (2009) The cell wall in heterocyst formation by *Anabaena* sp. PCC 7120. *Journal of Basic Microbiology* 49(1):5-24.
 34. Gambacorta A, Pagnotta E, Romano I, Sodano G, & Trincone A (1998) Heterocyst glycolipids from nitrogen-fixing cyanobacteria other than nostocaceae. *Phytochemistry* 48(5):801-805.
 35. Bauersachs T, *et al.* (2009) Distribution of heterocyst glycolipids in cyanobacteria. *Phytochemistry* 70(17):2034-2039.
 36. Cardemil L & Wolk CP (1979) The polysaccharides from heterocyst and spore envelopes of a blue-green alga. Structure of the basic repeating unit. (Translated from eng) *J Biol Chem* 254(3):736-741 (in eng).

37. Fay P (1969) Cell differentiation and pigment composition in *Anabaena cylindrica*. *Archiv für Mikrobiologie* 67(1):62-70.
38. Tel-Or E, Stewart WDP, & Fogg GE (1977) Photosynthetic components and activities of nitrogen-fixing isolated heterocysts of *Anabaena cylindrica*. *Proceedings of the Royal Society of London. Series B. Biological Sciences* 198(1130):61-86.
39. Burnat M, Herrero A, & Flores E (2014) Compartmentalized cyanophycin metabolism in the diazotrophic filaments of a heterocyst-forming cyanobacterium. (Translated from eng) *Proceedings of the National Academy of Sciences of the United States of America* 111(10):3823-3828 (in eng).
40. Adams DG & Carr NG (1981) The developmental biology of heterocyst and akinete formation in cyanobacteria. (Translated from eng) *Crit Rev Microbiol* 9(1):45-100 (in eng).
41. Adams DG & Duggan PS (1999) Tansley Review No. 107. Heterocyst and akinete differentiation in cyanobacteria. *New Phytologist* 144(1):3-33.
42. Perez R, Forchhammer K, Salerno G, & Maldener I (2016) Clear differences in metabolic and morphological adaptations of akinetes of two Nostocales living in different habitats. *Microbiology* 162(2):214-223.
43. Kaplan-Levy RN, Hadas O, Summers ML, Rücker J, & Sukenik A (2010) Akinetes: Dormant Cells of Cyanobacteria. *Dormancy and Resistance in Harsh Environments*, eds Lubzens E, Cerda J, & Clark M (Springer Berlin Heidelberg, Berlin, Heidelberg), pp 5-27.
44. Cardemil L & Wolk CP (1981) POLYSACCHARIDES FROM THE ENVELOPES OF HETEROCYSTS AND SPORES OF THE BLUE-GREEN ALGAE *ANABAENA VARIABILIS* AND *CYLINDROSPERMUM LICHENIFORME*1. *Journal of Phycology* 17(3):234-240.
45. Braune W (1980) Structural aspects of akinete germination in the cyanobacterium *Anabaena variabilis*. *Archives of Microbiology* 126(3):257-261.
46. Perez R, Wormer L, Sass P, & Maldener I (2018) A highly asynchronous developmental program triggered during germination of dormant akinetes of filamentous diazotrophic cyanobacteria. (Translated from eng) *FEMS Microbiol Ecol* 94(1) (in eng).
47. Skill SC & Smith RJ (1987) Synchronous Akinete Germination and Heterocyst Differentiation in *Anabaena* PCC 7937 and *Nostoc* PCC 6720. *Microbiology* 133(2):299-303.
48. Sili C, Ena A, Materassi R, & Vincenzini M (1994) Germination of desiccated aged akinetes of alkaliphilic cyanobacteria. *Archives of Microbiology* 162(1):20-25.
49. Moore D, McGregor GB, & Shaw G (2004) MORPHOLOGICAL CHANGES DURING AKINETE GERMINATION IN *CYLINDROSPERMOPSIS RACIBORSKII* (NOSTOCALES, CYANOBACTERIA)1. *Journal of Phycology* 40(6):1098-1105.
50. Meeks JC, Campbell EL, Summers ML, & Wong FC (2002) Cellular differentiation in the cyanobacterium *Nostoc punctiforme*. (Translated from eng) *Arch Microbiol* 178(6):395-403 (in eng).
51. Herdman M & Rippka R (1988) [22] Cellular differentiation: Hormogonia and baeocytes. *Methods in Enzymology*, (Academic Press), Vol 167, pp 232-242.
52. Damerval T, et al. (1991) Hormogonium Differentiation in the Cyanobacterium *Calothrix*: A Photoregulated Developmental Process. *The Plant Cell* 3(2):191-201.

53. Campbell EL & Meeks JC (1989) Characteristics of Hormogonia Formation by Symbiotic Nostoc spp. in Response to the Presence of Anthoceros punctatus or Its Extracellular Products. (Translated from eng) *Appl Environ Microbiol* 55(1):125-131 (in eng).
54. Cirés S & Ballot A (2016) A review of the phylogeny, ecology and toxin production of bloom-forming Aphanizomenon spp. and related species within the Nostocales (cyanobacteria). *Harmful Algae* 54:21-43.
55. Cirés S, Wörmer L, Wiedner C, & Quesada A (2013) Temperature-Dependent Dispersal Strategies of Aphanizomenon ovalisporum (Nostocales, Cyanobacteria): Implications for the Annual Life Cycle. *Microbial Ecology* 65(1):12-21.
56. Tashyreva D & Elster J (2016) Annual Cycles of Two Cyanobacterial Mat Communities in Hydro-Terrestrial Habitats of the High Arctic. (Translated from eng) *Microb Ecol* 71(4):887-900 (in eng).
57. Hershkovitz N, Oren A, & Cohen Y (1991) Accumulation of trehalose and sucrose in cyanobacteria exposed to matric water stress. (Translated from eng) *Appl Environ Microbiol* 57(3):645-648 (in eng).
58. Davey MC (1989) The Effects of Freezing and Desiccation on Photosynthesis and Survival of Terrestrial Antarctic Algae and Cyanobacteria. (Translated from English) *Polar Biology* 10(1):29-36 (in English).
59. Shang J-L, *et al.* (2019) Genomic and transcriptomic insights into the survival of the subaerial cyanobacterium Nostoc flagelliforme in arid and exposed habitats. *Environmental Microbiology* 21(2):845-863.
60. Richaud C, Zabulon G, Joder A, & Thomas J-C (2001) Nitrogen or Sulfur Starvation Differentially Affects Phycobilisome Degradation and Expression of the *nblA* Gene in *Synechocystis* Strain PCC 6803. *Journal of Bacteriology* 183(10):2989.
61. Baier A, Winkler W, Korte T, Lockau W, & Karradt A (2014) Degradation of Phycobilisomes in *Synechocystis* sp. PCC6803: EVIDENCE FOR ESSENTIAL FORMATION OF AN NblA1/NblA2 HETERODIMER AND ITS CODEGRADATION BY A Clp PROTEASE COMPLEX. *Journal of Biological Chemistry* 289(17):11755-11766.
62. Schlebusch M & Forchhammer K (2010) Requirement of the Nitrogen Starvation-Induced Protein Sll0783 for Polyhydroxybutyrate Accumulation in *Synechocystis* sp. Strain PCC 6803. *Appl Environ Microbiol* 76(18):6101.
63. Klotz A, *et al.* (2016) Awakening of a Dormant Cyanobacterium from Nitrogen Chlorosis Reveals a Genetically Determined Program. *Current Biology* 26(21):2862-2872.
64. Spät P, Klotz A, Rexroth S, Maček B, & Forchhammer K (2018) Chlorosis as a Developmental Program in Cyanobacteria: The Proteomic Fundament for Survival and Awakening. *Molecular & Cellular Proteomics* 17(9):1650.
65. Forchhammer K & Schwarz R (2019) Nitrogen chlorosis in unicellular cyanobacteria - a developmental program for surviving nitrogen deprivation. (Translated from eng) *Environ Microbiol* 21(4):1173-1184 (in eng).
66. Gram C (1884) Ueber die isolirte Färbung der Schizomyceten in Schnitt- und Trockenpräparaten. *Fortschritte der Medicin* 2:185-189.
67. Weise G, Drews G, Jann B, & Jann K (1970) Identification and analysis of a lipopolysaccharide in cell walls of the blue-green alga *Anacystis nidulans*. (Translated from eng) *Arch Mikrobiol* 71(1):89-98 (in eng).

68. Mikheyskaya LV, Ovodova RG, & Ovodov YS (1977) Isolation and characterization of lipopolysaccharides from cell walls of blue-green algae of the genus *Phormidium*. (Translated from eng) *Journal of Bacteriology* 130(1):1-3 (in eng).
69. Hoiczuk E & Hansel A (2000) Cyanobacterial cell walls: news from an unusual prokaryotic envelope. (Translated from eng) *J Bacteriol* 182(5):1191-1199 (in eng).
70. Work E (1957) Biochemistry of the Bacterial Cell Wall. *Nature* 179(4565):841-847.
71. Weidel W & Pelzer H (Bagshaped Macromolecules—A New Outlook on Bacterial Cell Walls.
72. Vollmer W, Blanot D, & de Pedro MA (2008) Peptidoglycan structure and architecture. (Translated from eng) *FEMS Microbiol Rev* 32(2):149-167 (in eng).
73. Holtje JV & Glauner B (1990) Structure and metabolism of the murein sacculus. (Translated from eng) *Res Microbiol* 141(1):75-89 (in eng).
74. de Pedro MA & Cava F (2015) Structural constraints and dynamics of bacterial cell wall architecture. (Translated from eng) *Front Microbiol* 6:449 (in eng).
75. Pazos M & Peters K (2019) Peptidoglycan. *Bacterial Cell Walls and Membranes*, ed Kuhn A (Springer International Publishing, Cham), pp 127-168.
76. Schleifer KH & Kandler O (1972) Peptidoglycan types of bacterial cell walls and their taxonomic implications. (Translated from eng) *Bacteriol Rev* 36(4):407-477 (in eng).
77. Mahapatra S, Crick DC, McNeil MR, & Brennan PJ (2008) Unique structural features of the peptidoglycan of *Mycobacterium leprae*. (Translated from eng) *J Bacteriol* 190(2):655-661 (in eng).
78. Guinand M, Ghuyssen JM, Schleifer KH, & Kandler O (1969) The peptidoglycan in walls of *Butyribacterium rettgeri*. (Translated from eng) *Biochemistry* 8(1):200-207 (in eng).
79. Gustafson J, Strässle A, Hächler H, Kayser FH, & Berger-Bächi B (1994) The femC locus of *Staphylococcus aureus* required for methicillin resistance includes the glutamine synthetase operon. *Journal of Bacteriology* 176(5):1460.
80. Bui NK, *et al.* (2012) Isolation and analysis of cell wall components from *Streptococcus pneumoniae*. *Analytical Biochemistry* 421(2):657-666.
81. Barreteau H, *et al.* (2008) Cytoplasmic steps of peptidoglycan biosynthesis. (Translated from eng) *FEMS Microbiol Rev* 32(2):168-207 (in eng).
82. Teo ACK & Roper DI (2015) Core Steps of Membrane-Bound Peptidoglycan Biosynthesis: Recent Advances, Insight and Opportunities. (Translated from eng) *Antibiotics (Basel)* 4(4):495-520 (in eng).
83. Mainardi J-L, Villet R, Bugg TD, Mayer C, & Arthur M (2008) Evolution of peptidoglycan biosynthesis under the selective pressure of antibiotics in Gram-positive bacteria. *FEMS Microbiology Reviews* 32(2):386-408.
84. Schneider T, *et al.* (2004) In vitro assembly of a complete, pentaglycine interpeptide bridge containing cell wall precursor (lipid II-Gly5) of *Staphylococcus aureus*. *Molecular microbiology* 53(2):675-685.
85. Bellais S, *et al.* (2006) Aslfm, the D-aspartate ligase responsible for the addition of D-aspartic acid onto the peptidoglycan precursor of *Enterococcus faecium*. (Translated from eng) *J Biol Chem* 281(17):11586-11594 (in eng).

86. Sham L-T, *et al.* (2014) MurJ is the flippase of lipid-linked precursors for peptidoglycan biogenesis. *Science* 345(6193):220.
87. Vollmer W & Bertsche U (2008) Murein (peptidoglycan) structure, architecture and biosynthesis in *Escherichia coli*. *Biochimica et Biophysica Acta (BBA) - Biomembranes* 1778(9):1714-1734.
88. Tipper DJ & Strominger JL (1965) Mechanism of action of penicillins: a proposal based on their structural similarity to acyl-D-alanyl-D-alanine. (Translated from eng) *Proceedings of the National Academy of Sciences of the United States of America* 54(4):1133-1141 (in eng).
89. Egan AJF, Biboy J, van't Veer I, Breukink E, & Vollmer W (2015) Activities and regulation of peptidoglycan synthases. (Translated from eng) *Philosophical transactions of the Royal Society of London. Series B, Biological sciences* 370(1679):20150031 (in eng).
90. Zapun A, Contreras-Martel C, & Vernet T (2008) Penicillin-binding proteins and β -lactam resistance. *FEMS Microbiology Reviews* 32(2):361-385.
91. Sauvage E, Kerff F, Terrak M, Ayala JA, & Charlier P (2008) The penicillin-binding proteins: structure and role in peptidoglycan biosynthesis. *FEMS Microbiology Reviews* 32(2):234-258.
92. Ghuysen J-M (1991) Serine β -lactamases and Penicillin-binding proteins. *Annual Review of Microbiology* 45(1):37-67.
93. Wise EM, Jr. & Park JT (1965) Penicillin: its basic site of action as an inhibitor of a peptide cross-linking reaction in cell wall mucopeptide synthesis. (Translated from eng) *Proceedings of the National Academy of Sciences of the United States of America* 54(1):75-81 (in eng).
94. Lavollay M, *et al.* (2008) The Peptidoglycan of Stationary-Phase *Mycobacterium tuberculosis* Predominantly Contains Cross-Links Generated by Transpeptidation. *Journal of Bacteriology* 190(12):4360.
95. Mainardi J-L, *et al.* (2005) A Novel Peptidoglycan Cross-linking Enzyme for a β -Lactam-resistant Transpeptidation Pathway. *Journal of Biological Chemistry* 280(46):38146-38152.
96. Magnet S, *et al.* (2007) Identification of the L,D-transpeptidases responsible for attachment of the Braun lipoprotein to *Escherichia coli* peptidoglycan. (Translated from eng) *Journal of Bacteriology* 189(10):3927-3931 (in eng).
97. Braun V & Rehn K (1969) Chemical characterization, spatial distribution and function of a lipoprotein (murein-lipoprotein) of the *E. coli* cell wall. The specific effect of trypsin on the membrane structure. (Translated from eng) *Eur J Biochem* 10(3):426-438 (in eng).
98. Hantke K & Braun V (1973) Covalent binding of lipid to protein. Diglyceride and amide-linked fatty acid at the N-terminal end of the murein-lipoprotein of the *Escherichia coli* outer membrane. (Translated from eng) *Eur J Biochem* 34(2):284-296 (in eng).
99. Cohen EJ, Ferreira JL, Ladinsky MS, Beeby M, & Hughes KT (2017) Nanoscale-length control of the flagellar driveshaft requires hitting the tethered outer membrane. *Science* 356(6334):197.
100. Nakayama H, Kurokawa K, & Lee BL (2012) Lipoproteins in bacteria: structures and biosynthetic pathways. (Translated from eng) *FEBS J* 279(23):4247-4268 (in eng).
101. Asmar AT & Collet J-F (2018) Lpp, the Braun lipoprotein, turns 50—major achievements and remaining issues. *FEMS Microbiology Letters* 365(18).
102. Armstrong JJ, Baddiley J, Buchanan JG, Carss B, & Greenberg GR (1958) 882. Isolation and structure of ribitol phosphate derivatives (teichoic acids)

- from bacterial cell walls. *Journal of the Chemical Society (Resumed)* (0):4344-4354.
103. Ward JB (1981) Teichoic and teichuronic acids: biosynthesis, assembly, and location. (Translated from eng) *Microbiol Rev* 45(2):211-243 (in eng).
 104. Araki Y & Ito E (1989) Linkage Units in Cell Walls of Gram-Positive Bacteria. *Critical Reviews in Microbiology* 17(2):121-135.
 105. Bhavsar AP, Beveridge TJ, & Brown ED (2001) Precise deletion of tagD and controlled depletion of its product, glycerol 3-phosphate cytidyltransferase, leads to irregular morphology and lysis of *Bacillus subtilis* grown at physiological temperature. (Translated from eng) *J Bacteriol* 183(22):6688-6693 (in eng).
 106. Eugster MR & Loessner MJ (2012) Wall teichoic acids restrict access of bacteriophage endolysin Ply118, Ply511, and PlyP40 cell wall binding domains to the *Listeria monocytogenes* peptidoglycan. (Translated from eng) *J Bacteriol* 194(23):6498-6506 (in eng).
 107. Wanner S, *et al.* (2017) Wall teichoic acids mediate increased virulence in *Staphylococcus aureus*. *Nature Microbiology* 2(4):16257.
 108. Ohno N, Yadomae T, & Miyazaki T (1982) Identification of 2-amino-2-deoxyglucose residues in the peptidoglycan of *Streptococcus pneumoniae*. *Carbohydrate Research* 107(1):152-155.
 109. Lacks S & Neuberger M (1975) Membrane location of a deoxyribonuclease implicated in the genetic transformation of *Diplococcus pneumoniae*. *Journal of Bacteriology* 124(3):1321.
 110. Zipperle Jr GF, Ezzell Jr JW, & Doyle RJ (1984) Glucosamine substitution and muramidase susceptibility in *Bacillus anthracis*. *Canadian Journal of Microbiology* 30(5):553-559.
 111. Rosenthal RS, Blundell JK, & Perkins HR (1982) Strain-related differences in lysozyme sensitivity and extent of O-acetylation of gonococcal peptidoglycan. *Infection and Immunity* 37(2):826.
 112. Coulombe F, *et al.* (2009) Increased NOD2-mediated recognition of N-glycolyl muramyl dipeptide. *The Journal of Experimental Medicine* 206(8):1709.
 113. Larson TR & Yother J (2017) Streptococcus pneumoniae; capsular polysaccharide is linked to peptidoglycan via a direct glycosidic bond to β -D-N-acetylglucosamine. *Proceedings of the National Academy of Sciences* 114(22):5695.
 114. Rausch M, *et al.* (2019) Coordination of capsule assembly and cell wall biosynthesis in *Staphylococcus aureus*. *Nat Commun* 10(1):1404.
 115. Du S & Lutkenhaus J (2019) At the Heart of Bacterial Cytokinesis: The Z Ring. *Trends in Microbiology* 27(9):781-791.
 116. Bi EF & Lutkenhaus J (1991) FtsZ ring structure associated with division in *Escherichia coli*. (Translated from eng) *Nature* 354(6349):161-164 (in eng).
 117. Erickson HP (1997) FtsZ, a tubulin homologue in prokaryote cell division. *Trends in Cell Biology* 7(9):362-367.
 118. Mukherjee A & Lutkenhaus J (1994) Guanine nucleotide-dependent assembly of FtsZ into filaments. *Journal of Bacteriology* 176(9):2754.
 119. Erickson HP, Taylor DW, Taylor KA, & Bramhill D (1996) Bacterial cell division protein FtsZ assembles into protofilament sheets and minirings, structural homologs of tubulin polymers. *Proceedings of the National Academy of Sciences* 93(1):519.

120. Lu C, Reedy M, & Erickson HP (2000) Straight and Curved Conformations of FtsZ Are Regulated by GTP Hydrolysis. *Journal of Bacteriology* 182(1):164.
121. Hale CA & de Boer PA (1997) Direct binding of FtsZ to ZipA, an essential component of the septal ring structure that mediates cell division in *E. coli*. (Translated from eng) *Cell* 88(2):175-185 (in eng).
122. Pichoff S & Lutkenhaus J (2005) Tethering the Z ring to the membrane through a conserved membrane targeting sequence in FtsA. (Translated from eng) *Mol Microbiol* 55(6):1722-1734 (in eng).
123. Chen Y, Huang H, Osawa M, & Erickson HP (2017) ZipA and FtsA* stabilize FtsZ-GDP miniring structures. *Scientific Reports* 7(1):3650.
124. Gueiros-Filho FJ & Losick R (2002) A widely conserved bacterial cell division protein that promotes assembly of the tubulin-like protein FtsZ. *Genes & Development* 16(19):2544-2556.
125. Dajkovic A, Pichoff S, Lutkenhaus J, & Wirtz D (2010) Cross-linking FtsZ polymers into coherent Z rings. *Molecular Microbiology* 78(3):651-668.
126. Espeli O, *et al.* (2012) A MatP-divisome interaction coordinates chromosome segregation with cell division in *E. coli*. (Translated from eng) *EMBO J* 31(14):3198-3211 (in eng).
127. Lutkenhaus J (2007) Assembly dynamics of the bacterial MinCDE system and spatial regulation of the Z ring. (Translated from eng) *Annu Rev Biochem* 76:539-562 (in eng).
128. LaBreck CJ, Conti J, Viola MG, & Camberg JL (2019) MinC N- and C-Domain Interactions Modulate FtsZ Assembly, Division Site Selection, and MinD-Dependent Oscillation in *Escherichia coli*. (Translated from eng) *Journal of Bacteriology* 201(4):e00374-00318 (in eng).
129. Adler HI, Fisher WD, Cohen A, & Hardigree AA (1967) Miniature *Escherichia coli* cells deficient in DNA. (Translated from eng) *Proc Natl Acad Sci U S A* 57(2):321-326 (in eng).
130. Mulder E & Woldringh CL (1989) Actively replicating nucleoids influence positioning of division sites in *Escherichia coli* filaments forming cells lacking DNA. (Translated from eng) *Journal of Bacteriology* 171(8):4303-4314 (in eng).
131. Bernhardt TG & de Boer PAJ (2005) SlmA, a nucleoid-associated, FtsZ binding protein required for blocking septal ring assembly over Chromosomes in *E. coli*. (Translated from eng) *Mol Cell* 18(5):555-564 (in eng).
132. Wu LJ & Errington J (2012) Nucleoid occlusion and bacterial cell division. *Nature Reviews Microbiology* 10(1):8-12.
133. Goehring NW, Gonzalez MD, & Beckwith J (2006) Premature targeting of cell division proteins to midcell reveals hierarchies of protein interactions involved in divisome assembly. *Molecular Microbiology* 61(1):33-45.
134. Boyle DS, Khattar MM, Addinall SG, Lutkenhaus J, & Donachie WD (1997) ftsW is an essential cell-division gene in *Escherichia coli*. (Translated from eng) *Mol Microbiol* 24(6):1263-1273 (in eng).
135. Mohammadi T, *et al.* (2011) Identification of FtsW as a transporter of lipid-linked cell wall precursors across the membrane. *The EMBO Journal* 30(8):1425-1432.
136. Taguchi A, *et al.* (2019) FtsW is a peptidoglycan polymerase that is functional only in complex with its cognate penicillin-binding protein. *Nature Microbiology* 4(4):587-594.

137. Botta GA & Park JT (1981) Evidence for involvement of penicillin-binding protein 3 in murein synthesis during septation but not during cell elongation. (Translated from eng) *J Bacteriol* 145(1):333-340 (in eng).
138. Wissel MC & Weiss DS (2004) Genetic analysis of the cell division protein FtsI (PBP3): amino acid substitutions that impair septal localization of FtsI and recruitment of FtsN. (Translated from eng) *Journal of Bacteriology* 186(2):490-502 (in eng).
139. Fraipont C, *et al.* (2011) The integral membrane FtsW protein and peptidoglycan synthase PBP3 form a subcomplex in *Escherichia coli*. *Microbiology* 157(1):251-259.
140. Bertsche U, *et al.* (2006) Interaction between two murein (peptidoglycan) synthases, PBP3 and PBP1B, in *Escherichia coli*. *Molecular Microbiology* 61(3):675-690.
141. Boes A, Olatunji S, Breukink E, & Terrak M (2019) Regulation of the Peptidoglycan Polymerase Activity of PBP1b by Antagonist Actions of the Core Divisome Proteins FtsBLQ and FtsN. (Translated from eng) *MBio* 10(1):e01912-01918 (in eng).
142. Gerding MA, *et al.* (2009) Self-enhanced accumulation of FtsN at Division Sites and Roles for Other Proteins with a SPOR domain (DamX, DedD, and RlpA) in *Escherichia coli* cell constriction. (Translated from eng) *Journal of Bacteriology* 191(24):7383-7401 (in eng).
143. Bisson-Filho AW, *et al.* (2017) Treadmilling by FtsZ filaments drives peptidoglycan synthesis and bacterial cell division. *Science* 355(6326):739.
144. Egan AJ & Vollmer W (2013) The physiology of bacterial cell division. (Translated from eng) *Ann N Y Acad Sci* 1277:8-28 (in eng).
145. Heidrich C, *et al.* (2001) Involvement of N-acetylmuramyl-L-alanine amidases in cell separation and antibiotic-induced autolysis of *Escherichia coli*. (Translated from eng) *Mol Microbiol* 41(1):167-178 (in eng).
146. Uehara T, Dinh T, & Bernhardt TG (2009) LytM-domain factors are required for daughter cell separation and rapid ampicillin-induced lysis in *Escherichia coli*. (Translated from eng) *Journal of Bacteriology* 191(16):5094-5107 (in eng).
147. Peters NT, *et al.* (2013) Structure-function analysis of the LytM domain of EnvC, an activator of cell wall remodelling at the *Escherichia coli* division site. (Translated from eng) *Molecular Microbiology* 89(4):690-701 (in eng).
148. Tsang M-J, Yakhnina AA, & Bernhardt TG (2017) NlpD links cell wall remodeling and outer membrane invagination during cytokinesis in *Escherichia coli*. (Translated from eng) *PLoS Genet* 13(7):e1006888-e1006888 (in eng).
149. Stohl EA, Lenz JD, Dillard JP, & Seifert HS (2015) The Gonococcal NlpD Protein Facilitates Cell Separation by Activating Peptidoglycan Cleavage by AmiC. (Translated from eng) *J Bacteriol* 198(4):615-622 (in eng).
150. Ercoli G, *et al.* (2015) LytM Proteins Play a Crucial Role in Cell Separation, Outer Membrane Composition, and Pathogenesis in Nontypeable *Haemophilus influenzae*. *mBio* 6(2):e02575-02514.
151. Rocaboy M, *et al.* (2013) The crystal structure of the cell division amidase AmiC reveals the fold of the AMIN domain, a new peptidoglycan binding domain. *Molecular Microbiology* 90(2):267-277.

152. Uehara T, Parzych KR, Dinh T, & Bernhardt TG (2010) Daughter cell separation is controlled by cytokinetic ring-activated cell wall hydrolysis. (Translated from eng) *EMBO J* 29(8):1412-1422 (in eng).
153. Yang DC, *et al.* (2011) An ATP-binding cassette transporter-like complex governs cell-wall hydrolysis at the bacterial cytokinetic ring. (Translated from eng) *Proceedings of the National Academy of Sciences of the United States of America* 108(45):E1052-E1060 (in eng).
154. Bernhardt TG & de Boer PA (2003) The Escherichia coli amidase AmiC is a periplasmic septal ring component exported via the twin-arginine transport pathway. *Mol Microbiol* 48(5):1171-1182.
155. Peters NT, Dinh T, & Bernhardt TG (2011) A Fail-Safe Mechanism in the Septal Ring Assembly Pathway Generated by the Sequential Recruitment of Cell Separation Amidases and Their Activators. *Journal of Bacteriology* 193(18):4973-4983.
156. Möll A, *et al.* (2014) Cell separation in Vibrio cholerae is mediated by a single amidase whose action is modulated by two nonredundant activators. (Translated from eng) *Journal of Bacteriology* 196(22):3937-3948 (in eng).
157. van Teeffelen S & Renner LD (2018) Recent advances in understanding how rod-like bacteria stably maintain their cell shapes. (Translated from eng) *F1000Res* 7:241-241 (in eng).
158. Cho H, *et al.* (2016) Bacterial cell wall biogenesis is mediated by SEDS and PBP polymerase families functioning semi-autonomously. (Translated from eng) *Nature microbiology* 1:16172-16172 (in eng).
159. Claessen D, *et al.* (2008) Control of the cell elongation–division cycle by shuttling of PBP1 protein in Bacillus subtilis. *Molecular Microbiology* 68(4):1029-1046.
160. Cleverley RM, *et al.* (2019) The cell cycle regulator GpsB functions as cytosolic adaptor for multiple cell wall enzymes. *Nature Communications* 10(1):261.
161. Van Den Ent F, *et al.* (2006) Dimeric structure of the cell shape protein MreC and its functional implications. *Molecular Microbiology* 62(6):1631-1642.
162. Leaver M & Errington J (2005) Roles for MreC and MreD proteins in helical growth of the cylindrical cell wall in Bacillus subtilis. *Molecular Microbiology* 57(5):1196-1209.
163. Garner EC, *et al.* (2011) Coupled, circumferential motions of the cell wall synthesis machinery and MreB filaments in B. subtilis. (Translated from eng) *Science (New York, N.Y.)* 333(6039):222-225 (in eng).
164. Salje J, van den Ent F, de Boer P, & Löwe J (2011) Direct membrane binding by bacterial actin MreB. (Translated from eng) *Mol Cell* 43(3):478-487 (in eng).
165. van den Ent F, Johnson CM, Persons L, de Boer P, & Löwe J (2010) Bacterial actin MreB assembles in complex with cell shape protein RodZ. (Translated from eng) *The EMBO Journal* 29(6):1081-1090 (in eng).
166. Liu X, Biboy J, Vollmer W, & den Blaauwen T (2019) MreC and MreD balance the interaction between the elongasome proteins PBP2 and RodA. *bioRxiv*:769984.
167. Meeske AJ, *et al.* (2016) SEDS proteins are a widespread family of bacterial cell wall polymerases. *Nature* 537(7622):634-638.
168. McPherson DC & Popham DL (2003) Peptidoglycan synthesis in the absence of class A penicillin-binding proteins in Bacillus subtilis. (Translated from eng) *J Bacteriol* 185(4):1423-1431 (in eng).

169. Wetzel RG (2001) 15 - PLANKTONIC COMMUNITIES: ALGAE AND CYANOBACTERIA. *Limnology (Third Edition)*, ed Wetzel RG (Academic Press, San Diego), pp 331-393.
170. ECHLIN P & MORRIS I (1965) THE RELATIONSHIP BETWEEN BLUE-GREEN ALGAE AND BACTERIA. *Biological Reviews* 40(2):143-184.
171. Fuhs GW (1958) [Enzymatic reduction of *Oscillatoria amoena* (Kutz.) Gomont membranes with lysozyme]. (Translated from ger) *Arch Mikrobiol* 29(1):51-52 (in ger).
172. Crespi HL, Mandeville SE, & Katz JJ (1962) The action of lysozyme on several blue-green algae. *Biochemical and Biophysical Research Communications* 9(6):569-573.
173. Foter MJ, Palmer CM, & Maloney TE (1953) Antialgal properties of various antibiotics. (Translated from eng) *Antibiot Chemother (Northfield)* 3(5):505-508 (in eng).
174. Work E & Dewey DL (1953) The Distribution of α , ϵ -Diaminopimelic Acid among various Micro-organisms. *Microbiology* 9(3):394-409.
175. Ris H & Singh RN (1961) Electron microscope studies on blue-green algae. (Translated from eng) *J Biophys Biochem Cytol* 9(1):63-80 (in eng).
176. Chapman JA & Salton MR (1962) A study of several blue-green algae in the electron microscope. (Translated from eng) *Arch Mikrobiol* 44:311-322 (in eng).
177. Jost M (1965) Die Ultrastruktur von *Oscillatoria rubescens* D. C. *Archiv für Mikrobiologie* 50(3):211-245.
178. Frank H, Lefort M, & Martin HH (1962) Elektronenoptische und chemische Untersuchungen an Zellwänden der Blaualge *Phormidium uncinatum*. in *Zeitschrift für Naturforschung B*, p 262.
179. Drews G & Meyer H (1964) Untersuchungen zum chemischen Aufbau der Zellwände von *Anacystis nidulans* und *Chlorogloea fritschii*. *Archiv für Mikrobiologie* 48(3):259-267.
180. Jensen TE & Sicko LM (1971) The Effect of Lysozyme on Cell Wall Morphology in a Blue-green Alga, *Cylindrospermum* sp. *Microbiology* 68(1):71-75.
181. Punnett T & Derrenbacker EC (1966) The Amino Acid Composition of Algal Cell Walls. *Microbiology* 44(1):105-114.
182. Golecki JR (1977) Studies on ultrastructure and composition of cell walls of the cyanobacterium *Anacystis nidulans*. *Archives of Microbiology* 114(1):35-41.
183. Jurgens UJ, Drews G, & Weckesser J (1983) Primary structure of the peptidoglycan from the unicellular cyanobacterium *Synechocystis* sp. strain PCC 6714. (Translated from eng) *J Bacteriol* 154(1):471-478 (in eng).
184. Jürgens UJ & Weckesser J (1986) Polysaccharide covalently linked to the peptidoglycan of the cyanobacterium *Synechocystis* sp. strain PCC6714. *Journal of Bacteriology* 168(2):568.
185. Jürgens UJ, Golecki JR, & Weckesser J (1985) Characterization of the cell wall of the unicellular cyanobacterium *Synechocystis* PCC 6714. *Archives of Microbiology* 142(2):168-174.
186. Hoiczuk E & Baumeister W (1995) Envelope structure of four gliding filamentous cyanobacteria. (Translated from eng) *Journal of Bacteriology* 177(9):2387-2395 (in eng).

187. Flores E, Herrero A, Wolk CP, & Maldener I (2006) Is the periplasm continuous in filamentous multicellular cyanobacteria? *Trends in Microbiology* 14(10):439-443.
188. Mariscal V, Herrero A, & Flores E (2007) Continuous periplasm in a filamentous, heterocyst-forming cyanobacterium. (Translated from eng) *Mol Microbiol* 65(4):1139-1145 (in eng).
189. Kodani S, Ishida K, & Murakami M (1999) Occurrence and identification of UDP-N-acetylmuramyl-pentapeptide from the cyanobacterium *Anabaena cylindrica*. *FEMS Microbiology Letters* 176(2):321-325.
190. Videau P, *et al.* (2016) Mutation of the murC and murB Genes Impairs Heterocyst Differentiation in *Anabaena* sp. Strain PCC 7120. (Translated from eng) *Journal of Bacteriology* 198(8):1196-1206 (in eng).
191. Lázaro S, Fernández-Piñas F, Fernández-Valiente E, Blanco-Rivero A, & Leganés F (2001) pbpB, a gene coding for a putative penicillin-binding protein, is required for aerobic nitrogen fixation in the cyanobacterium *Anabaena* sp. strain PCC7120. (Translated from eng) *Journal of Bacteriology* 183(2):628-636 (in eng).
192. Leganés F, *et al.* (2005) Wide variation in the cyanobacterial complement of presumptive penicillin-binding proteins. *Archives of Microbiology* 184(4):234-248.
193. Marbouty M, Mazouni K, Saguez C, Cassier-Chauvat C, & Chauvat F (2009) Characterization of the *Synechocystis* strain PCC 6803 penicillin-binding proteins and cytokinetic proteins FtsQ and FtsW and their network of interactions with ZipN. (Translated from eng) *Journal of Bacteriology* 191(16):5123-5133 (in eng).
194. Mazouni K, Domain F, Cassier-Chauvat C, & Chauvat F (2004) Molecular analysis of the key cytokinetic components of cyanobacteria: FtsZ, ZipN and MinCDE. *Molecular Microbiology* 52(4):1145-1158.
195. Koksharova OA & Wolk CP (2002) A novel gene that bears a DnaJ motif influences cyanobacterial cell division. (Translated from eng) *J Bacteriol* 184(19):5524-5528 (in eng).
196. Miyagishima S-y, Wolk CP, & Osteryoung KW (2005) Identification of cyanobacterial cell division genes by comparative and mutational analyses. *Molecular Microbiology* 56(1):126-143.
197. Schmitz O, Katayama M, Williams SB, Kondo T, & Golden SS (2000) CikA, a Bacteriophytochrome That Resets the Cyanobacterial Circadian Clock. *Science* 289(5480):765.
198. Herrero A, Stavans J, & Flores E (2016) The multicellular nature of filamentous heterocyst-forming cyanobacteria. *FEMS Microbiology Reviews* 40(6):831-854.
199. Mandakovic D, *et al.* (2016) CyDiv, a Conserved and Novel Filamentous Cyanobacterial Cell Division Protein Involved in Septum Localization. (Translated from English) *Frontiers in Microbiology* 7(94) (in English).
200. Doherty HM & Adams DG (1995) Cloning and sequence of ftsZ and flanking regions from the cyanobacterium *Anabaena* PCC 7120. *Gene* 163(1):93-96.
201. Zhang CC, Huguenin S, & Friry A (1995) Analysis of genes encoding the cell division protein FtsZ and a glutathione synthetase homologue in the cyanobacterium *Anabaena* sp. PCC 7120. *Research in Microbiology* 146(6):445-455.
202. Sakr S, Jeanjean R, Zhang C-C, & Arcondeguy T (2006) Inhibition of cell division suppresses heterocyst development in *Anabaena* sp. strain PCC

7120. (Translated from eng) *Journal of Bacteriology* 188(4):1396-1404 (in eng).
203. Kuhn I, Peng L, Bedu S, & Zhang CC (2000) Developmental regulation of the cell division protein FtsZ in *Anabaena* sp. strain PCC 7120, a cyanobacterium capable of terminal differentiation. (Translated from eng) *Journal of Bacteriology* 182(16):4640-4643 (in eng).
204. Wang Y & Xu X (2005) Regulation by *hetC* of Genes Required for Heterocyst Differentiation and Cell Division in *Anabaena* sp. Strain PCC 7120. *Journal of Bacteriology* 187(24):8489.
205. Khudyakov I & Wolk CP (1997) *hetC*, a gene coding for a protein similar to bacterial ABC protein exporters, is involved in early regulation of heterocyst differentiation in *Anabaena* sp. strain PCC 7120. (Translated from eng) *J Bacteriol* 179(22):6971-6978 (in eng).
206. Camargo S, *et al.* (2019) ZipN is an essential FtsZ membrane tether and contributes to the septal localization of SepJ in the filamentous cyanobacterium *Anabaena*. *Scientific Reports* 9(1):2744.
207. Hu B, Yang G, Zhao W, Zhang Y, & Zhao J (2007) MreB is important for cell shape but not for chromosome segregation of the filamentous cyanobacterium *Anabaena* sp. PCC 7120. *Molecular Microbiology* 63(6):1640-1652.
208. Burnat M, Schleiff E, & Flores E (2014) Cell Envelope Components Influencing Filament Length in the Heterocyst-Forming Cyanobacterium *Anabaena* sp. Strain PCC 7120. *Journal of Bacteriology* 196(23):4026.
209. Singh SP & Montgomery BL (2014) Morphogenes *bolA* and *mreB* mediate the photoregulation of cellular morphology during complementary chromatic acclimation in *Fremyella diplosiphon*. *Molecular Microbiology* 93(1):167-182.
210. Santos JM, Freire P, Vicente M, & Arraiano CM (1999) The stationary-phase morphogene *bolA* from *Escherichia coli* is induced by stress during early stages of growth. (Translated from eng) *Mol Microbiol* 32(4):789-798 (in eng).
211. Aldea M, Garrido T, Hernandez-Chico C, Vicente M, & Kushner SR (1989) Induction of a growth-phase-dependent promoter triggers transcription of *bolA*, an *Escherichia coli* morphogene. (Translated from eng) *Embo j* 8(12):3923-3931 (in eng).
212. Zhang LC, Chen YF, Chen WL, & Zhang CC (2008) Existence of periplasmic barriers preventing green fluorescent protein diffusion from cell to cell in the cyanobacterium *Anabaena* sp. strain PCC 7120. (Translated from eng) *Mol Microbiol* 70(4):814-823 (in eng).
213. Haselkorn R (2008) Cell-cell communication in filamentous cyanobacteria. *Molecular Microbiology* 70(4):783-785.
214. Zhang L-C, Risoul V, Latifi A, Christie JM, & Zhang C-C (2013) Exploring the size limit of protein diffusion through the periplasm in cyanobacterium *Anabaena* sp. PCC 7120 using the 13 kDa iLOV fluorescent protein. *Research in Microbiology* 164(7):710-717.
215. Mullineaux CW, *et al.* (2008) Mechanism of intercellular molecular exchange in heterocyst-forming cyanobacteria. (Translated from eng) *The EMBO Journal* 27(9):1299-1308 (in eng).
216. Metzner I (1955) Zur Chemie und zum submikroskopischen Aufbau der Zellwände, Scheiden und Gallerten von Cyanophyceen. *Archiv für Mikrobiologie* 22(1):45-77.
217. Wildon DC & Mercer FV (1963) The ultrastructure of the heterocyst and akinete of the blue-green algae. *Archiv für Mikrobiologie* 47(1):19-31.

218. Lang NJ, Fay P, & Fogg GE (1971) The heterocysts of blue-green algae II. Details of ultrastructure. *Proceedings of the Royal Society of London. Series B. Biological Sciences* 178(1051):193-203.
219. Wilk L, *et al.* (2011) Outer membrane continuity and septosome formation between vegetative cells in the filaments of *Anabaena* sp. PCC 7120. *Cellular Microbiology* 13(11):1744-1754.
220. Omairi-Nasser A, Haselkorn R, & Jotham Austin I (2014) Visualization of channels connecting cells in filamentous nitrogen-fixing cyanobacteria. *The FASEB Journal* 28(7):3016-3022.
221. Bornikoel J, *et al.* (2017) Role of Two Cell Wall Amidases in Septal Junction and Nanopore Formation in the Multicellular Cyanobacterium *Anabaena* sp. PCC 7120. *Front Cell Infect Microbiol* 7:386.
222. Nürnberg DJ, *et al.* (2015) Intercellular diffusion of a fluorescent sucrose analog via the septal junctions in a filamentous cyanobacterium. (Translated from eng) *MBio* 6(2):e02109-e02109 (in eng).
223. Lehner J, *et al.* (2013) Prokaryotic multicellularity: a nanopore array for bacterial cell communication. (Translated from eng) *FASEB J* 27(6):2293-2300 (in eng).
224. Giddings TH & Staehelin LA (1981) Observation of microplasmodesmata in both heterocyst-forming and non-heterocyst forming filamentous cyanobacteria by freeze-fracture electron microscopy. *Archives of Microbiology* 129(4):295-298.
225. Flores E, *et al.* (2007) Septum-Localized Protein Required for Filament Integrity and Diazotrophy in the Heterocyst-Forming Cyanobacterium *Anabaena* sp. Strain PCC 7120. *Journal of Bacteriology* 189(10):3884.
226. Nayar AS, Yamaura H, Rajagopalan R, Risser DD, & Callahan SM (2007) FraG is necessary for filament integrity and heterocyst maturation in the cyanobacterium *Anabaena* sp. strain PCC 7120. *Microbiology* 153(2):601-607.
227. Ramos-León F, Mariscal V, Frías JE, Flores E, & Herrero A (2015) Divisome-dependent subcellular localization of cell–cell joining protein SepJ in the filamentous cyanobacterium *Anabaena*. *Molecular Microbiology* 96(3):566-580.
228. Ramos-León F, Mariscal V, Battchikova N, Aro E-M, & Flores E (2017) Septal protein SepJ from the heterocyst-forming cyanobacterium *Anabaena* forms multimers and interacts with peptidoglycan. *FEBS Open Bio* 7(10):1515-1526.
229. Lehner J, *et al.* (2011) The morphogene *AmiC2* is pivotal for multicellular development in the cyanobacterium *Nostoc punctiforme*. *Molecular Microbiology* 79(6):1655-1669.
230. Mariscal V, Nürnberg DJ, Herrero A, Mullineaux CW, & Flores E (2016) Overexpression of SepJ alters septal morphology and heterocyst pattern regulated by diffusible signals in *Anabaena*. *Molecular Microbiology* 101(6):968-981.
231. Flores E, Nieves-Morion M, & Mullineaux CW (2018) Cyanobacterial Septal Junctions: Properties and Regulation. (Translated from eng) *Life (Basel)* 9(1) (in eng).
232. Weiss GL, Kieninger A-K, Maldener I, Forchhammer K, & Pilhofer M (2019) Structure and Function of a Bacterial Gap Junction Analog. *Cell* 178(2):374-384.e315.
233. Merino-Puerto V, Mariscal V, Mullineaux CW, Herrero A, & Flores E (2010) Fra proteins influencing filament integrity, diazotrophy and localization of

- septal protein SepJ in the heterocyst-forming cyanobacterium *Anabaena* sp. *Molecular Microbiology* 75(5):1159-1170.
234. Merino-Puerto V, *et al.* (2011) FraC/FraD-dependent intercellular molecular exchange in the filaments of a heterocyst-forming cyanobacterium, *Anabaena* sp. *Molecular Microbiology* 82(1):87-98.
 235. Bauer CC, Buikema WJ, Black K, & Haselkorn R (1995) A short-filament mutant of *Anabaena* sp. strain PCC 7120 that fragments in nitrogen-deficient medium. (Translated from eng) *Journal of Bacteriology* 177(6):1520-1526 (in eng).
 236. Berendt S, *et al.* (2012) Cell wall amidase AmiC1 is required for cellular communication and heterocyst development in the cyanobacterium *Anabaena* PCC 7120 but not for filament integrity. (Translated from eng) *J Bacteriol* 194(19):5218-5227 (in eng).
 237. Christman HD, Campbell EL, & Meeks JC (2011) Global transcription profiles of the nitrogen stress response resulting in heterocyst or hormogonium development in *Nostoc punctiforme*. (Translated from eng) *Journal of Bacteriology* 193(24):6874-6886 (in eng).
 238. Zhu J, *et al.* (2001) HcwA, an autolysin, is required for heterocyst maturation in *Anabaena* sp. strain PCC 7120. (Translated from eng) *Journal of Bacteriology* 183(23):6841-6851 (in eng).
 239. Brenes-Alvarez M, Vioque A, & Muro-Pastor AM (2020) The Integrity of the Cell Wall and Its Remodeling during Heterocyst Differentiation Are Regulated by Phylogenetically Conserved Small RNA Yfr1 in *Nostoc* sp. Strain PCC 7120. (Translated from eng) *MBio* 11(1) (in eng).
 240. Rudolf M, *et al.* (2015) The Peptidoglycan-Binding Protein SjcF1 Influences Septal Junction Function and Channel Formation in the Filamentous Cyanobacterium *Anabaena*. *MBio* 6(4):e00376-00315.
 241. Yang DC, Tan K, Joachimiak A, & Bernhardt TG (2012) A conformational switch controls cell wall-remodelling enzymes required for bacterial cell division. *Molecular Microbiology* 85(4):768-781.
 242. Büttner FM, Faulhaber K, Forchhammer K, Maldener I, & Stehle T (2016) Enabling cell–cell communication via nanopore formation: structure, function and localization of the unique cell wall amidase AmiC2 of *Nostoc punctiforme*. *FEBS Journal* 283(7):1336-1350.
 243. Faheem M, *et al.* (2016) Functional and structural characterization of a novel putative cysteine protease cell wall-modifying multi-domain enzyme selected from a microbial metagenome. *Scientific Reports* 6(1):38031.
 244. Faulhaber K (2017) Detaillierte Charakterisierung von AmiC2, einem Schlüsselenzym für die intrafilamentöse Kommunikation in *Nostoc punctiforme* ATCC29133. (University of Tübingen, Tübingen).
 245. Kumar A, *et al.* (2013) The structure of Rv3717 reveals a novel amidase from *Mycobacterium tuberculosis*. (Translated from eng) *Acta Crystallogr D Biol Crystallogr* 69(Pt 12):2543-2554 (in eng).
 246. Bornikoel J, Staiger J, Madlung J, Forchhammer K, & Maldener I (2018) LytM factor Alr3353 affects filament morphology and cell–cell communication in the multicellular cyanobacterium *Anabaena* sp. PCC 7120. *Molecular Microbiology* 108(2):187-203.
 247. Jensen KF (1993) The *Escherichia coli* K-12 "wild types" W3110 and MG1655 have an rph frameshift mutation that leads to pyrimidine starvation due to low pyrE expression levels. (Translated from eng) *J Bacteriol* 175(11):3401-3407 (in eng).

248. Hanahan D (1983) Studies on transformation of *Escherichia coli* with plasmids. (Translated from eng) *J Mol Biol* 166(4):557-580 (in eng).
249. Hanahan D, Jessee J, & Bloom FR (1991) Plasmid transformation of *Escherichia coli* and other bacteria. (Translated from eng) *Methods Enzymol* 204:63-113 (in eng).
250. Studier FW (2005) Protein production by auto-induction in high density shaking cultures. (Translated from eng) *Protein Expr Purif* 41(1):207-234 (in eng).
251. Laemmli UK (1970) Cleavage of structural proteins during the assembly of the head of bacteriophage T4. (Translated from eng) *Nature* 227(5259):680-685 (in eng).
252. Hayashi K (1975) A rapid determination of sodium dodecyl sulfate with methylene blue. *Analytical Biochemistry* 67(2):503-506.
253. Zhou R, Chen S, & Recsei P (1988) A dye release assay for determination of lysostaphin activity. (Translated from eng) *Anal Biochem* 171(1):141-144 (in eng).
254. Prigozhin DM, Mavrici D, Huizar JP, Vansell HJ, & Alber T (2013) Structural and Biochemical Analyses of Mycobacterium tuberculosis N-Acetylmuramyl-L-alanine Amidase Rv3717 Point to a Role in Peptidoglycan Fragment Recycling. *Journal of Biological Chemistry* 288(44):31549-31555.
255. Darrouzet-Nardi A, Ladd MP, & Weintraub MN (2013) Fluorescent microplate analysis of amino acids and other primary amines in soils. *Soil Biology and Biochemistry* 57:78-82.
256. Kühner D, Stahl M, Demircioglu DD, & Bertsche U (2014) From cells to muropeptide structures in 24 h: Peptidoglycan mapping by UPLC-MS. *Scientific Reports* 4(1):7494.
257. Tabor S & Richardson CC (1985) A bacteriophage T7 RNA polymerase/promoter system for controlled exclusive expression of specific genes. (Translated from eng) *Proc Natl Acad Sci U S A* 82(4):1074-1078 (in eng).
258. de Pedro MA, Quintela JC, Höltje JV, & Schwarz H (1997) Murein segregation in *Escherichia coli*. *Journal of bacteriology* 179(9):2823-2834.
259. Lehner J (2012) Funktionelle Charakterisierung der Zellwandproteine AmiC2 und SepJN und ihre Bedeutung für die Vielzelligkeit des filamentösen Cyanobakteriums *Nostoc punctiforme* ATCC 29133. PhD (University of Tübingen, Tübingen).
260. Turner RD, Mesnage S, Hobbs JK, & Foster SJ (2018) Molecular imaging of glycan chains couples cell-wall polysaccharide architecture to bacterial cell morphology. *Nature Communications* 9(1):1263.
261. Frain KM, Gangl D, Jones A, Zedler JAZ, & Robinson C (2016) Protein translocation and thylakoid biogenesis in cyanobacteria. *Biochimica et Biophysica Acta (BBA) - Bioenergetics* 1857(3):266-273.
262. Knyazev DG, *et al.* (2013) The Bacterial Translocon SecYEG Opens upon Ribosome Binding. *Journal of Biological Chemistry* 288(25):17941-17946.
263. Yeats C & Bateman A (2003) The BON domain: a putative membrane-binding domain. *Trends in Biochemical Sciences* 28(7):352-355.
264. Poon WW, *et al.* (2000) Identification of *Escherichia coli* ubiB, a Gene Required for the First Monooxygenase Step in Ubiquinone Biosynthesis. *Journal of Bacteriology* 182(18):5139.

265. Noinaj N, Guillier M, Barnard TJ, & Buchanan SK (2010) TonB-dependent transporters: regulation, structure, and function. (Translated from eng) *Annu Rev Microbiol* 64:43-60 (in eng).
266. Uehara T & Park JT (2007) An Anhydro-N-Acetylmuramyl-L-Alanine Amidase with Broad Specificity Tethered to the Outer Membrane of Escherichia coli. *Journal of Bacteriology* 189(15):5634.
267. Zhang J-Y, Lin G-M, Xing W-Y, & Zhang C-C (2018) Diversity of Growth Patterns Probed in Live Cyanobacterial Cells Using a Fluorescent Analog of a Peptidoglycan Precursor. (Translated from English) *Frontiers in Microbiology* 9(791) (in English).
268. Tiyanont K, *et al.* (2006) Imaging peptidoglycan biosynthesis in *Bacillus subtilis* with fluorescent antibiotics. *Proceedings of the National Academy of Sciences* 103(29):11033.
269. Deibert J, Kühner D, Stahl M, Koeksoy E, & Bertsche U (2016) The Peptidoglycan Pattern of Staphylococcus carnosus TM300-Detailed Analysis and Variations Due to Genetic and Metabolic Influences. (Translated from eng) *Antibiotics (Basel)* 5(4):33 (in eng).
270. Potluri L-P, de Pedro MA, & Young KD (2012) Escherichia coli low-molecular-weight penicillin-binding proteins help orient septal FtsZ, and their absence leads to asymmetric cell division and branching. (Translated from eng) *Molecular Microbiology* 84(2):203-224 (in eng).
271. Bonis M, Ecobichon C, Guadagnini S, Prévost M-C, & Boneca IG (2010) A M23B family metallopeptidase of Helicobacter pylori required for cell shape, pole formation and virulence. *Molecular Microbiology* 78(4):809-819.
272. Schäper S, *et al.* (2018) Seven-transmembrane receptor protein RgsP and cell wall-binding protein RgsM promote unipolar growth in Rhizobiales. (Translated from eng) *PLoS Genet* 14(8):e1007594-e1007594 (in eng).
273. Ashby MK & Houmard J (2006) Cyanobacterial two-component proteins: structure, diversity, distribution, and evolution. (Translated from eng) *Microbiology and molecular biology reviews : MMBR* 70(2):472-509 (in eng).
274. Dobihal GS, Brunet YR, Flores-Kim J, & Rudner DZ (2019) Homeostatic control of cell wall hydrolysis by the WalRK two-component signaling pathway in Bacillus subtilis. *eLife* 8:e52088.
275. Glauner B, Höltje JV, & Schwarz U (1988) The composition of the murein of Escherichia coli. *Journal of Biological Chemistry* 263(21):10088-10095.
276. Sycuro LK, *et al.* (2010) Peptidoglycan crosslinking relaxation promotes Helicobacter pylori's helical shape and stomach colonization. (Translated from eng) *Cell* 141(5):822-833 (in eng).
277. Loskill P, *et al.* (2014) Reduction of the peptidoglycan crosslinking causes a decrease in stiffness of the Staphylococcus aureus cell envelope. (Translated from eng) *Biophys J* 107(5):1082-1089 (in eng).
278. Mai-Prochnow A, Clauson M, Hong J, & Murphy AB (2016) Gram positive and Gram negative bacteria differ in their sensitivity to cold plasma. *Scientific Reports* 6(1):38610.
279. Gaysina LA, Saraf A, & Singh P (2019) Chapter 1 - Cyanobacteria in Diverse Habitats. *Cyanobacteria*, eds Mishra AK, Tiwari DN, & Rai AN (Academic Press), pp 1-28.
280. Battistuzzi FU & Hedges SB (2008) A Major Clade of Prokaryotes with Ancient Adaptations to Life on Land. *Molecular Biology and Evolution* 26(2):335-343.
281. Pisabarro AG, de Pedro MA, & Vazquez D (1985) Structural modifications in the peptidoglycan of Escherichia coli associated with changes in the state of

- growth of the culture. (Translated from eng) *J Bacteriol* 161(1):238-242 (in eng).
282. More N, *et al.* (2019) Peptidoglycan Remodeling Enables Escherichia coli To Survive Severe Outer Membrane Assembly Defect. (Translated from eng) *MBio* 10(1) (in eng).
 283. Sandoz KM, *et al.* (2016) Transcriptional Profiling of Coxiella burnetii Reveals Extensive Cell Wall Remodeling in the Small Cell Variant Developmental Form. (Translated from eng) *PLoS One* 11(2):e0149957-e0149957 (in eng).
 284. Zapun A, *et al.* (2013) In vitro reconstitution of peptidoglycan assembly from the Gram-positive pathogen Streptococcus pneumoniae. (Translated from eng) *ACS Chem Biol* 8(12):2688-2696 (in eng).
 285. Figueiredo TA, *et al.* (2012) Identification of genetic determinants and enzymes involved with the amidation of glutamic acid residues in the peptidoglycan of Staphylococcus aureus. (Translated from eng) *PLoS Pathog* 8(1):e1002508 (in eng).
 286. Ngadjeua F, *et al.* (2018) Critical Impact of Peptidoglycan Precursor Amidation on the Activity of L,d-Transpeptidases from Enterococcus faecium and Mycobacterium tuberculosis. *Chemistry – A European Journal* 24(22):5743-5747.
 287. Dajkovic A, *et al.* (2017) Hydrolysis of peptidoglycan is modulated by amidation of meso-diaminopimelic acid and Mg(2+) in Bacillus subtilis. (Translated from eng) *Molecular Microbiology* 104(6):972-988 (in eng).
 288. Munch D, *et al.* (2012) Identification and in vitro analysis of the GatD/MurT enzyme-complex catalyzing lipid II amidation in Staphylococcus aureus. (Translated from eng) *PLoS Pathog* 8(1):e1002509 (in eng).
 289. Morlot C, *et al.* (2018) Structure of the essential peptidoglycan amidotransferase MurT/GatD complex from Streptococcus pneumoniae. *Nature Communications* 9(1):3180.
 290. Quintela J, Caparrós M, & de Pedro MA (1995) Variability of peptidoglycan structural parameters in Gram-negative bacteria. *FEMS Microbiology Letters* 125(1):95-100.
 291. Schaechter M (2009) *The Desk Encyclopedia Of Microbiology*. (Academic Press, San Diego), 2. Ed, pp 836-837.
 292. Höltje JV, Mirelman D, Sharon N, & Schwarz U (1975) Novel type of murein transglycosylase in Escherichia coli. (Translated from eng) *Journal of Bacteriology* 124(3):1067-1076 (in eng).
 293. Moynihan PJ & Clarke AJ (2011) O-Acetylated peptidoglycan: Controlling the activity of bacterial autolysins and lytic enzymes of innate immune systems. *The International Journal of Biochemistry & Cell Biology* 43(12):1655-1659.
 294. Balomenou S, *et al.* (2013) Distinct functions of polysaccharide deacetylases in cell shape, neutral polysaccharide synthesis and virulence of Bacillus anthracis. (Translated from eng) *Mol Microbiol* 87(4):867-883 (in eng).
 295. Gründling A & Schneewind O (2006) Cross-Linked Peptidoglycan Mediates Lysostaphin Binding to the Cell Wall Envelope of Staphylococcus aureus. *Journal of Bacteriology* 188(7):2463.
 296. Bera A, *et al.* (2007) Influence of wall teichoic acid on lysozyme resistance in Staphylococcus aureus. (Translated from eng) *Journal of Bacteriology* 189(1):280-283 (in eng).
 297. Brown S, Santa Maria JP, Jr., & Walker S (2013) Wall teichoic acids of gram-positive bacteria. (Translated from eng) *Annual review of microbiology* 67:313-336 (in eng).

298. WOITZIK D, WECKESSER J, & JÜRGENS UJ (1988) Isolation and Characterization of Cell Wall Components of the Unicellular Cyanobacterium *Synechococcus* sp. PCC 6307. *Microbiology* 134(3):619-627.
299. Schneider S & Jürgens UJ (1991) Cell wall and sheath constituents of the cyanobacterium *Gloeobacter violaceus*. *Archives of Microbiology* 156(4):312-318.
300. Braun V & Sieglin U (1970) The Covalent Murein-Lipoprotein Structure of the *Escherichia coli* Cell Wall. *European Journal of Biochemistry* 13(2):336-346.
301. Oh J-T, *et al.* (2000) Cationic peptide antimicrobials induce selective transcription of *micF* and *osmY* in *Escherichia coli*. *Biochimica et Biophysica Acta (BBA) - Biomembranes* 1463(1):43-54.
302. Buist G, Steen A, Kok J, & Kuipers OP (2008) LysM, a widely distributed protein motif for binding to (peptido)glycans. *Molecular Microbiology* 68(4):838-847.
303. Bateman A & Bycroft M (2000) The structure of a LysM domain from *E. coli* membrane-bound lytic murein transglycosylase D (MltD)11 Edited by P. E. Wight. *Journal of Molecular Biology* 299(4):1113-1119.
304. Buist G, *et al.* (1995) Molecular cloning and nucleotide sequence of the gene encoding the major peptidoglycan hydrolase of *Lactococcus lactis*, a muramidase needed for cell separation. (Translated from eng) *J Bacteriol* 177(6):1554-1563 (in eng).
305. Beliveau C, Potvin C, Trudel J, Asselin A, & Bellemare G (1991) Cloning, sequencing, and expression in *Escherichia coli* of a *Streptococcus faecalis* autolysin. (Translated from eng) *J Bacteriol* 173(18):5619-5623 (in eng).
306. Boekhorst J, de Been MWHJ, Kleerebezem M, & Siezen RJ (2005) Genome-Wide Detection and Analysis of Cell Wall-Bound Proteins with LPxTG-Like Sorting Motifs. *Journal of Bacteriology* 187(14):4928.
307. Baba T & Schneewind O (1996) Target cell specificity of a bacteriocin molecule: a C-terminal signal directs lysostaphin to the cell wall of *Staphylococcus aureus*. (Translated from eng) *The EMBO Journal* 15(18):4789-4797 (in eng).
308. Garcia JL, Sanchez-Beato AR, Medrano FJ, & Lopez R (1998) Versatility of choline-binding domain. (Translated from eng) *Microb Drug Resist* 4(1):25-36 (in eng).
309. Mesnage S, *et al.* (2000) Bacterial SLH domain proteins are non-covalently anchored to the cell surface via a conserved mechanism involving wall polysaccharide pyruvylation. (Translated from eng) *The EMBO Journal* 19(17):4473-4484 (in eng).
310. Navarre WW, Daefler S, & Schneewind O (1996) Cell wall sorting of lipoproteins in *Staphylococcus aureus*. *Journal of Bacteriology* 178(2):441.
311. van der Aart LT, *et al.* (2018) High-Resolution Analysis of the Peptidoglycan Composition in *Streptomyces coelicolor*. *Journal of Bacteriology* 200(20):e00290-00218.
312. McKerrow J, *et al.* (2000) A simple HPLC method for analysing diaminopimelic acid diastereomers in cell walls of Gram-positive bacteria. (Translated from eng) *Lett Appl Microbiol* 30(3):178-182 (in eng).
313. Bui NK, *et al.* (2009) The peptidoglycan sacculus of *Myxococcus xanthus* has unusual structural features and is degraded during glycerol-induced myxospore development. (Translated from eng) *Journal of Bacteriology* 191(2):494-505 (in eng).

314. Höltje J-V, Kopp U, Ursinus A, & Wiedemann B (1994) The negative regulator of β -lactamase induction AmpD is a N-acetyl-anhydromuramyl-L-alanine amidase. *FEMS Microbiology Letters* 122(1-2):159-164.
315. Pennartz A, Génèreux C, Parquet C, Mengin-Lecreulx D, & Joris B (2009) Substrate-induced inactivation of the Escherichia coli AmiD N-acetylmuramoyl-L-alanine amidase highlights a new strategy to inhibit this class of enzyme. (Translated from eng) *Antimicrob Agents Chemother* 53(7):2991-2997 (in eng).
316. Büttner FM, Zoll S, Nega M, Götz F, & Stehle T (2014) Structure-function analysis of Staphylococcus aureus amidase reveals the determinants of peptidoglycan recognition and cleavage. (Translated from eng) *The Journal of biological chemistry* 289(16):11083-11094 (in eng).
317. Sadovskaya I, *et al.* (2017) Another Brick in the Wall: a Rhamnan Polysaccharide Trapped inside Peptidoglycan of *Lactococcus lactis*. *MBio* 8(5):e01303-01317.
318. Campbell EL, Summers ML, Christman H, Martin ME, & Meeks JC (2007) Global Gene Expression Patterns of *Nostoc punctiforme* in Steady-State Dinitrogen-Grown Heterocyst-Containing Cultures and at Single Time Points during the Differentiation of Akinetes and Hormogonia. *Journal of Bacteriology* 189(14):5247.
319. Patel Jignesh G, *et al.* (2020) Evolution, purification, and characterization of RC0497: a peptidoglycan amidase from the prototypical spotted fever species Rickettsia conorii. in *Biological Chemistry*, p 249.
320. Tulum I, Tahara YO, & Miyata M (2019) Peptidoglycan layer and disruption processes in Bacillus subtilis cells visualized using quick-freeze, deep-etch electron microscopy. *Microscopy* 68(6):441-449.
321. Li K, *et al.* (2018) Atomic Force Microscopy of Side Wall and Septa Peptidoglycan From Bacillus subtilis Reveals an Architectural Remodeling During Growth. (Translated from English) *Frontiers in Microbiology* 9(620) (in English).
322. Ehlert K, Schröder W, & Labischinski H (1997) Specificities of FemA and FemB for different glycine residues: FemB cannot substitute for FemA in staphylococcal peptidoglycan pentaglycine side chain formation. *Journal of Bacteriology* 179(23):7573.
323. Zheng Z, *et al.* (2017) An amidase is required for proper intercellular communication in the filamentous cyanobacterium *Anabaena* sp. PCC 7120. *Proceedings of the National Academy of Sciences* 114(8):E1405.
324. Cserti E, *et al.* (2017) Dynamics of the peptidoglycan biosynthetic machinery in the stalked budding bacterium Hyphomonas neptunium. *Molecular Microbiology* 103(5):875-895.
325. Mellroth P, *et al.* (2014) Structural and Functional Insights into Peptidoglycan Access for the Lytic Amidase LytA of *Streptococcus pneumoniae*. *MBio* 5(1):e01120-01113.
326. Sandalova T, *et al.* (2016) The crystal structure of the major pneumococcal autolysin LytA in complex with a large peptidoglycan fragment reveals the pivotal role of glycans for lytic activity. (Translated from eng) *Mol Microbiol* 101(6):954-967 (in eng).

